Nonlinear Vibration Analysis Using the Method of Direct Normal Forms

Ayman Mohammad Adel Nasir

Department of Mechanical Engineering

University of Sheffield

This thesis is submitted for the degree of

Doctor of Philosophy

Supervisor

Prof. David Wagg

February 2023

I would like to dedicate this thesis to my mother, for her help and support, and to the soul of my father. I would like also to devote this work to my beloved wife, for her support, love and patience.

Declaration

I hereby declare that except where specific reference is made to the work of others, the contents of this thesis are original and have not been submitted in whole or in part for consideration for any other degree or qualification in this, or any other university. This thesis is my own work and contains nothing which is the outcome of work done in collaboration with others, except as specified in the text and Acknowledgments.

Ayman Nasir

February, 2023

Acknowledgements

I would like to thank every person who helped me finish this thesis; special appreciations to my supervisors Prof. David Wagg and Prof. Neil Sims, for their great efforts and instructions, the guidance and advice I got from them made this work valuable. In addition, I would like to thank the PhD Viva examiners; Prof. Andrea Cammarano and Dr. Graeme Manson, for their valuable comments which lead to significant improvements to the overall quality of this thesis. I would like also to thank Eng. Nour Atieh for her help during the writing process of this thesis. Moreover, being sponsored by Alzaytoonah University of Jordan to obtain my PhD degree, I would like to appreciate their help and support during my PhD studying period.

Abstract

In this thesis, an approximative analysis of nonlinear dynamical systems utilising the direct normal forms method (DNF) is addressed. For certain engineering applications, this approach is used to analyse nonlinear equations of motion. Nonetheless, while dealing with its specifics, the DNF approach has several undesirable restrictions, particularly in regards to the enormous algebraic terms and solutions; thus, it is crucial to use computer-based procedures. In this thesis, Maple, a symbolic computing program, plays a crucial role in obtaining step-by-step solutions for difficult nonlinear dynamical engineering problems based on the DNF approach. In this thesis, it is shown that the implementation of such software permits the analysis of more complicated systems, particularly those with higher-order geometric nonlinear stiffness terms, combinations of nonlinear stiffness and viscous damping, and systems with fractional order damping terms.

The analysis in this thesis starts with a comprehensive investigation of single-degree-of-freedom (SDOF) nonlinear systems, beginning with conservative systems and progressing through viscously damped and forced systems with various forms of geometric nonlinearities. Higher order accuracies of the DNF method are then explored in detail; beginning with a reintroduction of the study of ε^2 accuracy using symbolic computations. A unique refinement of the DNF methodology in terms of higher order accuracies is then presented. With the use of symbolic computations tools, the precision of the DNF approach has been increased to any desired level of precision, ε^n, which has been shown with a number of applications. In addition, for viscously damped SDOF systems, a novel approach based on a variation of Burton's method along with a normal form technique to obtain the damped backbone curves is thoroughly discussed with examples.

Furthermore, the analysis is extended to multi-degree-of-freedom (MDOF) nonlinear systems; starting with two verification problems that show the capability of the proposed symbolic DNF technique with Maple software. Then, a more advanced system of 2-DOF cubic-quintic oscillator is briefly discussed, in which analytical expressions of *single-mode* and *double-mode* backbone curves are generated.

In conclusion, the overall study findings provide unique enhancements to the technique of DNF for investigating nonlinear SDOF and MDOF systems analytically; this includes creating a tool for the researcher to apply the method of DNF symbolically for systems with high orders of polynomial stiffness nonlinearities, systems with combinations of stiffness and damping nonlinearities, and systems with viscous damping with fractional orders. Moreover, the accuracy of the DNF method is discussed in detail and a general form for any ε order is obtained. In conclusion, the implementation of symbolic computations of DNF method for such systems is shown to be effective and trustworthy.

List of Publications

During my PhD study, I have published one journal paper and two conference articles as listed below:

1. (Journal paper) A. Nasir, N. Sims, and D. Wagg. Direct normal form analysis of oscillators with different combinations of geometric nonlinear stiffness terms. *Journal of Applied and Computational Mechanics*, 7:1167–1182, 2021.

2. (Conference article) A.M. Nasir, N.D. Sims and D.J. Wagg. Computing backbone curves for nonlinear oscillators with higher order polynomial stiffness terms. In: Papadrakakis, M., Fragiadakis, M. and Papadimitriou, C., (eds.) EURODYN 2020: Proceedings of the XI International Conference on Structural Dynamics. *EURODYN 2020: XI International Conference on Structural Dynamics*, 23-26 Nov 2020, Athens, Greece. European Association for Structural Dynamics (EASD), pp. 318-334. ISBN 9786188507203, 2020.

3. (Conference article) A. Nasir, N. Sims, D.J. Wagg. Exploring the Dynamics of Viscously Damped Nonlinear Oscillators via Damped Backbone Curves: A Normal Form Approach. In: Lacarbonara, W., Balachandran, B., Leamy, M.J., Ma, J., Tenreiro Machado, J.A., Stepan, G. (eds) *Advances in Nonlinear Dynamics*. NODYCON Conference Proceedings Series. Springer, Cham. https://doi.org/10.1007/978-3-030-81162-4_14, 2022.

Table of Contents

List of Figures

List of Tables

Nomenclature

$[h_{(j)}]$	An $\{N \times L_j\}$ matrix of the coefficients of the components in $h_{(j)}$, corresponding to the terms in $u^*_{(j)}$
$[N_{u(j)}]$	An $\{N \times L_j\}$ matrix of the coefficients of the components in $n_{u(j)}$, corresponding to the terms in $u^*_{(j)}$
$[n_{v(j)}]$	An $\{N \times L_j\}$ matrix of the coefficients of the components in $N_{v(j)}$, corresponding to the terms in $u^*_{(j)}$
β	The order of the fractional derivative, see Section 6.2
$\boldsymbol{\beta}_{(j)}$	An $\{N \times L_j\}$ matrix for identifying the resonant terms in the j^{th} homo-logical equation
$\boldsymbol{\Gamma}_{\boldsymbol{x}}$	An $\{N \times 1\}$ vector of nonlinear terms in x coordinates
$\boldsymbol{\Lambda}$	A diagonal $\{N \times N\}$ matrix of the squared linear frequencies
$\boldsymbol{\Phi}$	An $\{N \times N\}$ vector of linear mode shapes
$\boldsymbol{\Upsilon}$	A diagonal $\{N \times N\}$ matrix of the square of fundamental response frequencies
$\Gamma()$	Gamma function, a special function used in this thesis for the analysis of fractionally damped systems, Chapter 6
$\Im\{\}$	The imaginary part of the solution, see Chapter 6
$\mathbf{C}$	An $\{N \times 1\}$ damping matrix
$\mathbf{e}$	An $\{N \times 2\}$ matrix for removing non-resonant forcing terms

$\mathbf{e}_i$	A $\{1 \times 2\}$ vector representing the i^{th} row of matrix $\mathbf{e}$
$\mathbf{H}$	An $\{N \times 1\}$ vector of harmonic components of the modal displacements
$\mathbf{h}_{(j)}$	An $\{N \times 1\}$ vector of harmonic components in the i^{th} homo-logical equation
$\mathbf{i}$	Imaginary unit which is equal to $\sqrt{-1}$
$\mathbf{I}_N$	An $\{N \times N\}$ identity matrix
$\mathbf{K}$	An $\{N \times N\}$ stiffness matrix
$\mathbf{M}$	An $\{N \times N\}$ mass matrix
$\mathbf{N}_q$	An $\{N \times 1\}$ vector of nonlinear terms and linear damping terms in modal coordinates q
$\mathbf{N}_v$	An $\{N \times 2\}$ vector of nonlinear terms and linear damping terms in forcing transformed modal coordinates v
$\mathbf{P}_q$	An $\{N \times 2\}$ matrix of excitation amplitudes in modal coordinates q
$\mathbf{P}_u$	An $\{N \times 2\}$ matrix of excitation amplitudes in resonant coordinates u
$\mathbf{P}_v$	An $\{N \times 2\}$ matrix of excitation amplitudes in forcing-transformed modal coordinates v
$\mathbf{P}_x$	An $\{N \times 2\}$ matrix of force amplitudes in physical coordinates x
$\mathbf{P}_{q,i}$	An $\{N \times 1\}$ vector representing the i^{th} row of matrix $\mathbf{P}_q$
$\mathbf{P}_{v,i}$	An $\{1 \times 2\}$ vector representing the i^{th} row of matrix $\mathbf{P}_v$
$\mathbf{q}$	An $\{N \times 1\}$ vector of modal displacement
$\mathbf{r}$	A $\{2 \times 1\}$ complex exponential functions vector describing the sinusoidal component of external force
$\mathbf{u}$	An $\{N \times 2\}$ vector of the fundamental components of modal displacements
$\mathbf{u}^*_{(j)}$	An $\{L_j \times 1\}$ vector of unique combinations of the variables in the j^{th} homo-logical equation
$\mathbf{W}$	An $\{2 \times 2\}$ matrix of diagonal elements $\mathbf{i}\Omega$ and $-\mathrm{i}\Omega$

$\mathbf{x}$	An $\{N \times 1\}$ vector of physical displacement
e	Euler's number
Ω	The frequency of external force
ω_d	Damped natural frequency
ω_{ni}	The i^{th} linear frequency
ω_{ri}	The fundamental response frequency of the i^{th} mode
ϕ_i	The phase of the fundamental response component of the i^{th} mode
$\Re\{\}$	The real part of the solution, see Chapter 6
ε	A bookkeeping parameter denoting the smallness of the nonlinearity
C_j^β	The fractional binomial coefficient, see Section 6.2
h	Sample step size, see Section 6.2
N	The number of degrees-of-freedom of system
$N_{u,i}$	The i^{th} term in vector $\mathbf{N}_u$
N_{ui}^+	The time-invariant complex component of the i^{th} term in vector $\mathbf{N}_u$ corresponding to the positive conjugate of the resonating term
N_{ui}^-	The time-invariant complex component of the i^{th} term in vector $\mathbf{N}_u$ corresponding to the negative conjugate of the resonating term
$n_{v(j)}$	An $\{N \times 1\}$ vector of nonlinear and damping, including both resonant and harmonic, components in the j^{th} homo-logical equation
r_m	The negative complex component of the sinusoidal forcing
r_p	The positive complex component of the sinusoidal forcing
t	Time

t_n	Sample points, see Section 6.2
u_i	The i^{th} term of u vector, denoting the displacement of fundamental component of the i^{th} mode
u_m	An $\{N \times 1\}$ vector with u_{mi} as its i^{th}
u_p	An $\{N \times 1\}$ vector with u_{pi} as its i^{th}
U_i	The amplitude of the fundamental response component of the i^{th} mode
u_{mi}	The negative component of the complex conjugate pair that forms u_i
u_{pi}	The positive component of the complex conjugate pair that forms u_i
v	An $\{N \times 1\}$ vector of forcing-transformed modal displacements

Chapter 1

Introduction

The broad context of linear and nonlinear dynamical systems is explored in this Chapter, focusing on nonlinear systems and their general characteristics. The research motivations are then described in depth to demonstrate the necessity to improve the DNF technique, taking into considerations the projected advantages and drawbacks of such modifications. Finally, in Section 1.3 the outline of the thesis is discussed in detail.

1.1 Background and Motivations

For a given linear mechanical system, the equations of motion are generated according to the fact that the acceleration, velocity, and displacement are proportional to the inertial force, damping force, and elastic restoring force, respectively. Based on these assumptions, linear models can be perfect in many applications, nevertheless, in other situations, the presence of excessive deformations and other sources of nonlinearities limit the accuracy of these models; leading to inaccurate or even incorrect results. Accordingly, for these specific applications, nonlinear system analysis need to be performed.

In the literature, linear vibration theories have been matured significantly, for the purpose of tackling linear vibration problems; well-developed methods and analytical tools such as modal superposition, time domain, and frequency domain analysis are available for linear system analysis. In machine dynamics, for example, linear vibration analysis is often suitable for machines that run at low speeds and with relatively small com-

ponent deformations. However, in modern machine industry, two opposing tendencies are being chased at the same time: faster speeds and lighter weights, [1]. These tendencies cause significant greater deformations of machine components, requiring dynamic analysis based on nonlinear vibration theory to be adopted, in order to attain improved accuracy and more satisfying findings.

System modelling approach allows for a simple categorisation of vibrations into two broad classes: linear vibrations and nonlinear vibrations, regardless of the underlying causes. First, it's important to exercise caution when using the terms linear and nonlinear to classify systems in general; linear systems are those whose outputs are directly proportional to their inputs, allowing researchers to accurately forecast the system's behaviour when they know the input. Importantly, the linear system being studied is amenable to direct application of any number of linear theories, including the concepts of superposition and homogeneity. Moreover, advanced tools like Laplace transformations and Laplace inverse procedures are highly efficient for solving the equations of motion (EOM) of linear systems. Nevertheless, in mathematics, nonlinear functions can be studied using Laplace, but the results are more complicated and difficult to be adopted; they will not provide the same benefits as direct integration techniques, thus, numerous method of analysing nonlinear dynamical systems can be found in the literature.

In addition, features such as equilibrium and stability points, finite resonances, and clearly anticipated steady-state performance, are readily apparent for linear vibrational systems. While linear models are perfectly valid models and provide very accurate results in many cases, it is when they are improperly used beyond their limits that they are inaccurate and lead to incorrect results. Due to the fact that many engineering, physical, and mathematical applications are inherently nonlinear, applying linear approaches to explore these applications can be ineffective, in these specific cases, nonlinear models gain increasing importance for researchers and need to be feasibly practised.

In principle, when the displacement x or its derivatives, i.e. velocity, $\dot{x}$ and acceleration, $\ddot{x}$, appear in the equation of motion with degrees other than the first, the inertial force, damping force, and elastic restoring force are no longer proportional to the acceleration, velocity, and displacement, respectively. In that case, the

corresponding problems or systems are classified as nonlinear. Nonetheless, in numerous engineering applications other configurations of nonlinearities are observed, for which this definition is unsatisfied, for instance; the case of Coulomb friction, [8, 12]. In this case, and others similar, it is more realistic to rely on the principle of superposition and homogeneity to define nonlinear systems, see [10] for broader discussions regarding nonlinearities in engineering applications.

In terms of the steady-state performance and stability of a system, a nonlinear problem often displays characteristics that are not anticipated by or even hinted at in a linear problem. For instance, if a sinusoidal forcing scheme was used to drive a linear vibrational system, the system response would likewise be sinusoidal, but maybe with a variable amplitude, frequency, or phase shift. However, the system output cannot be anticipated if the same sinusoidal force is employed to drive a nonlinear system. The following are distinguishing features of nonlinear systems in comparison to linear ones, [11]:

- Nonlinear systems do not follow the principle of superposition (in terms of linearity and homogeneity).
- They may have multiple isolated equilibrium points, while linear systems can have only one.
- They may create additional subharmonic vibrations with constant frequency.
- They may have several steady-state amplitudes, additionally, they might exhibit properties such as limit-cycle, bifurcation and chaos.

Most practical engineering applications are themselves inherently nonlinear, with nonlinearities stemming from a wide variety of sources such as geometry, material, and contact or boundary conditions. The problem with these nonlinearities is the undesirable, unpredictable, and sometimes catastrophic vibrational motions which can be resulted. For instance, one of the devastating incidents is the collapse of the first Tacoma Narrows Bridge (1940), Fig. 1.1, where the catastrophic sudden collapse is mainly caused due to two nonlinear phenomena; namely the flatter phenomenon, and nonlinear interactions between the moving air and bridge components. Since most engineering structures must function in a linear fashion, nonlinear interactions and behaviours are often not taken into account throughout the design process. In reality, linearity may be seen as an idealisation or perfection, but dealing with nonlinear situations is needed in many current applications. For instance; in the field of mechanical vibrations, excessive deflections of beams, plates and wind turbines blades are well-known

examples of nonlinear dynamical systems, [8]. Moreover, in control systems, flight control of a fly-by-wire high performance jet is an important engineering application of nonlinear dynamical systems, [13].

Figure 1.1: Collapse of Tacoma Narrows Bridge (1940)
(*Source*: https://en.wikipedia.org/wiki/Tacoma_Narrows_Bridge_(1940))

The exact analytical technique is one of the many proposed approaches for solving nonlinear equations of motion, however it is often reserved for the simplest problems, refer to Section 2.1 for more details regarding the exact solutions of nonlinear systems. Therefore, the researchers had to implement approximation techniques which should be precise enough to capture the system's dynamic behaviours while also accounting for the nonlinear phenomena connected with it. The literature has many different analytical approximation approaches; some examples are the fundamental perturbation method, the harmonic balancing method, the averaging method, the multiple scales method, and the normal forms method. There are advantages and disadvantages to each of these approaches, and in certain circumstances one may be more desirable than the others.

Nonlinear vibration system's frequency-amplitude relationships are of great interest, because they indicate how the periodic responses of a nonlinear system change as the input frequency is varied, for linear systems this is captured by the frequency response function, which relates the magnitude and phase of the input to that of the output. In comparison to linear systems, the frequency-amplitude relationship of nonlinear systems are curved lines (hence called "backbone curves"), [33]. These relationships can be generated either analytically through

approximate analytical techniques or numerically with some numerical techniques (mainly continuation) such as COCO and MatCont continuation tool boxes in MATLAB [34, 116], which will be primarily used in this thesis to investigate backbone curves relations numerically and compare them to analytical solutions based on the DNF method.

There are a number of challenges that researchers face when trying to achieve a high level of accuracy in their proposed findings while using approximate analytical approaches for tackling complicated engineering problems. Thus, there is a growing need for software packages that may truncate solution terms with enhanced techniques that imply less computational time and efforts, but at the expense of precision. This thesis primarily uses Maple, a symbolic computations software, to solve difficult nonlinear equations of motion for various vibratory dynamical systems through the DNF approach.

In the literature, the method of DNF has been implemented to investigate the dynamics of numerous engineering applications for both forced-damped SDOF and MDOF systems, for which the damping is modelled in terms of viscous damping. However, when applied symbolically, the method has the potential to be further improved to study systems with non-conventional damping models. In this thesis, as a novel implementation of the method, DNF is used to symbolically investigate the dynamics of SDOF systems involving viscous damping with fractional order derivatives.

To conclude, the method of direct normal forms (DNF) is considered as a highly sophisticated method that involves many mathematically intense algebraic steps, moreover, it is a powerful technique for investigating nonlinear dynamical systems for both SDOF and MDOF applications. Nevertheless, when implemented symbolically, many accompanied mathematical steps can be performed with much less efforts. Practically, the symbolic implementation of the DNF method is to be discussed in detail through out this thesis. In the following subsection the research aims and objectives are accordingly clarified.

1.2 Research Objectives

This thesis studies the symbolic implementation of direct normal forms method (DNF), this is accomplished by developing novel usage of DNF for practical engineering applications. The DNF method, in its traditional implementation, requires mathematically intense hand calculations for the purpose of investigating the dynamics of nonlinear systems. The main purpose of this thesis is to introduce a novel symbolic implementation of the DNF method to create an efficient tool for researcher to use when adopting this method. In particular, the key objectives of this research are:

1. To study the method of DNF in detail and how it can be symbolically implemented for solving complex engineering applications.

2. To develop novel symbolic implementations of the DNF technique using Maple software, which can enable researchers to solve nonlinear equation of motions with enhanced accuracy and generate backbone curves for the corresponding vibratory systems.

3. To adopt the proposed symbolic computations approach to investigate the accuracy of DNF technique, and obtain closed-form solutions truncated to any desired accuracy, ε^n. For different nonlinear applications, the outcomes of these accuracies are to be investigated and compared.

4. To develop a novel normal forms technique to investigate the dynamics of viscously damped SDOF oscillators. This technique is used to obtain the damped backbone curves of the nonlinear systems.

5. To apply the proposed Maple symbolic algorithms for chosen practical SDOF and MDOF engineering problems, including: nonlinear oscillators, beams, and any relative engineering applications.

6. To develop a novel implementation of the DNF method to study SDOF systems with viscous damping of various fractional orders, and compare the findings with both numerical results and some other techniques found in the literature.

7. To compare analytical DNF results with simulation results (obtained using numerical continuation packages, i.e. COCO and Matcont).

1.3 Thesis Outline

The discussion in Chapter 1, as previously described, shows the introduction of the research topic. It contains background and motivations of the author on pursuing these research activities. A brief introduction of nonlinear dynamical systems and their solutions is presented. Moreover, the research objectives are described in detail, and finally the thesis outline is briefly discussed.

In Chapter 2, a brief literature review related to previous works is shown. Firstly, discussions regarding the nonlinear dynamical systems in the field of mechanical engineering are performed. Then, the methods for investigating nonlinear dynamical systems are briefly presented starting with approximate analytical methods, followed by specific discussion regarding the method of DNF and its applications. Moreover, the numerical techniques for analysing nonlinear dynamical systems are discussed to indicate the verification techniques used in this thesis. The modal analysis of linear systems is then shown with brief discussions of the nonlinear normal modes (NNMs) theory and applications. Furthermore, the concept of damped backbone curves of nonlinear systems is introduced, this is followed by reviewing the literature of oscillators with combinations of stiffness and damping nonlinear terms, and finally oscillators with fractional order damping are investigated.

In Chapter 3, an extended formulation for the method of DNF to solve nonlinear dynamical systems is shown. The analysis starts with the DNF procedure of conservative systems where no forcing or damping occurs, and then it is extended to systems with viscous damping and forcing. This is followed by a discussion of the stability conditions of DNF method. Moreover, two examples of using DNF method are shown in detail; the first example is a single-degree-of-freedom conservative oscillator with two types of geometric polynomial nonlinearities, while the second example describes a system of viscously damped Duffing oscillator that is driven by a forcing away from resonance.

In Chapter 4, the analysis is extended to include higher order accuracies of DNF starting with DNF analysis of ε^2 accuracy, which has been previously discussed in the literature in many conducted researches, for instance, refer to Wagg and Neild [8]. Then, a novel general DNF analysis for any required accuracy, ε^n, is discussed. This is followed by two examples that compare the DNF results for ε^1, ε^2 and ε^3 accuracies.

Moreover, the analysis of damped backbone curves is discussed for which a novel new procedure of calculating such type of backbone curves for systems with viscous damping is introduced with some detailed examples.

In Chapter 5, further applications of DNF methods to investigate the dynamics of nonlinear SDOF systems are discussed in detail. The discussion starts with the analysis of SDOF cubic-quintic oscillator, then, analysis of SDOF oscillators with any type of odd polynomial nonlinearities is presented. In the following subsection, DNF analysis of Van-der-Pol, Rayleigh, and oscillators with combinations of nonlinear stiffness and viscous damping is revealed.

In Chapter 6, a novel implementation of DNF technique is presented to investigate the dynamics of viscously damped nonlinear SDOF systems with fractional (or non-integer) order derivative (denoted as fractionally damped systems, [122]). In this Chapter, the method of DNF is modified to study systems with fractional order damping. Starting by DNF analysis of Duffing oscillator with fractional damping, analytical expressions of the frequency-amplitude relationships are obtained and compared to both numerical results and results of other methods found in the literature. At the final section of this Chapter, DNF analysis of the fractional Van-der-Pol oscillator is revealed.

In Chapter 7, applications of DNF methods to investigate the dynamics of nonlinear MDOF systems are discussed. Two verification problems are investigated to show the validity of symbolically applied DNF technique to explore MDOF systems. The first verification problem illustrates a nonlinearly coupled 2-DOF vertical-horizontal-spring-mass oscillator (or as called Touzé system, [46]). Initially, a new derivation for the equations of motion is introduced, then the method of DNF is applied in order to get the backbone curves of this system, these results are then compared to the literature to verify the outcomes obtained. Moreover, the second verification problem represents an investigation of 3-DOF system with cubic nonlinear coupling stiffness terms, results are verified by comparisons with relative works from the literature. Finally, using the symbolically applied DNF method, a more complicated system of cubic-quintic 2-DOF system is studied, in which *single-mode* and *double-mode* backbone curves are obtained. Finally, in Chapter 8, the conclusions and possible future works are briefly discussed.

Chapter 2

Literature Review

An overview of the literature is provided in this Chapter in relation to nonlinear dynamic properties and methods for analysing nonlinear systems. As such, it is crucial to comprehend the consequences of nonlinearity in structural dynamics for the purposes of either avoiding or capitalising on nonlinearities. Recent techniques for investigating nonlinear dynamics cover a lot of areas, but they can be classified into three major categories: numerical, analytical, and experimental. In this Chapter, a brief summary of some of these methods is discussed. This is followed by a brief discussion of the modal analysis approaches for nonlinear systems. Then, oscillators with combinations of stiffness and damping nonlinear terms are visited. Finally, nonlinear oscillators with fractional order damping term are discussed in details.

2.1 Nonlinear dynamical systems

Although the nonlinear vibration systems are mathematically well known for several centuries, the actual and real interests in this field started efficiently in the 19th century; this can be related to the mathematical tools developments, and one of the earliest work in this field was undertaken by J. H. Poincaré, a well-known French mathematician [39]. His contributions to pure and applied mathematics were of outstanding novelty in that era, he classified the singular points of nonlinear autonomous systems of nonlinear vibrations, and one of the modified perturbation methods was partially named after him; Lindstedt-Poincaré method [18].

For decades, the dynamics behind the nonlinear vibratory systems are discussed thoroughly in many books, [2–8, 18], and many unique features of nonlinear systems dynamical behaviours are found when comparing with linear systems, such as initial condition sensitivity and output to input varieties. These unique characteristics, contrary to linear systems, may yield to various nonlinear dynamic phenomena including multiple solutions, jump phenomena, harmonics, resonance distortion, quasi-periodic motions, etc.

In the literature, only limited number of nonlinear vibration systems have exact solutions, for instance, Kovacic and Brennan developed an exact solution of the Duffing oscillator based on the Jacobi elliptic functions approach, [87]. Nevertheless, a wide variety of other systems do not have these exact solutions, hence, approximate methods are presented. In the literature, perturbation methods are mainly used to investigate the dynamics of nonlinear systems, which depend on Taylor-series expansion [33]. These perturbation techniques enabled the engineering analyst to get some good analytical approximations for nonlinear systems, but it involves some undesired outcomes that cause solution divergence in some cases, mainly due to the appearance of secular terms, [36]. Many developed methods are found to overcome this problem, all of which contain mathematical complexities and high dimensionality of solutions, which increase the manipulation and simulation time. In the following subsection a brief review of the methods used for investigating the dynamics of nonlinear systems is given.

2.2 Methods of investigating nonlinear dynamical systems

The main concern in this Section is to focus on mathematically based techniques, including numerical and analytical methods, since they are most relevant to the thesis's central topic. In Subsection 2.2.1 the approximate analytical techniques for analysing nonlinear dynamical systems are briefly discussed, while in Subsection 2.2.2 the method of DNF is revisited in more depth. Finally, in Subsection 2.2.3 the numerical techniques of nonlinear dynamical systems are discussed.

2.2.1 Approximate analytical methods of nonlinear dynamical systems

Herein, a short summary of the main methods used in analysing the dynamics of nonlinear systems is presented, including harmonic balance technique, in addition to some perturbation techniques; namely, averaging, multiple scales, normal forms and finally direct normal forms techniques.

Starting with the harmonic balance method, [33], which is a frequency domain method for calculating the steady-state solution of the nonlinear systems. It was originally implemented by Baily [19] and Lindenlaub [20], where the solution is assumed to be summation of consecutive harmonics differing in amplitudes and frequencies. It is considered one of the simplest methods, but it has some problems of accuracy, and sometimes harmonics cannot be effectively balanced causing researcher to execute an endless loop of calculations, [8]. Comparisons of the harmonic balance technique and some perturbation techniques in determining the combination resonance for parametric dynamical systems can be found in [9].

The averaging method is based on the concept of substituting the actual differential EOM with its averaged form. Thus, the basic (or smaller) response is kept while solving the response, however, the rapid dynamics, i.e. the harmonics, are eliminated. More information regarding the averaging method used in nonlinear dynamic systems may be found in Sanders's textbook, [21]. Moreover, according to Verhulst, [22], the approach of averaging may be used to determine the steady-state response of a system, as well as its transient behaviour. Nevertheless, unlike the harmonic balance, the approach of averaging is only applicable to weakly-nonlinear systems in which the nonlinear terms are substantially less than the linear ones.

Another well-known method, especially for SDOF systems, is the multiple scales method [8]; a highly intense algebraic method in which two, or even more, time scales are used in the solution, this technique is outstanding in some SDOF cases, while it could be very difficult and time consuming in MDOF cases, and the technique becomes extremely complex for large systems. The difference between multiple scales and averaging method is that, in multiple scales, instead of removing the fast components by averaging, terms of equivalent order are collected together under the assumption that the terms of the same scale balance each other, this is accomplished by applying different time scales to the equation of motion.

Nonlinear DNF method, the method used in this work, is a well-structured technique of solving nonlinear EOMs with various types of nonlinearities, it can be used for either SDOF or MDOF problems, it is possible for the analyst to select a certain resonant (or non-resonant) case to study, and a part of mathematical

intensity could be avoided by making several nonlinear transformations for the EOM, these transformations include near-identity transforms and forcing transforms (for forced systems), [8], and matrix algebra techniques are adopted to solve matrices with multi-step approach, yielding to detection of the desired resonances and solving the SDOF or MDOF system.

While the DNF method looks fascinating for a wide range of applications, it contains many critical details; as mentioned, using several nonlinear transformations can reduce the mathematically intense steps, nevertheless, when used for complicated nonlinear systems, specifically those modelled by high orders of geometric polynomial nonlinear terms or combinations of nonlinear stiffness geometric and viscous damping terms, the method would still generate huge and complicated terms due to the system complicity, and when trying to use computer algorithms in the solution, researchers suffer intense symbolic computations and intermediate steps, thus, it could be very difficult to use numerical based packages, mainly MATLAB. Accordingly, as presented in this thesis, it could be helpful to use symbolic packages, i.e. Maple, which enhances the accuracy by increasing the number of terms truncated for the solution. Additionally, researchers who use the DNF method tend to make some system simplifications, mainly system reduction, in order to decrease the matrix sizes involved, this crucial step must be practised with much conscious and carefulness; because it can affect the results, while when using Maple software, it is possible to build a highly structured pattern that can be used for any degree-of-freedom and massive number of terms, hence, some analyst described this technique to lend itself to be used in symbolic programming packages [8]. More in-depth discussions of the DNF technique and its applications is revealed in the following subsection.

2.2.2 The method of direct normal forms

In the literature, starting by early Poincare's work, the application of normal forms for SDOF and MDOF is discussed; initially, Hamiltonian normal form (or Birkhoff normal form) technique was introduced in [24], where undamped unforced problem is considered, this work was followed by the first-order normal form technique [23], implemented firstly for nonlinear dynamic systems in [24], in this technique forced and damped systems are considered.

Because the majority of mechanical vibration applications are readily characterised by the second-order form, Neild and Wagg initially developed variant normal forms for second order dynamical problems in [8]; this method will be followed throughout the discussion and formulation of this work. Compared to previous techniques covered so far, the fundamental benefit of the DNF approach is that it can calculate harmonics without supposing particular harmonic components in trial solutions. This implies that no previous knowledge of the harmonic components of the system's response is necessary, nor is any extra complexity required when considering harmonics. In addition, the process of normal forms may be expressed in a matrix-based form, making its application to computer automation more suitable.

Several research projects addressing the nonlinear dynamics of mechanical systems use the direct normal forms approach. For example, Xin et al. [27] considered the SDOF nonlinear oscillators of polynomial-type nonlinearities using DNF technique. Their work involved investigation of velocities and displacements, while illustrating the contributions of the various polynomial nonlinearities in different forms to the system response by means of the resulting resonance response functions (denoted as RRFs). In addition, Shaw et al. examined the performance of the nonlinear vibration isolator using the DNF approach in [28]. The system was modelled as a SDOF oscillator with high orders of polynomial nonlinear components, and the authors generated a set of backbone curves for the nonlinear vibration isolator by taking into account the comparable conservative system. Furthermore, Cammarano et al. [29] examined the optimal load for the nonlinear energy harvester in the case of purely resistive loads. Their work was conducted both analytically and numerically, and they discovered that analytical results approximated using the DNF technique were very close to numerical results within the selected range of frequency.

The DNF method was also used to investigate the nonlinear dynamics of MDOF systems. In [30], the bifurcations of the backbone curves caused by the modal interaction are investigated by considering a 2-DOF oscillator with cubic nonlinearities. In addition, Hill et al. analysed the same system to introduce the *out-of-unison* resonance behaviour found in actual systems such as the taut cable. Then, in [32], the same authors highlighted how backbone curves derived using the normal form approach may assist the design and optimisation of weakly nonlinear systems with numerous degrees of freedom. The DNF approach has been used as the

primary method of analysis for estimating the dynamic response of the nonlinear systems investigated in this research.

Due to the fundamental nature of nonlinearities, the DNF approach is not restricted to nonlinear oscillators; many engineering applications in the real-life display sources of geometric, or even damping nonlinearities. Consequently, the direct normal form approach is used to examine nonlinear beams, cables, shells, plates, and multi-story structures; for a thorough discussion of several of these applications, refer to [8].

Another important application of nonlinearly coupled multi-degree-of-freedom system is the Touzé two-degree-of-freedom oscillator; a system of vertical-horizontal oscillator moves under the influence a harmonic forcing conditions. This system is early studied in detail by [45,46], and [47] introduced some advances for the effect of higher order terms on the dynamic behaviour of the system. In the present research, for verification purposes, the Touzé's system is studied in detail using DNF method, with the aid of Maple symbolic computation software, the results are then compared to corresponding results from the literature.

Due to the advances made in the field of computer packages software, accompanied with the more complex nature of arising nonlinear dynamical problems, many symbolic software started to appear, for instance, Mathematica, is one of these packages which was used in some applications in physics and engineering, like those mentioned in [25]. Maple software, which will be used for programming in this work, is a software package used mainly for symbolic computations, with many other applications. Maple was firstly introduced in 1982 by the University of Waterloo, in a funded project to build a powerful software for computational analysis, but it was not until 2005 that Maple became well-known for scientists all over the world, due to new graphical user interface and modified wizards.

To some extent, the implementation of Maple symbolic packages for solving nonlinear mathematical and physical problems can be found in the literature, and some textbooks were published considering this modern thinking, both for mathematical [37] and physical [38] applications. In addition, some works were specifically introduced to implement Maple analysis for nonlinear oscillations; in 1992 Wang and Huseyin [26] introduced

one of the earliest works in this field, where they produced two Maple programs for the application of the intrinsic harmonic balance method, one for autonomous and the other for nonautonomuos systems. Seven years later, X. Liu [40], in his PhD thesis, used Maple as the main program for introducing a complete analysis of nonlinear dynamical problems, where he illustrated methods of implementing symbolic computations for mathematical approximations of some nonlinear dynamical problems.

In the present study, a novel method of solving SDOF and MDOF nonlinear oscillators is introduced, using the nonlinear DNF method, with the aid of Maple symbolic software. Approximate analytical solutions for SDOF and MDOF with various types of nonlinearities is presented, furthermore, the implementation of this method for fractionally damped systems is discussed with some engineering applications; namely, the fractionally damped Duffing oscillator and the fractional Van-der-Pol oscillator.

When practising the method of DNF for SDOF and MDOF nonlinear oscillators with viscous damping and external forcing (usually harmonic, otherwise some special conversions to harmonic forcing are adopted, [89]), the analysis starts by applying the method for the undamped-unforced (or the conservative) case. Then, the forced system is considered, and compared to the conservative case. In fact, the solution of forced nonlinear systems using DNF method has some additional details regarding the nature of the forcing terms. Normally, it is desired to study the system under harmonic forcing, with forcing frequency to be either near resonance or away from resonance, step-by-step solution of the case of forced vibration can be seen in [8]. Specifically, one of the advantages of DNF is the flexibility of studying systems under variety of forcing and resonance conditions.

2.2.3 Numerical techniques

Given a mathematical dynamic model of a certain deterministic nonlinear system, numerical approaches may be direct techniques for determining its solutions. Since mathematical models for physical systems might be represented in a variety of ways, this thesis offers an overview of the techniques for solving nonlinear ordinary differential equations (ODEs), as this is the major approach used. Additionally, in Chapter 6 of this work, as a novel application to the method of DNF, it is used for investigating the dynamics of fractionally damped

nonlinear oscillators. In all of these aforementioned applications, it is vital to apply verifications of the resulted outcomes using numerical techniques, those are to be discussed in detail in this subsection.

Direct time-integration of the EOMs is one of the numerical methods for finding dynamic solutions. The fundamental benefit of this approach is its ease of use and availability; for instance, the ODE solvers included into MATLAB are useful tools, including solvers of explicit and implicit systems, refer to [51] for more in depth discussions regarding MATLAB solvers for numerous applications. Direct time-integration method may be used for both smooth and non-smooth systems[1], and it is not limited to any particular type of mathematical models. In addition, the time-integration technique may be used for modelling the transient dynamic responses of a system; these responses can then be processed to get solutions such as the steady-state response or frequency response functions (FRFs). As an example of this approach, Neild and Wagg used this method to verify their approximation findings of resonance curves in [53], where they determined the steady-state of a single-degree-of-freedom (DOF) Duffing oscillator. The apparent limitations of this approach, however, are also not to be overlooked. To provide just one example, in comparison to approximate analytical and numerical continuation techniques, applying direct time-integration techniques to the challenges of large-scale systems is very inefficient and time-consuming, [17]. Furthermore, for systems with mild damping, it may take a long time for such approaches to locate the steady-state or near steady-state solutions of the system. Moreover, using direct time-integration to the EOMs, and due to transient or numerical effects, it may be impossible to integrate the unstable steady-state solutions or even stable solutions but with weak attractions.

In the literature, the subject of uncertain nonlinear systems has been extensively investigated using a number of techniques, for instance, in [14], Manson and Worden proposed alternative techniques to the well-known Monte-Carlo approach for assessing parametric uncertainties effects to higher-order frequency response functions of SDOF systems. Furthermore, using Volterra series analytical approach, the same authors studied random vibrations of a Duffing oscillator in [15], and then obtained approximations to the coherence of this Duffing oscillator in [16]. When dealing with their details, and similar to other approximate analytical techniques, the aforementioned approaches are mathematically intense and time consuming.

[1] Generally speaking, if the system's equation of motion includes continuous nonlinear terms with no sudden changes in the type or magnitude of nonlinearity, then the system can be describes as smooth. On the other hand, non-smooth systems are resulted from severe nonlinearity sources, such as impacts, [52]. It is worth mentioning that some continuous nonlinearities can be non-smooth, this can be related to the presence of sharp edges in the graphical representation of the corresponding nonlinear term(s).

Numerical continuation is the alternative method, and it is tailored more for smooth nonlinear dynamic systems. Numerical continuation, also known as parameter continuation, is a conceptual modelling method of computing approximate numerical solutions of a system of parameterized nonlinear equations of motion, based on the fact that the manifold of points that assemble lines (in one-dimensional space), or planes (in two-dimensional space) represents the approximate solution to the nonlinear system, [17]. This indicates that the under-determined system's solution will undergo a similar, incremental shift if a single parameter of the EOMs is altered. Accordingly, when an initial solution point is provided in the parameter space, the solution corresponding to a little change in a studied parameter may be located in its near vicinity; this newly found solution can then be utilised to seek the next solution with still another small parameter change; etc. When trying to identify steady-state solutions, numerical continuation is more effective than direct time-integration methods. As an added bonus, this method may be used to track down unstable solutions.

Many programs now provide support for the theory of numerical continuation. Examples include AUTO-07p, which was first proposed by Doedel in [54] and can be accessed from [55]. MatCont is another example of numerical continuation packages, which was created by Dhooge et al. [56, 57] and is accessible in [58]. Moreover, COCO continuation package was introduced in [34] and can be accessed from [35]. Another well-known package is NNMcont, which was discussed in [59] by Peeters et al. and is accessible from [60].

Numerous continuation programs, like AUTO-07p, MatCont, and COCO, had their origins as tools for mathematicians. Their adaptability and scalability make them useful for modelling and analysing a wide variety of mechanical dynamic behaviours. In [64], for instance, AUTO-07p was used to perform an airplane's bifurcation analysis, an ostensibly useful task for designing airplanes. Furthermore, in [63], COCO was carefully modified to follow the location of the resonant response of an actual nonlinear oscillator setup, providing yet another example of the coordinated use of numerical continuation and other approaches for experimental testing.

Unlike other similar programs, NNMcont is tailored to calculating the reaction of nonlinear mechanical systems. In particular, this technique makes it possible to discover the periodic solution of analogous

conservative structures based on the nonlinear normal modes (NNMs) theory, [41], as opposed to calculating the forced and damped, i.e. non-conservative, response of the nonlinear mechanical systems. NNMcont is used in a wide variety of mechanical contexts. For instance, Kerschen et al. [42] used it to determine the NNMs of an airplane's airframe, while Renson et al. [61] used it to determine the NNMs of a satellite's structure, both in the aerospace industry.

Since the other three example numerical continuation algorithms are built in MATLAB, structural dynamists may be less acquainted with AUTO-07p and it may not be compatible with as many current software packages as the other two. In addition, both MatCont and NNMcont rely on a graphical user interface, which facilitates implementation but reduces customisation options for researchers. This thesis relies on the work of COCO, which has been used for comparison and verification purposes in this thesis. Nevertheless, MatCont is used for the numerical investigation of the frequency responses for oscillators that include both stiffness and damping nonlinear terms as will be discussed in Section 5.4. More in depth discussions regarding numerical continuation tools in MATLAB, specifically COCO in comparison to other tools can be found in [62].

2.3 Modal analysis

The idea behind modal analysis is that the system's output may be represented by a set of vibrational modes. Over the last decades, linear modal analysis has evolved and found widespread use in a variety of applications, including sub-structuring approaches [48] and structural health monitoring [49]. The overall response of a linear system may be written as the sum of the responses of its individual vibration modes since these modes are isolated from one another. Moreover, proportional damping is presumed between the masses in order to obtain meaningful response predictions. In fact, in modal analysis theory, the relevance of proportional damping will become apparent when recognised that a system with proportional damping will have exactly the same mode shapes to its counterparts that are undamped, [50]. Accordingly, vibration modes are governed solely by the system's mass, damping, and stiffness, as well as its structural features, such as boundary conditions. The system's degrees-of-freedom are equal to the number of its modes, for which the modal damping, natural frequency, and mode shape are all associated with each mode.

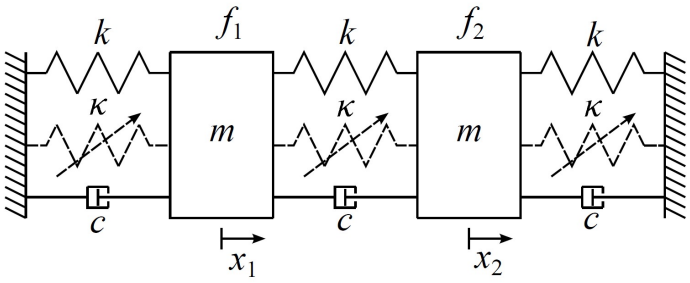

Figure 2.1: Schematic diagram of 2-DOF oscillator with lumped masses, m, linear stiffnesses k, linear damping c and nonlinear stiffness κ.

For instance, the linearised form of the 2-DOF oscillator system presented in Fig. 2.1 is described by the following equations of motion,

$$m\ddot{x}_1 + c\,(2\dot{x}_1 - \dot{x}_2) + k\,(2x_1 - x_2) = f_1 \tag{2.1a}$$

$$m\ddot{x}_2 + c\,(2\dot{x}_2 - \dot{x}_1) + k\,(2x_2 - x_1) = f_2 \tag{2.1b}$$

in this system, two modes of vibrations can be depicted, in which the two lumped masses will oscillate *in-phase* and *out-of-phase*. Thus, the mode shapes of this system are;

$$\phi_1^{\intercal} = [1 \quad 1] \tag{2.2a}$$

$$\phi_2^{\intercal} = [1 \quad -1] \tag{2.2b}$$

where ϕ_1 and ϕ_2 are the first and second mode shapes, respectively, and the superscript $\intercal$ denotes the matrix transpose. Now, using the modal transformation of $x \to q$, the equations of motion can be rearranged in terms of the natural frequencies, ω_{n1} and ω_{n2}, damping modal ratios, ζ_1 and ζ_2 and the modal forces f_{q1} and f_{q2} leading to the following perfectly decoupled EOMs,

$$\ddot{q}_1 + 2\zeta_1\omega_{n1}\dot{q}_1 + \omega_{n1}^2 q_1 = f_{q1} \tag{2.3a}$$

$$\ddot{q}_2 + 2\zeta_2\omega_{n2}\dot{q}_2 + \omega_{n2}^2 q_2 = f_{q2} \tag{2.3b}$$

where

$$\omega_{n1} = \frac{k}{m} \qquad \zeta_1 = \frac{c}{2\sqrt{mk}} \qquad f_{q1} = \frac{f_1 + f_2}{2m} \tag{2.4a}$$

$$\omega_{n2} = \frac{3k}{m} \qquad \zeta_2 = \frac{\sqrt{3}c}{2\sqrt{mk}} \qquad f_{q2} = \frac{f_1 - f_2}{2m} \tag{2.4b}$$

accordingly, two modes can be separately considered, this yields to the fact that the superposition principle can be applicable for the computations of the responses of the two lumped masses, which have the form;

$$x_1 = q_1 + q_2 \tag{2.5a}$$

$$x_2 = q_1 - q_2 \tag{2.5b}$$

Nonlinear normal modes (NNMs) theory is a viable option for analysing the modal behaviour of nonlinear structures. Firstly introduced by Rosenberg [84], NNMs were used in investigating the nonlinear dynamical systems and phenomena in several conducted researches, for instance in [66], Rand applied the concept of NNMs to obtain explicit approximate expressions for normal modal curves in nonlinear two DOF systems. Moreover, in [65] Manevich and Mikhlin used the idea of NNMs in the investigation of periodic solutions of nonlinear systems in a similar manner to normal vibrations with rectilinear trajectories. Additionally, in his PhD thesis, Vakakis performed a methodical overview at NNMs that were specified using conservative dynamical systems, refer to [67] for more details, this work was then expanded by Shaw and Pierre [68] to include non-conservative systems. Recently, one of the most current definitions of NNMs was provided in [41] by Kerschen et al.

A variety of NNMs definitions may be found in the literature. For instance, according to Rosenberg's definition, [84], a NNM occurs when all points in the system simultaneously experience their maximum and minimum values and go through zero. So, the displacement of one point may be utilised as a reference, and that point's displacement can characterise the displacements of the other locations. For instance, the EOMs of

the nonlinear two degree-of-freedom system seen in Fig. 2.1 may be represented as

$$m\ddot{x}_1 + k(2x_1 - x_2) + \kappa x_1^3 + \kappa(x_1 - x_2)^3 = 0 \tag{2.6a}$$

$$m\ddot{x}_2 + k(2x_2 - x_1) + \kappa x_2^3 + \kappa(x_2 - x_1)^3 = 0 \tag{2.6b}$$

Assuming the reference coordinate to be x_1, then x_2 can be written as

$$x_2 = \hat{x}_2(x_1) \tag{2.7}$$

where $\hat{x}_2$ denotes the modal curve of x_2, to proceed, it is convenient to differentiate Eq. 2.7 twice with respect to time, which gives

$$\ddot{x}_2 = \hat{x}_2''\dot{x}_1^2 + \hat{x}_2'\ddot{x}_1^2 \tag{2.8}$$

where differentiation with respect to x_1 is denoted by primes. It is possible to get $\hat{x}_2$ by replacing Eq. 2.7 and Eq. 2.8 by Eq. 2.6, and then removing time dependency, i.e. $\ddot{x}_1$ and $\dot{x}_1$. For more in-depth analysis, Kerschen et al. in [41] provides a comprehensive overview of the methods used to calculate NNMs. In contrast to other methods, the use of NNMs is not restricted to weakly nonlinear systems, which is perhaps its greatest benefit.

Modal analysis of nonlinear systems may also adopt the modal decomposition strategy. The nonlinear EOMs are broken down into a collection of linearly uncoupled but possibly nonlinearly coupled modes by using the linear mode shapes generated from the underlying linear structure of nonlinear systems. Using the linear mode shapes from Eq. 2.2, the nonlinear modal EOMs for the example system presented in Eq. 2.6 are

$$\ddot{q}_1 + \omega_{n_1}^2 q_1 + \frac{\kappa}{m}\left(q_1^3 + 3q_1q_2^2\right) = 0 \tag{2.9a}$$

$$\ddot{q}_2 + \omega_{n_2}^2 q_2 + \frac{\kappa}{m}\left(3q_1^2q_2 + 9q_2^3\right) = 0 \tag{2.9b}$$

With the inclusion of the linked nonlinear elements in Eq. 2.9, the modes may interact and are no longer completely independent of one another. That's why nonlinear systems can't benefit from the concept of superposition. Approximate solutions to Eq. 2.7 may be calculated using the normal form approach by applying a

sequence of transformations, [8] and the full derivation will be shown in Chapter 3. It is easier to handle modal interaction and modal superposition using the normal form approaches based on the modal decomposition approach than with NNMs, particularly for weakly nonlinear systems.

2.4 Damped backbone curves

A new novel approximative analytical method for estimating the damped backbone curves resulting from the introduction of viscous damping into the equation of motion is discussed in Chapter 4 of this thesis. Analysis of nonlinear systems has traditionally included studying the connection between the nonlinear frequency and the consequent vibration amplitudes. This may be achieved by estimating the system's conservative (undamped-unforced) backbone curves and comparing them to numerically calculated forced damped frequency responses. Although this method is very accurate for undamped and very mildly damped systems, increasing the damping decreases the correspondence between the conservative backbone curves and the forced damped frequency response curves. As a consequence, the precision of estimating the system's important properties, such as its bifurcation points, is diminished. In principle, this technique applies to both SDOF and MDOF systems and is based on a variation of Burton's method and normal forms technique.

Nonlinear oscillators are commonly used to represent SDOF and MDOF systems, among other real-world engineering applications. Typical examples of SDOF systems include single-mode approximations of structural components such as cables and beams, while MDOF systems have many applications depending on the type and complexity of the system under consideration. The presence of viscous damping and its effect on the dynamic behaviour of such nonlinear systems is a crucial aspect of these systems. In Section 4.4 of this thesis, a new approximative analytical method for estimating the damped backbone curves arising from the incorporation of viscous damping is presented.

Following the first study of Krack, [89], numerous works are published in the literature to calculate the damped backbone curves, often by adding a fictitious force to the equation of motion to produce an analogous system by discarding the term that involves viscous damping. In Section 4.4 of this thesis, the method presented can be applied directly in a similar way to the case of linear viscous damping, this leads to approximate

damped backbone curves expressions for nonlinear oscillators. The method is based on a variation of Wentzel, Kramers and Brilloun (WKB) method and Burton method [91], and can be directly applied to both SDOF and MDOF systems. In addition, the approach is extended to incorporate any order of polynomial nonlinear terms by using a normal form technique implemented symbolically through Maple software. Finally, some selected examples are provided to examine the dynamics of nonlinear SDOF and MDOF systems by analysing the resultant damped backbone curves.

2.5 Oscillators with combinations of stiffness and damping nonlinear terms

A wide class of oscillators can be modelled by a combination of stiffness and damping terms according to the following definition

$$\ddot{x}(t) + f\left(x(t), \dot{x}(t)\right) + g(x) = 0, \tag{2.10}$$

where the function $f\left(x(t), \dot{x}(t)\right)$ represents any combination of $x(t)$ and $\dot{x}(t)$; for instance, Van-der-Pol and Rayleigh oscillators are well known examples of such oscillators. Van-der-Pol oscillator represents the case when $f\left(x(t), \dot{x}(t)\right) = \mu\left(x^2(t) - 1\right)\dot{x}(t)$, and Rayleigh oscillator is obtained when $f\left(x(t), \dot{x}(t)\right) = \mu\left(\dot{x}^2(t) - 1\right)\dot{x}(t)$, moreover, some researchers studied the Van-der-Pol-Duffing oscillator in which a cubic stiffness term is added to the EOM; for instance, in [164] the authors investigate the steady-state response of the Van-der-Pol-Duffing oscillator used for weak signal detection applications. More complex systems involves the inclusion of higher order stiffness terms to the EOM, the cubic–quintic Duffing–van der Pol oscillator is one of these systems, it is studied in detail in [106] in which Homotopy, harmonic balance and multiple scales techniques are used to obtain analytical approximate and numerical solutions of the cubic–quintic Duffing–van der Pol equation with two-external periodic forcing terms.

In the case of Rayleigh oscillators more complex systems are also found in the literature; for instance, a cubic stiffness term is added to the equation of motion to model Rayleigh-Duffing oscillator, refer to [108–111, 114] for some of these researches. Nevertheless, the Rayleigh-Duffing oscillator can be considered as a special case of a system involving higher order stiffness terms, in specific the cubic and quintic powers of

$x(t)$, this system is studied in [112, 113]. In this thesis, this system is denoted as the "cubic-quintic Rayleigh oscillator" and it will be revisited in detail Subsection 5.4.5 in this work.

Direct normal forms method has been usually applied to systems with polynomial stiffness nonlinear terms such as the quadratic and cubic terms, and viscous damping is occasionally added to the system to model the damping effects. Nevertheless, according to the researcher best knowledge, the implementation of DNF for studying systems with combinations of stiffness and damping nonlinearities is limited to simple cases; for instance, in [8] DNF has been used to investigate the steady-state response of Van-der-Pol oscillator where frequency-amplitude and frequency-phase relations are obtained. In this work, DNF is used to explore the dynamics of Van-der-Pol, Rayleigh, and more complex systems involving high orders of nonlinear stiffness terms.

2.6 Oscillators with fractional order damping

In recent years, the development of fractional calculus in research has gained extensive attractions, and many publications have been proposed in this field; for instance, the interested reader is advised to visit [123, 124, 139–142]. In the field of engineering, fractional calculus has been strongly exercised for the modelling of many practical engineering applications, in which damping history is of interest for this thesis.

In the context of dynamics, fractional models enable researchers to easily represent the vibratory behaviour of elements that would require complex formulations, such as multi-element or hereditary models, this is related to the fact that fractional models can accurately reproduce the damping mechanisms using a small number of variables compared to other damping models found in the literature, [124–126].

From physical point of view, fractional damping models are specifically useful for modelling polymeric materials that exhibit some frequency dependence and arise naturally, for example, from specified Newtonian fluid movements, [127], or molecular theories that predict the behaviour of certain types of polymeric materials [128]. Indeed, fractional models are used to easily capture the viscoelastic nature of materials such as rubber or concrete [129], whose behaviour was previously modelled with a power law [130, 131], and it was

found that fractional operators can appear in the non-linear stress-strain relation of metals [132]. Moreover, viscoelastic constitutive models based on fractional derivatives have been proposed to reproduce the time dependent behaviour of real materials [133–138].

Considering the Duffing oscillator with fractional damping, driven by harmonic force of non-resonant type. In Chapter 6 of this thesis, it is required to get direct normal form frequency response for the system.

$$\ddot{x}(t) + 2\varepsilon\zeta\omega_n \mathrm{D}^{\beta}x(t) + \omega_n^2 x(t) + \varepsilon\alpha x^3(t) = \varepsilon R\cos(\Omega t) \tag{2.11}$$

where $x(t)$ denotes the displacement of the oscillator, ω_n is the natural frequency of the system and ζ is the viscous damping ratio. Moreover, $\mathrm{D}^{\beta}x(t)$ denotes the fractional damping of the system with β being the order of the fractional order of the system, where $(0 < \beta < 1)$, and when $\beta = 1$ then the system is viscously damped. Additionally, R and Ω appears in the right-hand-side of the equation represent the forcing amplitude and forcing frequency, respectively. Finally, ε is a bookkeeping parameter which is assumed to be unity through out this work.

In order to verify the precision of the approximate analytical frequency response computed, it is important to generate numerical solutions of the oscillator EOM, Eq. 2.11. In the literature, some numerical methods to solve fractional order differential equations can be found. For instance, Roberto Garrappa et al. have produced a series of publications dealing with the numerical approximations of fractional differential equations by means of predictor–corrector algorithms and trapezoidal rules, [146–149], and they have generated several MATLAB codes for various cases according to the system being considered; this includes, for instance, FDE routines which are, in principle, similar to the well-known ODE routines available in MATLAB, refer to [150, 151] for more details regarding FDE routines and their use. Nevertheless, the predictor-corrector algorithms were primarily used by Diethelm et al. in [152, 153], in which they presented multiple numerical algorithms for the numeration of fractional-order calculus, their work included computations of Caputo and Riemann–Liouville definitions as well.

Another well-known numerical technique used for fractional-order differential equations is the Grünwald-Letnikov's definition, [124, 154, 155], based on the backward difference generalisation of the fractional derivative. This definition was applied in [156] for developing discrete-time state-space equivalent model of a continuous linear time invariant (LTI) System, in addition, a MATLAB toolbox has been generated for simulating and analysing these LTI systems, refer to [157, 158]. Moreover, Grünwald-Letnikov's definition was used to obtain numerical solutions to the fractionally damped Duffing oscillator, and the fractional-order Van-der-Pol Duffing oscillator in [160, 161], respectively. In this work, Grünwald-Letnikov's definition is used for the numerical solutions for fractional Duffing oscillator in Eq. 2.11.

Moreover, in Chapter 6, it is required to get DNF solution of the Van-der-Pol oscillator with fractional order damping, driven by harmonic force of non-resonant type. As discussed in Section 2.5, Van-der-Pol oscillator is well-known example of non-conservative oscillators with nonlinear damping, and the nonlinearity evolves with time as briefly discussed in [163]. Additionally, Van-der-Pol oscillators have many real-life applications in the fields of physics, electronics, biology, neurology, sociology and economics, some of these applications can be found in [164].

Herein, the fractionally damped Van-der-Pol oscillator is specifically addressed, to some extent, this type of oscillators is studied in the literature both numerically and analytically using different techniques. For instance, as one of the earliest works for such types of oscillators, Barbosa et al. investigated the dynamics of the unforced fractional order Van-der-Pol oscillator using various numerical techniques in [165], after few years the same authors introduced a modified version of that work using the same techniques for which the fractional-order time derivatives were involved in the state-space model, [166].

Approximate analytical techniques were also implemented to investigate fractional-order Van-der-Pol oscillators; for instance, higher order angular frequency and the period approximations of the fractionally damped Van-der-Pol oscillator are introduced using the residue harmonic balance in [169]. In a more recent work, Chen et al. investigated the primary resonance amplitude-frequency response equation for this oscillator using the method of harmonic balance, and based on Lyapunov theory, [123, 124, 139], they have been able to apply

stability condition for the steady-state solutions obtained, refer to [168] for more details regarding this work. Finally, homotopy perturbation methods are also used by some researchers to investigate this type of oscillators; a general heuristic review of the homotopy perturbation methods for non-conservative oscillators is recently introduced by Chun-Hui He and El-Dib, [170]. More specifically, the homotopy perturbation method has been used to explore the approximate solution of the fractionally damped Van-der-Pol oscillator for which the fractional derivative is described using Caputo's definition, [167].

Based on the aforementioned, and according to the authors best knowledge, the DNF method has never been used to study non-conservative fractionally damped nonlinear oscillators, thus, in Chapter 6, a novel implementation of the DNF method to explore the dynamics of Van-der-Pol oscillators with fractional damping term is introduced, amplitude-frequency and phase-frequency relationships are to be generated. Where relevant, for verification purposes, the results are to be compared to both numerical solutions and previous works found in the literature.

2.7 Summary

To comprehend nonlinearity in mechanical systems, it is necessary to determine the response solutions of nonlinear systems. Therefore, in Section 2.2, numerical and analytical techniques for finding the solutions of mathematical models of nonlinear systems were explored. The primary advantage of the numerical approach is that it is not limited by the complexity of nonlinear systems; however, one of its disadvantages is that the numerical results alone can only provide limited insight into the explicit relationships between the physical properties and dynamic behaviour of systems. This numerical disadvantage may be remedied using analytical approaches. However, the top limit of the use of analytical methods is not known beforehand, which may be overcame by confirming the analytical findings with numerical ones. The direct normal form method is selected to research nonlinear behaviour in this thesis due to the capability of being used in symbolic programming algorithms in which Maple symbolic software is used for modifying the method to be applicable in more complicated engineering applications.

According to the discussions in this Chapter, the following main findings are seen;

- For SDOF systems, the method of DNF is normally used in the literature to systems with low orders of polynomial nonlinearities, regularly quadratic and cubic, in Section 5.1-Section 5.3 of the thesis, the applicability of this method is generalised to study any order of polynomial nonlinear terms.

- For oscillators with combinations of stiffness nonlinear and damping terms, such as Van-der-Pol, Rayleigh, etc., DNF method has not been used to in the literature for system analysis (except for Van-der-Pol oscillator in [8]), thus, in Section 5.4 of this thesis the analysis is extended to include these systems.

- According to the researcher best knowledge, the accuracy of the DNF technique in the literature is limited to ε^1 and ε^2 expansions, in Section 4.2-Section 4.3 a novel improvement is introduced by raising the accuracy of the DNF method to any desired expansion, ε^n.

- For viscously damped nonlinear SDOF oscillators, the usual in literature analysis is normally based on generating analytical expressions of the backbone curves, those can be compared to the numerically computed frequency response function, in Section 4.4 of this thesis a novel proposed technique describes the inclusion of the damping term to the backbone curves, which results in the damped backbone curves.

- For fractionally damped SDOF nonlinear oscillators, which have never been analysed using the method of DNF, Chapter 6 introduces a modified technique that enables the researcher effectively study these types of oscillators, comparisons with numerical solutions and other methods found in the literature are then introduced.

- For MDOF systems, DNF method has been used to some extent in the literature, in Section 7.3 of this thesis a 2-DOF oscillator with cubic and quintic nonlinearities is investigated, and according to the author's best knowledge, this system has never been analysed using the method of DNF.

Chapter 3

Nonlinear systems analysis using direct normal form method

In this Chapter, a brief step-by-step problem solving using DNF method is discussed, the first part of this Chapter shows the direct normal forms technique detailed procedure, further analysis for using this technique with more examples of SDOF and MDOF is found in [8]. In this work, the main purpose is to extend the analysis to more complex systems. Next part is the problem of a SDOF unforced, undamped nonlinear oscillator, with two different powers of geometric type nonlinearities, these powers can be changed to make quadratic-cubic, quadratic-quintic (to the power of 5), quadratic-septuple (to the power of 7), cubic-quintic, or any other configuration provided that at least one of the two powers is odd according to the energy analysis of system stability [8].

3.1 DNF procedure for conservative systems

Considering a general unforced, nonlinear, N-degree-of-freedom mechanical system, a general form of the equation of motion can be written as

$$\mathbf{M}\ddot{\mathbf{x}} + \mathbf{K}\mathbf{x} + \varepsilon \mathbf{N}_x(\mathbf{x}) = 0, \tag{3.1}$$

where $\mathbf{x}$ is an $\{N \times 1\}$ vector of physical displacements, $\boldsymbol{M}$ and $\boldsymbol{K}$ are $\{N \times N\}$ matrices of mass and linear stiffness respectively, $\mathbf{N}_x(\mathbf{x})$ is an $\{N \times 1\}$ vector of stiffness related nonlinear terms and ε is used to denote smallness of the nonlinear terms. It is worth mentioning that, for the DNF technique to be properly applied, an assumption that the nonlinear terms are able to be expressed in polynomial forms in terms of x is adopted. This assumption could be trivial for polynomial stiffness nonlinear terms, i.e. quadratic, cubic, etc., but for different types of nonlinearities the fulfilment of this assumption can be more difficult, for instance, refer to the DNF analysis of fractionally damped nonlinear oscillator, Chapter 6, specifically Eq. 6.19 and the discussions therein.

In order to decouple the linearly coupled terms, the initial step of the direct normal form procedure is the linear modal transform, which is expressed as

$$\mathbf{x} = \Phi\mathbf{q}, \tag{3.2}$$

and the resulting equation of motion in modal coordinates is

$$\ddot{\mathbf{q}} + \Lambda\mathbf{q} + \varepsilon\mathbf{N}_q(\mathbf{q}) = 0, \tag{3.3}$$

where $\mathbf{q}$ is $\{N \times 1\}$ vector of linear modal displacement and Φ is an $\{N \times N\}$ matrix of linear mode shape matrix, and Λ is an $\{N \times N\}$ diagonal matrix of the square of natural frequencies, which can be found from the eigenvalues problem $\Phi\Lambda = \mathbf{M}^{-1}\mathbf{K}\Phi$ provided that Φ is mass normalised. Then, the nonlinear terms vector becomes

$$\varepsilon\mathbf{N}_q(\mathbf{q}) = \varepsilon\Phi^{-1}\mathbf{M}^{-1}\mathbf{N}_x(\Phi\mathbf{q}), \tag{3.4}$$

The following step of the direct normal form technique is the nonlinear near-identity transformation, i.e.

$$\mathbf{q} = \mathbf{u} + \varepsilon\mathbf{H}(\mathbf{u}), \tag{3.5}$$

which results in a resonant equation of motion, written as

$$\ddot{\mathbf{u}} + \Lambda\mathbf{u} + \varepsilon\mathbf{N}_u(\mathbf{u}) = 0, \tag{3.6}$$

where $\mathbf{u}$ and $\mathbf{H}(\mathbf{u})$ are the fundamental and harmonic components of $\mathbf{q}$ respectively, and $\mathbf{N}_u(\mathbf{u})$ is an $\{N \times 1\}$ vector of resonant nonlinear terms.

To determine the resonant nonlinear terms, the vectors $\mathbf{N}_u(\mathbf{u})$ and $\mathbf{H}(\mathbf{u})$ are expressed in a series form as,

$$\varepsilon \mathbf{N}_u(\mathbf{u}) = \varepsilon \mathbf{n}_1(\mathbf{u}) + \varepsilon^2 \mathbf{n}_2(\mathbf{u}) + \ldots \tag{3.7a}$$

$$\varepsilon \mathbf{H}(\mathbf{u}) = \varepsilon \mathbf{h}_1(\mathbf{u}) + \varepsilon^2 \mathbf{h}_2(\mathbf{u}) + \ldots, \tag{3.7b}$$

where $\mathbf{n}_1(\mathbf{u})$ and $\mathbf{n}_2(\mathbf{u})$ are given in Eq. 3.12, and $\mathbf{N}_q(\mathbf{q})$ is expanded in a Taylor series about the equilibrium $q = u$, which can be written as

$$\varepsilon \mathbf{N}_q(\mathbf{q}) = \varepsilon \mathbf{N}_q(\mathbf{u}) + \varepsilon^2 \frac{\partial}{\partial \mathbf{u}} \mathbf{N}_q(\mathbf{u}) \mathbf{H}(\mathbf{u}) + \ldots, \tag{3.8}$$

Additionally, a frequency detuning expression is introduced, based on the fact that the response frequencies of nonlinear systems are often distinct from their natural frequencies, [8, 99], written as,

$$\Lambda = \Gamma + \varepsilon \Delta, \tag{3.9}$$

where Γ is an $\{N \times N\}$ diagonal matrix of square of resonant frequencies, and $\Delta = \Lambda - \Gamma$. Now, substituting Eq. 3.7-Eq. 3.9 into Eq. 3.3 to compare with Eq. 3.6 gives,

$$\begin{aligned} &\varepsilon \frac{\mathrm{d}^2}{\mathrm{d}t^2} \mathbf{h}_{(1)}(\mathbf{u}) + \varepsilon^2 \frac{\mathrm{d}^2}{\mathrm{d}t^2} \mathbf{h}_{(2)}(\mathbf{u}) + \varepsilon \Gamma \mathbf{h}_{(1)}(\mathbf{u}) + \varepsilon^2 \Delta \mathbf{h}_{(1)}(\mathbf{u}) + \varepsilon^2 \Lambda \mathbf{h}_{(2)}(\mathbf{u}) + \\ &\varepsilon^2 \frac{\partial}{\partial \mathbf{u}} \mathbf{N}_q(\mathbf{u}) \mathbf{h}_{(1)}(\mathbf{u}) + \ldots = \varepsilon \mathbf{N}_{u(1)}(\mathbf{u}) + \varepsilon^2 \mathbf{N}_{u(2)}(\mathbf{u}) \end{aligned} \tag{3.10}$$

this leads to expressions that must be balanced in the following order

$$\varepsilon^1 : \frac{\mathrm{d}^2}{\mathrm{d}t^2} \mathbf{h}_1 \mathbf{u} + \Gamma \mathbf{h}_1 \mathbf{u} + \mathbf{n}_1 \mathbf{u} = \mathbf{n}_{u(1)}(\mathbf{u}) \tag{3.11a}$$

$$\varepsilon^2 : \frac{\mathrm{d}^2}{\mathrm{d}t^2} \mathbf{h}_2 \mathbf{u} + \Gamma \mathbf{h}_2 \mathbf{u} + \mathbf{n}_2 \mathbf{u} = \mathbf{n}_{u(2)}(\mathbf{u}) \tag{3.11b}$$

where,

$$\mathbf{n}_1(\mathbf{u}) = \mathbf{N}_q(\mathbf{u}) \tag{3.12a}$$

$$\mathbf{n}_2(\mathbf{u}) = (\Lambda - \Gamma)\mathbf{h}_1(\mathbf{u}) + \frac{\partial}{\partial \mathbf{u}}\mathbf{N}_q(\mathbf{u})\mathbf{h}_1(\mathbf{u}) \tag{3.12b}$$

Here, an assumed solution of the form

$$u_n = u_{pn} + u_{mn} = \left(\frac{U_n}{2}\mathrm{e}^{-\,\mathbf{i}\phi_n}\right)\mathrm{e}^{\,\mathbf{i}\omega_{rn}t} + \left(\frac{U_n}{2}\mathrm{e}^{\,\mathbf{i}\phi_n}\right)\mathrm{e}^{-\,\mathbf{i}\omega_{rn}t}, \tag{3.13}$$

is adopted, where $n = 1, \ldots, N$, moreover, U_n, ϕ_n and ω_n are the displacement amplitude, phase lag, and response frequency of the n^{th} mode, respectively. Substituting Eq. 3.13, the vectors $\mathbf{n}_{(j)}$, $\mathbf{n}_{(j)}$ and $\mathbf{n}_{u(j)}$ may all be expressed in terms of a $\{\Im_j \times 1\}$ vector of nonlinear terms in the original problem, i.e., in $\mathbf{n}_{(j)}$. For example, if $\mathbf{n}_{(j)} = \left[n_{(j)}\right]\mathbf{u}^*_{(j)}$ is defined, then by mirroring this structure, $\mathbf{h}_{(j)} = \left[h_{(j)}\right]\mathbf{u}^*_{(j)}$ and $\mathbf{n}_{u(j)} = \left[n_{u(j)}\right]\mathbf{u}^*_{(j)}$ are obtained, where $[\,]$ denotes a $\{N \times \Im_j\}$ coefficient matrix. For the case of polynomial nonlinear terms under consideration, then the elements in $\mathbf{u}^*_{(j)}$ may be written as

$$u^*_{(j)\ell} = \prod_{n=1}^{N} u_{pn}^{s_{pj,\ell,n}} u_{mn}^{s_{mj,\ell,n}} \tag{3.14}$$

where $s_{pj,\ell,n}$ and $s_{mj,\ell,n}$ are exponents of u_{pn} and u_{mn} in any element of $\mathbf{u}^*_{(j)}$ respectively. In order to identify the resonant nonlinear terms retained in $\mathbf{n}_{u(j)}$from $\mathbf{n}_{(j)}$, $\beta_{(j)}$, is introduced, i.e.

$$\beta_{(j)n,\ell} = \left[\sum_{n=1}^{N}\left(s_{pj,\ell,n} - s_{mj,\ell,n}\right)\omega_{rn}\right]^2 - \omega_{rn}^2 \tag{3.15}$$

accompanied with the corresponding criteria that

$$\text{Non-resonant:} \quad \beta_{(j)n,\ell} \neq 0, \left[n_{u(j)}\right]_{n,\ell} = 0, \left[h_{(j)}\right]_{n,\ell} = \frac{\left[n_{(j)}\right]_{n,\ell}}{\beta_{(j)n,\ell}}, \tag{3.16a}$$

$$\text{Resonant:} \quad \beta_{(j)n,\ell} = 0, \left[n_{u(j)}\right]_{n,\ell} = \left[n_{(j)}\right]_{n,\ell}, \left[h_{(j)}\right]_{n,\ell} = 0 \tag{3.16b}$$

Once the resonant nonlinear terms are determined to a specific accuracy level, i.e., ε^j, with the substitutions of Eq. 3.13, Eq. 3.6 can be written in the form,

$$\chi_n \mathrm{e}^{\,\mathbf{i}\omega_{rn}t} + \tilde{\chi}_n \mathrm{e}^{-\,\mathbf{i}\omega_{rn}t} = 0, \tag{3.17}$$

where χ_n and $\tilde{\chi}_n$ are time-independent complex conjugates and, finally setting $\chi_n = 0$ leads to the backbone curve expressions. Practically, it can be feasible to employ normal form analysis to build codes for SDOF and MDOF oscillators using Maple software, which enables symbolic calculations to be carried out with greater precision and involving more complicated system analysis.

3.2 DNF procedure for forced damped systems

In this section, the analysis is extended to systems under the excitation of harmonic forcing and viscous damping. For convenience, only the main steps are to be discussed in this work, however, the complete detailed analysis of these types of systems using direct normal forms is briefly mentioned in [8]. Considering a general harmonically forced, viscously damped, nonlinear and N-degree-of-freedom mechanical system, whose equation of motion may be written as

$$\mathbf{M}\ddot{\mathbf{x}} + \mathbf{C}\dot{\mathbf{x}} + \mathbf{K}\mathbf{x} + \Upsilon(\mathbf{x}, \dot{\mathbf{x}}, \mathbf{r}) = \mathbf{P}_x \mathbf{r}, \tag{3.18}$$

where the amplitude of the forcing term is denoted by $\mathbf{P}_x$, and $\mathbf{r}$ is the vector of forcing term which can be written as $\mathbf{r} = \{r_p, r_m\}^\intercal = \{\mathrm{e}^{\,\mathbf{i}\Omega t}, \mathrm{e}^{-\,\mathbf{i}\Omega t}\}^\intercal$ where the forcing frequency is denoted as Ω. From Eq. 3.18 it can be seen that all nonlinear terms are gathered in one term, $\Upsilon(\mathbf{x}, \dot{\mathbf{x}}, \mathbf{r})$. Here it should be noticed that both damping term and nonlinear term are assumed to be small compared to the linear stiffness, hence, more conveniently Eq. 3.18 can be rewritten as

$$\mathbf{M}\ddot{\mathbf{x}} + \mathbf{K}\mathbf{x} + \overline{\Upsilon}(\mathbf{x}, \dot{\mathbf{x}}, \mathbf{r}) = \mathbf{P}_x \mathbf{r}, \tag{3.19}$$

where $\overline{\Upsilon}(\mathbf{x}, \dot{\mathbf{x}}, \mathbf{r}) = \Upsilon(\mathbf{x}, \dot{\mathbf{x}}, \mathbf{r}) + \mathbf{C}\dot{\mathbf{x}}(t)$. Now, the application of direct normal forms begins, similar to the case of unforced equation, by writing Eq. 3.19 in its linear modal normal form, using the transformation $\mathbf{x} \to \mathbf{q}$, simply

by applying $\mathbf{x} = \Phi\mathbf{q}$, with some matrix manipulation Eq. 3.19 becomes

$$\ddot{\mathbf{q}} + \Lambda\mathbf{q} + \mathbf{N}_\mathbf{q}(\mathbf{q}, \dot{\mathbf{q}}, \mathbf{r}) = \mathbf{P}_q\mathbf{r}, \tag{3.20}$$

where $\mathbf{N}_\mathbf{q}(\mathbf{x}, \dot{\mathbf{x}}, \mathbf{r}) = (\Phi^\intercal\mathbf{M}\Phi)^{-1}\Phi^\intercal\overline{\Upsilon}(\Phi\mathbf{q}, \Phi\dot{\mathbf{q}}, \mathbf{r})$ and $\mathbf{P}_q = (\Phi^\intercal\mathbf{M}\Phi)^{-1}\Phi^\intercal\mathbf{P}_x$.

Next step is to apply the forcing transformation in order to remove the non-resonant forcing terms, and this can be achieved using an additional transformation, $\mathbf{q} \to \mathbf{v}$; where for the system with N degrees-of-freedom, it is possible to introduce $\mathbf{e}$ of $\{N \times 2\}$ and the transformation becomes $\mathbf{q} = \mathbf{v} + \mathbf{e}\mathbf{r}$. Now, substituting in Eq. 3.20, and rearranging the dynamic equation, one shall find

$$\ddot{\mathbf{v}} + \Lambda\mathbf{v} + \mathbf{N}_\mathbf{v}(\mathbf{v}, \dot{\mathbf{v}}, \mathbf{r}) = \mathbf{P}_v\mathbf{r}, \tag{3.21}$$

where the nonlinear forcing vector is transformed using

$$\mathbf{N}_\mathbf{v}(\mathbf{v}, \dot{\mathbf{v}}, \mathbf{r}) = \mathbf{N}_\mathbf{q}(\mathbf{v} + \mathbf{e}\mathbf{r}, \dot{\mathbf{v}} + \mathbf{e}\mathbf{W}\mathbf{r}, \mathbf{r}) \tag{3.22}$$

where $W = \begin{bmatrix} \mathbf{i}\Omega & 0 \\ 0 & -\mathbf{i}\Omega \end{bmatrix}$.

The transformed matrix $\mathbf{e}$ is found element by element, depending on the type of forcing frequency Ω, according to the following criteria

- For near-resonant forcing ($\Omega \approx \omega_{nk}$), then

$$e_{k,1} = \frac{P_{q,k,1}}{\omega_{nk}^2 - \Omega^2}, \quad e_{k,2} = \frac{P_{q,k,2}}{\omega_{nk}^2 - \Omega^2}, \quad P_{v,k,1} = 0, \quad P_{v,k,2} = 0, \tag{3.23}$$

- For non-resonant forcing ($\Omega \neq \omega_{nk}$), then

$$e_{k,1} = 0, \quad e_{k,2} = 0, \quad P_{v,k,1} = P_{q,k,1}, \quad P_{v,k,2} = P_{q,k,2}, \tag{3.24}$$

To proceed with the analysis, it is convenient to recall the analysis of unforced case; where similar solution is to be followed, i.e. Eq. 3.6 to Eq. 3.13, except for adding the extra transformation $\mathbf{v} \to \mathbf{u}$. Additionally, $\mathbf{u}^*$

matrix is found element by element using the relation

$$u_{\ell}^{*} = r_{p}^{m_{p\ell}} r_{m}^{m_{m\ell}} \prod_{k=1}^{N} u_{pk}^{s_{pk,\ell}} u_{mk}^{s_{mk,\ell}} \tag{3.25}$$

where $m_{p\ell}$ and $m_{m\ell}$ are power indices of r_p and r_m, respectively.

Furthermore, in order to find $\boldsymbol{\beta}^{*}$ matrix, Eq. 3.15 in the unforced case shall be modified, and it can be found for the forced vibration element by element using the relation

$$\beta_{k,\ell} = \left[\left(m_{p\ell} - m_{m\ell} \right) \Omega + \sum_{n=1}^{N} \left[\left(s_{pj,\ell,n} - s_{mj,\ell,n} \right) \omega_{rn} \right] \right]^{2} - \omega_{rk}^{2} \tag{3.26}$$

Finally, same procedure as the case of unforced vibration is followed to get the solutions of the forced vibration equations. The following algorithm demonstrates the full symbolic implementation of the DNF technique. Moreover, the symbolic implementation of the DNF method is described in detail in Fig. 3.1.

Algorithm: ε^1-order DNF technique using symbolic computations

Inputs: Mass matrix M, Linear stiffness matrix K, nonlinear and linear damping vector N_x, forcing amplitude matrix P_x and forcing frequency Ω.

Outputs: Displacement response x, backbone curves.

Procedure:

- **Linear modal transformation**

  1. Calculate linear natural frequencies, Γ, and mode shapes Φ.

  2. Calculate nonlinear and linear damping terms vector N_x and forcing amplitudes P_q.

- **Forcing transformation**

  3. Determine resonant forcing amplitudes P_v.

  4. Calculate the forcing transform matrix e (if exists).

  5. Calculate nonlinear and linear damping terms after forcing transformation N_v.

- **Nonlinear near identity transformation (symbolically)**

  6. **Loop #1**: perform a loop over DOF, substitute $x's$ and their derivatives by corresponding u_p and u_m components (using several if clauses inside the loop).

  7. For each equation in N_v, calculate the number of terms (as vector) then convert to set, and then find the total number of terms for the whole system (unite all terms for all equations and convert to vector again.

  8. **Loop #2 (nested):** the outer loop over the DOF, and the inner loop over terms number in each equation, determine the nonlinear and linear damping coefficients, and corresponding unique combination of variables u^* (using if clauses and coefficients commands).

  9. **Loop #3 (nested):** calculating n^* matrix for the whole system.

  10. **Loop #4 (nested):** calculating power indexes s_p and s_m for u^* (whole system) and placing them in Table (or matrix) form.

  11. **Check:** multiply n^* by u^* and subtract initial equations, zeros must be obtained.

  12. **Loop #5 (nested):** Forming β matrix, for to DOF and then to the total number of terms, use corresponding β equation.

  13. **Loop #6 (nested):** Calculate coefficients of resonant terms n_u^*, and of harmonic terms h^*.

  14. Calculate the resonant nonlinear and linear damping terms by multiplying n_u^* by u^*.

- **Finding backbone curves and inverse transformation to find x.**

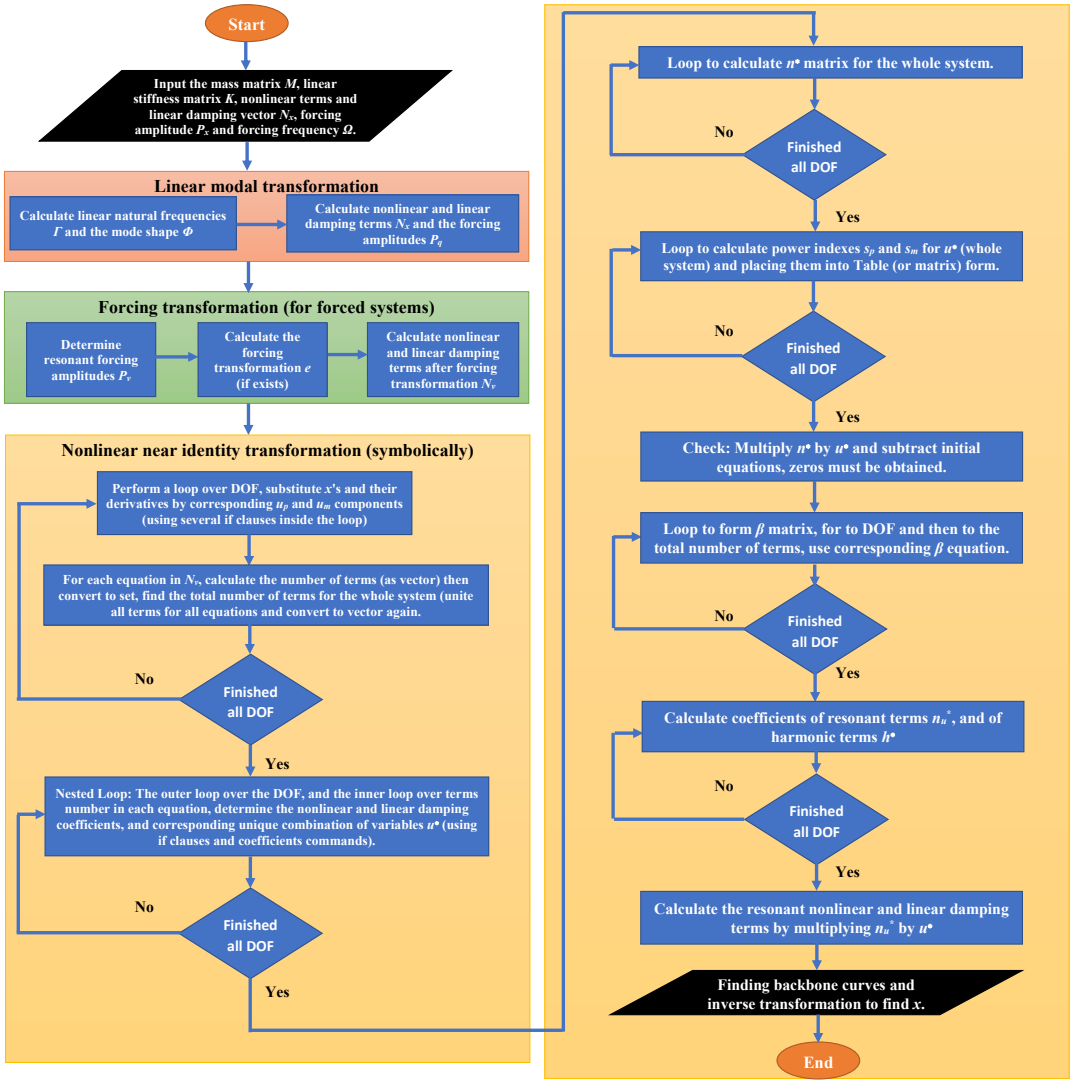

Figure 3.1: Flow chart for the symbolic implementation of the DNF method, truncated to ε^1 accuracy, same procedure with more algebraically intense mathematical steps can be followed to apply the method for higher ε accuracies, refer to Section 4.1 and Section 4.2.

3.3 Stability of the steady-state solution

In this subsection, the stability of the assumed direct normal form steady-state solution is discussed using a method that was firstly used in [27] and then it was rederived in [82]. The stability analysis to be followed is based on considering a perturbation technique about the steady-state solution, and then the stability of the solution is determined by examining the stability of the perturbation. Considering the i^{th} mode of deviation

about the steady-state solution, and denoting the nonlinear amplitude and the phase difference to be U_i and ϕ_i, respectively, then, the assumed solution can be written as

$$u_i = U_{pi}(\varepsilon t)\mathrm{e}^{\,\mathbf{i}\omega_{ri}t} + U_{mi}(\varepsilon t)\mathrm{e}^{-\,\mathbf{i}\omega_{ri}t} = \left[\frac{U_i(\varepsilon t)}{2}\mathrm{e}^{-\,\mathbf{i}\phi_i(\varepsilon t)}\right]\mathrm{e}^{\,\mathbf{i}\omega_{ri}t} + \left[\frac{U_i(\varepsilon t)}{2}\mathrm{e}^{\,\mathbf{i}\phi_i(\varepsilon t)}\right]\mathrm{e}^{-\,\mathbf{i}\omega_{ri}t} \tag{3.27}$$

herein, both the amplitude and the phase difference U_i and ϕ_i are varying with time but with small values, that is why ε is used to denote the smallness of these variations. Accordingly, neglecting higher order accuracies, the time-derivatives of the assumed solution is given by

$$\dot{u}_i(t) = \mathbf{i}\omega_{ri}\left(U_{pi}\mathrm{e}^{\,\mathbf{i}\omega_{ri}t} - U_{mi}\mathrm{e}^{-\,\mathbf{i}\omega_{ri}t}\right) \tag{3.28a}$$

$$\ddot{u}_i(t) = -\omega_{ri}^2 u_i + 2\,\mathbf{i}\varepsilon\omega_{ri}\left(U'_{pi}\mathrm{e}^{\,\mathbf{i}\omega_{ri}t} - U'_{mi}\mathrm{e}^{-\,\mathbf{i}\omega_{ri}t}\right) \tag{3.28b}$$

where the prime denotes the derivative with respect to (εt), thus

$$U'_{pi} = \frac{\mathrm{d}U_{pi}}{d(\varepsilon t)} \tag{3.29a}$$

$$U'_{mi} = \frac{\mathrm{d}U_{mi}}{d(\varepsilon t)} \tag{3.29b}$$

In Eq. 3.28, the term $\dot{u}_i$ is truncated to ε^1 order since the the terms related to velocity (or first derivative) are only appearing in nonlinear and damping terms which are all of ε^1 accuracy. However, the terms representing the acceleration, or the second derivative, are considered to be of ε^0 order, hence $\ddot{u}_i$ is to be truncated to ε^2. Accordingly, the complete expressions with their substitutions are truncated to ε^2 accuracy. Substituting Eq. 3.27 and Eq. 3.29 into the i^{th} resonant equation, the equation of motion, in its general form becomes

$$\begin{aligned}&\left[2\,\mathbf{i}\omega_{ri}U'_{pi} + \left(\omega_{ni}^2 - \omega_{ri}^2\right)U_{pi} + N_{ui}^{+} - P_{ui}\right]\mathrm{e}^{\,\mathbf{i}\omega_{ri}t} + \\ &\left[-2\,\mathbf{i}\omega_{ri}U'_{mi} + \left(\omega_{ni}^2 - \omega_{ri}^2\right)U_{mi} + N_{ui}^{-} - P_{ui}\right]\mathrm{e}^{-\,\mathbf{i}\omega_{ri}t} = 0,\end{aligned} \tag{3.30}$$

where the complex conjugate N_{ui}^{+} and N_{ui}^{-} are those obtained from N_{ui} in the same manner as those from Eq. 3.7a. To satisfy Eq. 3.30, the contents of the square brackets must be equated to zeros, such that

$$U'_{pi} = \frac{+\mathbf{i}}{2\omega_{ri}}\left[\left(\omega_{ni}^2 - \omega_{ri}^2\right)U_{pi} + N_{ui}^{+} - P_{ui}\right], \tag{3.31a}$$

$$U'_{mi} = \frac{-\mathbf{i}}{2\omega_{ri}}\left[\left(\omega_{ni}^2 - \omega_{ri}^2\right)U_{mi} + N_{ui}^{+} - P_{ui}\right] \tag{3.31b}$$

Now, introducing a vector of amplitude and phase components, written as $\mathbf{U}$, such that

$$\mathbf{U} = \begin{Bmatrix} U_{p1} & U_{m1} & U_{p2} & U_{m2} & \dots & U_{pN} & U_{mN} \end{Bmatrix}^{\mathsf{T}} \tag{3.32}$$

thus

$$\mathbf{U}' = \begin{Bmatrix} U'_{p1} & U'_{m1} & U'_{p2} & U'_{m2} & \dots & U'_{pN} & U'_{mN} \end{Bmatrix}^{\mathsf{T}} = \mathbf{f}(\mathbf{U}) \tag{3.33}$$

Accordingly, the initial definition of the solution will slightly deviate from the steady-state solution, and thus it can be written as

$$\mathbf{U} = \mathbf{U_{ss}} + \varepsilon\mathbf{U_{pb}} \tag{3.34}$$

where $\mathbf{U_{ss}}$ is the steady-state solution and $\varepsilon\mathbf{U_{pb}}$ is the small perturbation around the steady-state conditions. Combining Eq. 3.33 with Eq. 3.34, and applying ε^1 Taylor series expansion yields to

$$\mathbf{U} = \mathbf{U'_{ss}} + \varepsilon\mathbf{U'_{pb}} = \mathbf{f}\left(\mathbf{U_{ss}} + \varepsilon\mathbf{U_{pb}}\right) = \mathbf{f}(\mathbf{U_{ss}}) + \varepsilon\mathbf{f_U}(\mathbf{U_{ss}})\mathbf{U_{bp}} + \mathscr{O}(\varepsilon^2) \tag{3.35}$$

where the term $\mathbf{f_U}$ denotes the Jacobian matrix of $\mathbf{f}$ with respect to $\mathbf{U}$ defined as

$$\mathbf{f_U} = \begin{bmatrix} \frac{\partial f_1}{\partial U_{p1}} & \frac{\partial f_1}{\partial U_{m1}} & \cdots & \frac{\partial f_1}{\partial U_{pi}} & \frac{\partial f_1}{\partial U_{mi}} & \cdots & \frac{\partial f_1}{\partial U_{pN}} & \frac{\partial f_1}{\partial U_{mN}} \\ \frac{\partial f_2}{\partial U_{p1}} & \frac{\partial f_2}{\partial U_{m1}} & \cdots & \frac{\partial f_2}{\partial U_{pi}} & \frac{\partial f_2}{\partial U_{mi}} & \cdots & \frac{\partial f_2}{\partial U_{pN}} & \frac{\partial f_2}{\partial U_{mN}} \\ \vdots & \vdots & \ddots & \vdots & \vdots & \ddots & \vdots & \vdots \\ \frac{\partial f_{2N-1}}{\partial U_{p1}} & \frac{\partial f_{2N-1}}{\partial U_{m1}} & \cdots & \frac{\partial f_{2N-1}}{\partial U_{pi}} & \frac{\partial f_{2N-1}}{\partial U_{mi}} & \cdots & \frac{\partial f_{2N-1}}{\partial U_{pN}} & \frac{\partial f_{2N-1}}{\partial U_{mN}} \\ \frac{\partial f_{2N}}{\partial U_{p1}} & \frac{\partial f_{2N}}{\partial U_{m1}} & \cdots & \frac{\partial f_{2N}}{\partial U_{pi}} & \frac{\partial f_{2N}}{\partial U_{mi}} & \cdots & \frac{\partial f_{2N}}{\partial U_{pN}} & \frac{\partial f_{2N}}{\partial U_{mN}} \end{bmatrix} \tag{3.36}$$

and if $\mathbf{U}'_{\mathbf{ss}} = \mathbf{f}(\mathbf{U}_{\mathbf{ss}})$, then Eq. 3.35 can be rewritten as

$$\mathbf{U}'_{\mathbf{pb}} = \mathbf{f}_{\mathbf{U}}(\mathbf{U}_{\mathbf{ss}})\mathbf{U}_{\mathbf{pb}} \tag{3.37}$$

It can be shown from Eq. 3.34 that if the solution of the perturbation is stable at zero, then the steady-state solution is also stable. To evaluate the stability of the steady-state solution, one may look at the eigenvalues of $\mathbf{f}_{\mathbf{U}}$, and the stability analysis may become an eigenvalue problem as a result. According to the stability theorem, if an eigenvalue moves over the imaginary axis in the complex plane, the solution is no longer stable. The conditions for establishing stability are, hence,

i. The steady-state solution is considered to be stable if and only if all of the eigenvalues have real components that are negative.

ii. The steady-state solution is neutral if and only if one of the eigenvalues has a real component of zero and all the rest have real components of negative.

iii. Finally, the steady-state solution is unstable if and only if any eigenvalue has a positive real component.

3.4 Examples

In this section, two examples of nonlinear equations will be shown. The first example depicts a SDOF conservative oscillator with two nonlinear geometric stiffness terms, whereas the second example discusses a SDOF oscillator with viscous damping and harmonic forcing away from resonance. It is essential to note that all of the manipulations and solutions to be presented are derived using Maple symbolic computation packages, while COCO numerical continuation toolbox in MATLAB is employed for numerical comparisons and verifications.

3.4.1 SDOF conservative oscillator with two nonlinear geometric stiffness terms

Considering the following general formula for unforced, undamped SDOF oscillator,

$$\ddot{x}(t) + \omega_n^2 x(t) + \alpha_1 x^{\mu}(t) + \alpha_2 x^{\nu}(t) = 0, \tag{3.38}$$

where ω_n is the natural frequency of the system, α_1 and α_2 are arbitrary small coefficients for the nonlinear terms, μ and ν are two integers denoting the lower and higher orders of the nonlinear terms, respectively. Furthermore, due to the stability conditions of nonlinear systems, at least one of the nonlinear integer orders (i.e. μ or ν) should be an odd number, for detailed discussion of the potential functions and how they are used to study the stability of the system refer to [8].

Using the DNF method, it is feasible to compare the oscillator's dynamics for various μ and ν configurations. Theoretically, such systems with distinct parameters and orders of nonlinearities may be utilised to represent certain engineering applications. In theory, the symbolic computations approach proposed in this work may be extended to broader SDOF systems with any number of nonlinear variables; this will be briefly explored in Chapter 4. By starting with two nonlinear terms defined by Eq. 3.38 and increasing the order for evaluating this approach, it is feasible to grasp its capabilities and limitations.

The following procedure illustrates the use of symbolic computations of a normal form method in order to solve Eq. 3.38 for $\mu = 2$ and $\nu = 7$, nevertheless, following the same procedure, it is possible to solve the equation for any other values, as long as at least one exponent is odd. Practically, DNF analysis of such systems undergoes a series of transformations that involve complex mathematical manipulations, in this work the most important results are shown, focusing on the utilisation of symbolic computation software, i.e. Maple. Rewriting Eq. 3.38 with $\mu = 2$ and $\nu = 7$, leads to

$$\ddot{x}(t) + \omega_n^2 x(t) + \alpha_1 x^2(t) + \alpha_2 x^7(t) = 0, \tag{3.39}$$

The first step is using Eq. 3.3 in view of Eq. 3.2 to make the linear modal transformation, in this step it should be noticed that for SDOF systems the transform is unity and $x = q$, then

$$\ddot{q} + \Gamma q + N_q(q) = 0, \tag{3.40}$$

where $\Gamma = \omega_n^2$ and $N_q(q) = \alpha_1 q^2 + \alpha_2 q^7$. The second step is the near-identity transformation, and for $\varepsilon = 1$, rewriting the nonlinear terms using $\mathbf{u}$, one should obtain $N_q(u) = \alpha_1 u_1^2 + \alpha_2 u_1^7$ and $\mathbf{u_1} = \mathbf{u_{p1}} + \mathbf{u_{m1}}$, thus

$$\boldsymbol{n}_{(1)}(\boldsymbol{u}) = \mathbf{n}^*\mathbf{u}^*(\mathbf{u_p} + \mathbf{u_m}) = \alpha_1(u_p + u_m)^2 + \alpha_2(u_p + u_m)^7, \tag{3.41}$$

By expanding Eq. 3.41, $\mathbf{n}_{(\mathbf{1})}(\mathbf{u})$ will contain many terms (11 terms in this case), these terms have to be primarily decomposed into coefficients and nonlinear functions vectors $\mathbf{n}^*$ and $\mathbf{u}^*$, respectively.

$$\mathbf{n}^* = \begin{bmatrix} \alpha_1 & \alpha_1 & \alpha_2 & \alpha_2 & 2\alpha_1 & 7\alpha_2 & 21\alpha_2 & 35\alpha_2 & 35\alpha_2 & 21\alpha_2 & 7\alpha_2 \end{bmatrix} \tag{3.42}$$

$$\mathbf{u}^* = \begin{bmatrix} u_{m1}^2 & u_{p1}^2 & u_{m1}^7 & u_{p1}^7 & u_{p1}u_{m1} & u_{p1}u_{m1}^6 & u_{p1}^2u_{m1}^5 & u_{p1}^3 & u_{m1}^4 & u_{p1}^4u_{m1}^3 & u_{p1}^5u_{m1}^2 & u_{p1}^6u_{m1} \end{bmatrix}^{\mathsf{T}} \tag{3.43}$$

As the number of nonlinear terms and their associated orders rise, or when higher order accuracy (i.e. ε^2, ε^3, etc.) is considered, it becomes more difficult to alter this first step using conventional hand calculations. Symbolically, the suggested technique may be performed quickly to accomplish this step and generate $\mathbf{n}^*$ and $\mathbf{u}^*$ matrices.

Using the suggested symbolic technique, the author has been able to investigate several SDOF oscillators with two weak nonlinearities of varying orders. The amount of terms included in the matrix is crucial when implementing the DNF approach, particularly for SDOF problems. Table 3.1 displays the number of terms for conservative nonlinear oscillators of different orders of nonlinearities, i.e. for different μ and ν configurations. The values in the highlighted cells show the scenario when the EOM has just one nonlinear component.

The increasing number of terms appearing in Table 3.1 leads to additional difficulties for hand calculations to be performed. Importantly, more complex systems will lead to a higher number of terms; some examples of more complex cases include:

- the EOM involves viscous damping (in this case two additional terms are to be added to those in Table 3.1),
- the system contains more than two types of polynomial nonlinearities,
- solving the EOM for a higher order accuracy (i.e. ε^2)
- and when using the direct normal forms technique for MDOF systems,

all of the aforementioned cases can yield to a dramatic increase in the matrix size, thus, the mathematical complexity is also increased, and this can justify turning to symbolic computation method.

Table 3.1: Number of terms involved in matrices for selected values of ν and μ.

μ \ ν	3	5	7	9	11	13
2	7	9	11	13	15	17
3	4	10	12	14	16	18
4	9	11	13	15	17	19
5	10	6	14	16	18	20
6	11	13	15	17	19	21
7	12	14	8	18	20	22
8	13	15	17	19	21	23
9	14	16	18	10	22	24
10	15	17	19	21	23	25
11	16	18	20	22	12	26
12	17	19	21	23	25	27
13	18	20	22	24	26	14

In order to complete the analysis, by applying Eq. 3.15, $\boldsymbol{\beta}^*$ can be written as

$$\boldsymbol{\beta}^* = \omega_r^2 \begin{bmatrix} 3 & 48 & 3 & 48 & -1 & 24 & 8 & 0 & 0 & 8 & 24 \end{bmatrix} \tag{3.44}$$

It should be emphasised that, according to direct normal forms analysis, any zero value in $\boldsymbol{\beta}^*$ matrix indicates the presence of a resonant term; while any non-zero value indicates a non-resonant or harmonic term.

The next step, illustrates the resulting coefficients of resonant terms $\mathbf{n}_\mathbf{u}^*$ and $\mathbf{h}^*$ of harmonic terms for both resonant and non-resonant cases (refer to [8] for detailed analysis). In symbolic programming, this step is based on conditional loop manipulation for each element in $\boldsymbol{\beta}^*$ with respect to $\mathbf{n}^*$. The results are

$$\mathbf{n}_\mathbf{u}^* = \alpha_2 \begin{bmatrix} 0 & 0 & 0 & 0 & 0 & 0 & 0 & 35 & 35 & 0 & 0 \end{bmatrix} \tag{3.45}$$

$$\mathbf{h}^* = \frac{1}{\omega_r^2} \begin{bmatrix} \frac{\alpha_1}{3} & \frac{\alpha_1}{48} & \frac{\alpha_2}{3} & \frac{\alpha_2}{48} & -2\alpha_1 & \frac{7\alpha_2}{24} & \frac{21\alpha_2}{8} & 0 & 0 & \frac{21\alpha_2}{8} & \frac{7\alpha_2}{24} \end{bmatrix} \tag{3.46}$$

If the analysis is only truncated to ε^1 accuracy, which regularly leads to acceptable inspection of the nonlinear effects for systems with weak nonlinearities, the final step is rewriting the transformed equation of motion. For the non-resonant case, Eq. 3.40 in u-transformed coordinate system becomes

$$\ddot{u}+\Lambda u+\mathbf{n}_{\mathbf{u}}^{*}\mathbf{u}^{*}=0 \quad \rightsquigarrow \quad \ddot{u}+\omega_n^2 u+35\left(u_{p1}^3u_{m1}^4+u_{p1}^4u_{m1}^3\right)=0 \tag{3.47}$$

and the near identity transform is written as

$$q=u+\mathbf{h}^{*}\mathbf{u}^{*}, \tag{3.48}$$

which leads to

$$\begin{aligned} q=u+\frac{1}{3\omega_r^2}\Bigg(&\alpha_1u_{m1}^2+\frac{\alpha_1u_{p1}^2}{16}+\alpha_2u_{m1}^7-6\alpha_1u_{p1}u_{m1}+\frac{7\alpha_2u_{p1}u_{m1}^6}{8}+\frac{63\alpha_2u_{p1}^2u_{m1}^5}{8}+\\ &\frac{63\alpha_2u_{p1}^5u_{m1}^2}{8}+\frac{7\alpha_2u_{p1}^6u_{m1}}{8}\Bigg) \end{aligned} \tag{3.49}$$

Substituting the assumed solution, Eq. 3.27, into Eq. 3.47, and solving the positive (or negative) complex exponential terms by exact balancing, one can get the equation of the backbone curve for this system, truncated to ε^1 accuracy, which is

$$\omega_r^2=\omega_n^2+\frac{35}{64}\alpha_2U^6 \tag{3.50}$$

Following the same aforementioned procedure, one should be able to find the backbone curve for any values of ν and μ in Eq. 3.38. One advantage of having a computer pattern in such case is the ability of doing several runs with different conditions. Table 3.2 shows the backbone curve obtained for the first four values of ν when $\mu=2$ for the ε^1 expansion. It is clear that a general pattern is repeated for the backbone equation found, so if $\mu=2$ it could be generalized for any value of ν that

$$\omega_r^2=\omega_n^2+\eta_i\alpha_2U^{\nu-1} \tag{3.51}$$

where η_i denotes a constant that directly depends on the order of the nonlinear term, refer to Table 3.4 for some values of η_i for numerous orders of polynomial nonlinear terms.

Table 3.2: Backbone curve equation of ε^1 accuracy for different values of ν while $\mu = 2$.

Value of ν	Equation of motion	Backbone curve equation
3	$\ddot{x}(t) + \omega_n^2 x(t) + \alpha_1 x^2(t) + \alpha_2 x^3(t) = 0$	$\omega_r^2 = \omega_n^2 + \frac{3}{4}\alpha_2 U^2$
5	$\ddot{x}(t) + \omega_n^2 x(t) + \alpha_1 x^2(t) + \alpha_2 x^5(t) = 0$	$\omega_r^2 = \omega_n^2 + \frac{5}{8}\alpha_2 U^4$
7	$\ddot{x}(t) + \omega_n^2 x(t) + \alpha_1 x^2(t) + \alpha_2 x^7(t) = 0$	$\omega_r^2 = \omega_n^2 + \frac{35}{64}\alpha_2 U^6$
9	$\ddot{x}(t) + \omega_n^2 x(t) + \alpha_1 x^2(t) + \alpha_2 x^9(t) = 0$	$\omega_r^2 = \omega_n^2 + \frac{63}{128}\alpha_2 U^8$

Practically, for the weak nonlinear case, the values of α_1 and α_2 should be small, typically less than unity, Fig. 3.2 shows the backbone curves for the conservative oscillators appearing in Table 3.2, using the following numerical values; $\alpha_1 = 0.2$, $\alpha_2 = 0.1$ and $\omega_n = \pi$ rad/s.

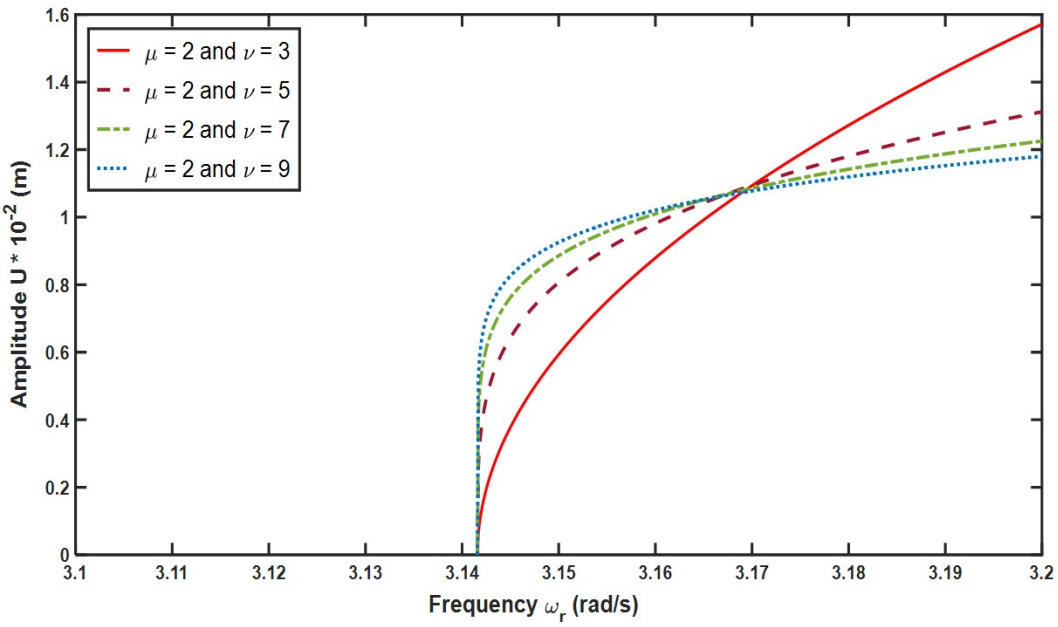

Figure 3.2: Conservative backbone curves for different values of ν while $\mu_1 = 2$. All results are obtained analytically using the findings in Eq. 3.51 or equivalently Table 3.2, and the natural frequency is $\omega_n = \pi$ rad/s.

Furthermore, it is possible to obtain the backbone curve relation, truncated to ε^1 accuracy, for any values of ν and μ in Eq. 3.38. Table 3.3 shows some examples of these results.

The following findings are noted:

- For SDOF systems, any even nonlinearity found in the EOM is removed by the normal form transformation and does not appear in the backbone curve. This phenomenon is found in the literature in terms of

Table 3.3: Backbone curve equation of ε^1 accuracy for different values of ν and μ.

Value of ν	Value of μ	Equation of motion	Backbone curve equation
3	5	$\ddot{x}(t)+\omega_n^2 x(t)+\alpha_1 x^3(t)+\alpha_2 x^5(t)=0$	$\omega_r^2=\omega_n^2+\frac{3}{4}\alpha_1 U^2+\frac{5}{8}\alpha_2 U^4$
4	7	$\ddot{x}(t)+\omega_n^2 x(t)+\alpha_1 x^4(t)+\alpha_2 x^7(t)=0$	$\omega_r^2=\omega_n^2+\frac{35}{64}\alpha_2 U^6$
5	9	$\ddot{x}(t)+\omega_n^2 x(t)+\alpha_1 x^5(t)+\alpha_2 x^9(t)=0$	$\omega_r^2=\omega_n^2+\frac{5}{8}\alpha_1 U^4+\frac{63}{128}\alpha_2 U^8$
6	9	$\ddot{x}(t)+\omega_n^2 x(t)+\alpha_1 x^6(t)+\alpha_2 x^9(t)=0$	$\omega_r^2=\omega_n^2+\frac{63}{128}\alpha_2 U^8$
7	11	$\ddot{x}(t)+\omega_n^2 x(t)+\alpha_1 x^7(t)+\alpha_{11} x^9(t)=0$	$\omega_r^2=\omega_n^2+\frac{35}{64}\alpha_2 U^6+\frac{231}{512}\alpha_2 U^{10}$

quadratic nonlinearity appearing in SDOF nonlinear oscillator, [8], based upon the analysis introduced, this finding is generalised for any even nonlinearity that appears in SDOF systems.

- Referring to Table 3.3 and Table 3.2, it is clear that the nonlinear frequency resulting by ε^1 DNF accuracy consists of the linear natural frequency of the system, in addition to the nonlinear frequency shift which depends on the nonlinear terms appearing in the original equation of motion.

- Some of these results are numerically verified using COCO numerical continuation toolbox in MATLAB (see Fig. 3.3 & Fig. 3.4 in the following subsection), and acceptable agreement between analytical backbone curves and numerical results can be observed.

In conclusion, in order to generalise the ε^1 backbone curve relation for any SDOF nonlinear oscillator with two types of nonlinearities, Eq. 3.38, in view of Table 3.1 & Table 3.2, provided that ν and μ are both odd, the following relation can be obtained

$$\omega_r^2=\omega_n^2+\eta_{i,1}\alpha_1 U^{\nu-1}+\eta_{i,2}\alpha_2 U^{\mu-1} \tag{3.52}$$

where $\eta_{i,1}$ and $\eta_{i,2}$ are constants directly related to the order of the nonlinearity, Table 3.4 shows the values of these constants for several orders of the nonlinear terms. Finally, as mentioned earlier, any even nonlinearity in the EOM will be removed by the normal form and will not appear in Eq. 3.52.

Table 3.4: Values of the constants η_i appearing in the backbone curve relation, Eq. 3.52

Order of nonlinearity	3	5	7	9	11	13	15	17
η_i	$\frac{3}{4}$	$\frac{5}{8}$	$\frac{35}{64}$	$\frac{63}{128}$	$\frac{231}{512}$	$\frac{429}{1024}$	$\frac{6435}{16384}$	$\frac{12155}{32768}$

Using Eq. 3.52 and Table 3.4 it is possible to get the conservative backbone curve relation for any nonlinear oscillator with two different types of polynomial nonlinearities. As an example, if the EOM contains both cubic and quintic nonlinearities, i.e.

$$\ddot{x}(t) + \omega_n^2 x(t) + \alpha_1 x^3(t) + \alpha_2 x^5(t) = 0, \tag{3.53}$$

then, the conservative backbone curve of ε^1 accuracy will be

$$\omega_r^2 = \omega_n^2 + \frac{3}{4}\alpha_1 U^2 + \frac{5}{8}\alpha_2 U^4, \tag{3.54}$$

In the following subsection, in order to investigate the accuracy of the symbolically applied DNF technique, as a verification problem, the system of a Duffing oscillator with cubic nonlinearity, viscous damping and forcing away from resonance is considered, this example system is priorly studied using traditional DNF method by Wagg and Neild in [8].

3.4.2 Verification problem: Non-resonant Duffing oscillator with cubic nonlinearity

The equation of motion of Duffing oscillator with cubic nonlinearity, viscous damping and forcing away from resonance where the ratio between the driving frequency and the natural frequency is 1/3 (i.e. $a = \frac{1}{3}$) is given by

$$\ddot{x}(t) + 2\zeta\omega_n\dot{x}(t) + \omega_n^2 x(t) + \alpha x^3(t) = R\cos(\Omega t), \tag{3.55}$$

Using the proposed DNF technique applied symbolically, it is required to analytically generate conservative backbone curve equations for ε^1 accuracy, and compare with forced (and lightly damped) response curves. The step-by-step procedure involves large matrices and algebraic terms, hence, only the key results are to be shown, while further results for matrix algebra manipulations can be found in [8]. Upon analysing the system using

DNF, one can get

$$\begin{aligned}\frac{1}{4}\left[3\alpha U^3+\left(24\alpha e^2+4\left(\omega_n^2-\omega_r^2\right)\right)\right]\cos\left(\omega_r t-\phi\right)+2\alpha e^3\cos\left(\omega_r t\right)\\ -2\zeta\omega_n\omega_r U\sin\left(\omega_r t-\phi\right)=0,\end{aligned} \tag{3.56}$$

where $e=\dfrac{R}{2\left(\omega_n^2-\Omega^2\right)}$.

Applying the suitable trigonometric identities, and then balancing the sines and cosines terms in Eq. 3.56, yields to

$$\zeta\omega_n\omega_r U=-\alpha e^3\sin(\phi) \tag{3.57}$$

$$3\alpha e^2+\frac{3}{8}\alpha U^3+\frac{1}{2}\left(\omega_n^2-\omega_r^2\right)=-\alpha e^3\cos(\phi) \tag{3.58}$$

Hence, it is possible to use Eq. 3.57 & Eq. 3.58 to get an expression for U as a function of ω_r, therefore, computing the forced response curve analytically, this has been previously done in [8] by applying traditional hand calculations. In order to compare with our proposed symbolic computation method, the same problem has been solved in conservative case (unforced-undamped case), and the conservative backbone curve is computed using Eq. 3.52 and Table 3.4 and plotted in Fig. 3.3, along with the numerically computed forced-damped frequency response curves for several values of R. The numerical values chosen for this figure are $\omega_n=2$ rad/s, $\zeta=0.01$ and $\alpha=0.2$.

Fig. 3.3 represents a typical backbone curve and frequency response curves for any forced damped nonlinear system in hardening case. From this figure, several important observations can be noticed; first of all, as the value of α is positive, the hardening behaviour is clearly seen, in contrast, as will be shown later on in Fig. 3.4, if α is negative softening behaviour will be noticed. Furthermore, as the figure shows the relation between natural frequency and amplitude, the conservative backbone curves do not perfectly coincide with the manifolds' peaks, and this is due to the presence of damping, however, in order to overcome this issue, the following Chapter introduces a novel method of obtaining the damped backbone curves for such viscously damped systems. Moreover, as the forcing amplitude R becomes higher, more matching between the conservative backbone curves and their corresponding manifolds occurs.

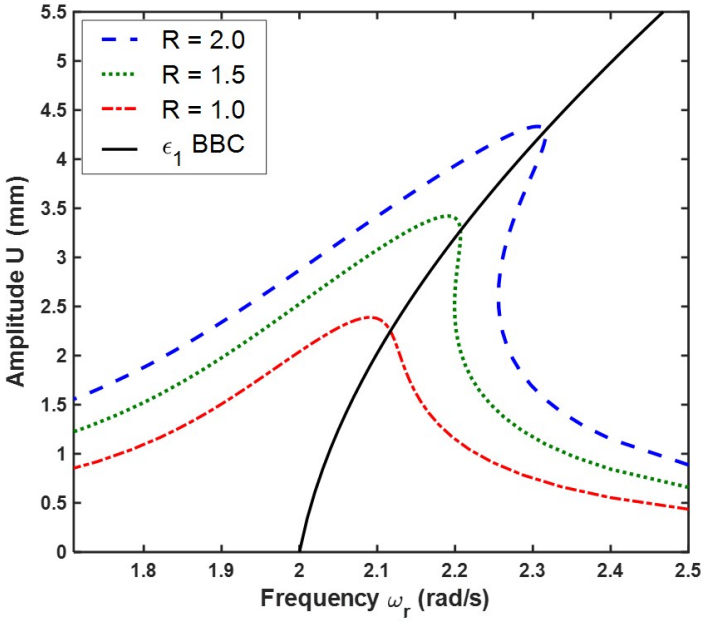

Figure 3.3: Conservative backbone curve and the forced-damped frequency responses for the Duffing oscillator with cubic nonlinearity. The solid black line represents the conservative backbone curve obtained analytically using Eq. 3.52 and Table 3.4, while the coloured dashed lines are the forced-damped frequency responses computed numerically using COCO toolbox in MATLAB for different values of R. The numerical values are: $\omega_n = 2$ rad/s, $\zeta = 0.01$ and $\alpha = 0.2$.

Finally, in order to compare the frequency response of several nonlinear terms in combination, recall Eq. 3.38 in its forced damped case, that is

$$\ddot{x}(t) + 2\zeta\omega_n\dot{x}(t) + \omega_n^2 x(t) + \alpha_1 x^{\nu}(t) + \alpha_2 x^{\mu}(t) = R\cos(\Omega t), \tag{3.59}$$

Various values of ν and μ can be considered, the corresponding EOM can be studied using the method of DNF and analytical backbone curve relations are then obtained. Three cases are studied, linear oscillator and cubic-quintic oscillator in both hardening and softening cases (3-5 Hardening, 3-5 Softening). Fig. 3.4 represents backbone equation for all previous cases along with their forcing manifolds obtained numerically using COCO, this figure is generated using the numerical data: general parameters for all cases $\omega_n = 2$ rad/s, $\zeta = 0.05$ and $R = 1$. In the case of hardening cubic-quintic oscillator $\alpha_1 = 0.2$ and $\alpha_2 = 0.3$. And finally, for softening cubic-quintic oscillator $\alpha_1 = -0.2$ and $\alpha_2 = -0.3$.

Fig. 3.4 illustrates the effect of both hardening and softening nonlinear terms on the frequency response of the system. Using this figure, the following can be noticed; firstly, compared to the linear case, hardening

polynomial nonlinearities shift the peak to the right whilst minimising the maximum vibration amplitude of the system. On the other hand, softening nonlinear terms cause shifting to the left and maximising the vibration amplitude. However, using Eq. 3.52 along with Table 3.4 it is possible to obtain the conservative backbone curves for SDOF oscillator with two nonlinear terms, and compare with the forced-damped frequency response computed numerically using COCO toolbox in MATLAB.

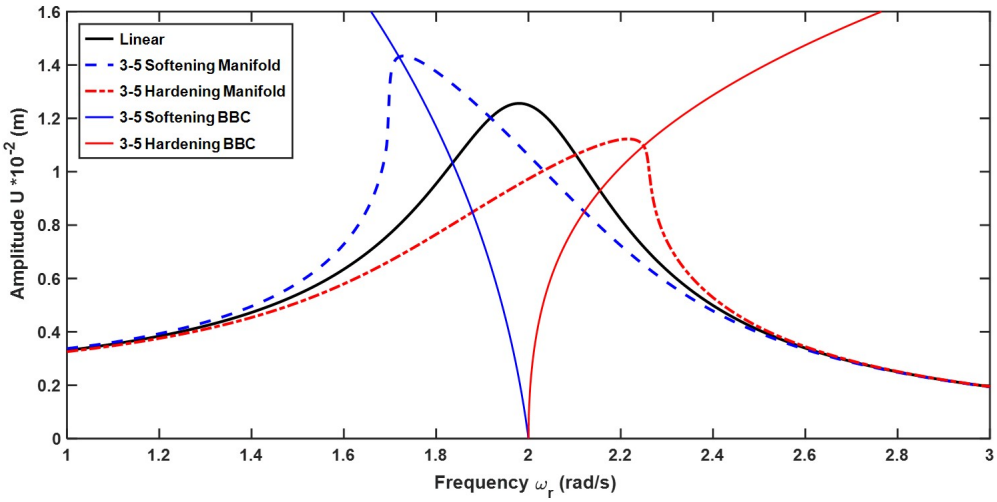

Figure 3.4: Frequency responses and conservative backbone curves for the cubic-quintic oscillator for various types of nonlinearities. The red and blue solid lines illustrate the conservative backbone curves computed analytically using the DNF results for the hardening and softening cases, respectively. Moreover, the black solid line, dashed-dotted red line and dashed blue line represent the numerically computed frequency responses for the linear, hardening and softening cases, respectively, all generated using COCO toolbox in MATLAB. Common parameters for all cases are $\omega_n = 2$ rad/s, $\zeta = 0.05$ and $R = 1$. Moreover, for hardening cases, $\alpha_1 = 0.2$ and $\alpha_2 = 0.3$, and finally for softening cases, $\alpha_1 = -0.2$ and $\alpha_2 = -0.3$.

3.5 Summary

In this Chapter, the theoretical procedure of the DNF analysis is shown in detail. Firstly, the DNF procedure for conservative (or unforced, undamped) systems is presented. Then, the procedure for forced damped systems is substantially revealed. The vital difficulties using this technique are mainly related to the complexity of the matrix manipulations, specifically for systems with numerous number of polynomial nonlinear terms and/or the high orders of the nonlinearities involved in the EOM. Despite the fact that building symbolic algorithms to deal with such type of method has consumed considerable time and effort, these algorithms greatly helped the researcher investigate complex systems such that the SDOF system studied in Subsection 3.4.1 rapidly and efficiently.

Based upon the analysis performed in this Chapter, the following can be observed;

- The DNF procedures presented are considered to be greatly complicated and sophisticated if handled by traditional hand calculations, specifically when the size of the matrices involved become considerably large, thus the utilisation of symbolic computations can be efficiently helpful.
- The general formula for the backbone curve in Eq. 3.51 is for the special case when ε^1 accuracy is considered and one single odd and one single even nonlinear terms appearing in the original EOM, which indicates that ε^1 accuracy is unable to capture the effect of even nonlinear terms to the frequency response (or backbone) curves. Nevertheless, this restriction will be resolved when studying higher order accuracies in Section 4.1-Section 4.3.
- In Subsection 3.4.2, the Duffing oscillator is investigated under non-resonant conditions, for which the driving frequency is away from the natural frequency of the system, i.e. $\Omega \neq \omega_n$, however, more examples of the resonant cases can be found in [8].
- The backbone curves generated in this Chapter are restricted to the conservative systems, however, in the following Chapter, a novel approximate method of obtaining the damped backbone curve is shown.
- In Chapter 5, more comprehensive examples for SDOF systems using DNF method are discussed in detail.

Chapter 4

Higher order accuracies and applications to damped systems

In this Chapter, DNF analysis is extend to include higher order accuracies (i.e. $\varepsilon^2, \varepsilon^3, ...$), and the resulting backbone curves are then compared to show the benefits of extending the analysis to these higher orders of accuracies. Firstly, the DNF analysis truncated to ε^2 is presented, the procedure shown in this section can be found in the literature in [8, 47]. In the following subsections, a novel implementation of the DNF method is derived to generalise the analysis; closed-form mathematical expressions for any desired DNF accuracy is obtained, and, in principle, these expressions can be applied with the aid of symbolic computations software to get approximate analytical results for the systems to any desired accuracy. Finally, a general closed-form expression that enables the researcher to investigate the results for any desired n^{th} accuracy is produced. Two examples are then studied, the first example illustrates the analysis of conservative Duffing oscillator while the second example shows the conservative quadratic-cubic oscillator, in both examples DNF analysis is held to ε^1, ε^2 and ε^3 accuracies, and the resulting backbone curves are compared.

4.1 DNF procedure for ε^2 accuracy

While in many cases the first order of truncated solution, (i.e. ε^1 accuracy), yields to acceptable results (compared to numerical solutions), sometimes it can be beneficial (or even required) to extend the analysis to a

higher order accuracies. In this section, a brief formulation to ε^2 accuracy is discussed, more details regarding the derivation of this high order of accuracy can be found in [8].

To start the derivation of ε^2 accuracy, one may refer to Eq. 3.10, for which it is possible to obtain $h_2(u)$ and $n_{u2}(u)$ vectors. In analogy to Eq. 3.12 it is possible to write

$$\widetilde{\mathbf{n}}_{\mathbf{2}}(\mathbf{u}) + \Gamma \mathbf{h}_{\mathbf{2}}(\mathbf{u}) + \frac{\mathrm{d}^2}{\mathrm{d}t^2}\mathbf{h}_{\mathbf{2}}(\mathbf{u}) = \mathbf{n}_{\mathbf{u2}}(\mathbf{u}) \tag{4.1}$$

where $\widetilde{\mathbf{n}}_{\mathbf{2}}(\mathbf{u}) = \mathbf{n}_{\mathbf{2}}(\mathbf{u}) + (\Lambda - \Gamma)\mathbf{h}_{\mathbf{1}}(\mathbf{u}) + \dfrac{\mathrm{d}}{\mathrm{d}\mathbf{u}}\{\mathbf{n}_{\mathbf{1}}(\mathbf{u})\}\mathbf{h}_{\mathbf{1}}(\mathbf{u})$

Herein, more complexity can be clearly noticed regarding the nonlinear term, so it is more difficult to obtain the solution to ε^2 accuracy. However, according to the system being approximated, it will be shown that rather than being considered as a compromising procedure to improve the accuracy, the need of extending the analysis to ε^2 highly depends on the orders of the nonlinear terms. In matrix form, and similar to the analysis of ε^1, the following terms can be introduced,

$$\widetilde{\mathbf{n}}_{\mathbf{2}}(u) = \mathbf{n}^{(2)}\mathbf{u}^{(2)}(u_p, u_m), \qquad \mathbf{h}_{\mathbf{2}}(u) = \mathbf{h}^{(2)}\mathbf{u}^{(2)}(u_p, u_m), \qquad \mathbf{n}_{\mathbf{u2}}(u) = \mathbf{n}_u^{(2)}\mathbf{u}^{(2)}(u_p, u_m) \tag{4.2}$$

where, for SDOF systems, $\mathbf{n}^{(2)}$, $\mathbf{h}^{(2)}$, $\mathbf{n}_u^{(2)}$ are row vectors, and $\mathbf{u}^{(2)}(u_p, u_m)$ is a column vector, hence, the resulting products will be scalars. The step-by-step analysis is performed exactly as the case of ε^1, and $\boldsymbol{\beta}^{(2)}$ is computed accordingly, [8]. Finally, the near-identity transformation, to ε^2 order is written as

$$\mathrm{q} = \mathbf{u} + \mathbf{h}^{(1)}\mathbf{u}^{(1)} + \mathbf{h}^{(2)}\mathbf{u}^{(2)}, \tag{4.3}$$

and the resulting EOM is found to be,

$$\ddot{\mathbf{u}} + \Lambda\mathbf{u} + \mathbf{n}^{(1)}\mathbf{u}^{(1)} + \mathbf{n}_u^{(2)}\mathbf{u}^{(2)} = 0 \tag{4.4}$$

The same procedure with some additional steps can be followed for forced-damped systems, and for systems studied in the resonant case, refer to [8] for detailed analysis of such systems.

4.2 DNF analysis for ε^n accuracy

In this part, thanks to the symbolic computations algorithms generated, a novel improvement of the DNF method is introduced in order to find any accuracy of the DNF solution ε^n. The analysis to be performed in this Section builds of the ε^1 analysis shown in Chapter 3; by referring to Eq. 3.10, it is possible to obtain the ε^2 accuracy solution by finding the $h_2(u)$ and $n_{u2}(u)$ vectors, in analogy to Eq. 3.10 it is possible to write

$$\widetilde{\mathbf{n}}_{\mathbf{2}}(\mathbf{u}) + \Gamma \mathbf{h}_{\mathbf{2}}(\mathbf{u}) + \frac{\mathrm{d}^2}{\mathrm{d}t^2}\mathbf{h}_{\mathbf{2}}(\mathbf{u}) = \mathbf{n}_{\mathbf{u2}}(\mathbf{u}), \tag{4.5}$$

where $\widetilde{\mathbf{n}}_{\mathbf{2}}(\mathbf{u}) = \mathbf{n}_{\mathbf{2}}(\mathbf{u}) + (\Lambda - \Gamma)\mathbf{h}_{\mathbf{1}}(\mathbf{u}) + \dfrac{\mathrm{d}}{\mathrm{d}\mathbf{u}}\{\mathbf{n}_{\mathbf{1}}(\mathbf{u})\}\mathbf{h}_{\mathbf{1}}(\mathbf{u})$.

As discussed earlier, the need of extending the analysis to ε^2 highly depends on the orders of the nonlinear terms, however, in some cases it can be necessary to find ε^2 solution, for instance, refer to [47]. In matrix form, and similar to the analysis of ε^1, the following terms can be introduced,

$$\begin{aligned} \widetilde{\mathbf{n}}_{\mathbf{2}}(u) &= \mathbf{n}^{(2)}\mathbf{u}^{(2)}(u_p, u_m) \\ \mathbf{h}_{\mathbf{2}}(u) &= \mathbf{h}^{(2)}\mathbf{u}^{(2)}(u_p, u_m) \\ \mathbf{n}_{\mathbf{u2}}(u) &= \mathbf{n}_u^{(2)}\mathbf{u}^{(2)}(u_p, u_m) \end{aligned} \tag{4.6}$$

where, for SDOF systems, $\mathbf{n}^{(2)}$, $\mathbf{h}^{(2)}$, $\mathbf{n}_u^{(2)}$ are row vectors, and $\mathbf{u}^{(2)}(u_p, u_m)$ is a column vector, hence, the resulting products will be scalars. The step-by-step analysis is performed exactly as the case of ε^1, and $\boldsymbol{\beta}^{(2)}$ is computed accordingly, [8]. Finally, the near-identity transformation, to ε^2 order, along with the resulted EOM are found to be,

$$\mathbf{q} = \mathbf{u} + \mathbf{h}^{(1)}\mathbf{u}^{(1)} + \mathbf{h}^{(2)}\mathbf{u}^{(2)} \quad \rightsquigarrow \quad \ddot{\mathbf{u}} + \Lambda\mathbf{u} + \mathbf{n}^{(1)}\mathbf{u}^{(1)} + \mathbf{n}_u^{(2)}\mathbf{u}^{(2)} = 0 \tag{4.7}$$

The same procedure with some additional steps can be followed for forced-damped systems, and for systems studied in the resonant case. In the literature, most of the DNF analysis is restricted to ε^1 accuracy, for which acceptable levels of agreements with the numerical results are obtained. Moreover, some researchers extended the analysis to ε^2 accuracy, and normally this yields to desirable improvements of the findings, the interested reader is advised to visit [8] for detailed analysis of some examples. However, according to author's best knowledge, DNF method has never been used with accuracies higher than ε^2 to investigate the dynamics of

nonlinear systems, this is mainly related to the increasing mathematical complexities, and since the results of lower orders accuracies could normally yield to sufficient levels of accuracy. However, in this work, it is desired to extend the analysis to include any order of DNF accuracy, and by using symbolic computations it is possible to overcome the complicated mathematical manipulations usually accompanied to such analysis.

Now, in order to obtain ε^3 solution, or any higher order accuracy, the following relation is considered;

$$\mathbf{q} = \mathbf{u} + \mathbf{h}(\mathbf{u}) \tag{4.8}$$

where the harmonic solution can be perturbed in the following form

$$\mathbf{h}(\mathbf{u}) = \varepsilon \mathbf{h_1}(\mathbf{u}) + \varepsilon^2 \mathbf{h_2}(\mathbf{u}) + \varepsilon^3 \mathbf{h_3}(\mathbf{u}) + \varepsilon^4 \mathbf{h_4}(\mathbf{u}) + \varepsilon^5 \mathbf{h_5}(\mathbf{u}) + ... \tag{4.9}$$

The conservative EOM, in terms of $\mathbf{u}$, is written as

$$\ddot{\mathbf{u}} + \Lambda \mathbf{u} + \mathbf{N_u}(\mathbf{u}) = 0 \tag{4.10}$$

Where the nonlinear vector (or matrix), $\mathbf{N_u}(\mathbf{u})$, is approximated in the following form

$$\mathbf{N_u}(\mathbf{u}) = \varepsilon \mathbf{N_u}(\mathbf{u}) + \varepsilon^2 \mathbf{N_u}(\mathbf{u}) + \varepsilon^3 \mathbf{N_u}(\mathbf{u}) + \varepsilon^4 \mathbf{N_u}(\mathbf{u}) + \varepsilon^5 \mathbf{N_u}(\mathbf{u}) + ..., \tag{4.11}$$

Substituting in the EOM, while considering ε^5 as the highest accuracy to be considered, it is possible to write;

$$\begin{gathered}
\ddot{\mathbf{u}} + \varepsilon \frac{\mathrm{d}}{\mathrm{d}t^2}\mathbf{h_1}(\mathbf{u}) + \varepsilon^2 \frac{\mathrm{d}}{\mathrm{d}t^2}\mathbf{h_2}(\mathbf{u}) + \varepsilon^3 \frac{\mathrm{d}}{\mathrm{d}t^2}\mathbf{h_3}(\mathbf{u}) + \varepsilon^4 \frac{\mathrm{d}}{\mathrm{d}t^2}\mathbf{h_4}(\mathbf{u}) + \varepsilon^5 \frac{\mathrm{d}}{\mathrm{d}t^2}\mathbf{h_5}(\mathbf{u}) + \\
\Lambda \left(\mathbf{u} + \varepsilon \mathbf{h_1}(\mathbf{u}) + \varepsilon^2 \mathbf{h_2}(\mathbf{u}) + \varepsilon^3 \mathbf{h_3}(\mathbf{u}) + \varepsilon^4 \mathbf{h_4}(\mathbf{u}) + \varepsilon^5 \mathbf{h_5}(\mathbf{u}) + ... \right) + \\
\varepsilon \mathbf{n_1} \left(\mathbf{u} + \varepsilon \mathbf{h_1}(\mathbf{u}) + \varepsilon^2 \mathbf{h_2}(\mathbf{u}) + \varepsilon^3 \mathbf{h_3}(\mathbf{u}) + \varepsilon^4 \mathbf{h_4}(\mathbf{u}) + ... \right) + \\
\varepsilon^2 \mathbf{n_2} \left(\mathbf{u} + \varepsilon \mathbf{h_1}(\mathbf{u}) + \varepsilon^2 \mathbf{h_2}(\mathbf{u}) + \varepsilon^3 \mathbf{h_3}(\mathbf{u}) + ... \right) + \varepsilon^3 \mathbf{n_3} \left(\mathbf{u} + \varepsilon \mathbf{h_1}(\mathbf{u}) + \varepsilon^2 \mathbf{h_2}(\mathbf{u}) + ... \right) + \\
\varepsilon^4 \mathbf{n_4} \left(\mathbf{u} + \varepsilon \mathbf{h_1}(\mathbf{u}) + ... \right) + \varepsilon^5 \mathbf{n_5} \left(\mathbf{u} + ... \right) = 0
\end{gathered} \tag{4.12}$$

Using Taylor series expansion given in the following form

$$\begin{aligned}\mathbf{n_i}\left(\mathbf{u}+\varepsilon\mathbf{h_1}(\mathbf{u})+\varepsilon^2\mathbf{h_2}(\mathbf{u})+\varepsilon^3\mathbf{h_3}(\mathbf{u})+\varepsilon^4\mathbf{h_4}(\mathbf{u})+\varepsilon^5\mathbf{h_5}(\mathbf{u})+...\right)=\mathbf{n_i}(u)+\\ \varepsilon\mathbf{h_1}(\mathbf{u})\frac{\mathrm{d}}{\mathrm{d}u}\{\mathbf{n_i}\}+\varepsilon^2\mathbf{h_2}(\mathbf{u})\frac{\mathrm{d}^2}{\mathrm{d}u^2}\{\mathbf{n_i}\}+\varepsilon^3\mathbf{h_3}(\mathbf{u})\frac{\mathrm{d}^3}{\mathrm{d}u^3}\{\mathbf{n_i}\}+\varepsilon^4\mathbf{h_4}(\mathbf{u})\frac{\mathrm{d}^4}{\mathrm{d}u^4}\{\mathbf{n_i}\}+...,\end{aligned} \tag{4.13}$$

hence, Eq. 4.9 becomes

$$\begin{aligned}\varepsilon\frac{\mathrm{d}^2}{\mathrm{d}t^2}\{\mathbf{h_1}(\mathbf{u})\}+\varepsilon^2\frac{\mathrm{d}^2}{\mathrm{d}t^2}\{\mathbf{h_2}(\mathbf{u})\}+\varepsilon^3\frac{\mathrm{d}^2}{\mathrm{d}t^2}\{\mathbf{h_3}(\mathbf{u})\}+\varepsilon^4\frac{\mathrm{d}^2}{\mathrm{d}t^2}\{\mathbf{h_4}(\mathbf{u})\}+\varepsilon^5\frac{\mathrm{d}^2}{\mathrm{d}t^2}\{\mathbf{h_5}(\mathbf{u})\}+\\ \Lambda\left(\varepsilon\mathbf{h_1}(\mathbf{u})+\varepsilon^2\mathbf{h_2}(\mathbf{u})+\varepsilon^3\mathbf{h_3}(\mathbf{u})+\varepsilon^4\mathbf{h_4}(\mathbf{u})+\varepsilon^5\mathbf{h_5}(\mathbf{u})+...\right)+\varepsilon\mathbf{n_1}(\mathbf{u})+\varepsilon^2\mathbf{h_1}(\mathbf{u})\frac{\mathrm{d}}{\mathrm{d}u}\{\mathbf{n_1}\}+\\ \varepsilon^3\mathbf{h_2}(\mathbf{u})\frac{\mathrm{d}^2}{\mathrm{d}u^2}\{\mathbf{n_1}\}+\varepsilon^4\mathbf{h_3}(\mathbf{u})\frac{\mathrm{d}^3}{\mathrm{d}u^3}\{\mathbf{n_1}\}+\varepsilon^5\mathbf{h_4}(\mathbf{u})\frac{\mathrm{d}^4}{\mathrm{d}u^4}\{\mathbf{n_1}\}+\varepsilon^2\mathbf{n_2}(\mathbf{u})+\varepsilon^3\mathbf{h_1}(\mathbf{u})\frac{\mathrm{d}}{\mathrm{d}u}\{\mathbf{n_2}\}+\\ \varepsilon^4\mathbf{h_2}(\mathbf{u})\frac{\mathrm{d}^2}{\mathrm{d}u^2}\{\mathbf{n_2}\}+\varepsilon^5\mathbf{h_3}(\mathbf{u})\frac{\mathrm{d}^3}{\mathrm{d}u^3}\{\mathbf{n_2}\}+\varepsilon^3\mathbf{n_3}(\mathbf{u})+\varepsilon^4\mathbf{h_1}(\mathbf{u})\frac{\mathrm{d}}{\mathrm{d}u}\{\mathbf{n_3}\}+\varepsilon^5\mathbf{h_2}(\mathbf{u})\frac{\mathrm{d}^2}{\mathrm{d}u^2}\{\mathbf{n_3}\}+\\ \varepsilon^4\mathbf{n_4}(\mathbf{u})+\varepsilon^4\mathbf{h_1}(\mathbf{u})\frac{\mathrm{d}}{\mathrm{d}u}\{\mathbf{n_4}\}+\varepsilon^5\mathbf{n_5}(\mathbf{u})=\varepsilon\mathbf{n_{u1}}(\mathbf{u})+\varepsilon^2\mathbf{n_{u^2}}(\mathbf{u})+\varepsilon^3\mathbf{n_{u^3}}(\mathbf{u})+\varepsilon^4\mathbf{n_{u^4}}(\mathbf{u})+\varepsilon^5\mathbf{n_{u^5}}(\mathbf{u})\end{aligned} \tag{4.14}$$

Now, the detuning step of $\Lambda=\Gamma+\varepsilon\Delta$ is adopted, where $\Delta=\omega_{nk}^2-\omega_{rk}^2$ and for small nonlinearity $\omega_{nk}\approx\omega_{rk}$, this step is performed in [8] in order to obtain ε^2 accuracy, however, in this step the analysis is generalised to include any higher order of ε. Accordantly, Eq. 4.14 can be rewritten as

$$\begin{aligned}\varepsilon\frac{\mathrm{d}^2}{\mathrm{d}t^2}\{\mathbf{h_1}(\mathbf{u})\}+\varepsilon^2\frac{\mathrm{d}^2}{\mathrm{d}t^2}\{\mathbf{h_2}(\mathbf{u})\}+\varepsilon^3\frac{\mathrm{d}^2}{\mathrm{d}t^2}\{\mathbf{h_3}(\mathbf{u})\}+\varepsilon^4\frac{\mathrm{d}^2}{\mathrm{d}t^2}\{\mathbf{h_4}(\mathbf{u})\}+\varepsilon^5\frac{\mathrm{d}^2}{\mathrm{d}t^2}\{\mathbf{h_5}(\mathbf{u})\}+\\ \Gamma\left(\varepsilon\mathbf{h_1}(\mathbf{u})+\varepsilon^2\mathbf{h_2}(\mathbf{u})+\varepsilon^3\mathbf{h_3}(\mathbf{u})+\varepsilon^4\mathbf{h_4}(\mathbf{u})+\varepsilon^5\mathbf{h_5}(\mathbf{u})+...\right)+\varepsilon^2\Delta\mathbf{h_1}(\mathbf{u})+\varepsilon^3\Delta\mathbf{h_2}(\mathbf{u})+\\ \varepsilon^4\Delta\mathbf{h_3}(\mathbf{u})+\varepsilon^5\Delta\mathbf{h_4}(\mathbf{u})+\varepsilon\mathbf{n_1}(\mathbf{u})+\varepsilon^2\mathbf{h_1}(\mathbf{u})\frac{\mathrm{d}}{\mathrm{d}u}\{\mathbf{n_1}\}+\varepsilon^3\mathbf{h_2}(\mathbf{u})\frac{\mathrm{d}^2}{\mathrm{d}u^2}\{\mathbf{n_1}\}+\varepsilon^4\mathbf{h_3}(\mathbf{u})\frac{\mathrm{d}^3}{\mathrm{d}u^3}\{\mathbf{n_1}\}+\\ \varepsilon^5\mathbf{h_4}(\mathbf{u})\frac{\mathrm{d}^4}{\mathrm{d}u^4}\{\mathbf{n_1}\}+\varepsilon^2\mathbf{n_2}(\mathbf{u})+\varepsilon^3\mathbf{h_1}(\mathbf{u})\frac{\mathrm{d}}{\mathrm{d}u}\{\mathbf{n_2}\}+\varepsilon^4\mathbf{h_2}(\mathbf{u})\frac{\mathrm{d}^2}{\mathrm{d}u^2}\{\mathbf{n_2}\}+\varepsilon^5\mathbf{h_3}(\mathbf{u})\frac{\mathrm{d}^3}{\mathrm{d}u^3}\{\mathbf{n_2}\}+\\ \varepsilon^3\mathbf{n_3}(\mathbf{u})+\varepsilon^4\mathbf{h_1}(\mathbf{u})\frac{\mathrm{d}}{\mathrm{d}u}\{\mathbf{n_3}\}+\varepsilon^5\mathbf{h_2}(\mathbf{u})\frac{\mathrm{d}^2}{\mathrm{d}u^2}\{\mathbf{n_3}\}+\varepsilon^4\mathbf{n_4}(\mathbf{u})+\varepsilon^5\mathbf{h_1}(\mathbf{u})\frac{\mathrm{d}}{\mathrm{d}u}\{\mathbf{n_4}\}+\varepsilon^5\mathbf{n_5}(\mathbf{u})=\\ \varepsilon\mathbf{n_{u1}}(\mathbf{u})+\varepsilon^2\mathbf{n_{u2}}(\mathbf{u})+\varepsilon^3\mathbf{n_{u3}}(\mathbf{u})+\varepsilon^4\mathbf{n_{u4}}(\mathbf{u})+\varepsilon^5\mathbf{n_{u5}}(\mathbf{u})\end{aligned} \tag{4.15}$$

by equating the similar powers of ε it is found that

$$\varepsilon^1: \quad \widetilde{\mathbf{n}}_1(\mathbf{u}) = \mathbf{n}_1(\mathbf{u})$$

$$\varepsilon^2: \quad \widetilde{\mathbf{n}}_2(\mathbf{u}) = \mathbf{n}_2(\mathbf{u}) + \Delta\mathbf{h}_1(\mathbf{u}) + \mathbf{h}_1(\mathbf{u})\frac{\mathrm{d}}{\mathrm{d}u}\{\mathbf{n}_1(\mathbf{u})\}$$

$$\varepsilon^3: \quad \widetilde{\mathbf{n}}_3(\mathbf{u}) = \mathbf{n}_3(\mathbf{u}) + \Delta\mathbf{h}_2(\mathbf{u}) + \mathbf{h}_1(\mathbf{u})\frac{\mathrm{d}}{\mathrm{d}u}\{\mathbf{n}_2(\mathbf{u}) + \mathbf{h}_2(\mathbf{u})\frac{\mathrm{d}^2}{\mathrm{d}u^2}\{\mathbf{n}_1(\mathbf{u})\}$$

$$\varepsilon^4: \quad \widetilde{\mathbf{n}}_4(\mathbf{u}) = \mathbf{n}_4(\mathbf{u}) + \Delta\mathbf{h}_3(\mathbf{u}) + \mathbf{h}_1(\mathbf{u})\frac{\mathrm{d}}{\mathrm{d}u}\{\mathbf{n}_3(\mathbf{u}) + \mathbf{h}_2(\mathbf{u})\frac{\mathrm{d}^2}{\mathrm{d}u^2}\{\mathbf{n}_2(\mathbf{u})\} + \mathbf{h}_3(\mathbf{u})\frac{\mathrm{d}^3}{\mathrm{d}u^3}\{\mathbf{n}_1(\mathbf{u})\}$$

$$\varepsilon^5: \quad \widetilde{\mathbf{n}}_5(\mathbf{u}) = \mathbf{n}_5(\mathbf{u}) + \Delta\mathbf{h}_4(\mathbf{u}) + \mathbf{h}_1(\mathbf{u})\frac{\mathrm{d}}{\mathrm{d}u}\{\mathbf{n}_4(\mathbf{u}) + \mathbf{h}_2(\mathbf{u})\frac{\mathrm{d}^2}{\mathrm{d}u^2}\{\mathbf{n}_3(\mathbf{u})\} + \mathbf{h}_3(\mathbf{u})\frac{\mathrm{d}^3}{\mathrm{d}u^3}\{\mathbf{n}_2(\mathbf{u})\} + \mathbf{h}_4(\mathbf{u})\frac{\mathrm{d}^4}{\mathrm{d}u^4}\{\mathbf{n}_1(\mathbf{u})\}$$

.

.

$$\varepsilon^n: \quad \widetilde{\mathbf{n}}_\mathbf{n}(\mathbf{u}) = \mathbf{n}_\mathbf{n}(\mathbf{u}) + \Delta\mathbf{h}_{\mathbf{n}-1}(\mathbf{u}) + \mathbf{h}_1(\mathbf{u})\frac{\mathrm{d}}{\mathrm{d}u}\{\mathbf{n}_{\mathbf{n}-1}(\mathbf{u}) + \mathbf{h}_2(\mathbf{u})\frac{\mathrm{d}^2}{\mathrm{d}u^2}\{\mathbf{n}_{\mathbf{n}-2}(\mathbf{u})\} +$$
$$\mathbf{h}_3(\mathbf{u})\frac{\mathrm{d}^3}{\mathrm{d}u^3}\{\mathbf{n}_{\mathbf{n}-3}(\mathbf{u})\} + \ldots + \mathbf{h}_{\mathbf{n}-1}(\mathbf{u})\frac{\mathrm{d}^{n-1}}{\mathrm{d}u^{n-1}}\{\mathbf{n}_1(\mathbf{u})\} = \mathbf{n}_\mathbf{n}(\mathbf{u}) + \Delta\mathbf{h}_{\mathbf{n}-1}(\mathbf{u}) + \sum_{j=1}^{n-1}\mathbf{h}_\mathbf{j}(\mathbf{u})\frac{\mathrm{d}^j}{\mathrm{d}u^j}\{\mathbf{n}_{\mathbf{n}-\mathbf{j}}(\mathbf{u})\} \tag{4.16}$$

Using Eq. 4.16, it is possible to investigate the accuracy of the solutions to any order of ε. As mentioned earlier, in the literature, the highest DNF accuracy computed is ε^2, however, in the following section two examples are selected to study the effect of raising the accuracy to ε^3; the conservative Duffing oscillator and the conservative quadratic-cubic oscillator. This effect is explored by means of computing the conservative backbone curves of the oscillators and comparing to those backbone curves computed for lower accuracies.

4.3 Examples

In this section, the conservative Duffing and the conservative quadratic-cubic oscillators are explored using the first three DNF accuracies, and the resulting backbone curves are obtained and compared.

4.3.1 Duffing oscillator

Considering the conservative Duffing oscillator governed by the EOM

$$\ddot{x}(t) + \omega_n^2 x(t) + \alpha x^3(t) = 0, \tag{4.17}$$

herein, the nonlinear term can be expressed as $N_u = \alpha x^3(t)$, so the DNF method can be symbolically applied to obtain analytical expressions of the conservative backbone curves for this oscillator as going to be shown. Final DNF analysis results are written in this section, for detailed analysis refer to discussion in Chapter 3.

Summary of ε^1 results

In this subsection, the first order term expansion; ε^1, is to discussed for the Duffing oscillator in order to compute the resulting conservative backbone curve equation. The matrices used for starting DNF analysis for the Duffing oscillator are as follows,

$$\begin{aligned}
\mathbf{u}^{(\mathbf{1})} = \begin{bmatrix} u_m^3 \\ u_p^3 \\ u_p u_m^2 \\ u_p^2 u_m \end{bmatrix} \rightsquigarrow \mathbf{n}^{(\mathbf{1})} = \alpha \begin{bmatrix} 1 \\ 1 \\ 3 \\ 3 \end{bmatrix}^{\mathsf{T}} \rightsquigarrow \boldsymbol{\beta}^{(1)} = \omega_r^2 \begin{bmatrix} 8 \\ 8 \\ 0 \\ 0 \end{bmatrix}^{\mathsf{T}} \rightsquigarrow \\
\mathbf{h}^{(\mathbf{1})} = \frac{\alpha}{8\omega_r^2} \begin{bmatrix} 1 \\ 1 \\ 0 \\ 0 \end{bmatrix}^{\mathsf{T}} \rightsquigarrow \mathbf{n}_{\mathbf{u}}^{(\mathbf{1})} = 3\alpha \begin{bmatrix} 0 \\ 0 \\ 1 \\ 1 \end{bmatrix}^{\mathsf{T}}
\end{aligned} \tag{4.18}$$

thus, ε^1 solution of Eq. 4.17 is given by

$$q = u + \mathbf{h}^{(\mathbf{1})}\mathbf{u}^{(\mathbf{1})} = (u_p + u_m) + \frac{\alpha}{8\omega_r^2}\left(u_p^3 + u_m^3\right), \tag{4.19}$$

Now, the assumed solution has the form

$$u = u_p + u_m = \frac{U}{2}\mathrm{e}^{\mathbf{i}(\omega_r t - \phi)} + \frac{U}{2}\mathrm{e}^{-\mathbf{i}(\omega_r t - \phi)}, \tag{4.20}$$

Finally, the resulting backbone curve, computed to ε^1 accuracy, is found to be

$$\omega_r^2 = \omega_n^2 + \frac{3}{4}\alpha U^2, \tag{4.21}$$

The result in Eq. 4.21 is well-known for the case of cubic nonlinearity and can be obtained using any approximate analytical technique. However, in the following subsection, the DNF analysis is extended to ε^2 in order to explore the resulting backbone curve.

Summary of ε^2 results

In this section, the first higher order term expansion; ε^2, is to be discussed for the Duffing oscillator in order to illustrate the difference of the resulting backbone curve equation compared to ε^1.

Based on ε^1 analysis, it is convenient to start by defining the following matrices

$$u_{u1}\left(u_p,u_m\right) = \mathbf{n}_{\mathbf{u}}^{(\mathbf{1})}\mathbf{u}^{(\mathbf{1})} = 3\alpha \begin{bmatrix} 0 & 0 & 1 & 1 \end{bmatrix} \begin{bmatrix} u_m^3 \\ u_p^3 \\ u_p u_m^2 \\ u_p^2 u_m \end{bmatrix} = 3\alpha\left(u_p u_m^2 + u_p^2 u_m\right), \tag{4.22}$$

$$h_1\left(u_p,u_m\right) = \mathbf{h}^{(\mathbf{1})}\mathbf{u}^{(\mathbf{1})} = \frac{\alpha}{8\omega_r^2} \begin{bmatrix} 1 & 1 & 0 & 0 \end{bmatrix} \begin{bmatrix} u_m^3 \\ u_p^3 \\ u_p u_m^2 \\ u_p^2 u_m \end{bmatrix} = \frac{\alpha}{8\omega_r^2}\left(u_p^3 + u_m^3\right), \tag{4.23}$$

Recalling that the nonlinear term is $n_1(u) = \alpha u^3$ and its Jacobian is $\dfrac{\mathrm{d}}{\mathrm{d}u}\left\{n_1(u)\right\} = 3\alpha u^2$, which gives

$$\begin{aligned} \widetilde{n}_2(u) = \mathbf{n}^{(\mathbf{2})}\mathbf{u}^{(\mathbf{2})} &= \Delta h_1\left(u_p,u_m\right) + \frac{\mathrm{d}}{\mathrm{d}u}\left\{n_1(u)\right\} h_1\left(u_p,u_m\right) \\ &= \frac{\alpha}{8\omega_r^2}\left(u_p^3 + u_m^3\right)\left(\delta + 3\alpha\left(u_p^2 + u_m^2\right)\right) \end{aligned} \tag{4.24}$$

where $\Delta = \delta = \omega_n^2 - \omega_r^2$, by expanding and decomposing $\mathbf{n}^{(\mathbf{2})}$ and $\mathbf{u}^{(\mathbf{2})}$, then the symbolic computation algorithm generated leads to the following matrices

$$\begin{aligned}
\mathbf{u}^{(\mathbf{2})} = \begin{bmatrix} u_m^3 \\ u_m^5 \\ u_p^3 \\ u_p^5 \\ u_p^3 u_m^2 \\ u_p u_m^4 \\ u_p^2 u_m^3 \\ u_p^4 u_m \end{bmatrix} \rightsquigarrow \mathbf{n}^{(\mathbf{2})} = \frac{3\alpha}{8\omega_r^2} \begin{bmatrix} \delta \\ \delta \\ 3\alpha \\ 3\alpha \\ 6\alpha \\ 6\alpha \\ 3\alpha \\ 3\alpha \end{bmatrix}^\intercal \rightsquigarrow \boldsymbol{\beta}^{(2)} = 8\omega_r^2 \begin{bmatrix} 1 \\ 3 \\ 1 \\ 3 \\ 0 \\ 1 \\ 0 \\ 1 \end{bmatrix}^\intercal \rightsquigarrow \\
\mathbf{n}_{\mathbf{u}}^{(\mathbf{2})} = \frac{3\alpha^2}{8\omega_r^2} \begin{bmatrix} 0 \\ 0 \\ 0 \\ 0 \\ 1 \\ 0 \\ 1 \\ 1 \end{bmatrix}^\intercal \rightsquigarrow \mathbf{h}^{(\mathbf{2})} = \frac{\alpha}{64\omega_r^4} \begin{bmatrix} \delta \\ \alpha \\ \delta \\ \alpha \\ 0 \\ 6\alpha \\ 0 \\ 6\alpha \end{bmatrix}^\intercal
\end{aligned} \tag{4.25}$$

thus, ε^2 equation of motion for the near identity transformation becomes

$$\ddot{u} + \omega_n^2 u + \mathbf{n}_{\mathbf{u}}^{(\mathbf{1})} \mathbf{u}^{(\mathbf{1})} + \mathbf{n}_{\mathbf{u}}^{(\mathbf{2})} \mathbf{u}^{(\mathbf{2})} = 0, \tag{4.26}$$

Finally, by substituting the assumed solution and decomposing into real and imaginary parts, one could find

the resulting backbone curve, truncated to ε^2 accuracy, which is found to be

$$\omega_r^2 = \omega_n^2 + \frac{3}{4}\alpha U^2 + \frac{3}{128\omega_r^2}\alpha^2 U^4 \tag{4.27}$$

Compared to the backbone curve computed for ε^1 accuracy, Eq. 4.21, an additional term is appearing in Eq. 4.27 which can be considered as a correction for the resulting backbone curve. Nevertheless, in the following subsection, the analysis is extended to find results of ε^3 DNF expansion for the Duffing oscillator.

Summary of ε^3 results

In this subsection, the next higher order term expansion; ε^3, is to be discussed for the Duffing oscillator in order to illustrate the difference of the resulting backbone curve equation compared to both ε^1 and ε^2.

Based on ε^2 analysis, start by defining the following

$$u_{u2}(u_p, u_m) = \mathbf{n}_{\mathbf{u}}^{(\mathbf{2})}\mathbf{u}^{(\mathbf{2})} = \frac{3\alpha^2}{8\omega_r^2}\left(u_p^3 u_m^2 + u_p^2 u_m^3\right) \tag{4.28}$$

$$h_2(u_p, u_m) = \mathbf{h}^{(\mathbf{2})}\mathbf{u}^{(\mathbf{2})} = \frac{\alpha}{64\omega_r^4}\left(\delta u_m^3 + \alpha u_m^5 + \delta u_p^3 + \alpha u_p^5 + 6\alpha u_p u_m^4 + 6\alpha u_p^4 u_m\right) \tag{4.29}$$

Referring to the derivation of ε^3 in Eq. 4.16, one may find that

$$\widetilde{n}_3(u) = \Delta h_2(u_p, u_m) + h_2(u_p, u_m)\frac{\mathrm{d}^2}{\mathrm{d}u^2}\{n_1(u)\} + h_1(u_p, u_m)\frac{\mathrm{d}}{\mathrm{d}u}\{n_2(u)\} + n_3(u_p, u_m) \tag{4.30}$$

Recalling that the nonlinear term is $n_1(u) = \alpha u^3$ and it Jacobians are $\frac{\mathrm{d}}{\mathrm{d}u}\{n_1(u)\} = 3\alpha u^2$ and $\frac{\mathrm{d}^2}{\mathrm{d}u^2}\{n_1(u)\} = 6\alpha u$. Additionally, in Eq. 4.30, $n_2(u) = n_3(u) = 0$ since no ε^2 or ε^3 terms appear in the original equation of motion, Eq. 4.17. Thus,

$$\begin{aligned}\widetilde{n}_3(u) = \mathbf{n}^{(\mathbf{3})}\mathbf{u}^{(\mathbf{3})} &= h_2(u)\left(\delta + \frac{\mathrm{d}^2}{\mathrm{d}u^2}\{n_1(u)\}\right) \\ &= \frac{\alpha}{64\omega_r^4}\left(\delta u_m^3 + \alpha u_m^5 + \delta u_p^3 + \alpha u_p^5 + 6\alpha u_p u_m^4 + 6\alpha u_p^4 u_m\right)\left(\delta + 6\alpha(u_p + u_m)\right)\end{aligned} \tag{4.31}$$

where $\Delta = \delta = \omega_n^2 - \omega_r^2$, by expanding and decomposing $\mathbf{n}^{(\mathbf{3})}$ and $\mathbf{u}^{(\mathbf{3})}$, and then the symbolic computation algorithm generated leads to the following matrices

$$\mathbf{u}^{(3)} = \begin{bmatrix} u_m^3 \\ u_m^4 \\ u_m^5 \\ u_m^6 \\ u_p^3 \\ u_p^4 \\ u_p^5 \\ u_p^6 \\ u_p^3 u_m \\ u_p u_m^3 \\ u_p u_m^4 \\ u_p u_m^5 \\ u_p^2 u_m^4 \\ u_p^4 u_m \\ u_p^4 u_m^2 \\ u_p^5 u_m \end{bmatrix} \rightsquigarrow \mathbf{n}^{(3)} = \frac{\alpha}{64\omega_r^6} \begin{bmatrix} \delta^2 \\ 6\alpha\delta \\ \alpha\delta \\ 6\alpha^2 \\ 6\alpha\delta \\ 6\alpha^2 \\ 6\alpha\delta \\ 6\alpha\delta \\ 6\alpha\delta \\ 42\alpha^2 \\ 36\alpha^2 \\ 6\alpha\delta \\ 36\alpha^2 \\ 42\alpha^2 \end{bmatrix}^{\mathsf{T}} \rightsquigarrow \boldsymbol{\beta}^{(3)} = \omega_r^2 \begin{bmatrix} 8 \\ 15 \\ 24 \\ 35 \\ 8 \\ 15 \\ 24 \\ 35 \\ 3 \\ 3 \\ 8 \\ 15 \\ 3 \\ 8 \\ 3 \\ 15 \end{bmatrix}^{\mathsf{T}} \rightsquigarrow$$

$$\mathbf{n}_{\mathbf{u}}^{(3)} = \frac{3\alpha^2}{8\omega_r^2} \begin{bmatrix} 0 \\ 0 \\ 0 \\ 0 \\ 0 \\ 0 \\ 0 \\ 0 \\ 0 \\ 0 \\ 0 \\ 0 \\ 0 \\ 0 \\ 0 \\ 0 \end{bmatrix}^{\mathsf{T}} \rightsquigarrow \mathbf{h}^{(3)} = \frac{\alpha}{64\omega_r^4} \begin{bmatrix} \frac{\delta^2}{8} \\ \frac{6\alpha\delta}{15} \\ \frac{\alpha\delta}{24} \\ \frac{6\alpha^2}{35} \\ \frac{6\alpha\delta}{15} \\ \frac{\delta^2}{8} \\ \frac{6\alpha\delta}{15} \\ \frac{6\alpha^2}{35} \\ \frac{6\alpha\delta}{3} \\ \frac{6\alpha\delta}{3} \\ \frac{6\alpha\delta}{8} \\ \frac{42\alpha^2}{15} \\ \frac{36\alpha^2}{3} \\ \frac{6\alpha\delta}{8} \\ \frac{36\alpha^2}{3} \\ \frac{42\alpha^2}{15} \end{bmatrix}^{\mathsf{T}} \tag{4.32}$$

thus, ε^3 equation of motion for the near identity transformation becomes

$$\ddot{u} + \omega_n^2 u + \mathbf{n}_{\mathbf{u}}^{(\mathbf{1})}\mathbf{u}^{(\mathbf{1})} + \mathbf{n}_{\mathbf{u}}^{(\mathbf{2})}\mathbf{u}^{(\mathbf{2})} + \mathbf{n}_{\mathbf{u}}^{(\mathbf{3})}\mathbf{u}^{(\mathbf{3})} = 0, \tag{4.33}$$

since all the elements in $\mathbf{n}_{\mathbf{u}}^{(\mathbf{3})}$ are zeros, then the term $\mathbf{n}_{\mathbf{u}}^{(\mathbf{3})}\mathbf{u}^{(\mathbf{3})} = 0$ and so it can be seen that for the Duffing oscillator, ε^3 accuracy is exactly equal to ε^2, and using the generated symbolic computations algorithm this finding can be generalised for any oscillator with odd nonlinearity (or combinations of odd stiffness nonlinearities) such as the cubic-quintic oscillator.

4.3.2 Conservative quadratic-cubic oscillator

Considering the conservative quadratic-cubic oscillator governed by the following EOM;

$$\ddot{x}(t) + \omega_n^2 x(t) + \alpha_1 x^2(t) + \alpha_2 x^3(t) = 0, \tag{4.34}$$

By repeating the same previous procedure the backbone curves, truncated to ε^1, ε^2, and ε^3 can be found to be

$$\begin{aligned}
\varepsilon^1: &\quad \omega_r^2 = \omega_n^2 + \frac{3}{4}\alpha_2 U^2 \\
\varepsilon^2: &\quad \omega_r^2 = \omega_n^2 + \frac{3}{4}\alpha_2 U^2 + \frac{3}{128\omega_r^2}\alpha_2^2 U^4 - \frac{5}{6\omega_r^2}\alpha_1^2 U^2 \\
\varepsilon^3: &\quad \omega_r^2 = \omega_n^2\left(1 - \frac{19}{6\omega_r^4}\alpha_1\alpha_2 U^2\right) + \frac{3}{4}\alpha_2 U^2 + \frac{3}{128\omega_r^2}\alpha_2^2 U^4 + \frac{105}{32\omega_r^4}\alpha_2^2\alpha_1 U^4 - \\
&\qquad \frac{5}{6\omega_r^2}\alpha_1^2 U^2 - \frac{19}{6\omega_r^2}\alpha_1\alpha_2 U^2
\end{aligned} \tag{4.35}$$

In Fig. 4.1, the analytical conservative backbone curves for quadratic-cubic oscillator in Eq. 4.34 are plotted, using ε^1, ε^2 and ε^3 DNF analysis results in Eq. 4.35, additionally, the COCO numerically computed backbone curve is also generated and plotted in this figure. The numerical values are: $\omega_n = 1$ rad/s, $\alpha_1 = 0.1$, $\alpha_2 = 0.1$ and for COCO backbone curve very small damping ratio of $\zeta = 0.001$ is used. It is worth mentioning that the nonlinear coefficients, α_1 and α_2, are selected to be small in order to indicate weak nonlinearities. The results in Fig. 4.1 reveal that ε^3 accuracy backbone curve represents an intermediate solution compared to both ε^1 and ε^2, and due to the small effects of the nonlinear terms the difference between the solutions is small. Moreover, perfect matching between the analytically computed ε^3 backbone curve and numerically generated backbone

curve (using COCO), which indicate that the DNF technique truncated to ε^3 gives high accuracy in comparison to the numerical results.

An important point to mention, according to the researcher best knowledge, in order to find the numerically computed backbone curve in COCO, a certain damping ratio should be assigned, thus the value of $\zeta = 0.001$ is adopted which best fits with the conservative backbone curves computed using the proposed results in Eq. 4.35. Nevertheless, having a precise vision of the simulation results, it is possible to find very minor differences between the DNF conservative backbone curve of ε^3 and COCO backbone curve; for instance, due to the natural frequency selected, the conservative DNF backbone curves are initiated at the exact value of $\omega_n = 1.0$, while the generated COCO backbone curve is initiated at $\omega_d = \sqrt{1.0-(0.001)^2} = 0.9999995$, accordingly, the differences between the two curves are negligible, and the matching is described to be perfect.

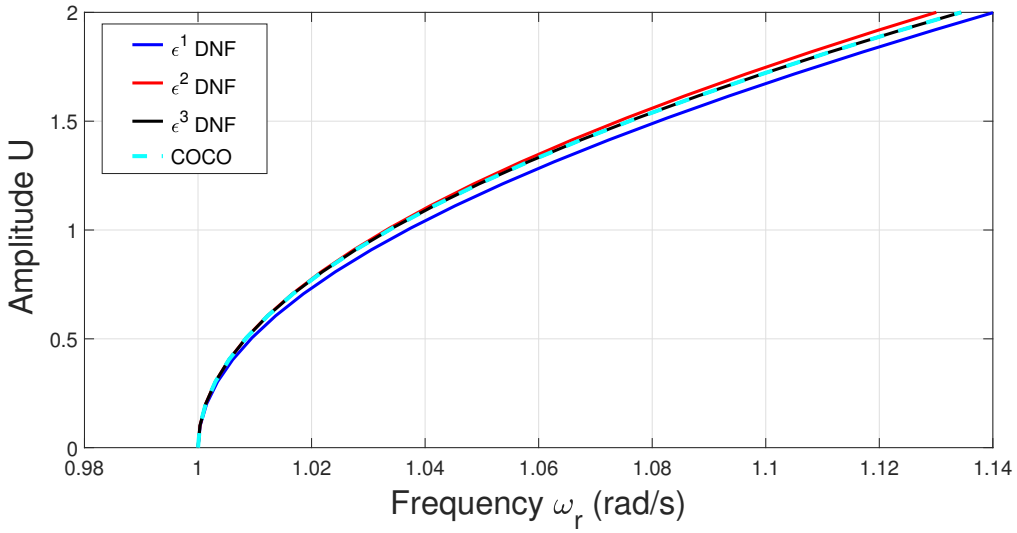

Figure 4.1: Comparing ε^1 (solid blue line), ε^2 (solid red line) and ε^3 (solid black line) DNF conservative backbone curves with the numerically computed backbone curve (dashed line) using COCO toolbox in MATLAB for the conservative quadratic-cubic oscillator in Eq. 4.34. Parameter values are: $\omega_n = 1$ rad/s, $\alpha_1 = 0.1$ and $\alpha_2 = 0.1$.

Similarly, if the effect of the nonlinear terms is significantly raised, greater differences between ε^1, ε^2 and ε^3 results are noticed for this quadratic-cubic oscillator. In Fig. 4.2 the nonlinear coefficients, α_1 and α_2, are selected to have higher values so that the differences are clearly visible. Nonetheless, compared to the numerically generated COCO backbone curve (plotted with small damping of $\zeta = 0.001$), the DNF backbone curve truncated to ε^3 still shows perfect matching.

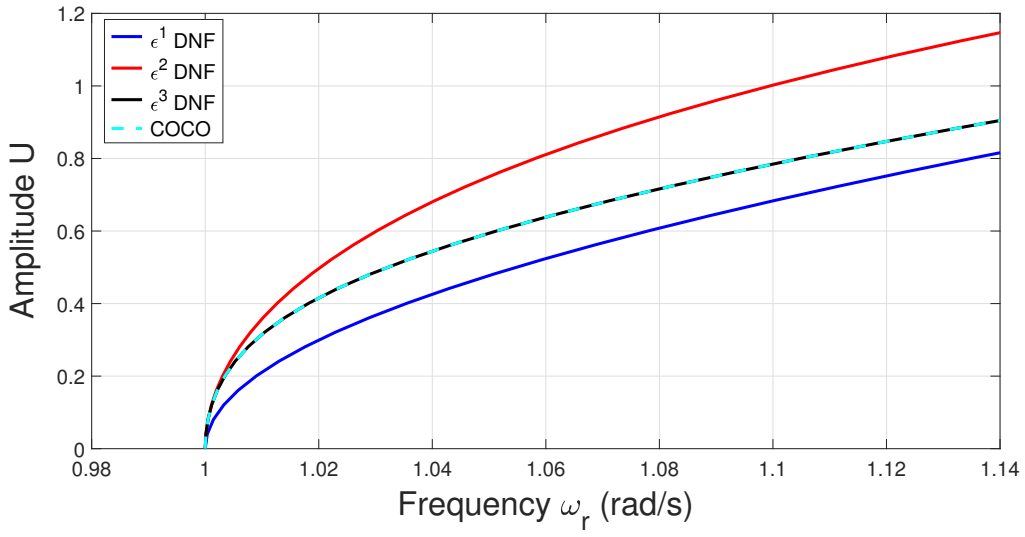

Figure 4.2: Comparing ε^1 (solid blue line), ε^2 (solid red line) and ε^3 (solid black line) DNF conservative backbone curves with the numerically computed backbone curve (dashed line) using COCO toolbox in MATLAB for the conservative quadratic-cubic oscillator in Eq. 4.34. Parameter values are: $\omega_n = 1$ rad/s, $\alpha_1 = 0.6$ and $\alpha_2 = 0.6$.

4.4 Damped backbone curves

In this subsection, a method is presented that can be applied directly for the case of linear viscous damping, and leads to approximate damped backbone curves expressions for nonlinear oscillators. To start, consider the example of a damped nonlinear oscillator of the form

$$\ddot{x} + 2\zeta\omega_n\dot{x} + \omega_n^2 x + \varepsilon f(x) = 0, \tag{4.36}$$

where $\omega_n = \sqrt{k/m}$ is the linear natural frequency, $\zeta = c/2m\omega_n$ is the damping ratio, ε is a small parameter and $f(x)$ is a nonlinear function of x. Here m is the mass in kg, k is linear stiffness in N/m and c is viscous damping coefficient in kg/s. For linear differential equations with viscous damping, using the Wentzel, Kramers & Brillouin (WKB) transformation, [93–95], one can remove the damping term as will be discussed later on. This method of transformation is also called the "method of reduction of order" [92] or the "normal form" [96]. The method in the form presented here is a variation on the WKB method, where an assumed solution is selected such that when substituted into Eq. 4.36 the transformed equation of motion does

$$x = \quad q(t)\mathrm{e}^{-\zeta\omega_n t}. \tag{4.37}$$

Then for the linear case, when $\varepsilon = 0$, substituting Eq. 4.37 into Eq. 4.36 gives

$$\ddot{q} + \omega_d^2 q = 0, \tag{4.38}$$

where $\omega_d = \omega_n \sqrt{1-\zeta^2}$ is the damped natural frequency. Eq. 4.38 is a linearised version of Eq. 4.36 that has been transformed into what appears to be an undamped (conservative) oscillator with a damped natural frequency, ω_d. Eq. 4.38 has solutions which are an infinite family of periodic solutions that depend on the initial conditions, $q(0)$ and $\dot{q}(0)$. For the nonlinear case, when $\varepsilon \neq 0$, this family of periodic solutions will correspond to the the *damped nonlinear normal mode(s)* with associated *damped backbone curve(s)*. In the next section, using the case of cubic nonlinearity, it is shown how the WKB approach is directly applied to nonlinear systems in order to compute approximations for damped backbone curves.

4.4.1 The cubic nonlinearity case

Considering the case when $\varepsilon \neq 0$, and $f(x) = \alpha x^3$ (i.e. the Duffing oscillator), then substituting Eq. 4.37 into Eq. 4.36 leads to

$$\ddot{q} + \omega_d^2 q + \varepsilon \mathrm{e}^{-3\zeta\omega_n t} \alpha q^3 = 0, \tag{4.39}$$

so that a time dependent exponential function appears as part of the nonlinear term. Dealing with this type of equation presents obvious difficulties, those to be discussed in detail later. But first a method is designed to overcome the difficulties for a more general class of nonlinear oscillators.

4.4.2 Burton's method

In the work of Burton, [90], the approximation $\omega^2(t)x = \omega_n^2 x + \varepsilon f(x)$ is made, so that the general expression for the nonlinear oscillator, Eq. 4.36, becomes

$$\ddot{x} + 2\zeta\omega_n \dot{x} + \omega^2(t)x = 0, \tag{4.40}$$

where $\omega(t)$ is a time varying "frequency" function. Using the transformation where $x(t) = q(t)e^{-\zeta\omega_n t}$ substituted into Eq. 4.40 the following can be obtain

$$\ddot{q} + \hat{\omega}_d(t)^2 q = 0, \tag{4.41}$$

where $\hat{\omega}_d(t)^2 = \omega^2 - \zeta^2\omega_n^2$ is a time varying approximation to the damped natural frequency of the system (similar results where obtained by [98]). Note also that in the case $\omega(t)$ is periodic, then Eq. 4.41 is a form of the widely studied Hill equation, [97].

4.4.3 Finding approximate solutions to Eq. 4.41

Using a similar approach to [90, 98], a trial solution of $q = u_p + u_m$ is now assumed, where

$$u_p = \frac{U(t)}{2}e^{\mathbf{i}\psi(t)} \quad \text{and} \quad u_m = \frac{U(t)}{2}e^{-\mathbf{i}\psi(t)}, \tag{4.42}$$

where $U(t)$ is a time dependent amplitude, and $\psi(t)$ is a time dependent phase. The following relationships are assumed to hold for $\psi(t)$

$$\frac{\mathrm{d}}{\mathrm{d}t}\psi(t) = \omega_r(t) \quad \text{and} \quad \psi(0) = \psi_0 \tag{4.43}$$

where $\omega_r(t)$ is the time dependent response frequency and ψ_0 is the phase lag (assumed to be independent of time). Using those definitions, it is possible to get

$$q(t) = U(t)\left(\frac{e^{\mathbf{i}\psi(t)} + e^{-\mathbf{i}\psi(t)}}{2}\right) = U(t)\cos(\psi(t)) \tag{4.44}$$

Substituting into Eq. 4.41 and equating the coefficients of the exponential terms gives

$$\begin{aligned} \ddot{U} + \mathbf{i}\dot{\omega}_r U + 2\mathbf{i}\omega_r\dot{U} + (\omega_d(t)^2 - \omega_r^2)U = 0, \\ \ddot{U} - \mathbf{i}\dot{\omega}_r U - 2\mathbf{i}\omega_r\dot{U} + (\omega_d(t)^2 - \omega_r^2)U = 0. \end{aligned} \tag{4.45}$$

which are complex conjugate expressions. Now, it is possible to compare the coefficients of the real and imaginary parts of either equations in Eq. 4.45 to get

$$\begin{aligned} \text{Re:} \quad & \ddot{U} + (\hat{\omega}_d^2 - \omega_r^2)U = 0, \\ \text{Im:} \quad & \frac{\dot{\omega}_r}{2\omega_r} + \frac{\dot{U}}{U} = 0. \end{aligned} \tag{4.46}$$

The second equation in Eq. 4.46 can be solved in the following way

$$\begin{aligned} \int_0^t -\frac{\dot{\omega}_r(\tau)}{2\omega_r(\tau)}\mathrm{d}\tau = \int_0^t \frac{\dot{U}(\tau)}{U(\tau)}\mathrm{d}\tau \quad &\rightsquigarrow \quad -\frac{1}{2}\ln\left(\omega_r(\tau)\right)\Big|_0^t = \ln\left(U(\tau)\right)\Big|_0^t \quad \rightsquigarrow \quad \ln\left(\frac{\omega_r(t)}{\omega_r(0)}\right)^{-\frac{1}{2}} = \ln\left(\frac{U(t)}{U(0)}\right) \\ &\rightsquigarrow \quad \left(\frac{\omega_r(0)}{\omega_r(t)}\right)^{\frac{1}{2}} = \frac{U(t)}{U(0)} \quad \rightsquigarrow \quad U(t) = U(0)\left(\frac{\omega_r(0)}{\omega_r(t)}\right)^{\frac{1}{2}} \end{aligned} \tag{4.47}$$

where τ is a dummy variable. Then, the final result in Eq. 4.47 gives the relationship between the time-dependent amplitude and the time-dependent frequency. As a result, based on the finding in Eq. 4.44 and the transformation of $x(t) = q(t)\mathrm{e}^{-\zeta\omega_n t}$, Eq. 4.40, the complete solution can be written as

$$\frac{x(t)\mathrm{e}^{\zeta\omega_n t}}{\cos\psi(t)} = U(0)\left(\frac{\omega_r(0)}{\omega_r(t)}\right)^{\frac{1}{2}} \quad \rightsquigarrow \quad x(t) = \mathrm{e}^{-\zeta\omega_n t}X(0)\left(\frac{\omega_r(0)}{\omega_r(t)}\right)^{\frac{1}{2}}\cos\psi(t) \tag{4.48}$$

where $X(0) = Q(0) = U(0)$ is the initial amplitude of displacement at time $t = 0$ (assuming for now that $\psi_0 = 0$). From Eq. 4.48 the amplitude decay of the solution can be defined as

$$\frac{x(t)}{X(0)} = \mathrm{e}^{-\zeta\omega_n t}\left(\frac{\omega_r(0)}{\omega_r(t)}\right)^{\frac{1}{2}} \quad \rightsquigarrow \quad t = \frac{1}{\zeta\omega_n}\ln\left[\frac{X(0)}{x(t)}\left(\frac{\omega_r(0)}{\omega_r(t)}\right)^{\frac{1}{2}}\right] \tag{4.49}$$

which can be used to get an expression for the time dependent amplitude decay of the oscillator. As noted, the first equation of Eq. 4.46 is a conservative oscillator equation with frequency $\sqrt{\hat{\omega}_d^2 - \omega_r^2}$. To find a solution for this and Eq. 4.49, more specific details are needed for the exact form of $\omega(t)$. Generally this type of Hill equation is approximated using a Fourier type expansion, but it depends on the specific properties of the frequency function. To proceed, it is convenient to discuss Burton's method for the solutions of the Duffing oscillator [90].

4.4.4 Burton's solution for the Duffing oscillator

To continue, Burton's method then computes the response frequency by studying the original problem Eq. 4.36 but without damping ($\zeta = 0$) and with $f(x)$ defined. Using harmonic balance, or a normal from method (see for example [99]) applied to the Duffing oscillator (i.e. $f(x) = \alpha x^3$), the following backbone curve relationship is obtained up to ε^1 accuracy

$$\omega_r(t) = \sqrt{\omega_n^2 + \varepsilon \frac{3\alpha}{4} U(t)^2} \quad \text{and} \quad \omega_r(0) = \sqrt{\omega_n^2 + \varepsilon \frac{3\alpha}{4} U(0)^2}. \tag{4.50}$$

These expressions give frequency approximations, and can be used in Eq. 4.49 to give amplitude approximations.

4.4.5 An approximation for small damping

If the viscous damping is sufficiently small, then an assumption that $2\zeta\omega_n = \hat{\varepsilon}$ can be assumed, where $\hat{\varepsilon} \ll 1$ and the nonlinear parameter α can be rescaled such that $\hat{\varepsilon}\hat{\alpha} = \varepsilon\alpha$. Then it is possible to rewrite the oscillator equation of motion as

$$\ddot{x} + \hat{\varepsilon}\dot{x} + \omega_n^2 x + \hat{\varepsilon} f(x) = 0, \tag{4.51}$$

or for the example of the Duffing oscillator

$$\ddot{x} + \hat{\varepsilon}\dot{x} + \omega_n^2 x + \hat{\varepsilon}\hat{\alpha}x^3 = 0, \tag{4.52}$$

then, by applying the WKB approach using $x = q(t)\mathrm{e}^{-\frac{\hat{\varepsilon}}{2}t}$, which gives

$$\ddot{q} + \omega_d^2 q + \hat{\varepsilon}\mathrm{e}^{-\hat{\varepsilon}t}\hat{\alpha}q^3 = 0. \tag{4.53}$$

Now, by applying an approximation of the exponential function $\mathrm{e}^{-\hat{\varepsilon}t} = 1 - \hat{\varepsilon}t + \ldots\mathscr{O}(\hat{\varepsilon}^2 t^2)$ one should obtain

$$\ddot{q} + \omega_d^2 q + \hat{\varepsilon}(1 - \hat{\varepsilon}t)\hat{\alpha}q^3 = 0 \rightsquigarrow \ddot{q} + \omega_d^2 q + \hat{\varepsilon}\hat{\alpha}q^3 + \ldots\mathscr{O}(\hat{\varepsilon}^2) = 0. \tag{4.54}$$

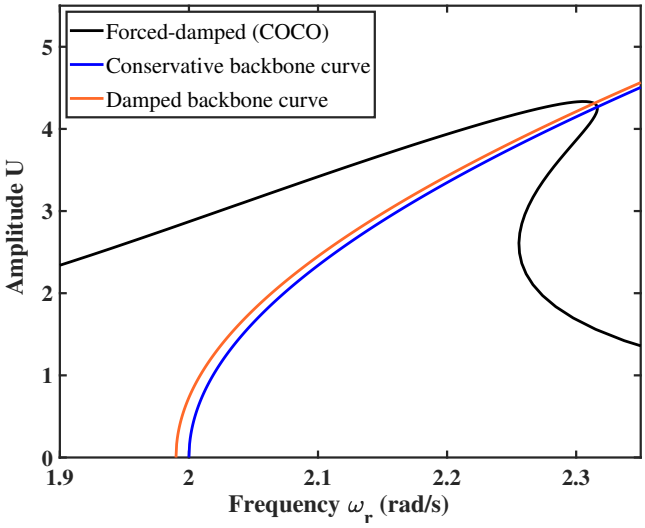

Figure 4.3: Conservative (undamped) and damped backbone curves when $\varepsilon\alpha = 0.4$, $\omega_n = 2$ rad/s and $\zeta = 0.1$. The damped backbone curve can be compared to the forced-damped frequency response curves (denoted 'Forced-damped (COCO)' in the legend) computed using COCO, this forced-damped frequency response shows both stable and unstable parts as a single solid line.

Finally, by applying a normal form transformation (or harmonic balance method) to Eq. 4.54, an approximate frequency-amplitude relationship is obtained, or the damped backbone curve of this oscillator, [8].

$$\omega_r \approx \sqrt{\omega_d^2 + \varepsilon \frac{3\alpha}{4} U^2} \tag{4.55}$$

where the rescaling has been removed, and since a steady-state solution is desired, ω_r and U are both assumed to be time independent. A numerical example is shown in Fig. 4.3, where the damped backbone curves (given by Eq. 4.55) are plotted along with the undamped (conservative) backbone curves, which is governed by the same expression as Eq. 4.55 but with ω_d replaced by ω_n on the right-hand side.

In order to study the effect of changing the nonlinear coefficient, α, for the Duffing oscillator, in both hardening and softening cases, Fig. 4.4 has been generated for the case when $\omega_n = 1$ rad/s and $\zeta = 0.1$ and a range of both negative and positive α values. The damped backbone curves are computed using the proposed approximate technique while the forced-damped frequency response curves are found using numerical continuation (COCO toolbox in MATLAB). From Fig. 4.4 it is clear that, for each value of the nonlinear coefficient, the damped backbone curves follow the curvature of the resonant peak defined by the forced-damped frequency response curves, and the two lines cross close to the peak of each forced-damped frequency response curve.

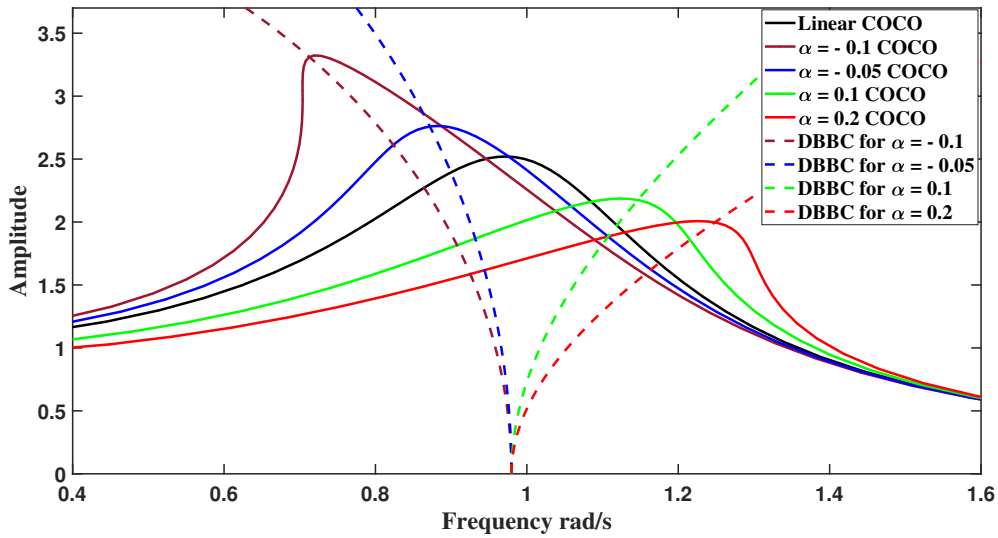

Figure 4.4: Damped backbone curves (denoted DBBC in the legend) for different values of α, when $\varepsilon = 1$, $\omega_n = 1$ rad/s and $\zeta = 0.1$ compared to the forced-damped frequency response curves (denoted COCO in the legend). The linear forced-damped frequency response curve (denoted 'Linear COCO' in the legend) is plotted for comparison. Note that because ζ and ω_n are constants the damped backbone curves all start from the same point on the Frequency axis.

This level of matching occurs, despite the truncation at order ε^2, and demonstrates the potential usefulness of this simple and direct method in order to obtain an approximation to the damped backbone curve.

In order to investigate the effect of varying the damping ratio on the overall results of this method, Fig. 4.5 shows the frequency-amplitude response for the damped Duffing oscillator when ζ is varied. The numerical values chosen for this graph are $\varepsilon\alpha = 0.4$, $\omega_n = 1$ rad/s. From this figure, it is noticed that the damped backbone curves start from the damped natural frequency, ω_d on the horizontal axis, and for each value of ζ the damped backbone curves and the forced-damped frequency response curves intersect at a similar position to the results shown in the previous two figures.

4.5 Analysis of SDOF systems with polynomial type nonlinearities

Considering a SDOF nonlinear oscillator with polynomial nonlinear stiffness term and small viscous damping, then the EOM can be studied using the method of direct normal form, Section 3.1. The general form for this SDOF oscillator is

$$\ddot{x} + \varepsilon\dot{x} + \omega_n^2 x + \varepsilon f(x) = 0, \tag{4.56}$$

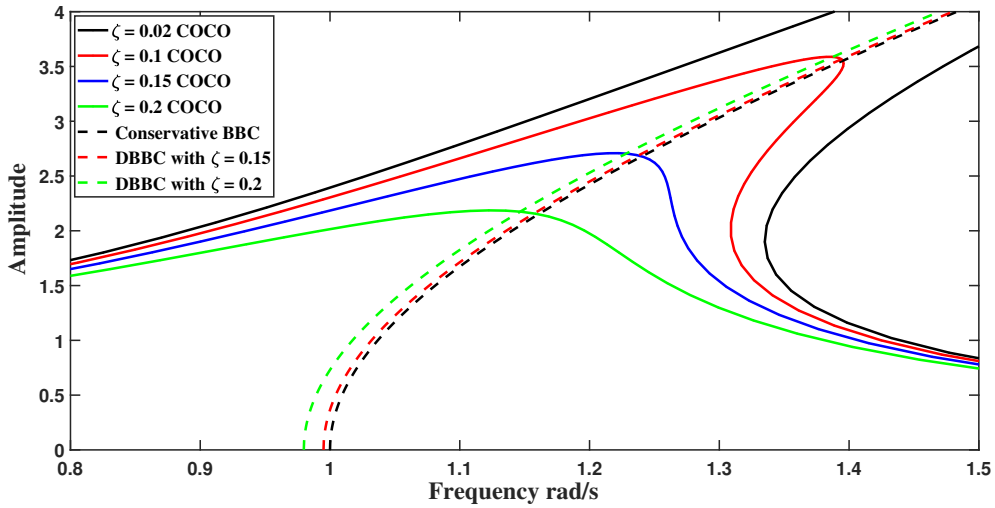

Figure 4.5: Damped backbone curves (denoted DBBC in the legend) for different values of ζ, when $\varepsilon\alpha = 0.4$ and $\omega_n = 1$ rad/s, compared to the forced-damped frequency response curves (denoted COCO in the legend). The conservative backbone curve with $\zeta = 0$ (denoted 'conservative BBC' in the legend) is shown for comparison. The forced-damped frequency response curves represent both stable and unstable parts of the solution.

where the nonlinear vector $f(x)$ contains all the polynomial nonlinear stiffness terms. Using a normal form method (or any other appropriate method such as harmonic balance), it is possible to find the conservative backbone curve, computed in this case to ε^1 accuracy (and in principle, for any degree of the polynomial nonlinearity). As shown above, the approximate expressions for the damped backbone obtained in this way replace the natural frequency, ω_n, with the damped natural frequency, ω_d. This approximation of the damped backbone curve is restricted to weak nonlinearities and small damping, however, compared to other techniques, the simplicity of this technique has the potential to be useful for some non-conservative systems. It is noteworthy that ε^1 normal form analysis in this work is able to precisely detect the effect of odd nonlinear terms appearing in the equations of motion, while for even nonlinearities the analysis needs to extended to include ε^2.

4.5.1 Example: Cubic-quintic oscillator with viscous damping

The problem of a cubic-quintic viscously damped SDOF oscillator will be briefly discussed using the method of DNF in Section 5.1, however, based on the aforementioned discussions in this Chapter, it will be shown how the damped backbone curves can be directly obtained from the conservative backbone curves for this kind of oscillators. In the literature, the conservative case of this oscillator has been studied by a number of authors, e.g. [18, 102, 103]. The equation of motion for the damped-unforced cubic-quintic nonlinear oscillator can be

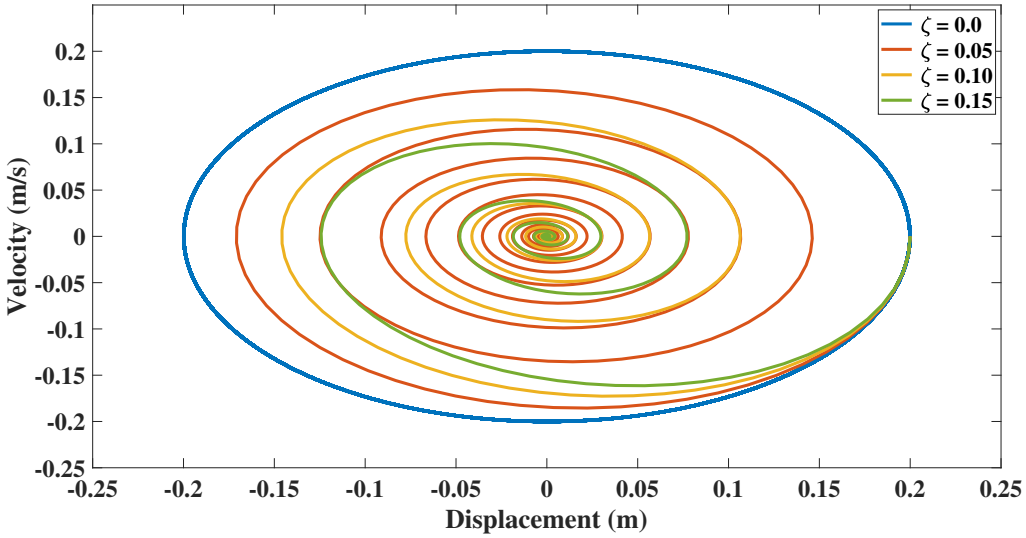

Figure 4.6: Phase portrait for the damped cubic-quintic when $\varepsilon\alpha = 0.1$, $\omega_n = 2$ rad/s and different values of ζ.

written as

$$\ddot{x} + \varepsilon\dot{x} + \omega_n^2 x + \varepsilon\alpha_1 x^3 + \varepsilon\alpha_2 x^5 = 0, \tag{4.57}$$

where $\varepsilon \approx 2\zeta\omega_n$ and the the coefficients of the nonlinear terms are assumed to be relatively small. In order to visually illustrate the damping effect for this system, Eq. 4.48 can be used to generate the phase portrait for this oscillator for the any given initial condition. For example, Fig. 4.6 shows the phase portrait for the cubic-quintic oscillator for various values of ζ at the following initial conditions $x(0) = 0.2$ m and $\dot{x}(0) = 0.0$ m/s.

Now, ε^1 normal form analysis can be applied to Eq. 4.57 in order to find the damped backbone curve of this oscillator, [104], which gives

$$\omega_r = \sqrt{\omega_d^2 + \varepsilon\frac{3\alpha_1}{4}U^2 + \varepsilon\frac{5\alpha_2}{8}U^4} \tag{4.58}$$

Accordingly, Eq. 4.58 can be directly used to obtain the damped backbone curves for this oscillator for small damping.

4.6 Summary

In this Chapter, two main topics are briefly discussed; the higher order accuracies of the DNF method, and the damped backbone curves. For the higher order accuracies, after discussing ε^2 case of accuracy, this is followed,

thanks to the powerful mathematical tools of the symbolic computations approach, by a novel improvement to the method of DNF to be investigated to any order of accuracy, i.e. ε^n.

Regarding higher order accuracies, the discussions practised in this Chapter yield to the following observations;

- In Section 4.1, ε^2 accuracy is investigated symbolically to give the same results found in literature by the traditionally applied DNF, refer to [8].
- The analysis performed in Section 4.2 represents the capability of applying the method of DNF to any accuracy ε^n, and this is applied to the example of a conservative Duffing oscillator and conservative quadratic-cubic oscillator in Section 4.3.
- For the example system of Duffing oscillator, it is observed that the results of ε^3 is exactly equivalent to those of ε^2, thus for the Duffing oscillator, and any oscillator with only odd nonlinear term (or terms), the DNF technique should be only applied to ε^2 accuracy.
- For the example system of quadratic-cubic oscillator, ε^3 accuracy lead to modified results compared to lower order accuracies, which implies the need of extending the analysis to higher order accuracies, as discussed in Section 4.2.
- The aforementioned analysis can lead to broader discussions regarding the nature of the DNF method in comparison with other normal forms technique; as a primary finding, it is possible to classify the method of DNF as minimal normal form technique, refer to [69] for broader discussions regarding this type of normal forms.

In connection to the subject of damped backbone curves, the following observations are seen;

- The method described in Section 4.4 represents a novel approximate technique of calculating the damped backbone curves of viscously damped systems.
- Although it needs more in-depth improvements, this method is considered sufficiently accurate for systems with light damping, so it can be practically used to many engineering applications.
- Compared to conservative backbone curves, the damped backbone curves yield to better matching between the backbone curves and the forcing frequency manifolds, refer to Fig. 4.3 and the discussions

beneath it.

- As a potential future frame work, this direct technique can be applied to MDOF systems considering the fact that, when generating the frequency-amplitude relationship for weakly nonlinear MDOF systems with small damping, the natural frequencies can be directly replaced with the damped natural frequencies and then the backbone curves can be compared to the forced frequency response curves.

Chapter 5

Applications to SDOF systems

In this Chapter, the DNF method is applied to several engineering applications of SDOF cases. Initially, an analytical study of nonlinear oscillators with different combinations of geometric polynomial stiffness nonlinearities is presented. To do this, the method of direct normal forms (DNF) is applied symbolically using Maple software. Accordingly, closed form (approximate) expressions of the corresponding frequency-amplitude relationships (or backbone curves) are obtained for both ε^1 and ε^2 expansions, and a general pattern for ε^1 truncation is presented in the case of odd nonlinear terms.

Furthermore, direct normal form analysis (DNF) is used to analytically explore the steady-state frequency response of Van der Pol, Rayleigh oscillators, in addition to some other oscillators with combinations of stiffness and damping nonlinearities, including Van-der-Pol-Duffing, Rayleigh-Duffing, Van-der-Pol cubic-quintic and Rayleigh cubic-quintic oscillators. In all cases under consideration, the oscillators are driven by a harmonic excitation near the resonance. The approximate analytical results are truncated to ε^1 accuracy and, for verification purposes, they are compared to numerical results obtained by MatCont numerical continuation toolbox in MATLAB.

5.1 Analysis of cubic-quintic SDOF oscillator

In this section, the analysis of different types of nonlinear oscillator is briefly discussed. The first example illustrates the conservative (undamped and unforced) cubic-quintic oscillator, which has been previously studied

by a range of other researchers and so the results of DNF can be compared to their work. For instance, in [83], Lai et al. have implemented a Newton-harmonic balancing approach to obtain first, second, and third-order approximations to the frequency-amplitude relationship for this type of SDOF oscillators. The interested reader can also find some other related works that study this system, see for example [33, 102, 103].

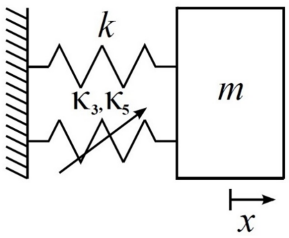

Figure 5.1: Schematic diagram of the cubic-quintic oscillator shown in Eq. 5.1.

The conservative cubic-quintic oscillator, as shown schematically in Fig. 5.1, is governed by the following equation of motion.

$$m\ddot{x}(t)+kx(t)+\kappa_3 x^3(t)+\kappa_5 x^5(t)=0 \Rightarrow \ddot{x}(t)+\omega_n^2 x(t)+\alpha_1 x^3(t)+\alpha_2 x^5(t)=0, \tag{5.1}$$

where over dots represent the derivative with respect to time, x represents the physical displacement, m is the mass of the oscillator, and the linear, cubic and quintic stiffnesses are k, κ_3 and κ_5, respectively. The subscripts are chosen to reflect the order of the nonlinearity (this can be helpful when studying multi-degree-of-freedom systems, as will be discussed in Chapter 7). Moreover, ω_n is the natural frequency of the system, α_1 and α_2 are (assumed to be small) coefficients for the cubic and quintic nonlinear terms, respectively. Firstly, by applying the linear modal transformation, the transformation is unity so $x=q$, and this is applicable for any SDOF system, then

$$\ddot{q}+\Lambda q+N_q(q)=0, \tag{5.2}$$

where $\Lambda=\omega_n^2$ and $N_q(q)=\alpha_1 q^3+\alpha_2 q^5$. The second step is the near-identity transformation, and for ε^1 accuracy, rewriting the nonlinear terms using u, in view of Eq. 3.1, one should obtain $N_q(u)=\alpha_1 u_1^3+\alpha_2 u_1^5$, thus

$$n_{(1)}(u)=\mathbf{n}^*\mathbf{u}^*\ (u_p,m_m)=\alpha_1(u_p+u_m)^3+\alpha_2(u_p+u_m)^5, \tag{5.3}$$

By expanding Eq. 5.3, $n_{(1)}(u)$ will contain many terms (ten terms in this case), these terms have to be primarily decomposed into coefficients and nonlinear functions vectors $\mathbf{n}^*$ and $\mathbf{u}^*$, respectively. For this example

$$\mathbf{n}^* = \begin{bmatrix} \alpha_1 & \alpha_2 & \alpha_1 & \alpha_2 & 3\alpha_1 & 5\alpha_2 & 3\alpha_1 & 10\alpha_2 & 10\alpha_2 & 5\alpha_2 \end{bmatrix} \tag{5.4}$$

$$\mathbf{u}^* = \begin{bmatrix} u_m^3 & u_m^5 & u_p^3 & u_p^5 & u_p u_m^2 & u_p u_m^4 & u_p^2 u_m & u_p^2 u_m^3 & u_p^3 u_m^2 & u_p^4 u_m \end{bmatrix} \tag{5.5}$$

The crucial step in this solution is solving the homological equation by finding the $\boldsymbol{\beta}^*$ matrix (refer to Eq. 3.14 and Eq. 3.15). To proceed, the polynomial term indices (defined by s_p and s_m) in the vector $\mathbf{u}^*$ need to be found.

In the present study, the above analysis has been implemented symbolically, and in principle this approach can be extended to any finite number of terms in Eq. 5.4. The next step defines the transformed nonlinear terms ($\mathbf{n}^*_{\mathbf{u},\mathbf{l}}$) and harmonics ($\mathbf{h}^*_{\mathbf{l}}$) matrices, (refer to Eq. 3.16). Practically, in Maple, this is performed by applying several iterative loops for each element in $\boldsymbol{\beta}^*$.

For this example system, Table 5.1 shows all the terms in Eq. 5.3 and the corresponding s_p, s_m and $\boldsymbol{\beta}^*$. It is noteworthy to mention that traditional hand calculations are performed by generating matrices (or tables) similar to Table 3.1, which quickly becomes impractical for more complex systems. On the other hand, the proposed symbolic computation method automatically generates all of these matrices, thus eliminates the chance of any mathematical errors, reduces the time and effort of computation and enables the study of more complex systems (within the constraint of the available computing power). If the truncated solution is limited to ε^1 order, the final step is rewriting the transformed equation of motion. For the non-resonant terms to ε^1 accuracy, the equation of motion in the u-transformed coordinate system becomes

$$\ddot{u} + \Lambda u + \mathbf{N}^*_{\mathbf{u}} \mathbf{u}^* = 0, \tag{5.6}$$

which can be written as

$$\ddot{u} + \omega_n^2 u + 3\alpha_1 (u_p u_m^2 + u_p^2 u_m) + 10\alpha_2 (u_p^2 u_m^3 + u_p^3 u_m^2) = 0, \tag{5.7}$$

and the near identity transformation is written as

$$q = u + \mathbf{h}^* \mathbf{u}^*, \tag{5.8}$$

which leads to

$$q = u + \frac{1}{8\omega_r^2}\left(\alpha_1(u_p^3 + u_m^3) + \frac{\alpha_2}{3}(u_p^5 + u_m^5) + 5\alpha_2(u_p^4 u_m + u_p u_m^4)\right) \tag{5.9}$$

In order to generate a time domain solution of the system, one can easily substitute the assumed solution, Eq. 3.27 into Eq. 5.9. Nevertheless, the focus in this work is to study the frequency amplitude relationship for the conservative (i.e., undamped) system, or the so-called conservative backbone curve. This can be also obtained by substituting in the assumed solution and solving the positive (or negative) complex exponential terms using exact harmonic balancing. Finally, using this approach the backbone curve, truncated to ε^1 accuracy, is expressed as

$$\omega_r^2 = \omega_n^2 + \frac{3}{4}\alpha_1 U^2 + \frac{5}{8}\alpha_2 U^4 \tag{5.10}$$

This form of ε^1 order backbone curve will be adopted for analysing the nonlinear frequency of the cubic-quintic oscillator, however, the results of Eq. 5.10 will also be compared to ε^2 solution, as will be discussed in the next Section.

Table 5.1: DNF matrix results for the cubic-quintic oscillator computed to ε^1 accuracy, if β^*=0, a resonance is indicated, otherwise the term is considered to be a non-resonant term

$\mathbf{u}^*$	$\mathbf{s_p}$	$\mathbf{s_m}$	β^*	$\mathbf{n}^*_{\mathbf{u,l}}$	$\mathbf{h}^*_{\mathbf{l}}$
u_m^3	0	3	$8\omega_r^2$	0	$\frac{\alpha_1}{8\omega_r^2}$
$3u_m^5$	0	5	$24\omega_r^2$	0	$\frac{\alpha_1}{24\omega_r^2}$
u_p^3	3	0	$8\omega_r^2$	0	$\frac{\alpha_1}{8\omega_r^2}$
u_p^5	5	0	$24\omega_r^2$	0	$\frac{\alpha_1}{24\omega_r^2}$
$u_p u_m^2$	1	2	0	$3\alpha_1$	0
$u_p u_m^4$	1	4	$8\omega_r^2$	0	$\frac{5\alpha_2}{8\omega_r^2}$
$u_p^2 u_m$	2	1	0	$3\alpha_1$	0
$u_p^2 u_m^3$	2	3	0	$10\alpha_2$	0
$u_p^3 u_m^2$	3	2	0	$10\alpha_2$	0
$u_p^4 u_m$	4	1	$8\omega_r^2$	0	$\frac{5\alpha_2}{8\omega_r^2}$

5.1.1 Higher order accuracy

A direct normal form analysis of ε^2 expansion for the same cubic-quintic oscillator is to be discussed in this subsection. The solution is based on the results of ε^1 accuracy, hence, it is possible to write

$$u_u = \mathbf{n}_\mathbf{u}^* \mathbf{u}^* = 3\alpha_1(u_p u_m^2 + u_p^2 u_m) + 10\alpha_2(u_p^2 u_m^3 + u_p^3 u_m^2) \tag{5.11}$$

$$\mathbf{n}_\mathbf{u}^* \mathbf{u}^* = \frac{1}{8\omega_r^2}\left(\alpha_1(u_p^3 + u_m^3) + \frac{\alpha_2}{3}(u_p^5 + u_m^5) + 5\alpha_2(u_p^4 u_m + u_p u_m^4)\right) \tag{5.12}$$

moreover, $n_1(u) = \alpha_1 u^3 + \alpha_2 u^5$ and its Jacobian is $\dfrac{\mathrm{d}}{\mathrm{d}u}(n_1(u)) = 3\alpha_1 u^2 + 5\alpha_2 u^4$. Now, the pre-transformed nonlinear term, $\tilde{n}_2$, is given by

$$\tilde{n}_2 = \frac{1}{4\omega_r^2}\left(\frac{\alpha_1}{4} + \frac{\alpha_2}{12} + \frac{5\alpha_2}{4}\right)\left((\omega_n^2 - \omega_r^2) + (3\alpha_1 u^2 + 5\alpha_2 u^4)\right) \tag{5.13}$$

Herein, it is important to notice that no ε^2 related terms appear in the original EOM, and so $n_2 = 0$. To complete the analysis, Eq. 5.13 needs to be expanded and the same previous procedure is repeated, with more terms appearing in the expansion compared to ε^1 accuracy (26 terms compared to 10 terms), due to the large number of terms, only the key results are to be shown here, detailed results are shown in Table A.1 (in Appendix A). The equation of motion in the u-transformed coordinate system becomes

$$\begin{aligned} \ddot{u} + \Lambda u + \mathbf{n}_\mathbf{u}^* \mathbf{u}^* + \mathbf{n}_\mathbf{u}^+ \mathbf{u}^+ &= 0, \\ \ddot{u} + \omega_n^2 u + 3\alpha_1\left(u_p u_m^3 + u_p^2 u_m\right) + 10\alpha_2\left(u_p^2 u_m^3 + u_p^3 u_m^2\right) &= 0, \end{aligned} \tag{5.14}$$

and the near identity transformation is written as

$$q = u + \mathbf{h}^* \mathbf{u}^* + \mathbf{h}^+ \mathbf{u}^+ \tag{5.15}$$

which leads to

$$q = u + \frac{1}{8\omega_r^2}\left(\alpha_1\left(u_p^3 + u_m^3\right) + \frac{\alpha_2}{3}\left(u_p^5 + u_m^5\right) + 5\alpha_2\left(u_p^4 u_m + u_p u_m^4\right)\right) \tag{5.16}$$

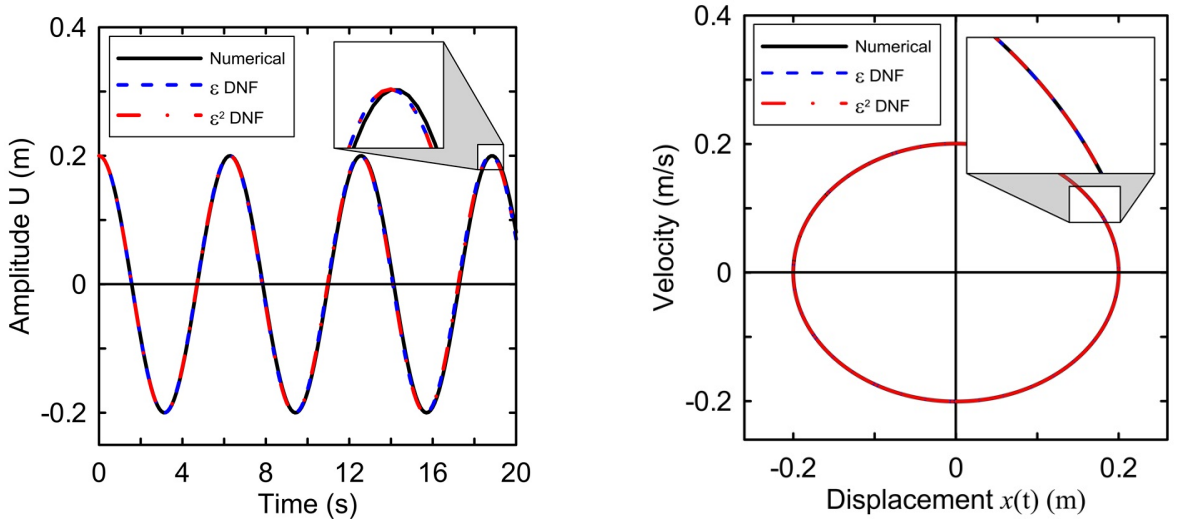

(a) (b)

Figure 5.2: DNF results compared to numerical results: (a) Steady-state response, (b) Phase portrait. The dashed blue curve and dash-dotted lines are computed from the analytical DNF solution for both ε^1 and ε^2, respectively, while the solid black curves are the numerical solutions computed using 4^{th} order Runge-Kutta computation in MATLAB. Parameter values are: $\omega_n = 1$ rad/s, $\alpha_1 = \alpha_2 = 0.1$.

The conservative backbone curve, truncated to ε^2, can be obtained by substituting in the assumed solution Eq. 5.16, and solving the positive (or negative) complex exponential terms using exact balancing, primarily, the following form shall be obtained;

$$\omega_r^2 = \omega_n^2 + \frac{3}{4}\alpha_1 U^2 + \frac{5}{8}\alpha_2 U^4 + \frac{3}{128\omega_r^2}\alpha_1^2 U^4 + \frac{5}{64\omega_r^2}\alpha_1\alpha_2 U^6 + \frac{95}{1536\omega_r^2}\alpha_2^2 U^8 \tag{5.17}$$

In Eq. 5.17, the effect of ε^2 can be interpreted as a type of frequency correction parameter. While most of the researchers using DNF technique are only considering ε^1 accuracy in the solution, it has previously been noticed that in some cases extending the analyses to include ε^2 accuracy can effectively enhance the results - refer to [47] as an example. In order to verify the accuracy of the solution, both ε^1 and ε^2 solutions will be compared to the numerical solution obtained using a 4^{th} order Runge-Kutta computation in MATLAB, and sample results are shown in Fig. 5.2. In Fig. 5.2a and Fig. 5.2b, both steady-state response of the oscillator and phase portrait plots are clarified for ε^1 and ε^2 along with the numerical solution. Overall, results in Fig. 5.2 show excellent agreement between the approximate DNF solutions and the numerical solution.

5.1.2 Comparisons with other methods

In order to verify the results of both ε^1 and ε^2 accuracies, it is possible to compare with some previous results in the literature. For ε^1 accuracy, Nayfeh's approximation for small amplitudes [33] has the following form

$$\omega_r = 1 + \left(\frac{3}{8}\alpha_1 + \frac{5}{16}\alpha_2 U^2\right) U^2 \tag{5.18}$$

Hence, ε^1 DNF solution given by Eq. 5.10 can be compared to Eq. 5.18 for primary verification of the validity of the DNF solution; thus Fig. 5.3a shows a comparison between both solutions for the following numerical values: $\alpha_1 = 0.2$, $\alpha_2 = 0.1$. This figure shows good agreement between the two approximations, specifically when the forcing frequency is close to the linear frequency, while at higher frequencies the two methods diverge. Furthermore, in the literature, some researchers studied the cubic quintic oscillator to ε^2 accuracy. For instance, Sulemen and Wu [102] used a modified homotopy method (modified HPM) to derive the backbone curve of this oscillator in the form

$$\omega_r = \sqrt{\frac{1}{2}\left(1 + \frac{3}{4}\alpha_1 U^2 + \sqrt{\left(\left(1 + \frac{3}{4}\alpha_1 U^2\right)^2 + \frac{15}{4}\alpha_1^2 U^4 + \frac{35}{144}\alpha_2^2 U^4\right)}\right)} \tag{5.19}$$

For verification purposes, the results of DNF for ε^2 accuracy, Eq. 5.17, can be compared to Eq. 5.19, in addition to the numerical solution of the cubic-quintic oscillator, as will be shown in Table 5.2-Table 5.4. However, as a primary comparison, Fig. 5.3b shows a comparison between the approximated backbone curves from both techniques. The two curves in Fig. 5.3b show identical behaviour at low amplitude, but the curves diverge as amplitudes of vibration increase, particularly for amplitude values above one. Further details regarding the accuracy of the two solutions will be shown in the next Sections.

5.1.3 Numerical investigation of the frequency-amplitude relationship

In order to verify the results of the analytical approximate methods previously described, some numerical techniques can be used. Specifically, numerical continuation technique using COCO toolbox in MATLAB can be used to find the steady-state frequency response of Eq. 5.1 for any given parameter values. And when comparing these numerical results to the results of RN, HPM and DNF (ε^1 and ε^2), it can be possible to investigate the

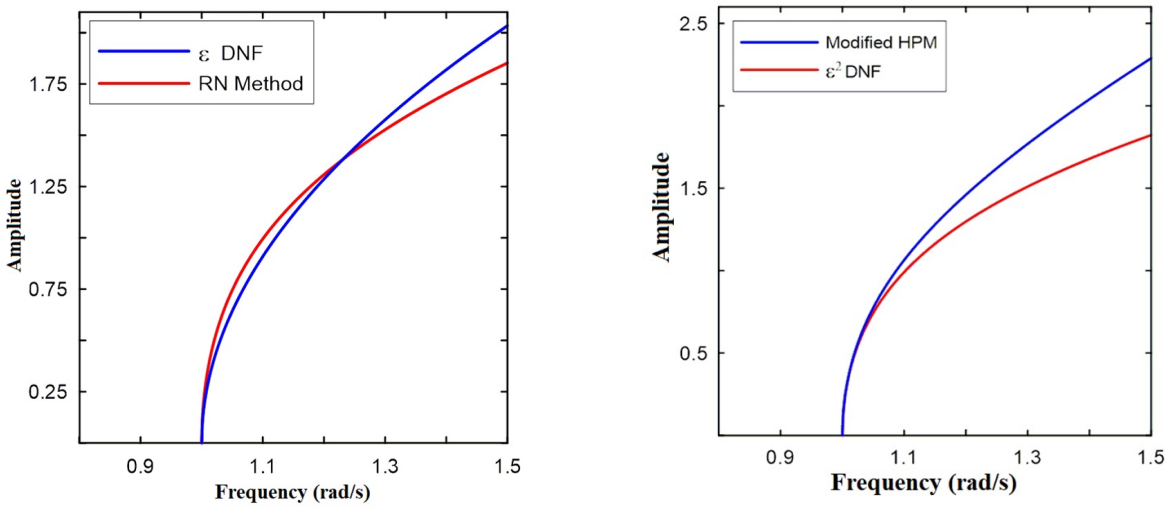

(a) (b)

Figure 5.3: Comparison between DNF results and other methods for the cubic-quintic oscillator: (a) ε^1-order DNF and the method of Renormalisation (RN method), (b) ε^2-order DNF and the modified homotopy method (Modified HPM). Parameter values are: $\omega_n = 1$ rad/s, $\alpha_1 = 0.2$, $\alpha_2 = 0.1$.

accuracy of these approximate analytical methods. For numerical verification purposes, the numerical continuation solution is generated using COCO in MATLAB with a very small damping value of $\zeta = 0.001$; in this sense, it can be possible to compare the numerical results to the analytical results of this conservative oscillator. Additionally, the following discussions reveal how numerical continuation results can be compared to the exact solution of Duffing oscillator which already exists in the literature.

Based on the Jacobi elliptic functions, the elliptical function solution (EPS) of Duffing oscillator has been studied by several authors, and the results are summarized by Kovacic and Brennan [87]. This work is to be adopted for validating the numerical solution. Accordingly, by setting $\alpha_2 = 0$ in Eq. 5.1, the equation of the conservative Duffing oscillator is obtained, which is

$$\ddot{x}(t) + \omega_n^2 x(t) + \alpha_1 x^3(t) = 0, \tag{5.20}$$

According to Kovacic and Brennan [87], the nonlinear frequency of this oscillator is

$$\omega_r^2 = \left(\omega_n^2 + \alpha_1 U^2\right)\left(1 - \frac{\alpha_1 U^2}{4\omega_n^2}\left(1 - \frac{\alpha_1 U^2}{4}\right)\right) + \ldots \tag{5.21}$$

For verification purposes, the numerical solution used in this work is applied to the Duffing oscillator, Eq. 5.20 and the numerical results of the nonlinear frequency are compared to the results of Kovacic and Brennan [87]. Sample results of this comparison can be found in Fig. 5.4, in which both the EPS and the numerically obtained backbone curves are plotted for $\alpha_1 = 0.1$. From this figure, it can be seen that numerical solutions have acceptable levels of accuracy at frequencies that are close to the natural frequency of the system while the accuracy decreases at higher values of the dimensionless nonlinear frequency.

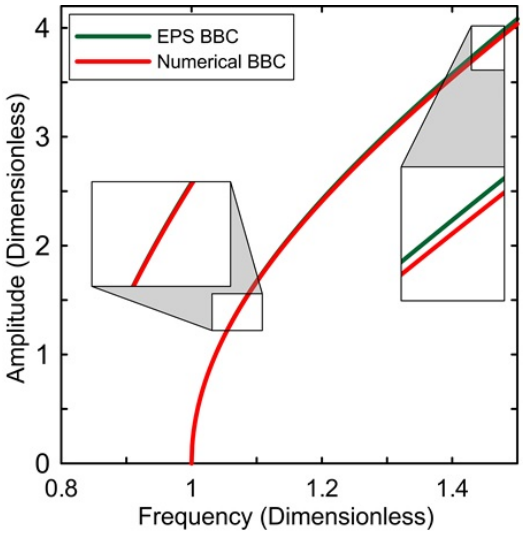

Figure 5.4: Comparison between elliptical functions (EPS) and numerical backbone curves for the Duffing oscillator. Parameter values are: $\omega_n = 1$ rad/s and $\alpha_1 = 0.2$.

5.1.4 Comparing analytical results with numerical results for the cubic-quintic oscillator

Table 5.2 & Table 5.3 show comparisons between Nayfeh's results (denoted by RN method), Sulemen and Wu results (denoted by Modified HPM) and the proposed method using DNF for both ε^1 and ε^2, all compared to the numerical continuation results (as a reference for comparison). The comparison is carried out for different selected amplitude values in order to evaluate the nonlinear amplitude-frequency response of the system while the linear natural frequency is assumed to be unity in all cases. Absolute error relative to the numerical continuation solution is also shown as a percentage underneath each of the relevant entries in the Tables. In Table 5.2, the values selected for comparison are $\alpha_1 = 0.2$ and $\alpha_2 = 0.1$ in order to represent weak nonlinear terms in comparison to the linear term. While in Table 5.3, the effect of larger nonlinear terms is shown using the numerical values of $\alpha_1 = 1$ and $\alpha_2 = 1$.

Table 5.2: DNF method results compared with other methods for $\alpha_1 = 0.2$, $\alpha_2 = 0.1$

Amplitude U	Numerical	RN method	Modified HPM	ε^1 DNF	ε^2 DNF
0.05	1.000186	1.000302 0.0116 %	1.000188 0.0002 %	1.000187 0.0001 %	1.000187 0.0001 %
0.2	1.003061	1.004833 0.1767 %	1.003026 0.0035 %	1.003045 0.0016 %	1.003045 0.0016 %
0.5	1.020497	1.030208 0.0016 %	1.019777 0.0706 %	1.020493 0.0004 %	1.020543 0.0045 %
1.0	1.103012	1.120833 1.6157 %	1.090601 1.1252 %	1.101136 0.1701 %	1.101986 0.0930 %
2.0	1.620928	1.483333 8.4888 %	1.509942 6.8471 %	1.612451 0.5230 %	1.633491 0.7750 %
5.0	6.753684	4.020833 40.465 %	5.916005 12.403 %	6.619101 1.9927 %	6.979045 3.3369 %

Table 5.3: DNF method results compared with other methods for $\alpha_1 = 1$, $\alpha_2 = 1$

Amplitude U	Numerical	RN method	Modified HPM	ε^1 DNF	ε^2 DNF
0.05	1.001979	1.001979 0.0950 %	1.000938 0.0090 %	1.000939 0.0089 %	1.000939 0.0089 %
0.2	1.031667	1.031667 1.597 %	1.015216 0.0231 %	1.015382 0.0068 %	1.015414 0.0036 %
0.5	1.197917	1.197917 8.092 %	1.101490 0.6095 %	1.107503 0.0670 %	1.108546 0.0272 %
1.0	1.791668	1.791667 16.915 %	1.473823 3.8262 %	1.554790 1.4573 %	1.541104 0.5642 %
2.0	4.166667	4.166667 9.5086 %	3.379416 11.182 %	3.741657 1.6615 %	3.882786 2.0477 %
5.0	25.79167	20.79167 22.970 %	18.07842 13.805 %	20.25772 3.4148 %	21.49016 2.4612 %

The results in Table 5.2 & Table 5.3 show the accuracy of DNF method compared to some other well established approximate methods that already exist in the literature. It is clear that, in terms of accuracy, the DNF method gives acceptable approximation of the frequency shift due to the presence of nonlinear terms in the equations of motion. The DNF method has been classified into two approaches ε^1 and ε^2, and in terms

of the series expansion, and this should correlate to lower and higher accuracies, respectively. However, the higher order accuracy does not always show a reduction in error compared to ε^1. A potential reason for this is due to the fact that only odd nonlinear terms are present, further explanation of this point is given in Section 5.2.

From another point of view, in order to explore the effect of changing the nonlinear coefficients, α_1 and α_2, on the nonlinear frequency of the system, ω_r, it is possible to make a parametric study of the resulting backbone curve equations. For instance, in Fig. 5.5, 3-dimensional representations of the variations of the nonlinear frequency, ω_r, when the nonlinear coefficients, α_1 and α_2 are varied steadily from -1 to 1, this is plotted for different values of the amplitude U while the natural frequency is $\omega_n = 1.0$ rad/s for all cases. This figure reveals that, when $U < 1$, the nonlinear frequency of the system increases steadily whenever α_1 and α_2 increase, however, this behaviour changes for higher values of U. It is also noted that the method of DNF is able to detect the nonlinear frequency of the system efficiently for lower values of U compared to higher values, i.e. $U > 2$, which present some limitations to the technique when used for excessive amplitudes of deflections provided that the natural frequency is relatively low. Nevertheless, for this conservative cubic-quintic oscillator further parametric studies can be held using the aforementioned analysis. Tabulated results for the sample amplitude value of $U = 0.2m$ can be found in Table 5.4, for which the nonlinear frequency of the system is computed to ε^1 accuracy, while the nonlinear coefficients are changing steadily from -1.0 to 1.0 and $\omega_n = 1.0$ rad/s.

To conclude, the results of cubic-quintic nonlinear oscillator with different values of the nonlinear coefficients can be implemented to study various cases of oscillators in both hardening and softening cases. And the approximate analytical results of DNF can be verified using numerical continuation techniques such as the COCO toolbox in MATLAB [34, 35]. COCO is used to numerically compute the frequency response functions representing the locus of points joining the maximum amplitude per period of the forced damped systems by adding viscous damping and periodic forcing terms to the cubic-quintic oscillator described in Eq. 5.1. Accordingly, using small damping value, $\zeta = 0.01$, Fig. 5.6 is generated for combinations of the nonlinear coefficients in the original equations of motion, the numerical values for this figure are: the natural frequency $\omega_n = 2$ rad/s, the forcing amplitude $R = 1$ (for the forced frequency manifolds), $\alpha_1 = \alpha_2 = 0.1$ for the hardening cases, and $\alpha_1 = \alpha_2 = -0.1$ for the softening casee. In this figure, results for the linear oscillator, Duffing oscillator

in both hardening and softening cases and the cubic-quintic oscillator in both hardening and softening cases are shown. The forced frequency response functions (dashed coloured lines) are numerically computed using COCO, while the conservative backbone curves (solid-coloured lines) are computed using ε^1 DNF results, Eq. 5.9. In Fig. 5.6, the idea is that the backbone curve should align along the centre of the resonance curve (e.g. the COCO curve). The only point that the COCO and backbone should cross is near the peak of the resonance (COCO) curve. In Fig. 5.6, it can be seen that this is true, for all the cases considered. So, in this sense, the matching is good.

Table 5.4: DNF method results for various values of the nonlinear coefficients

Nonlinear coefficients	Frequency ω_r (computed to ε^1 accuracy)				
α_2 \ α_1	-1.0	-0.5	0.0	0.5	1.0
-1.0	0.984378	0.984653	0.984886	0.985140	0.985393
-0.5	0.991968	0.992225	0.992472	0.992724	0.992975
0.0	0.999500	0.999750	1.000000	1.000250	1.000500
0.5	1.006976	1.007224	1.007472	1.007720	1.007968
1.0	1.014412	1.014643	1.014889	1.015135	1.015402

5.2 Analysis of generic cubic-quintic SDOF oscillator

In the previous Section, the results of ε^1 DNF were shown to be accurate enough for the analyst to adopt, without the need to consider higher order accuracies, this is due the presence of (only) odd nonlinear terms in the original EOM. On the other hand, the presence of even nonlinear terms can raise the difficulty of the analysis. In this section, the system considered represents a more complicated case in which the oscillator has four different orders of polynomial nonlinear terms, in this example the effect of higher order accuracy, ε^2, can be explored. Finally, a general closed form relation of the backbone curve, truncated to ε^1 accuracy is obtained

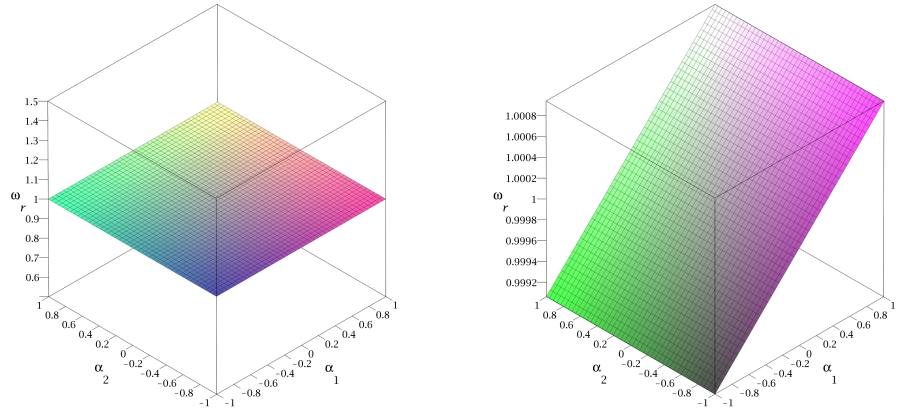

(a) $U = 0.00$

(b) $U = 0.05$

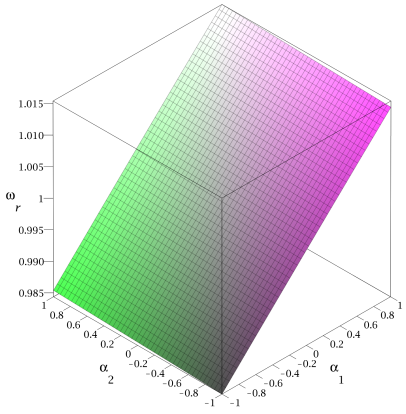

(c) $U = 0.20$

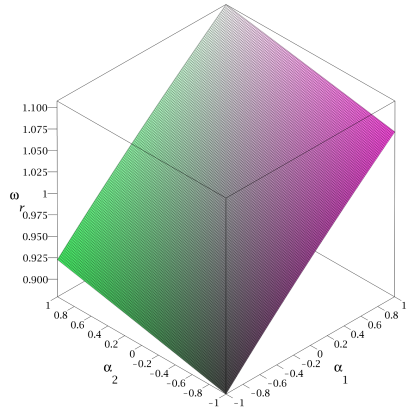

(d) $U = 0.50$

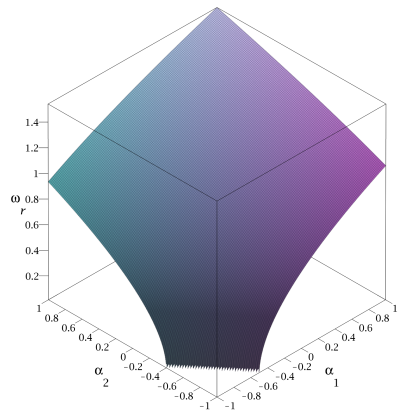

(e) $U = 1.00$

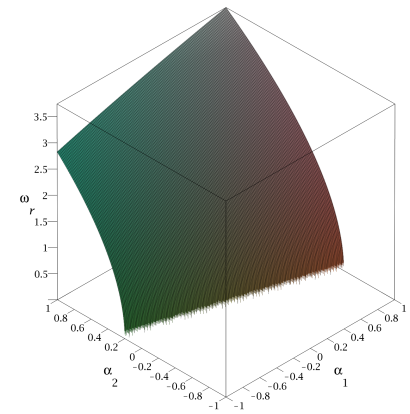

(f) $U = 2.00$

Figure 5.5: DNF results for the Cubic-quintic oscillator, truncated to ε^1 accuracy provided by Eq. 5.10. The results represent the variations of the nonlinear frequency ω_r for various values of the nonlinear coefficients, α_1 and α_2. The natural frequency for all cases is $\omega_n = 1.0$ rad/s while various values of the amplitude U is considered (in metres); (a) $U = 0.00$, (b) $U = 0.05$, (c) $U = 0.20$, (d) $U = 0.50$, (e) $U = 1.00$ and (f) $U = 2.00$.

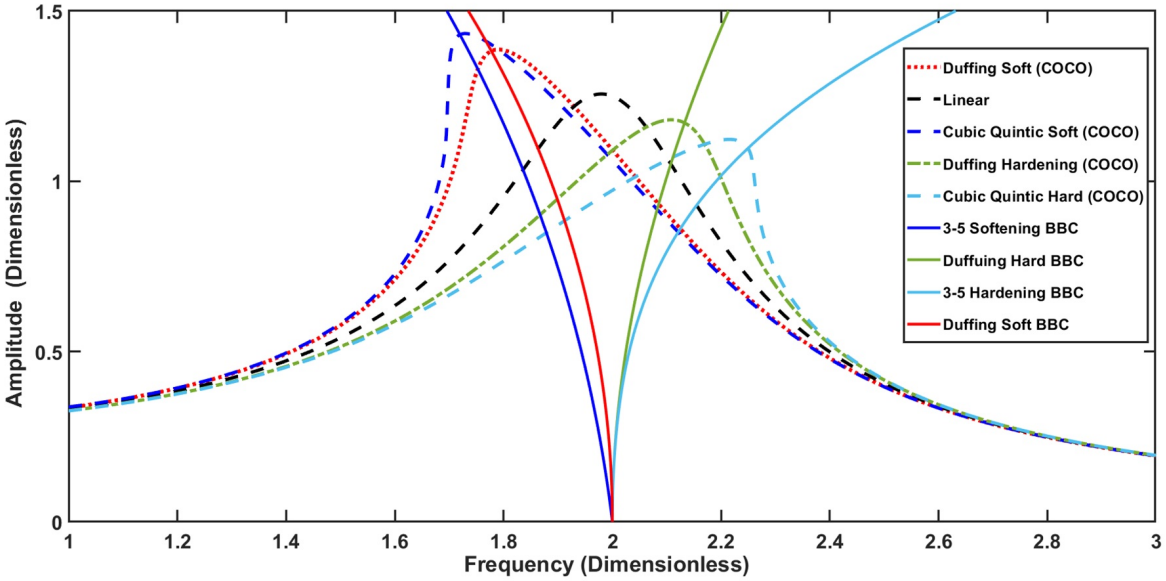

Figure 5.6: Conservative backbone curves and the forced-damped frequency response functions for different values of the nonlinear coefficients; solid lines represent the conservative backbone curves obtained analytically using DNF method, and dashed lines show the locus of the maximum displacement amplitude of the equivalent period orbit with forcing and damping added, those are obtained numerically using COCO. Parameter values are: natural frequency $\omega_n = 2$ rad/s, forcing amplitude $R = 1$, $\alpha_1 = \alpha_2 = 0.1$ for the hardening cases, and $\alpha_1 = \alpha_2 = -0.1$ for the softening cases.

for any oscillator with N number of stiffness polynomial nonlinear terms. In principle, Wagg and Neild [8] showed that, for the quadratic nonlinear oscillator, ε^1 DNF will not be able to capture the nonlinear frequency-amplitude curve of the system, while extending the analysis to ε^2 leads to a satisfactory approximation. In this section, using a SDOF oscillator with both odd and even nonlinear terms it is shown that the presence of even nonlinearities makes it necessary to compute ε^2.

Considering a SDOF nonlinear oscillator with four different orders of polynomial geometric nonlinear terms (with orders two to five, respectively), in its conservative form. The equations of motion of this oscillator can be written as

$$\ddot{x}(t) + \omega_n^2 x(t) + \alpha_1 x^2(t) + \alpha_2 x^3(t) + \alpha_3 x^4(t) + \alpha_4 x^5(t) = 0, \tag{5.22}$$

where the nonlinear coefficients are all assumed to be relatively small when compared to the linear term. Using the DNF, it is required to find the backbone curves of this system. In such unforced systems, the analysis will be similar to that in the previous cubic-quintic system, with more terms to be computed (or correspondingly larger matrix sizes). For a DNF computed to ε^1 accuracy, to find the number of terms, the following can be considered;

- any nonlinear power γ will contribute by $\gamma+1$ terms, and this is accumulative according to the number of nonlinear terms in the EOM. Hence, the analysis of the oscillator in Eq. 5.22 involves 18 terms to be computed in the ε^1 order solution.

- a viscous damping term, if appears in the equation of motion, will result in two additional terms, hence, the damped cubic-quintic oscillator involves 12 terms in that case.

- for the case of forced systems, more terms are to be included in the analysis according to the forcing type; either resonant or non-resonant. However, the analysis of this work is restricted to unforced, and non-resonant cases only.

Accordingly, the ε^1 solution of the conservative oscillator in Eq. 5.22 results in 18 terms in the matrices, this number of terms is difficult to be manipulated by hand calculations, and this can justify turning to symbolic computations. Moreover, the number of terms will also increase dramatically if considering ε^2 solution, in fact the number of terms involved in ε^2 analysis of Eq. 5.22 will be 52 terms. Practically, DNF analysis of Eq. 5.22 will be similar to the cubic-quintic oscillator, with more terms to be included in the solution. Accordingly, only final results are shown in this section. The backbone curve, truncated to ε^1 is found to be

$$\omega_r^2 = \omega_n^2 + \frac{3}{4}\alpha_1 U^2 + \frac{5}{8}\alpha_2 U^4 \tag{5.23}$$

which is identical to the equation obtained for the cubic-quintic oscillator, thus, it is clear that the effect of the even nonlinear terms in the original EOM is not appearing in the ε^1 order results. Nevertheless, if the analysis is extended to ε^2, the resulting backbone curve will be

$$\begin{gathered}\omega_r^2 = \omega_n^2 + \frac{3}{4}\alpha_1 U^2 + \frac{5}{8}\alpha_2 U^4 + \\ \frac{1}{\omega_r^2}\left(\frac{3}{128}\alpha_2^2 U^4 + \frac{5}{64}\alpha_2\alpha_4 U^6 + \frac{95}{1536}\alpha_4^2 U^8 - \frac{5}{6}\alpha_1^2 U^2 - \frac{7}{4}\alpha_1\alpha_3 U^4 - \frac{63}{80}\alpha_3^2 U^6\right)\end{gathered} \tag{5.24}$$

Table 5.5 shows a comparison between ε^1 and ε^2 frequency results of this oscillator and the numerical results obtained using COCO numerical continuation toolbox in MATLAB. For non-dimensionalisation purposes, similar to the cubic-quintic oscillator, the nondimensional numerical data chosen for Table 5.5 are $\alpha_1 = \alpha_2 = \alpha_3 = \alpha_4 = 0.1$. The results in Table 5.5 clearly show that the solutions truncated to ε^2 are more ac-

curate than those truncated a ε^1, which is a consequence of the presence of even nonlinear terms in the original equations of motion. For this particular system, the accuracy of the approximate analytical results is slightly modified due to calculating the higher order expansion. Nevertheless, in some other cases it can be necessary to find ε^2 solution; for example, if only even nonlinear terms appear in the equation of motion. It has been shown that the analysis of a nonlinear oscillator with a single quadratic nonlinearity (the escape equation) using DNF truncated to ε^1 accuracy (refer to [8] for more details) is not sufficient to compute the backbone curve relation, in fact the ε^2 order analysis is required.

In this work, it is shown that this result is true for higher order even nonlinear terms, and Table B.1 (in Appendix B) summarizes the results of the backbone curves for both lower and higher accuracies computed up to the 15^{th} polynomial order of the nonlinear terms. For verification purposes of the approximate analytical results of DNF, it is possible to compare with numerical continuation (COCO). Hence, Fig. 5.7 shows a comparison between DNF truncated to both ε^1 and ε^2, along with the numerical solution of the related forced damped system. The numerical data are $\alpha_1 = \alpha_2 = \alpha_3 = \alpha_4 = 0.1$.

Using Fig. 5.7, good matching between DNF results and the numerical results can be observed, in terms of the backbone curve curvature being very close to the centre line of the COCO computed curve, refer to Fig. 5.6 in Section 5.1 and the discussions therein. However, in Fig. 5.7, the backbone curves are not intersecting exactly at the peak of the COCO curve. One reason for this is related to the damping used for computing the numerical results; COCO simulations include a viscous damping term, which was chosen to be $\zeta = 0.01$ in this case, while the backbone curves are computed for conservative systems. If damped backbone curves were computed, better matching between the backbones and COCO curves would be expected, refer to Section 4.4. Another possible approach to refine the resulting analytical backbone curve in this figure so that it can be closer to the centre line of COCO numerical results, is to compute the ε^3 backbone curve for this system, similar to the discussions in Section 4.3, however, this practise will be highly complicated for such system and thus it can be performed in future works.

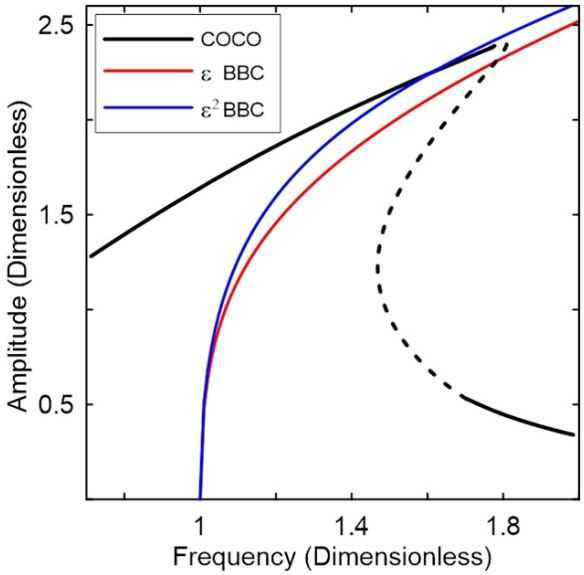

Figure 5.7: Comparison of DNF results and COCO results for the nonlinear oscillator in Eq. 5.22, the solid blue and red curves denote the analytical DNF results for ε^1 and ε^2 accuracies, respectively. Moreover, the black line denotes the frequency-response curve computed using COCO; the solid black line shows the stable region of the response while the dashed black line represents the unstable region. Parameter values are: $\omega_n = 1$ rad/s, and $\alpha_1 = \alpha_2 = \alpha_3 = \alpha_4 = 0.1$.

Table 5.5: DNF results for various values of the nonlinear coefficients

U	Numerical	ε^1	ε^2
0.05	1.00018	1.00009 0.008 %	1.00014 0.005 %
0.1	1.00043	1.00033 0.010 %	1.00035 0.008 %
0.2	1.00147	1.00155 0.007 %	1.00137 0.011 %
0.5	1.01017	1.01126 0.108 %	1.00967 0.049 %
1	1.06428	1.06653 1.21 %	1.05288 0.869 %
2	1.45567	1.51657 1.52 %	1.47312 1.25 %
3	2.75600	2.59567 2.51 %	2.61570 1.86 %
4	3.83312	4.86614 3.21 %	4.30962 2.10 %
5	6.5698	6.27592 4.47 %	6.65439 2.45 %

5.3 Analysis of SDOF oscillators with any type of odd polynomial nonlinearities

The equation of motion for a general SDOF conservative oscillator, with multiple geometric (polynomial) odd nonlinearities can be written as

$$\ddot{x}(t) + \omega_n^2 x(t) + \mathbf{N_x} = 0, \tag{5.25}$$

where ω_n is the natural frequency and the nonlinear terms vector N_x, in its general form, is written as

$$N_x = \sum_{i=1}^{R} \alpha_i x^i(t) \tag{5.26}$$

Herein, α_i, the coefficient of the i^{th} nonlinear stiffness term is considered to be relatively small, and R denotes the number of odd nonlinear terms. Using the method of DNF (implemented symbolically), the corresponding backbone curves of Eq. 5.22 have been generated. It was found that, for ε^1 order only, the effect of any odd nonlinearity appearing in the equation of motion is additive in the resulting expression for the backbone curve. For instance, the ε^1 order solution of the cubic-quintic oscillator will contain the terms of the cubic oscillator plus a term from the quintic oscillator. As a result, the corresponding expression for the backbone curve truncated to ε^1 order can be written as

$$\omega_r^2 = \omega_n^2 + \sum_{j=1}^{R} \xi_j \alpha_j U^{2j+1} \tag{5.27}$$

where ξ_j are constant coefficients appearing in the backbone curve equation, (these coefficients are independent of the nonlinear coefficients, or α values appearing in the original equation of motion). Table 5.6 shows the leading values of these constant coefficients for the first four orders of odd nonlinearities.

Table 5.6: Values of the constants ξ_j for ε^1 order DNF

Order of nonlinearity	3	5	7	9
ξ_j	$\frac{3}{4}$	$\frac{5}{8}$	$\frac{35}{64}$	$\frac{63}{128}$

Thus, using Eq. 5.27 and the values from Table 5.6, DNF results truncated to ε^1 accuracy, for the conservative backbone curve can be obtained. However, by using the binomial coefficients, it can be shown that for any odd order j, the coefficients ξ_j are given by the general expression

$$\xi_j = \frac{1}{2^{j-1}} \binom{j}{\frac{j+1}{2}}, \quad j = 1,3,5,... \tag{5.28}$$

Hence, the backbone curve equation, truncated to ε^1 order, for a SDOF oscillator with odd polynomial nonlinear stiffness terms, can be written as

$$\omega_r^2 = \omega_n^2 + \sum_{j=1}^{R} \frac{1}{2^{2j}} \binom{2j+1}{j+1} \alpha_j U^{2j+1} \tag{5.29}$$

For ε^2 accuracy, due to the appearance of some cross coupling terms, for instance, the term including $\alpha_1\alpha_3$ in Eq. 5.24, it is much more difficult to find a closed form solution similar to that in Eq. 5.29. However, using the proposed symbolic computation approach, ε^2 DNF analysis is applied for some selected SDOF oscillators, and the corresponding expressions for the conservative backbone curves are resulted, refer to Table B.2, Appendix B.

5.4 DNF analysis of Van-der-Pol, Rayleigh and oscillators with combinations of nonlinear stiffness and viscous damping terms

In this part, the method of DNF is used to analytically explore the steady-state frequency response of Van-der-Pol, Rayleigh oscillators, in addition to some other oscillators with combinations of stiffness and damping nonlinearities, including Van-der-Pol-Duffing, Rayleigh-Duffing, Van-der-Pol cubic-quintic and Rayleigh cubic-quintic oscillators. In all cases under consideration, the oscillators are driven by a harmonic excitation near the resonance. The approximate analytical results are truncated to ε^1 accuracy and, for verification purposes, they are compared to numerical results obtained by MatCont numerical continuation toolbox in MATLAB.

5.4.1 DNF analysis of Van-der-Pol oscillator

Starting with Van-der-Pol oscillator, it is desired to apply DNF to calculate the steady-state response of the oscillator close to resonance. The equation of motion of Van-der-Pol oscillator subjected to harmonic excitation is given by

$$\ddot{x}(t)+\mu\left(x^2(t)-1\right)\dot{x}(t)+\omega_n^2 x(t)=R\cos(\Omega t) \tag{5.30}$$

herein, ω_n is the oscillator's natural frequency, μ is a scalar constant, R is the forcing amplitude and Ω is the forcing frequency. It is important to consider that the nonlinearity is illustrated by the damping term, $\dot{x}(t)$, which is considered to be relatively small. To apply DNF analysis of this oscillator, it is convenient to use the following

$$\begin{aligned}\mathbf{P_x}&=\left\{\frac{R}{2},\frac{R}{2}\right\}\\ \mathbf{r}&=\{r_p,r_m\}^{\mathsf{T}}=\{\mathrm{e}^{\,\mathbf{i}\Omega t},\mathrm{e}^{-\,\mathbf{i}\Omega t}\}^{\mathsf{T}}\\ \widetilde{\mathbf{N}}(\mathbf{q},\dot{\mathbf{q}},\mathbf{r})&=\mu\left(q^2(t)-1\right)\dot{q}(t)\end{aligned} \tag{5.31}$$

and thus the equation of motion becomes

$$\ddot{x}(t)+\omega_n^2 x(t)+\widetilde{\mathbf{N}}(\mathbf{q},\dot{\mathbf{q}},\mathbf{r})=\mathbf{P_x r} \tag{5.32}$$

The linear modal transformation is $\mathbf{q}=\mathbf{x}=x$ since SDOF is considered, thus

$$\ddot{q}+\Lambda q+N_q(\mathbf{q},\dot{\mathbf{q}},\mathbf{r})=\mathbf{P_q r} \tag{5.33}$$

where $\Lambda=\omega_n^2$, $N_q(\mathbf{q},\dot{\mathbf{q}},\mathbf{r})=\mu\left(q^2-1\right)\dot{q}$ and $\mathbf{P_q}=\mathbf{P_x}$.

Now, the forcing transformation is considered to be $\mathbf{q}=\mathbf{v}+\mathbf{er}$, this transformation is used to eliminate the non-resonant forcing terms. Due to the fact that the analysis is close to resonant, $\Omega=\omega_r$ and $[\mathbf{e}]=0$, this results in

$$\ddot{v}+\Lambda v+N_v(\mathbf{v},\dot{\mathbf{v}},\mathbf{r})=\mathbf{P_v r} \tag{5.34}$$

with $N_v(\mathbf{v},\dot{\mathbf{v}},\mathbf{r})=\mu\left(v^2-1\right)\dot{v}$ and $\mathbf{P_v}=\mathbf{P_q}$.

The near-identity transformation is computed to ε^1 accuracy, by rewriting the nonlinear terms using $\mathbf{u}$, one should obtain $n_1(\mathbf{u},\dot{\mathbf{u}},\mathbf{r}) = \mu\left(u^2-1\right)\dot{u}$ for which $\mathbf{u} = \mathbf{u_p} + \mathbf{u_m}$, thus

$$\mathbf{u}^* = \begin{bmatrix} u_m^3 \\ u_p^3 \\ u_p u_m^2 \\ u_p^2 u_m \\ u_m \\ u_p \end{bmatrix} \rightsquigarrow \mathbf{n}^* = \mathbf{i}\mu\omega_r \begin{bmatrix} -1 \\ 1 \\ -1 \\ 1 \\ 1 \\ -1 \end{bmatrix}^{\mathsf{T}} \rightsquigarrow \boldsymbol{\beta}^* = \omega_r^2 \begin{bmatrix} 8 \\ 8 \\ 0 \\ 0 \\ 0 \\ 0 \end{bmatrix}^{\mathsf{T}} \rightsquigarrow$$
$$\mathbf{h}^* = \frac{\mathbf{i}\mu}{8\omega_r} \begin{bmatrix} -1 \\ 1 \\ 0 \\ 0 \\ 0 \\ 0 \end{bmatrix}^{\mathsf{T}} \rightsquigarrow \mathbf{n}_\mathbf{u}^* = \mathbf{i}\mu\omega_r \begin{bmatrix} 0 \\ 0 \\ -1 \\ 1 \\ 1 \\ -1 \end{bmatrix}^{\mathsf{T}} \tag{5.35}$$

For ε^1 accuracy, the equation of motion can then be written in the u-transformed coordinates as

$$\ddot{u} + \mu\left(\frac{U^2}{4} - 1\right)\dot{u} + \omega_n^2 u = R\cos(\omega_r t) \tag{5.36}$$

and by substituting the assumed solution it is possible to get

$$\left(\omega_n^2 - \omega_r^2\right)\frac{U}{2}\left(\mathrm{e}^{\,\mathbf{i}(\omega_r t-\phi)} + \mathrm{e}^{-\,\mathbf{i}(\omega_r t-\phi)}\right) + \mathbf{i}\mu\left(\frac{U^2}{4}-1\right)\omega_r\frac{U}{2}\left(\mathrm{e}^{\,\mathbf{i}(\omega_r t-\phi)} - \mathrm{e}^{-\,\mathbf{i}(\omega_r t-\phi)}\right) = \frac{R}{2}\left(\mathrm{e}^{\,\mathbf{i}\omega_r t} + \mathrm{e}^{-\,\mathbf{i}\omega_r t}\right) \tag{5.37}$$

Now, the real and imaginary parts of Eq. 5.37 can be balanced to get the following

$$\begin{aligned} \text{Re:} \quad & \left(\omega_n^2 - \omega_r^2\right)U = R\cos(\phi) \\ \text{Im:} \quad & \mu\left(\frac{U^2}{4}-1\right)\omega_r U = R\sin(\phi) \end{aligned} \tag{5.38}$$

and finally, by squaring and adding the real and imaginary solutions, it is possible to write expressions for the amplitude relationship, furthermore, by dividing them the phase relationship for the Van-der-Pol oscillator are obtained, such that

$$\begin{aligned} \text{Amplitude:} \quad U^2 &= \frac{R^2}{(\omega_n^2-\omega_r^2)^2+\mu^2\omega_r^2\left(\frac{U^2}{4}-1\right)^2} \\ \text{Phase:} \quad \phi &= \tan^{-1}\left[\frac{\mu\omega_r\left(\frac{U^2}{4}-1\right)}{(\omega_n^2-\omega_r^2)}\right] \end{aligned} \tag{5.39}$$

In the literature, the same results appears in Eq. 5.39 for Van-der-Pol-oscillator can be found in [8] using DNF applied traditionally with hand calculations, in this work moving to symbolic computations enables the researcher to extend the analysis in order to investigate more complex systems as will be discussed in the following sections. Moreover, in order to investigate the accuracy of the results in Eq. 5.39, MatCont numerical continuation toolbox in MATLAB is used; MatCont is an interactive numerical tool used to investigate dynamical systems, it is based on numerical continuation and could be to calculate equilibria curves and limiting points, as well as Hopf points, limit cycles fold bifurcation points, and other important dynamical characteristics of the system, refer to [116, 117] for further discussions regarding MatCont and its applications. In Fig. 5.8 MatCont is used to investigate the steady-state frequency response of Van-der-Pol oscillator in Eq. 5.30 for various excitation frequencies $R = 0.5, 1, 1.5, 2, 2.5, 3$ and 3.5.

Moreover, using the amplitude frequency relationship in Eq. 5.39, as Fig. 5.8 reveals, it is possible to analytically calculate ε^1 DNF frequency response manifolds for the same parameters in Fig. 5.8, by comparing the two figures similar behaviour of the two responses are found, however, some differences can be noticed; especially for lower excitation frequencies. In more details, the numerical continuation solution using MatCont can detect the subharmonic resonances that might occur (1 : 3 subharmonic resonances occur in this case), while the DNF method, in the current form applied, is unable to detect these subharmonic (or even super-harmonic) resonances that can happen. Furthermore discussions regarding the subharmonic and super-harmonic resonances for the case of Duffing oscillators can be found in [118] and references therein.

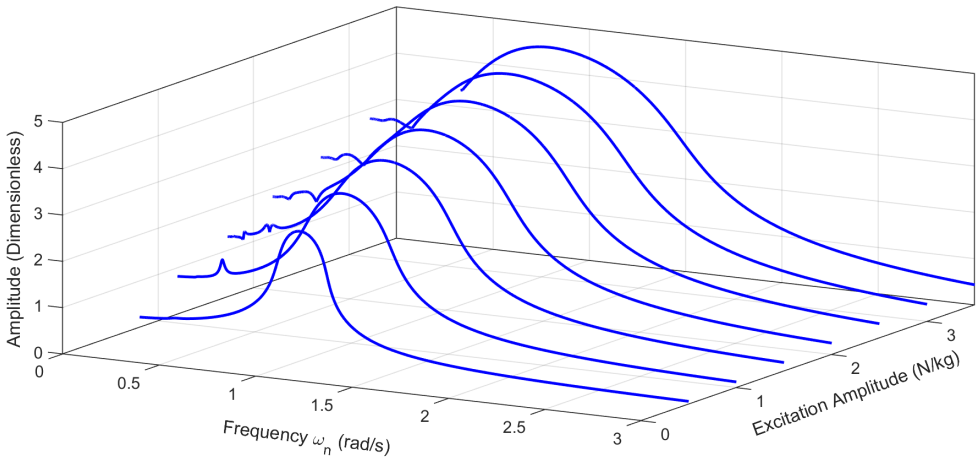

Figure 5.8: Steady-state frequency response manifolds for Van-der-Pol oscillator, the manifolds are computed numerically using MatCont toolbox. Parameter values are: $\omega_n = 1$ rad/s and $\mu = 0.2$. Curves from left to right represent the excitation amplitudes of $R = 0.5, 1, 1.5, 2, 2.5, 3$ and 3.5, respectively.

The amplitude-frequency variations with the excitation amplitude, R, are shown in Fig. 5.9. This figure is analytically generated using ε^1 DNF results in Eq. 5.39 for the excitation amplitudes of $R = 0.5 - 4$, while the natural frequency is $\omega_n = 1$ rad/s and $\mu = 0.2$. As clearly seen in Fig. 5.9, increasing the excitation amplitude results in higher peak frequency of the system around the natural frequency.

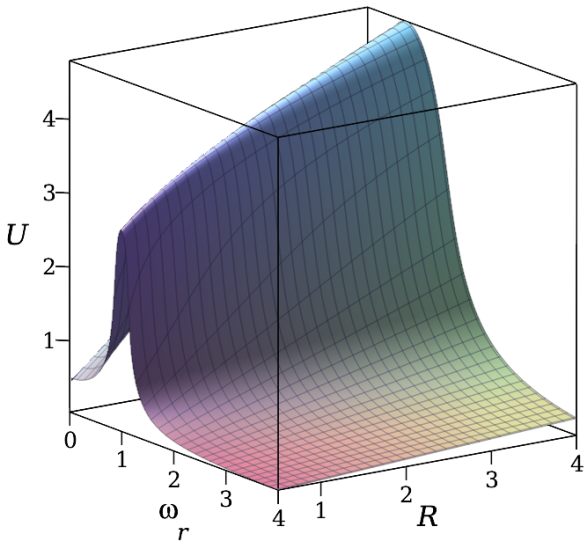

Figure 5.9: Steady-state frequency response manifolds for Van-der-Pol oscillator, the manifolds are computed analytically using ε^1 results appearing in Eq. 5.39. Parameter values are: $\omega_n = 1$ rad/s and $\mu = 0.2$.

In order to investigate the differences between the analytical and numerical solutions, Fig. 5.10 is generated with R values of $1,2$ and 3, the figure shows good agreement between the analytical and numerical solutions for lower values of R, while increasing R leads to less matching, this can be related to the accuracy of both DNF and MatCont.

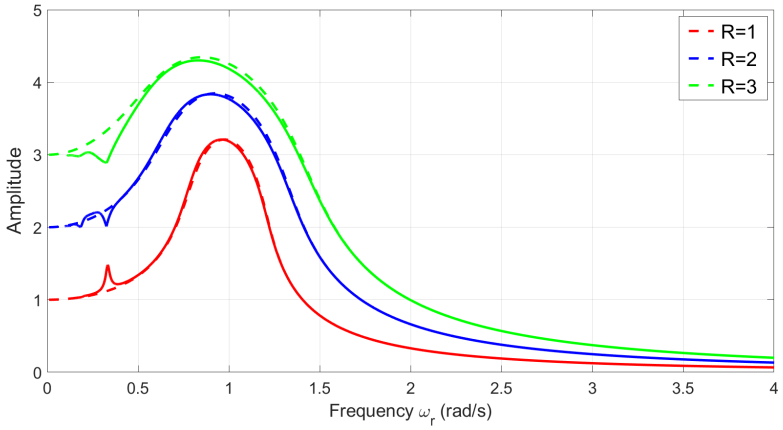

Figure 5.10: Steady-state frequency response comparison of the Van-der-Pol oscillator for both analytical DNF and numerical MatCont solutions for $R = 1,2$ and 3. Parameter values are: $\omega_n = 1$ rad/s and $\mu = 0.2$. Solid lines show numerical results from MatCont while dashed lines show analytical results from Eq. 5.39.

In order to investigate the effect of μ to the frequency response of the system, it is possible to choose a certain excitation amplitude, R, and varying μ which results in the steady-state frequency response manifolds for the selected μ and R values. Thus, Fig. 5.11 shows the MatCont numerically computed steady-state frequency responses while in Fig. 5.12 the analytically computed ε^1 DNF manifolds are noted. As seen in both figures, increasing the value of μ leads to decreasing the frequency responses, this decreasing process starts with high rates at small μ values but is rapidly becomes slower at higher μ values for which flatter response curves are noticed.

In the following subsection, in order to study their effects to the frequency responses, high orders of nonlinear stiffness terms (i.e. cubic and quintic) are added to the Van-der-Pol's EOM, and the dynamics of these systems are investigated using DNF method, the effects of adding these terms are discussed by means of steady-state amplitude comparisons.

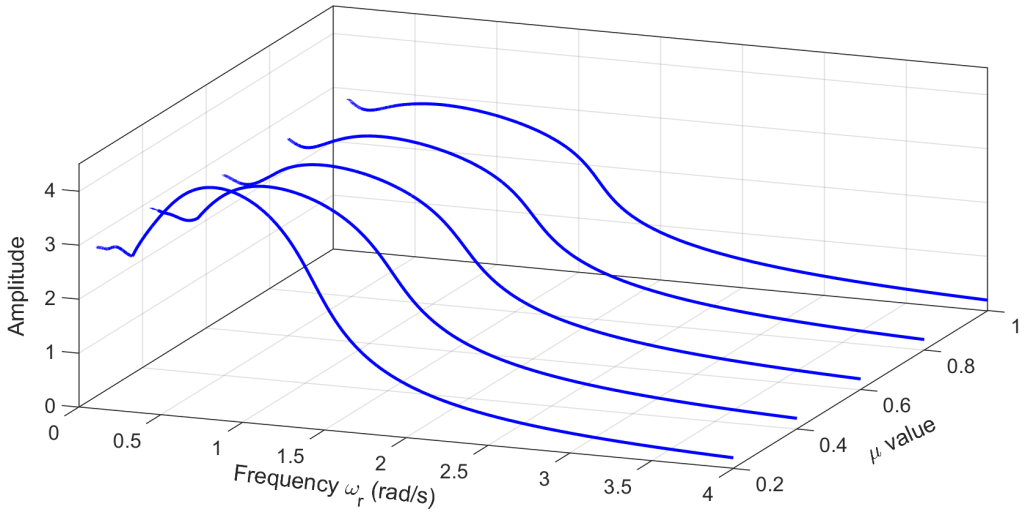

Figure 5.11: Steady-state frequency response variations with μ of Van-der-Pol oscillator. The excitation amplitude of $R = 3$ is chosen, and the responses are numerically computed with MatCont, the natural frequency considered is $\omega_n = 1$ rad/s. Curves from left to right represent the excitation amplitudes of $\mu = 0.2, 0.4, 0.6, 0.8$ and 1.0, respectively.

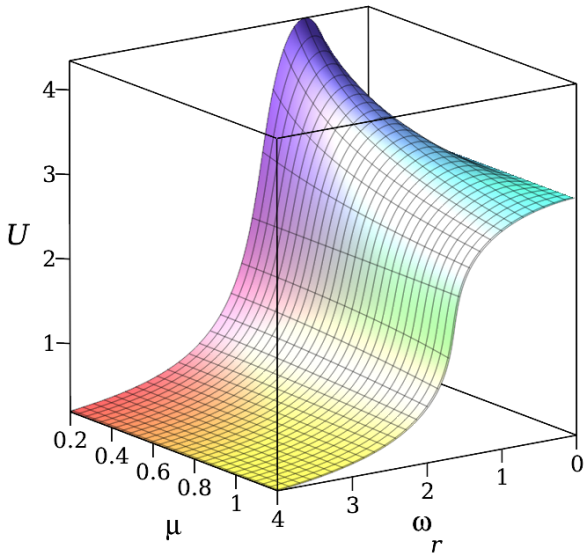

Figure 5.12: Steady-state frequency response variations with μ of Van-der-Pol oscillator. The excitation amplitude of $R = 3$ is chosen, the responses are analytically computed using the result in Eq. 5.39, the natural frequency considered is $\omega_n = 1$ rad/s.

5.4.2 DNF analysis of Van-der-Pol-Duffing and Van-der-Pol cubic-quintic oscillators

In this subsection, using DNF, an investigation of the steady-state frequency response of Van-der-Pol-Duffing oscillator is firstly performed, this is followed by the Van-der-Pol cubic-quintic system for which higher order stiffness term is involved.

Van-der-Pol-Duffing oscillator can be modelled using the following equation of motion [164],

$$\ddot{x}(t)+\mu\left(x^2(t)-1\right)\dot{x}(t)+\omega_n^2 x(t)+\varepsilon\alpha x^3(t)=R\cos(\Omega t) \tag{5.40}$$

with all parameters having the same definition as in Eq. 5.30, and ε is a bookkeeping parameter which is assumed to be unity. Moreover, α is a constant denoting the coefficient of the nonlinear term. Now, in order to apply DNF, the following preliminary steps are generated

$$\begin{aligned}\mathbf{P_x}&=\left\{\frac{R}{2},\frac{R}{2}\right\}\\ \mathbf{r}&=\{r_p,r_m\}^\intercal=\{\mathrm{e}^{\mathrm{i}\Omega t},\mathrm{e}^{-\mathrm{i}\Omega t}\}^\intercal\\ \widetilde{\mathbf{N}}(\mathbf{q},\dot{\mathbf{q}},\mathbf{r})&=\mu\left(x^2(t)-1\right)\dot{x}(t)\end{aligned} \tag{5.41}$$

and the equation of motion becomes

$$\ddot{x}(t)+\omega_n^2 x(t)+\widetilde{\mathbf{N}}(\mathbf{q},\dot{\mathbf{q}},\mathbf{r})=\mathbf{P_x r} \tag{5.42}$$

The linear modal transformation is $\mathbf{q}=\mathbf{x}=x$ since SDOF is considered, thus the EOM becomes

$$\ddot{q}+\Lambda q+N_q(\mathbf{q},\dot{\mathbf{q}},\mathbf{r})=\mathbf{P_q r} \tag{5.43}$$

where $\Lambda=\omega_n^2$, $N_q(\mathbf{q},\dot{\mathbf{q}},\mathbf{r})=\mu\left(q^2-1\right)\dot{q}+\alpha q^3$ and $\mathbf{P_q}=\mathbf{P_x}$.

In order to eliminate the non-resonant forcing terms, the transformation $\mathbf{q}=\mathbf{v}+\mathbf{er}$ is considered, moreover, $\Omega=\omega_r$ and $[\mathbf{e}]=0$, this results in

$$\ddot{v}+\Lambda v+N_v(\mathbf{v},\dot{\mathbf{v}},\mathbf{r})=\mathbf{P_v r} \tag{5.44}$$

with $N_v(\mathbf{v},\dot{\mathbf{v}},\mathbf{r})=\mu\left(v^2-1\right)\dot{v}+\alpha v^3$ and $\mathbf{P_v}=\mathbf{P_q}$.

The near-identity transformation is computed to ε^1 accuracy, by rewriting the nonlinear terms using $\mathbf{u}$, and then one can find that $n_1(\mathbf{u},\dot{\mathbf{u}},\mathbf{r}) = \mu\left(u^2-1\right)\dot{u}+\alpha u^3$ for which $\mathbf{u}=\mathbf{u_p}+\mathbf{u_m}$, all of these algebraic steps are symbolically produced using the proposed algorithm, hence, the analysis presented here is restricted to the main findings.

For ε^1 accuracy, the equation of motion can be written in the transformed coordinates, and by substituting the assumed solution the following will be obtained

$$\begin{gathered}\left(\omega_n^2-\omega_r^2\right)\frac{U}{2}\left(\mathrm{e}^{\,\mathbf{i}(\omega_r t-\phi)}+\mathrm{e}^{-\,\mathbf{i}(\omega_r t-\phi)}\right)+\\ \left(\frac{\mathbf{i}\mu U^2}{4}-\mathbf{i}\mu+\frac{3}{4}U^2\alpha\right)\omega_r\frac{U}{2}\left(\mathrm{e}^{\,\mathbf{i}(\omega_r t-\phi)}-\mathrm{e}^{-\,\mathbf{i}(\omega_r t-\phi)}\right)=\frac{R}{2}\left(\mathrm{e}^{\,\mathbf{i}\omega_r t}+\mathrm{e}^{-\,\mathbf{i}\omega_r t}\right)\end{gathered} \tag{5.45}$$

Now, it is possible to balance real and imaginary parts of Eq. 5.45, to get the following

$$\begin{aligned}\text{Re:}\quad &\left(\omega_n^2-\omega_r^2\right)U+\frac{3}{4}U^3\alpha=R\cos(\phi)\\ \text{Im:}\quad &\mu\left(\frac{U^2}{4}-1\right)\omega_r U=R\sin(\phi)\end{aligned} \tag{5.46}$$

Finally, similar to the Van-der-Pol oscillator in the previous subsection, it is possible to find the amplitude and phase relationships for the Van-der-Pol Duffing oscillator as

$$\begin{aligned}\text{Amplitude:}\quad U^2 &= \frac{R^2}{\left(\left(\omega_n^2-\omega_r^2\right)+\frac{3}{4}U^2\alpha\right)^2+\mu^2\omega_r^2\left(\frac{U^2}{4}-1\right)^2}\\ \text{Phase:}\quad \phi &= \tan^{-1}\left[\frac{\mu\omega_r\left(\frac{U^2}{4}-1\right)}{\left(\omega_n^2-\omega_r^2\right)+\frac{3}{4}U^2\alpha}\right]\end{aligned} \tag{5.47}$$

In order to investigate the differences between the analytical and numerical solutions, Fig. 5.13 is generated with R values of $1,2$ and 3, the figure shows good agreement between the analytical and numerical solutions specifically for low values of R.

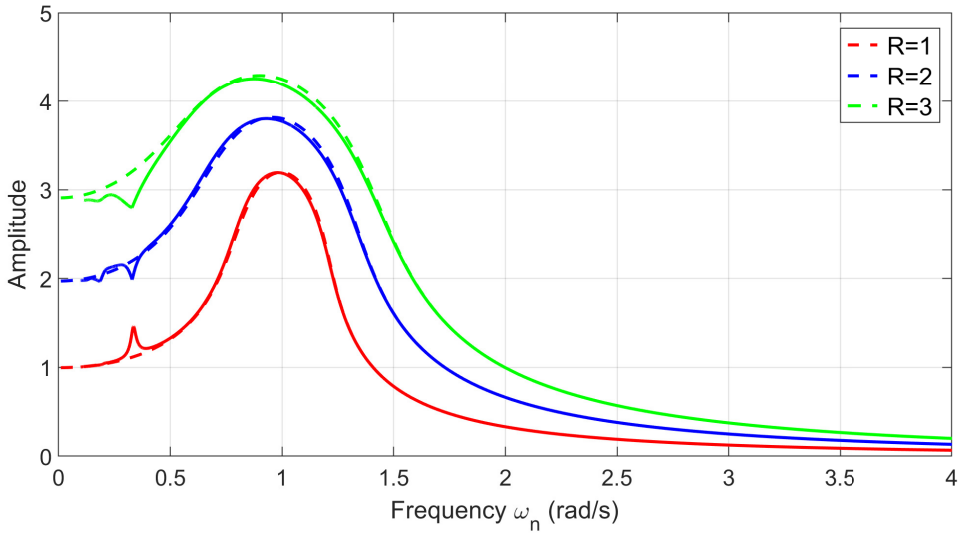

Figure 5.13: Van-der-Pol-Duffing steady-state frequency response comparison for both analytical DNF and numerical MatCont solutions for $R = 1, 2$ and 3, solid lines denote the numerical results obtained using MatCont, while the dashed lines represent ε^1 DNF solutions obtained using Eq. 5.47a). Parameter values are: $\omega_n = 1$ rad/s and $\mu = 0.2$ and $\alpha = 0.005$.

Similarly, it is possible to study the case of Van de Pol cubic-quintic oscillator governed by the following EOM,

$$\ddot{x}(t) + \mu\left(x^2(t) - 1\right)\dot{x}(t) + \omega_n^2 x(t) + \varepsilon\alpha_1 x^3(t) + \varepsilon\alpha_2 x^5(t) = R\cos(\Omega t) \tag{5.48}$$

and by repeating the previous procedure, the equation of motion in the transformed coordinates is eventually obtained. Then, by substituting the assumed solution, it is possible to write

$$\begin{gathered}\left(\omega_n^2 - \omega_r^2\right)\frac{U}{2}\left(\mathrm{e}^{\mathbf{i}(\omega_r t-\phi)} + \mathrm{e}^{-\mathbf{i}(\omega_r t-\phi)}\right) + \\ \left(\frac{\mathbf{i}\mu U^2}{4} - \mathbf{i}\mu + \frac{3}{4}U^2\alpha_1 + \frac{5}{8}U^4\alpha_2\right)\omega_r\frac{U}{2}\left(\mathrm{e}^{\mathbf{i}(\omega_r t-\phi)} - \mathrm{e}^{-\mathbf{i}(\omega_r t-\phi)}\right) = \frac{R}{2}\left(\mathrm{e}^{\mathbf{i}\omega_r t} + \mathrm{e}^{-\mathbf{i}\omega_r t}\right)\end{gathered} \tag{5.49}$$

Now, it is possible to balance real and imaginary parts of Eq. 5.49 to get

$$\begin{aligned}\text{Re:}\quad & \left(\omega_n^2 - \omega_r^2\right)U + \frac{3}{4}U^3\alpha_1 + \frac{5}{8}U^4\alpha_5 = R\cos(\phi) \\ \text{Im:}\quad & \mu\left(\frac{U^2}{4} - 1\right)\omega_r U = R\sin(\phi)\end{aligned} \tag{5.50}$$

Finally, it is possible to find the amplitude and phase relationships for Van-der-Pol cubic-quintic oscillator as

$$\begin{aligned} \text{Amplitude:} \quad U^2 &= \frac{R^2}{\left((\omega_n^2-\omega_r^2)+\frac{3}{4}U^2\alpha_1+\frac{5}{8}U^4\alpha_2\right)^2+\mu^2\omega_r^2\left(\frac{U^2}{4}-1\right)^2} \\ \text{Phase:} \quad \phi &= \tan^{-1}\left[\frac{\mu\omega_r\left(\frac{U^2}{4}-1\right)}{(\omega_n^2-\omega_r^2)+\frac{3}{4}U^2\alpha_1+\frac{5}{8}U^4\alpha_2}\right] \end{aligned} \tag{5.51}$$

By comparing the results of the Van-der-Pol cubic-quintic oscillator, Eq. 5.51, with the results of Van-der-Pol Duffing, Eq. 5.47 and those for the Van-der-Pol oscillator, Eq. 5.39, a certain pattern can be noticed; each nonlinear stiffness term leads to a new term appearing in the frequency response curve, and this is found to be applicable to any odd nonlinear term (i.e. cubic, quintic, ...). Accordingly, in the following subsection, a generalisation of the frequency-amplitude and phase-amplitude relationships for the Van-der-Pol oscillator with any type of odd polynomial nonlinearities is drawn.

5.4.3 Analysis of Van-der-Pol oscillators with any type of odd polynomial nonlinearities

In order to generalise the aforementioned results, it is possible to consider the equation of motion for a general Van-der-Pol oscillator, with multiple geometric (polynomial) odd nonlinearities, which can be written as

$$\ddot{x}(t)+\omega_n^2 x(t)+\mathbf{N_x}=R\cos(\Omega t), \tag{5.52}$$

where ω_n is the natural frequency and the nonlinear terms vector N_x, in its general form, is written as

$$N_x=\mu\left(x^2(t)-1\right)\dot{x}(t)+\sum_{i=1}^{M}\alpha_i x^i(t) \tag{5.53}$$

Herein, α_i, the coefficient of the i^{th} nonlinear stiffness term is considered to be relatively small, and M denotes the number of odd nonlinear terms. Using the method of DNF (implemented symbolically), the corresponding amplitude and phase relationships are obtained to ε^1 accuracy and this can be written in a general form to include any odd nonlinear stiffness terms, in addition to any combination of odd nonlinear stiffness terms. If considering the amplitude and phase relationships for Van-der-Pol, Duffing Van-der-Pol and cubic-quintic Van-

der-Pol oscillators, Eq. 5.39, Eq. 5.47 and Eq. 5.51, respectively, a pattern is clearly noticed for both U^2 and ϕ, which is

$$\begin{aligned} \text{Amplitude:} \quad U^2 &= \frac{R^2}{\left((\omega_n^2-\omega_r^2)+\sum_{j=1}^{M}\left(\frac{1}{2^{2j}}\binom{2j+1}{j+1}\alpha_j U^{2j+1}\right)\right)^2+\mu^2\omega_r^2\left(\frac{U^2}{4}-1\right)^2} \\ \text{Phase:} \quad \phi &= \tan^{-1}\left[\frac{\mu\omega_r\left(\frac{U^2}{4}-1\right)}{(\omega_n^2-\omega_r^2)+\sum_{j=1}^{M}\left(\frac{1}{2^{2j}}\binom{2j+1}{j+1}\alpha_j U^{2j+1}\right)}\right] \end{aligned} \tag{5.54}$$

where j in the summation represents the order of the odd nonlinear term appearing in the EOM, starting from $j=1$ for cubic nonlinearity, $j=2$ for quintic nonlinearity and so on, moreover, α_j denotes the coefficient of the corresponding nonlinear term.

In the following section, the Rayleigh oscillator is investigated using DNF in order to compare the steady-state amplitudes for Van-der-Pol and Rayleigh oscillators.

5.4.4 DNF analysis of Rayleigh oscillator

In this section, an investigation of the steady-state frequency response of Rayleigh oscillator is performed using DNF, similar to the Van-der-Pol oscillator, the Rayleigh oscillator is assumed to be forced with a harmonic force near the resonance. In analogy to Van-der-Pol oscillator in Eq. 5.30, Rayleigh oscillator can be modelled using the following equation of motion [110],

$$\ddot{x}(t)+\mu\left(\dot{x}^2(t)-1\right)\dot{x}(t)+\omega_n^2 x(t)=R\cos(\Omega t) \tag{5.55}$$

where all parameters have the same definition as in Eq. 5.30, the only difference here is the term $\dot{x}^3(t)$ appearing in the EOM rather than the term $x^2(t)\dot{x}(t)$ for Van-der-Pol case, and due to the fact that the assumed solution has an exponential form, then DNF method is applicable.

In order to apply DNF, the following preliminary steps are practised

$$\begin{aligned} \mathbf{P_x} &= \left\{ \frac{R}{2}, \frac{R}{2} \right\} \\ \mathbf{r} &= \{r_p, r_m\}^\intercal = \{\mathrm{e}^{\,\mathrm{i}\Omega t}, \mathrm{e}^{-\,\mathrm{i}\Omega t}\}^\intercal \\ \widetilde{\mathbf{N}}(\mathbf{q}, \dot{\mathbf{q}}, \mathbf{r}) &= \mu \left(\dot{x}^2(t) - 1\right) \dot{x}(t) \end{aligned} \tag{5.56}$$

and thus the equation of motion becomes

$$\ddot{x}(t) + \omega_n^2 x(t) + \widetilde{\mathbf{N}}(\mathbf{q}, \dot{\mathbf{q}}, \mathbf{r}) = \mathbf{P_x r} \tag{5.57}$$

The linear modal transformation is $\mathbf{q} = \mathbf{x} = x$ since SDOF is considered, thus

$$\ddot{q} + \Lambda q + N_q(\mathbf{q}, \dot{\mathbf{q}}, \mathbf{r}) = \mathbf{P_q r} \tag{5.58}$$

where $\Lambda = \omega_n^2$, $N_q(\mathbf{q}, \dot{\mathbf{q}}, \mathbf{r}) = \mu \left(\dot{q}^2 - 1\right) \dot{q}$ and $\mathbf{P_q} = \mathbf{P_x}$.

In order to eliminate the non-resonant forcing terms, the transformation of $\mathbf{q} \to \mathbf{v}$ to be $\mathbf{q} = \mathbf{v} + \mathbf{er}$ is considered, moreover, $\Omega = \omega_r$ and $[\mathbf{e}] = 0$, this results in

$$\ddot{v} + \Lambda v + N_v(\mathbf{v}, \dot{\mathbf{v}}, \mathbf{r}) = \mathbf{P_v r} \tag{5.59}$$

with $N_v(\mathbf{v}, \dot{\mathbf{v}}, \mathbf{r}) = \mu \left(\dot{v}^2 - 1\right) \dot{v}$ and $\mathbf{P_v} = \mathbf{P_q}$.

The near-identity transformation is computed to ε^1 accuracy, by rewriting the nonlinear terms using $\mathbf{u}$, one can find that $n_1(\mathbf{u}, \dot{\mathbf{u}}, \mathbf{r}) = \mu \left(\dot{u}^2 - 1\right) \dot{u}$ for which $\mathbf{u} = \mathbf{u_p} + \mathbf{u_m}$, thus

$$\mathbf{u}^* = \begin{bmatrix} u_m^3 \\ u_p^3 \\ u_p u_m^2 \\ u_p^2 u_m \\ u_m \\ u_p \end{bmatrix} \rightsquigarrow \mathbf{n}^* = \mathbf{i}\mu\omega_r \begin{bmatrix} \omega_r^2 \\ -\omega_r^2 \\ -3\omega_r^2 \\ 3\omega_r^2 \\ 1 \\ -1 \end{bmatrix}^{\mathsf{T}} \rightsquigarrow \boldsymbol{\beta}^* = \omega_r^2 \begin{bmatrix} 8 \\ 8 \\ 0 \\ 0 \\ 0 \\ 0 \end{bmatrix}^{\mathsf{T}} \rightsquigarrow$$
$$\mathbf{h}^* = \frac{\mathbf{i}\mu\omega_r}{8} \begin{bmatrix} 1 \\ -1 \\ 0 \\ 0 \\ 0 \\ 0 \end{bmatrix}^{\mathsf{T}} \rightsquigarrow \mathbf{n}_{\mathbf{u}}^* = \mathbf{i}\mu\omega_r \begin{bmatrix} 0 \\ 0 \\ -3\omega_r^2 \\ 3\omega_r^2 \\ 1 \\ -1 \end{bmatrix}^{\mathsf{T}} \tag{5.60}$$

Compared to the matrix manipulation of Van-der-Pol oscillator in Eq. 5.35, same matrix dimensions and similar terms appearing in Eq. 5.60 except for some higher orders of ω_r, and this is expected due to the oscillators' equation of motions being similar to each other with minor differences as previously shown.

For ε^1 accuracy, the equation of motion can then be written in the transformed coordinates, and upon substituting the assumed solution, the following can be found

$$\begin{aligned} \left(\omega_n^2 - \omega_r^2\right) \frac{U}{2} \left(\mathrm{e}^{\,\mathbf{i}(\omega_r t - \phi)} + \mathrm{e}^{-\,\mathbf{i}(\omega_r t - \phi)}\right) + \mathbf{i}\mu \left(\frac{3U^2\omega_r^2}{4} - 1\right) \omega_r \frac{U}{2} \left(\mathrm{e}^{\,\mathbf{i}(\omega_r t - \phi)} - \mathrm{e}^{-\,\mathbf{i}(\omega_r t - \phi)}\right) \\ = \frac{R}{2} \left(\mathrm{e}^{\,\mathbf{i}\omega_r t} + \mathrm{e}^{-\,\mathbf{i}\omega_r t}\right) \end{aligned} \tag{5.61}$$

Now, it is possible to balance real and imaginary parts of Eq. 5.61, which gives

$$\begin{aligned} \text{Re:} \quad & \left(\omega_n^2 - \omega_r^2\right) U = R\cos(\phi) \\ \text{Im:} \quad & \mu \left(\frac{3U^2\omega_r^2}{4} - 1\right) \omega_r U = R\sin(\phi) \end{aligned} \tag{5.62}$$

Finally, it is possible to find the amplitude and phase relationships for the Rayleigh oscillator as

$$\begin{aligned} \text{Amplitude:} \quad U^2 &= \frac{R^2}{(\omega_n^2-\omega_r^2)^2+\mu^2\omega_r^2\left(\frac{3U^2\omega_r^2}{4}-1\right)^2} \\ \text{Phase:} \quad \phi &= \tan^{-1}\left[\frac{\mu\omega_r\left(\frac{3U^2\omega_r^2}{4}-1\right)}{(\omega_n^2-\omega_r^2)}\right] \end{aligned} \tag{5.63}$$

In order to investigate the accuracy of the results in Eq. 5.63, similar to the analysis held for Van-der-Pol oscillator, MatCont toolbox is used to investigate the steady-state frequency response of Rayleigh oscillator in Fig. 5.14 for various excitation frequencies of $R = 0.5, 1, 1.5, 2, 2.5, 3, 3.5$ and 4, moreover, the same results can be seen in Fig. 5.15 using the analytical results in Eq. 5.63. Furthermore, similar to the generated plots of Van-der-Pol oscillator, the amplitude-frequency variations with the excitation amplitude for Rayleigh oscillator are shown in Fig. 5.14. This figure is analytically generated using ε^1 DNF results in Eq. 5.63 for the excitation amplitudes of $R = 0.5-4$, while the natural frequency is $\omega_n = 1$ rad/s and $\mu = 0.2$. From Fig. 5.14, it is noticed that, similar to Van-der-Pol case, increasing the excitation amplitude results in higher peak frequency of the system around the selected natural frequency.

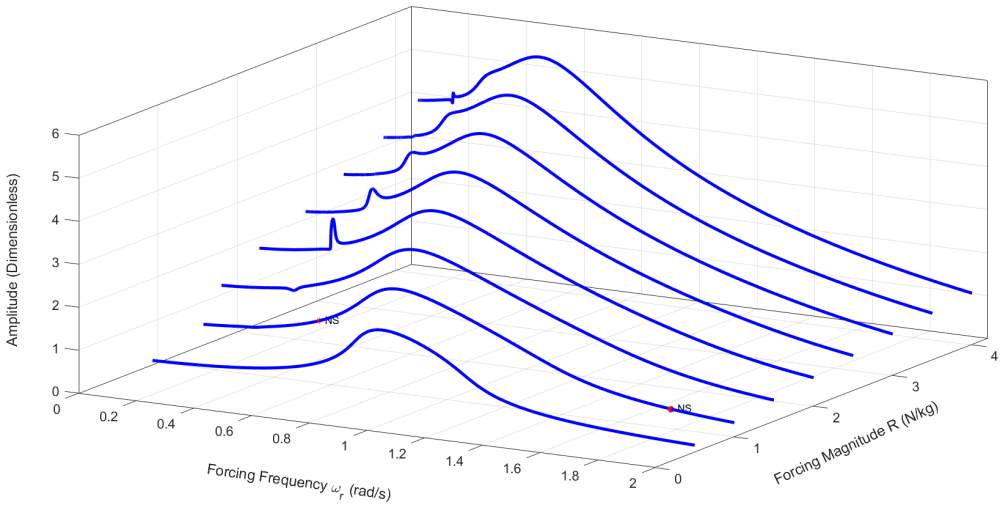

Figure 5.14: Steady-state frequency response manifolds for Rayleigh oscillator, the manifolds are computed numerically using MatCont toolbox. Parameter values are: $\omega_n = 1$ rad/s and $\mu = 0.2$. Curves from left to right represent the excitation amplitude of $R = 0.5, 1, 1.5, 2, 2.5, 3, 3.5$ and 4, respectively.

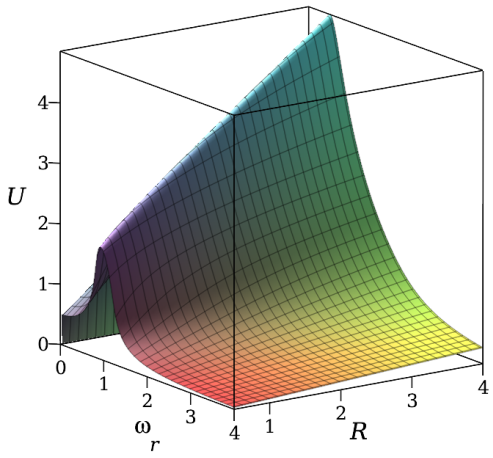

Figure 5.15: Steady-state frequency response manifolds for Rayleigh oscillator, the manifolds are computed analytically using ε^1 DNF results obtained from Eq. 5.63. Parameter values are: $\omega_n = 1$ rad/s and $\mu = 0.2$.

To In order to investigate the differences between the analytical and numerical solutions, Fig. 5.16 is generated, in which a comparison of the steady-state amplitude for R values of $1, 2$ and 3 is performed, the figure shows good agreement between the analytical and numerical solutions for lower values of R, while increasing R leads to less matching, this can be related to the accuracy of both DNF and MatCont.

The comparison in Fig. 5.16 shows that, as in the case of Van-der-Pol oscillator, MatCont continuation technique is able to capture the subharmonic resonances while ε^1 DNF method is unable to detect such types of behaviour. Moreover, both numerical and analytical results show the same trend with slight differences especially at lower values of R, nevertheless, the differences tend to grow with increasing R values.

In the literature, more complex systems involving stiffness and damping combinations can be found; this includes, as previously discussed, the Rayleigh-Duffing oscillator and cubic-quintic Rayleigh oscillator, and even the hybrid Rayleigh-Van der pol-Duffing oscillator recently introduced in [115], exploring such systems using traditional DNF method can be challenging due to the increasing number of terms involved. In addition, the effect of some higher orders polynomial stiffness terms cannot be captured with ε^1 DNF, this practically occurs for even nonlinear terms, refer to the discussions in Section 5.2 and the analysis in [8] for some examples, thus, higher order accuracies need to be considered which enormously increase the computations difficulty.

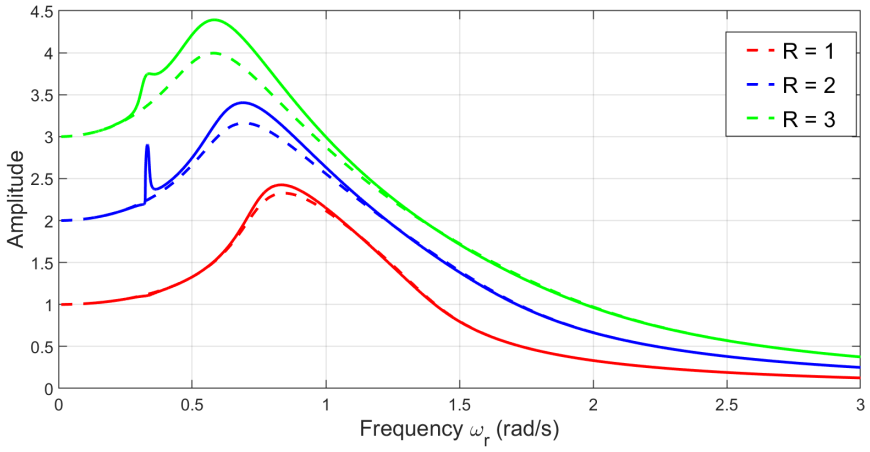

Figure 5.16: Rayleigh oscillator steady-state frequency response comparison for both analytical DNF and numerical MatCont solutions for excitation magnitudes of $R = 1, 2$ and 3, solid lines show numerical results obtained using MatCont while dashed lines represent the analytical results obtained using Eq. 5.62. Parameter values are: $\omega_n = 1$ rad/s and $\mu = 0.2$.

In the following subsection, ε^1 DNF is used for exploring the Rayleigh-Duffing oscillator and cubic-quintic Rayleigh oscillator for which symbolic computations show reliable tool to make the mathematical manipulations needed for the analysis.

5.4.5 DNF analysis of Rayleigh-Duffing and Rayleigh cubic-quintic oscillators

In this subsection, an investigation of the steady-state frequency response of Rayleigh-Duffing oscillator is performed using DNF, in addition to the appearance of $\dot{x}^3$ as in Rayleigh oscillator, this system involves a higher order stiffness term. i.e. x^3. Accordingly, Rayleigh-Duffing oscillator can be modelled using the following equation of motion [110],

$$\ddot{x}(t) + \mu\left(\dot{x}^2(t) - 1\right)\dot{x}(t) + \omega_n^2 x(t) + \varepsilon\alpha x^3(t) = R\cos(\Omega t) \tag{5.64}$$

where α is a constant denoting the coefficient of the cubic nonlinear stiffness term, ε is a bookkeeping parameter which is assumed to be unity, and all other parameters have the same definition as in Eq. 5.55.

In order to apply DNF, the following preliminary steps are practised

$$\begin{aligned} \mathbf{P_x} &= \left\{ \frac{R}{2}, \frac{R}{2} \right\} \\ \mathbf{r} &= \{r_p, r_m\}^\intercal = \{\mathrm{e}^{\,\mathbf{i}\Omega t}, \mathrm{e}^{-\,\mathbf{i}\Omega t}\}^\intercal \\ \widetilde{\mathbf{N}}(\mathbf{q}, \dot{\mathbf{q}}, \mathbf{r}) &= \mu \left(\dot{x}^2(t) - 1\right) \dot{x}(t) + \varepsilon \alpha x^3(t) \end{aligned} \tag{5.65}$$

and thus the equation of motion becomes

$$\ddot{x}(t) + \omega_n^2 x(t) + \widetilde{\mathbf{N}}(\mathbf{q}, \dot{\mathbf{q}}, \mathbf{r}) = \mathbf{P_x r} \tag{5.66}$$

The linear modal transformation is $\mathbf{q} = \mathbf{x} = x$ since SDOF is considered, thus

$$\ddot{q} + \Lambda q + N_q(\mathbf{q}, \dot{\mathbf{q}}, \mathbf{r}) = \mathbf{P_q r} \tag{5.67}$$

where $\Lambda = \omega_n^2$, $N_q(\mathbf{q}, \dot{\mathbf{q}}, \mathbf{r}) = \mu \left(\dot{q}^2 - 1\right) \dot{q} + \alpha q^3$ and $\mathbf{P_q} = \mathbf{P_x}$.

In order to eliminate the non-resonant forcing terms, the transformation of $\mathbf{q} \to \mathbf{v}$ to be $\mathbf{q} = \mathbf{v} + \mathbf{e}\mathbf{r}$ is considered, moreover, $\Omega = \omega_r$ and $[\mathbf{e}] = 0$, this results in

$$\ddot{v} + \Lambda v + N_v(\mathbf{v}, \dot{\mathbf{v}}, \mathbf{r}) = \mathbf{P_v r} \tag{5.68}$$

with $N_v(\mathbf{v}, \dot{\mathbf{v}}, \mathbf{r}) = \mu \left(\dot{v}^2 - 1\right) \dot{v} + \alpha v^3$ and $\mathbf{P_v} = \mathbf{P_q}$.

The near-identity transformation is computed to ε^1 accuracy, by rewriting the nonlinear terms using $\mathbf{u}$, it is possible to find that $n_1(\mathbf{u}, \dot{\mathbf{u}}, \mathbf{r}) = \mu \left(\dot{u}^2 - 1\right) \dot{u} + \alpha u^3$ for which $\mathbf{u} = \mathbf{u_p} + \mathbf{u_m}$, all of these algebraic steps are symbolically produced using the proposed algorithm and here the analysis is limited to the main findings.

For ε^1 accuracy, the equation of motion can then be written in the transformed coordinates, and by substituting the assumed solution, it is possible to write

$$\begin{aligned} &\left(\omega_n^2 - \omega_r^2\right) \frac{U}{2} \left(\mathrm{e}^{\,\mathbf{i}(\omega_r t - \phi)} + \mathrm{e}^{-\,\mathbf{i}(\omega_r t - \phi)}\right) + \\ &\left(\frac{3\,\mathbf{i}\mu U^2 \omega_r^2}{4} - \mathbf{i}\mu + \frac{3}{4} U^2 \alpha\right) \omega_r \frac{U}{2} \left(\mathrm{e}^{\,\mathbf{i}(\omega_r t - \phi)} - \mathrm{e}^{-\,\mathbf{i}(\omega_r t - \phi)}\right) = \frac{R}{2} \left(\mathrm{e}^{\,\mathbf{i}\omega_r t} + \mathrm{e}^{-\,\mathbf{i}\omega_r t}\right) \end{aligned} \tag{5.69}$$

Now, it is possible to balance real and imaginary parts of Eq. 5.69 to get the following

$$\begin{aligned} \text{Re:} \quad & \left(\omega_n^2 - \omega_r^2\right) U + \frac{3}{4} U^3 \alpha = R\cos(\phi) \\ \text{Im:} \quad & \mu \left(\frac{3U^2\omega_r^2}{4} - 1\right) \omega_r U = R\sin(\phi) \end{aligned} \tag{5.70}$$

Finally, it is possible to find the amplitude and phase relationships for the Rayleigh-Duffing oscillator as

$$\begin{aligned} \text{Amplitude:} \quad & U^2 = \frac{R^2}{\left((\omega_n^2 - \omega_r^2) + \frac{3}{4}U^2\alpha\right)^2 + \mu^2\omega_r^2\left(\frac{3U^2\omega_r^2}{4} - 1\right)^2} \\ \text{Phase:} \quad & \phi = \tan^{-1}\left[\frac{\mu\omega_r\left(\frac{3U^2\omega_r^2}{4} - 1\right)}{(\omega_n^2 - \omega_r^2) + \frac{3}{4}U^2\alpha}\right] \end{aligned} \tag{5.71}$$

As for the case of Rayleigh oscillator, Fig. 5.17 shows a comparison of the steady-state frequency response for both MatCont numerical results and DNF analytical results using Eq. 5.71. By comparing the peaks in Fig. 5.17 to the corresponding peaks in Fig. 5.17, the effects of adding the $\dot{x}^3$ term (i. e. Rayleigh-Duffing case) are clearly observed, for which significant reduction of the peak amplitude responses is found.

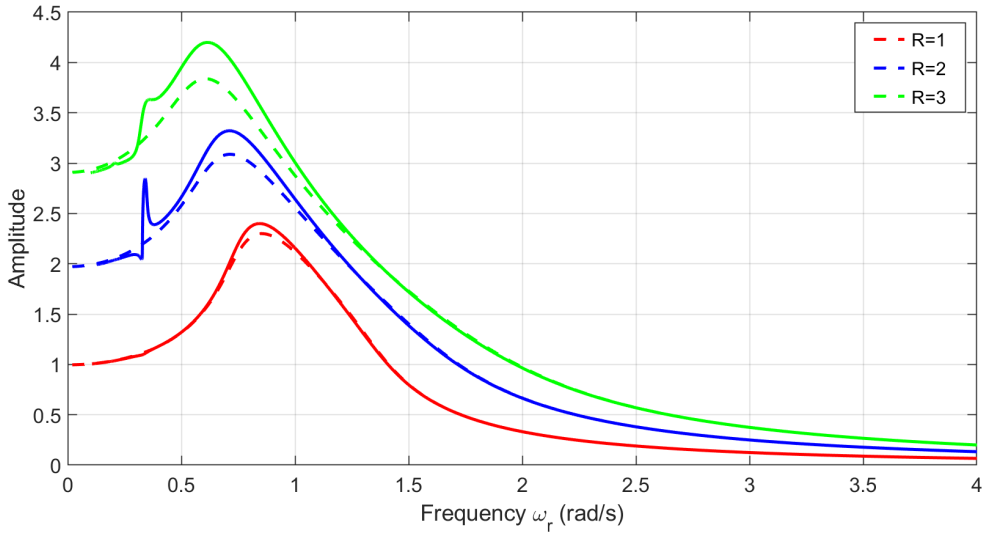

Figure 5.17: Steady-state frequency response comparison of the Rayleigh-Duffing oscillator for both analytical DNF and numerical MatCont solutions for $R = 1, 2$ and 3. Solid lines show numerical results from MatCont while dashed lines show analytical results from Eq. 5.71. Parameter values are: $\omega_n = 1$ rad/s and $\mu = 0.2$.

Similarly, one could study the case of Rayleigh cubic-quintic oscillator governed by the following EOM,

$$\ddot{x}(t)+\mu\left(\dot{x}^2(t)-1\right)\dot{x}(t)+\omega_n^2 x(t)+\varepsilon\alpha_1 x^3(t)+\varepsilon\alpha_2 x^5(t)=R\cos(\Omega t) \tag{5.72}$$

and by repeating the previous procedure, the equation of motion in the transformed coordinates is finally obtained, and by substituting the assumed solution. Then, it is possible to get

$$\begin{gathered}\left(\omega_n^2-\omega_r^2\right)\frac{U}{2}\left(\mathrm{e}^{\,\mathbf{i}(\omega_r t-\phi)}+\mathrm{e}^{-\,\mathbf{i}(\omega_r t-\phi)}\right)+\\ \left(\frac{3\,\mathbf{i}\mu U^2\omega_r^2}{4}-\mathbf{i}\mu+\frac{3}{4}U^2\alpha_1+\frac{5}{8}U^4\alpha_2\right)\omega_r\frac{U}{2}\left(\mathrm{e}^{\,\mathbf{i}(\omega_r t-\phi)}-\mathrm{e}^{-\,\mathbf{i}(\omega_r t-\phi)}\right)=\frac{R}{2}\left(\mathrm{e}^{\,\mathbf{i}\omega_r t}+\mathrm{e}^{-\,\mathbf{i}\omega_r t}\right)\end{gathered} \tag{5.73}$$

Now, ot is possible to balance the real and imaginary parts of Eq. 5.73, which gives

$$\begin{aligned}\text{Re:}\quad &\left(\omega_n^2-\omega_r^2\right)U+\frac{3}{4}U^3\alpha_1+\frac{5}{8}U^4\alpha_5=R\cos(\phi)\\ \text{Im:}\quad &\mu\left(\frac{3U^2\omega_r^2}{4}-1\right)\omega_r U=R\sin(\phi)\end{aligned} \tag{5.74}$$

Finally, it is possible to find the amplitude and phase relationships for the Rayleigh cubic-quintic oscillator as

$$\begin{aligned}\text{Amplitude:}\quad U^2&=\frac{R^2}{\left(\left(\omega_n^2-\omega_r^2\right)+\frac{3}{4}U^2\alpha_1+\frac{5}{8}U^4\alpha_2\right)^2+\mu^2\omega_r^2\left(\frac{3U^2\omega_r^2}{4}-1\right)^2}\\ \text{Phase:}\quad \phi&=\tan^{-1}\left[\frac{\mu\omega_r\left(\frac{3U^2\omega_r^2}{4}-1\right)}{\left(\omega_n^2-\omega_r^2\right)+\frac{3}{4}U^2\alpha_1+\frac{5}{8}U^4\alpha_2}\right]\end{aligned} \tag{5.75}$$

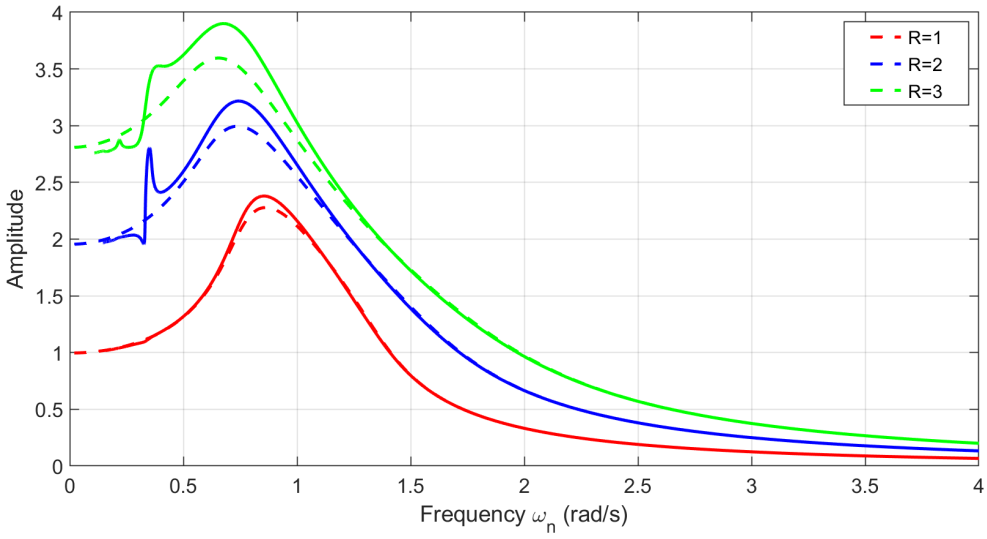

Figure 5.18: Steady-state frequency response comparison of the Rayleigh-cubic-quintic oscillator for both analytical DNF and numerical MatCont solutions for $R = 1, 2$ and 3. Solid lines show numerical results from MatCont while dashed lines show analytical results from Eq. 5.75. Parameter values are: $\omega_n = 1$ rad/s and $\mu = 0.2$.

5.4.6 Analysis of Rayleigh oscillators with any type of odd polynomial nonlinearities

In order to generalise the aforementioned results, it is possible to consider the equation of motion for a general Rayleigh oscillator, with multiple geometric (polynomial) odd nonlinearities, which can be written as

$$\ddot{x}(t) + \omega_n^2 x(t) + \mathbf{N_x} = R\cos(\Omega t), \tag{5.76}$$

where ω_n is the natural frequency and the nonlinear terms vector N_x, in its general form, is written as

$$N_x = \mu\left(\dot{x}^2(t) - 1\right)\dot{x}(t) + \sum_{i=1}^{M} \alpha_i x^i(t) \tag{5.77}$$

Herein, α_i, the coefficient of the i^{th} nonlinear stiffness term is considered to be relatively small, and M denotes the number of odd nonlinear terms. Using the method of DNF (implemented symbolically), the corresponding amplitude and phase relationships are obtained to ε^1 accuracy and this can be written in a general form to include any odd nonlinear stiffness terms, in addition to any combination of odd nonlinear stiffness terms. When considering the amplitude and phase relationships for Rayleigh, Duffing Rayleigh and cubic-quintic Rayleigh oscillators in Eq. 5.63, Eq. 5.71 and Eq. 5.75, respectively, a pattern is clearly noticed for both U^2

and ϕ, which is

$$\begin{aligned} \text{Amplitude:} \quad U^2 &= \frac{R^2}{\left((\omega_n^2-\omega_r^2)+\sum_{j=1}^{M}\left(\frac{1}{2^{2j}}\binom{2j+1}{j+1}\alpha_j U^{2j+1}\right)\right)^2+\mu^2\omega_r^2\left(\frac{3U^2\omega_r^2}{4}-1\right)^2} \\ \text{Phase:} \quad \phi &= \tan^{-1}\left[\frac{\mu\omega_r\left(\frac{3U^2\omega_r^2}{4}-1\right)}{(\omega_n^2-\omega_r^2)+\sum_{j=1}^{M}\left(\frac{1}{2^{2j}}\binom{2j+1}{j+1}\alpha_j U^{2j+1}\right)}\right] \end{aligned} \tag{5.78}$$

where j in the summation represents the order of the odd nonlinear term appearing in the EOM, starting from $j=1$ for cubic nonlinearity, $j=2$ for quintic nonlinearity and so on, moreover, α_j denotes the coefficient of the corresponding nonlinear term.

5.4.7 Numerical comparison of the six types of oscillators

For comparison purposes, it is possible to plot the frequency-response manifolds for each oscillator in 3-dimensional coordinates, with x, y and z axes denoting the frequency, amplitude, and excitation amplitude, respectively. Fig. 5.19 shows this comparison for the numerical values of $\omega_n = 1$ rad/s, $\mu = 0.2$, $\alpha_1 = 0.02$ and $\alpha_2 = 0.05$. In this figure, the U-axis limits are chosen to be similar for comparison purposes. Moreover, to investigate the effect of μ value to the steady-state frequency response of the six oscillators considered in this work, Fig. 5.20 is generated for the numerical values of $\omega_n = 1$ rad/s, $R = 5$, $\alpha_1 = 0.03$ and $\alpha_2 = 0.01$. In this figure, since the amplitudes of U are different between Van-der-Pol and Rayleigh oscillators, U-axis limits are kept similar for plots of the same types (i.e. Van-der-Pol and Rayleigh). According to the aforementioned discussions, one can study the difference between Van-der-Pol and Rayleigh oscillators, and the effect of adding geometric stiffness terms to each type of those oscillators. For instance, using the manifolds in Fig. 5.19, Table 5.7 is generated for the numerical values of the maximum amplitudes U and the frequencies they occur at, for each oscillator type. From Fig. 5.19 & Fig. 5.20, and Table 5.7, for the selected (specific) parameters, the following outcomes can be observed;

- The maximum amplitude resulting of Van-der-Pol is greater than that of Rayleigh, this due to the effect of the term $\dot{x}(t)$ in Rayleigh oscillators, refer to Eq. 5.55.

- Adding geometric stiffness terms to the EOM of both oscillators yields to reduction of the peak amplitudes while shifting the peaks to higher values.
- In some cases, adding higher orders of the geometric stiffness terms results in certain discontinuities in the frequency manifolds, this can be related to the overall effects of these stiffness terms to the oscillations (i.e. making the system highly stiff), this observation needs more extended research related to these oscillators which is out of the scope of this thesis.

Table 5.7: Numerical comparison of maximum amplitudes U for each type of oscillators plotted in Fig. 5.19

Oscillator type	Corresponding ε^1 DNF results	Maximum amplitude U_{min}	ω_r at maximum amplitude
Van-der-Pol	Eq. 5.39	4.345	0.829
Van-der-Pol-Duffing	Eq. 5.47	4.104	1.088
Van-der-Pol cubic-quintic	Eq. 5.51	3.739	1.577
Rayleigh	Eq. 5.63	3.987	0.568
Rayleigh-Duffing	Eq. 5.71	3.372	0.694
Rayleigh cubic-quintic	Eq. 5.75	2.849	0.856

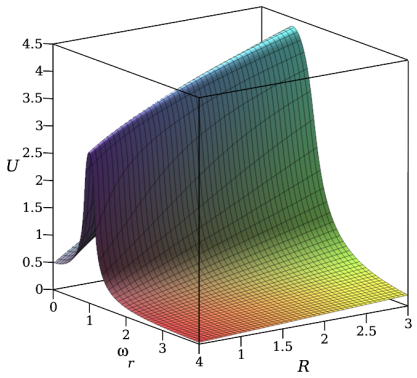

(a) Van-der-Pol

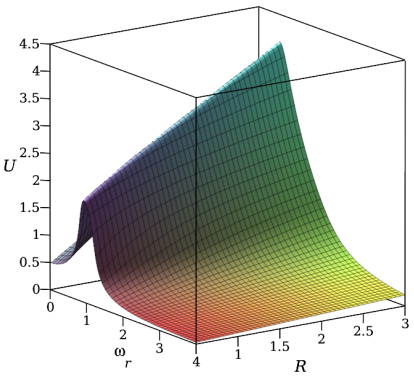

(b) Rayleigh

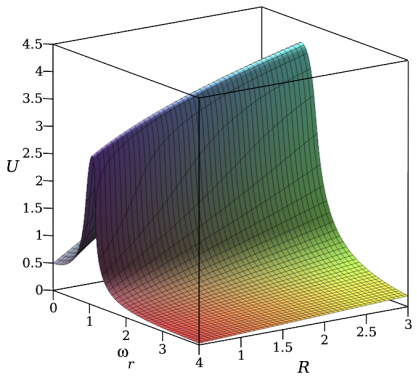

(c) Van-der-Pol-Duffing

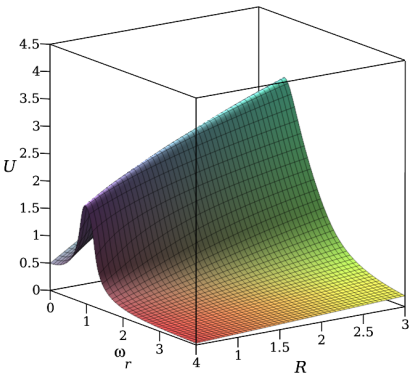

(d) Rayleigh-Duffing

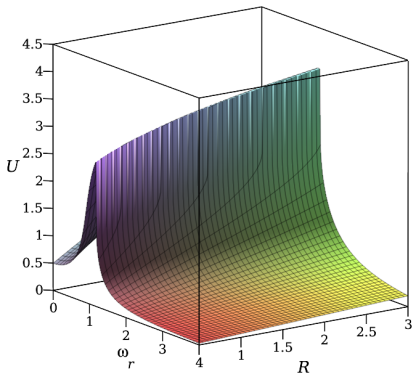

(e) Van-der-Pol-cubic quintic

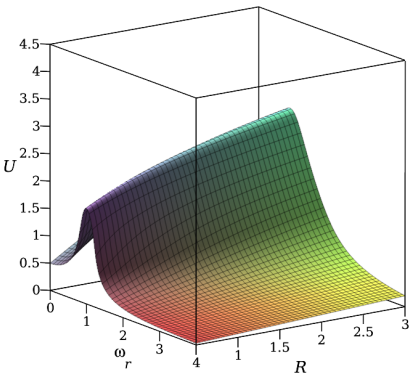

(f) Rayleigh-cubic quintic

Figure 5.19: Frequency response variations with forcing frequency for the six oscillators considered, all manifolds are computed using the analytical results discussed earlier. Parameter values are: $\omega_n = 1$ rad/s, $\mu = 0.2$, $\alpha_1 = 0.02$ and $\alpha_2 = 0.05$.

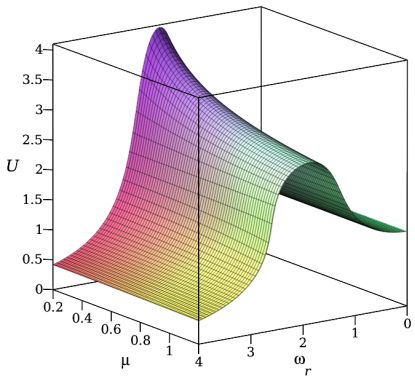

(a) Van-der-Pol

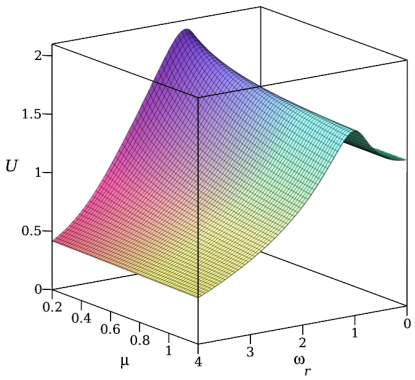

(b) Rayleigh

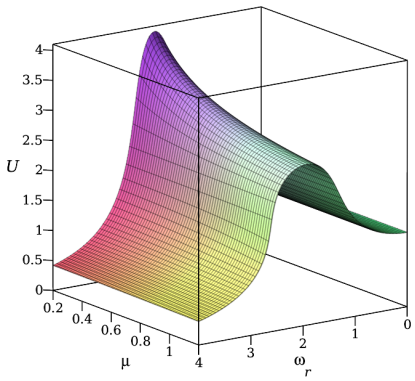

(c) Van-der-Pol-Duffing

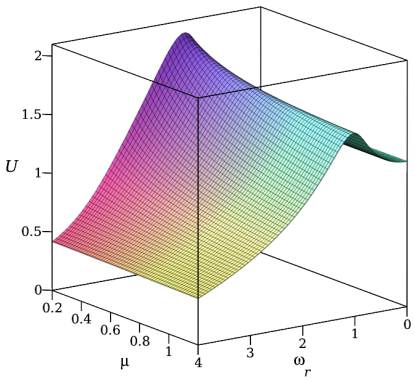

(d) Rayleigh-Duffing

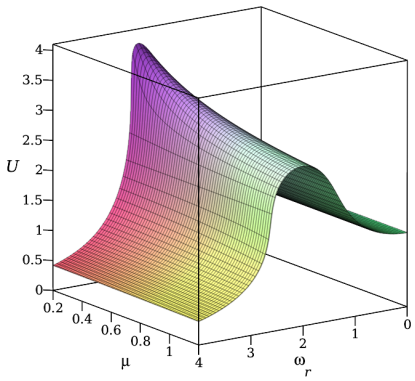

(e) Van-der-Pol-cubic quintic

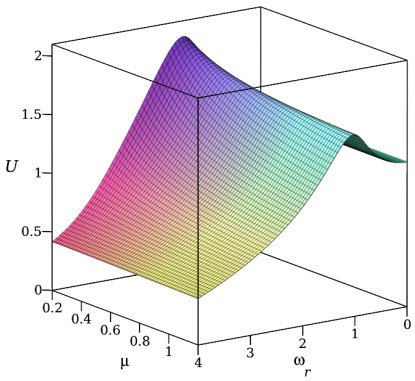

(f) Rayleigh-cubic quintic

Figure 5.20: Frequency response variations with μ for the six oscillators considered, all manifolds are computed using the analytical results discussed earlier. Parameter values are: $\omega_n = 2$ rad/s, $R = 5$, $\alpha_1 = 0.03$ and $\alpha_2 = 0.01$.

5.5 Summary

In this Chapter, applications of the symbolically applied DNF method for various types of SDOF systems are shown, two main topics are studied; the analysis of cubic-quintic oscillators (which eventually led to generic SDOF oscillators), and the analysis of oscillators with combinations of nonlinear stiffness and damping terms. Starting by the conservative cubic-quintic oscillator, analytical expressions of the backbone curves for both ε^1 and ε^2 are obtained, and a general formula to obtain the backbone curves for oscillators with odd polynomial stiffness (geometric) nonlinear terms is then concluded. Based on the analysis of these types of oscillators the following findings are observed;

- When compared to the numerical solutions (as a benchmark), if only odd nonlinear terms (such as the cubic-quintic) are found in the EOM, the outcomes of ε^2 order solutions were not always more accurate than the ε^1 order solutions.

- When even nonlinear terms were added, as with the generic cubic-quintic oscillator this observation is changed, and here, as would be expected, ε^2 order solutions were always more accurate than the ε^1 order solutions.

- Finally, it was shown that, for the SDOF oscillators considered with only odd nonlinear terms, the expression for the backbone curve of the system up to ε^1 order could be generalized. However, this was not the case when even nonlinearities were present and ε^2 accuracy was needed.

On the other hand, the second topic discussed in this Chapter is oscillators with combinations of nonlinear stiffness and damping terms, including Van-der-Pol, Rayleigh, Van-der-Pol Duffing, Rayleigh Duffing, cubic-quintic Van-der-Pol and finally the cubic-quintic Rayleigh oscillator. Referring to the aforementioned discussions for this topic, the following outcomes are seen;

- In the literature, upon these types of oscillators, only the Van-der-Pol oscillator was priorly discussed using DNF method, thus, using the symbolic computations the author has been able to extend the capabilities of DNF to analyse more complicated systems of that kind.

- For all of these oscillators, analytical frequency-response and phase relationships are obtained, and for verification purposes, those are compared to the numerical results obtained using MatCont continuation

package in MATLAB.

- Comparing the frequency-amplitude relationship of Van-der-Pol and Rayleigh oscillators, a similar trend can be observed, refer to Eq. 5.39 and Eq. 5.63, thus, for some specific applications, comparisons between these two types of oscillators are performed, refer to [121] for an example.

- For ε^1 DNF accuracy, the effect of adding odd nonlinear stiffness terms to Van-der-Pol or Rayleigh EOM's appears in the frequency response relationships in the form of additional stiffness terms, those terms are identical to those computed in Section 5.2, i.e. refer to the summation terms appearing in Eq. 5.29, Eq. 5.54, and Eq. 5.78.

- To conclude, it is important to mention that the analysis practised in this Section is based on ε^1 DNF accuracy, however, for future potential work, if odd nonlinear terms included into the EOMs, the effect of raising the accuracy to ε^2 can be investigated, while if even nonlinear terms are included, it can be also beneficial to study ε^3 accuracy, recall the discussions regarding higher order accuracies and their effect to the frequency-responses of the systems, Section 4.6.

Chapter 6

Exploring fractional nonlinear systems using modified DNF technique

Direct normal form (DNF) analysis of nonlinear oscillators with fractional damping of order β is shown in this Chapter, where $(0 < \beta < 1)$. Traditionally, the method of DNF is used to investigate the dynamics of nonlinear oscillators, for which the nonlinearity has been resulted from the inclusion of polynomial stiffness terms with low orders such as quadratic or cubic. In the previous Chapters, the DNF method is applied to oscillators with higher orders of polynomial stiffness terms, in addition to oscillators with combinations of viscous damping and polynomial nonlinear stiffness terms. In this Chapter, a novel implementation of the DNF method for the case of fractionally damped oscillators is to be investigated. Two main examples are to be discussed, the Duffing oscillator with fractional damping and the fractionally damped Van-der-Pol oscillator. Where relevant, the proposed results are to be compared to numerical results and to other analytical results in the literature.

6.1 Introduction to fractional calculus

Fractional calculus is a branch of mathematical analysis that studies the possibility of taking real number powers or complex number powers of the differentiation operator and the integration operator. An important point is that the fractional derivative at a point x is a local property only when a is an integer; on the other hand, in non-integer cases we cannot say that the fractional derivative at x of a function f depends only on

values of f very near x, in the way that integer-power derivatives certainly do. Therefore it is expected that the theory involves some sort of boundary conditions, involving information on the function further out. To use a metaphor, the fractional derivative requires some peripheral vision.

As far as the existence of such a theory is concerned, the foundations of the subject were laid by Liouville in a paper from 1832. The fractional derivative of a function to the order a is often defined by means of the Fourier or Mellin integral transforms. In the following subsection, the fractional derivative of a a basic power function, $f(x) = x^k$, is demonstrated. Accordingly, the most important fractional derivative definitions; the Riemann-Liouville and Caputo fractional derivatives are shown.

6.1.1 Fractional derivative of a basic power function

Let us assume that $f(x)$ is a monomial of the form

$$f(x) = x^k \tag{6.1}$$

where k is a real number, then the first derivative is as usual

$$f'(x) = kx^{k-1} \tag{6.2}$$

In general, the a^{th} derivative of the function $f(x)$ in Eq. 6.1 is written as

$$\frac{\mathrm{d}^a}{\mathrm{d}x^a}\left(x^k\right) = \frac{k!}{(k-a)!}x^{k-a} \tag{6.3}$$

In mathematics, the Gamma function (represented by the capital Greek letter Γ) is an extension of the factorial function, with its argument shifted down by 1, to real and complex numbers. That is, if n is a positive integer then

$$\Gamma = (n-1)! \tag{6.4}$$

in addition, when solving the fractional differential equation, another form of Γ function is obtained, which includes two operators. In mathematics, this form is called the incomplete Γ function, $\Gamma(a,z)$, and it is defined for all complex numbers except the non-positive integers, in case the real value of a is positive, $\Re\{a\} > 0$, the

incomplete Γ function is defined via a convergent to the improper integral

$$\Gamma(z) = \int_0^\infty \mathrm{e}^{-x} x^{t-1}\,\mathrm{d}x \tag{6.5}$$

Now, using the Gamma definition defined in Eq. 6.5, the a^{th} derivative of the function $f(x)$ in Eq. 6.3 can be rewritten as

$$\frac{\mathrm{d}^a}{\mathrm{d}x^a}\left(x^k\right) = \frac{\Gamma(k+1)}{\Gamma(k-a+1)} x^{k-a}, \qquad k \geq 0 \tag{6.6}$$

In order to apply the fractional derivative appearing in Eq. 6.6, it is possible to consider the simple case of $k = 1$ and $a = 0.5$, which represents the half-derivative of the function $f(x) = x$. Thus,

$$\frac{\mathrm{d}^{0.5}}{\mathrm{d}x^{0.5}}(x) = \frac{\Gamma(2)}{\Gamma(1.5)} x^{0.5} = \frac{1}{\left(\frac{\sqrt{\pi}}{2}\right)} \sqrt{x} \tag{6.7}$$

For any negative integer power k, the gamma function is undefined, alternatively the following relation is adopted;

$$\frac{\mathrm{d}^a}{\mathrm{d}x^a}\left(x^{-k}\right) = (-1)^a \frac{\Gamma(k+a)}{\Gamma(k)} x^{-(k+a)}, \qquad k \geq 0 \tag{6.8}$$

In general, the fractional derivative of function $f(x)$ and $0 < \alpha < 1$ can be written as

$$\mathrm{D}^\alpha(f(x)) = \frac{1}{\Gamma(1-\alpha)} \frac{\mathrm{d}}{\mathrm{d}x} \left(\int_0^x \frac{f(t)}{(x-t)^\alpha}\,\mathrm{d}t \right) \tag{6.9}$$

The previous definition of the fractional derivative was firstly introduced by Riemann and Liouville, whereas another well-known definition is introduced by Caputo and it is defined as, [124]

$$\mathrm{D}^\alpha(f(x)) = \frac{1}{\Gamma(k-\alpha)} \left(\int_0^x \frac{f(t)}{(x-t)^{\alpha+1-k}} \frac{\mathrm{d}^k}{\mathrm{d}x^k}\,\mathrm{d}t \right) \tag{6.10}$$

Considering the theory of fractional calculus, and according to different backgrounds, there are several definitions of the fractional-order derivatives [123, 124], however, under some special conditions, they are equivalent. For instance, Caputo and Riemann-Liouville fractional derivatives in Eq. 6.9 and Eq. 6.10 are two of the most well-known definitions of the fractional derivatives. Nevertheless, many other definitions have

been introduced in the literature for both fractional derivatives and fractional integrals, refer to [143] for some of these definitions. In this Chapter, another definition of the fractional is to be used; namely, Davison-Essex (D-E) definition, justifications of selecting this definition is provided in Section 6.2. In the following Section, more details of Davison-Essex are presented.

6.1.2 Davison-Essex (DE) fractional derivative

In 1998, Davison and Essex [144], published a paper which provides a variation to the Riemann-Liouville definition suitable for conventional initial value problems within the realm of fractional calculus. The definition presented in their work is;

$$\mathrm{D_0}^{\alpha}\left(f(x)\right) = \frac{\mathrm{d}^{n+1-k}}{\mathrm{d}x^{n+1-k}}\left(\int_0^x \frac{(x-t)^{-\alpha}}{\Gamma(1-\alpha)}\frac{\mathrm{d}^k f(t)}{\mathrm{d}t^k}\,\mathrm{d}t\right) \tag{6.11}$$

The DE definition given in Eq. 6.11 is shown to be valid for only limited values of t, thus, to develop the definition, Cavanati introduced an algorithm that is a particular case obtained with $k = N-1$, [145]. Accordingly, the definition in Eq. 6.11 becomes

$$\mathrm{D}^{\beta}u(t) = \frac{1}{\Gamma(n-\beta)}\int_0^t (t-s)^{n-\beta-1}\left(\frac{\mathrm{d}^n}{\mathrm{d}t^n}u(s)\right)\mathrm{d}s \tag{6.12}$$

in order to apply this definition, the primary and crucial step is to find the value of n, defined as $n = ceil(\beta)$ where in our case the fractional derivative is $0 < \beta < 1$ and thus $n = 1$. Accordingly, Davison-Essex definition in Eq. 6.12 can be rewritten as

$$\mathrm{D}^{\beta}u(t) = \frac{1}{\Gamma(1-\beta)}\int_0^t (t-s)^{-\beta}\left(\frac{\mathrm{d}}{\mathrm{d}t}u(s)\right)\mathrm{d}s \tag{6.13}$$

where the Gamma function, $\Gamma(\,)$, is defined in Eq. 6.4. In this thesis, this form of the DE fractional derivative is used to investigate the dynamics of fractionally damped nonlinear oscillators using the method of DNF.

6.2 Duffing oscillator with fractional order damping

Considering the Duffing oscillator with fractional damping, driven by harmonic force of non-resonant type. It is required to use DNF technique to investigate the frequency response for this system.

$$\ddot{x}(t)+2\varepsilon\zeta\omega_n \mathrm{D}^{\beta}x(t)+\omega_n^2 x(t)+\varepsilon\alpha x^3(t)=\varepsilon R\cos(\Omega t) \tag{6.14}$$

where $x(t)$ denotes the displacement of the oscillator, ω_n is the natural frequency of the system and ζ is the viscous damping ratio. Moreover, $\mathrm{D}^{\beta}x(t)$ denotes the fractional damping of the system with β being the order of the fractional order of the system, where $(0<\beta<1)$, and when $\beta=1$ then the system is viscously damped. Additionally, R and Ω appearing in the right-hand-side of the equation represent the forcing amplitude and forcing frequency, respectively. Finally, ε is a bookkeeping parameter which is assumed to be unity in this section, but it will be used for comparisons to other methods of analysis in Section 6.3. Finally, α is a constant denoting the smallness of the weak nonlinearity. Discussions regarding the fractional damping model, its importance, and how it complements with the existing damping models in the literature is provided in Section 2.6.

By applying the method of DNF, and since the system in Eq. 6.14 is SDOF, then $\mathbf{q}=\mathbf{x_1}=x$ with q_1 is the only element in $\mathbf{q}$, by applying the near-identity transform one can get

$$\ddot{q}+\Lambda q+N_q\left(q,\mathrm{D}^{\beta}\{q\}\right)=0, \tag{6.15}$$

where $\Lambda=\omega_n^2$ and $N_q\left(q,\mathrm{D}^{\beta}\{q\}\right)=2\zeta\omega_n\mathrm{D}^{\beta}q+\alpha q^3$.

For systems with integer order viscous damping, i.e. $\beta=1$, when applying the DNF method, the assumed solution has the form

$$u=u_p+u_m=\left(\frac{U}{2}\mathrm{e}^{-\mathrm{i}\phi}\right)\mathrm{e}^{\mathrm{i}\omega_r t}+\left(\frac{U}{2}\mathrm{e}^{\mathrm{i}\phi}\right)\mathrm{e}^{-\mathrm{i}\omega_r t}, \tag{6.16}$$

however, for systems with fractional order damping, i.e. $0<\beta<1$, the fractional derivative of the assumed solution can be expressed as

$$\mathrm{D}^{\beta}u=\mathrm{D}^{\beta}\left(u_p+u_m\right), \tag{6.17}$$

Now, the near identity transformation is applied to Eq. 6.15 using ε^1 order, yielding to

$$\begin{aligned} N_u &= 2\zeta\omega_n \mathrm{D}^\beta[u] + \alpha u^3 = 2\zeta\omega_n \mathrm{D}^\beta[u_p + u_m] + \alpha\left(u_p + u_m\right)^3 \\ &= 2\zeta\omega_n \mathrm{D}^\beta u_p + 2\zeta\omega_n \mathrm{D}^\beta u_m + \alpha u_p^3 + 3\alpha u_p^2 u_m + 3\alpha u_p u_m^2 + \alpha u_m^3 \end{aligned} \tag{6.18}$$

To emphasise, for systems with integer order derivative, i.e. $\beta = 1$, the assumed solution, Eq. 6.16, has some desirable characteristics that make the application of the DNF technique easily reachable, these characteristics are mainly related to the exponential terms appearing in the solution. The derivatives of the exponents in Eq. 6.16 can be imagined as multiples of the assumed solution, thus, for any integer value of n, it is possible to write

$$\frac{\mathrm{D}^n}{\mathrm{d}t^n}\left(u_p\right) = \left(\mathbf{i}\omega_r\right)^n u_p \tag{6.19a}$$

$$\frac{\mathrm{D}^n}{\mathrm{d}t^n}\left(u_m\right) = \left(-\mathbf{i}\omega_r\right)^n u_m \tag{6.19b}$$

As discussed in Subsection 6.1.2, the implementation of DNF for fractionally damped systems is based on the type of fractional derivative; when using DNF method for fractionally damped equations of motion it is difficult to rely on the characteristics in Eq. 6.19, since the application of the fractional derivatives (such as Caputo's derivative) regularly yields to completely different forms. In this work, the author is trying to find some acceptable approximations of the fractional derivatives that makes the DNF technique applicable. To accomplish that, it is convenient to refer to the Davison-Essex (D-E) definition of the fractional derivatives, Eq. 6.13; by performing Davison-Essex definition, it is possible to find the fractional damping of the system by evaluating the integral in Eq. 6.13 according to the order of the fractional derivative β. Our purpose in this work is to use Davison-Essex fractional derivative definition in Eq. 6.13, to evaluate the fractional derivatives of the assumed solution in Eq. 6.16, in a form that is similar to that seen in Eq. 6.19, and then it is possible proceed with the application of the DNF method.

By applying D-E definition of fractional derivative in Eq. 6.13 to the assumed solution, it is found that

$$\mathrm{D}^{\beta}(u_p) = \frac{1}{\Gamma(1-\beta)}\left(\frac{U}{2}\mathrm{e}^{\mathbf{i}\omega_r t}(\mathbf{i}\omega_r)^{\beta}\right)\left(\Gamma(1-\beta)-\Gamma((1-\beta),\mathbf{i}\omega_r t)\right) \tag{6.20a}$$

$$\mathrm{D}^{\beta}(u_m) = \frac{1}{\Gamma(1-\beta)}\left(\frac{U}{2}\mathrm{e}^{-\mathbf{i}\omega_r t}(-\mathbf{i}\omega_r)^{\beta}\right)\left(\Gamma(1-\beta)-\Gamma((1-\beta),-\mathbf{i}\omega_r t)\right) \tag{6.20b}$$

which are equivalent to

$$\mathrm{D}^{\beta}(u_p) = \left[\frac{1}{\Gamma(1-\beta)}\left((\mathbf{i}\omega_r)^{\beta}\right)\left(\Gamma(1-\beta)-\Gamma((1-\beta),\mathbf{i}\omega_r t)\right)\right]u_p \tag{6.21a}$$

$$\mathrm{D}^{\beta}(u_m) = \left[\frac{1}{\Gamma(1-\beta)}\left((-\mathbf{i}\omega_r)^{\beta}\right)\left(\Gamma(1-\beta)-\Gamma((1-\beta),-\mathbf{i}\omega_r t)\right)\right]u_m \tag{6.21b}$$

where the terms $\Gamma(1-\beta)$, $(\mathbf{i}\omega_r)^{\beta}$ and $(-\mathbf{i}\omega_r)^{\beta}$ are constants for a given value of β, whereas the terms $\Gamma((1-\beta),\mathbf{i}\omega_r t)$ and $\Gamma((1-\beta),-\mathbf{i}\omega_r t)$ are time dependent terms which represent the decaying terms of the solution caused by the fractional damping. In view of Eq. 6.20 and Eq. 6.21, the assumed solution in Eq. 6.16 can be rewritten as

$$N_u = \alpha u_p^3 + 3\alpha u_p^2 u_m + 3\alpha u_p u_m^2 + \alpha u_m^3 + 2\zeta\omega_n\eta_1(\beta,t)u_p + 2\zeta\omega_n\eta_2(\beta,t)u_m \tag{6.22}$$

where

$$\eta_1(\beta,t) = \left[\frac{1}{\Gamma(1-\beta)}\left((\mathbf{i}\omega_r)^{\beta}\right)\left(\Gamma(1-\beta)-\Gamma((1-\beta),\mathbf{i}\omega_r t)\right)\right] \tag{6.23a}$$

$$\eta_2(\beta,t) = \left[\frac{1}{\Gamma(1-\beta)}\left((-\mathbf{i}\omega_r)^{\beta}\right)\left(\Gamma(1-\beta)-\Gamma((1-\beta),-\mathbf{i}\omega_r t)\right)\right] \tag{6.23b}$$

Now, it is possible to proceed with the DNF analysis; $\mathbf{n}^*$, $\mathbf{u}^*$ and $\boldsymbol{\beta}^*$ matrices are obtained as

$$\begin{aligned}
\mathbf{u}^* &= \begin{bmatrix} u_p^3 & u_p^2 u_m & u_p u_m^2 & u_m^3 & u_p & u_m \end{bmatrix}^{\mathsf{T}} \\
\mathbf{n}^* &= \begin{bmatrix} \alpha & 3\alpha & 3\alpha & \alpha & 2\zeta\omega_n\eta_1 & 2\zeta\omega_n\eta_2 \end{bmatrix} \\
\boldsymbol{\beta}^* &= \omega_r^2 \begin{bmatrix} 8 & 0 & 0 & 8 & 0 & 0 \end{bmatrix}
\end{aligned} \tag{6.24}$$

As usual, according to the values of the elements in $\boldsymbol{\beta}^*$, it is possible to classify the type of expected resonances as follows:

- If the value of $\beta_j^* = 0$, then there exists an unconditional resonant term at this element.
- If the value of $\beta_j^* \neq 0$, then there exists a conditional resonant term at this element.

Now, the matrix $\boldsymbol{\beta}^*$ can be used to find the near-identity transform and the resonant nonlinear terms that remain in the dynamic equation for u giving

$$\begin{aligned} \mathbf{n}_{\mathbf{u}}^* &= \begin{bmatrix} 0 & 3\alpha & 3\alpha & 0 & 2\zeta\omega_n\eta_1 & 2\zeta\omega_n\eta_2 \end{bmatrix} \\ \mathbf{h}^* &= \frac{\alpha}{\omega_r^2}\begin{bmatrix} \frac{1}{8} & 0 & 0 & \frac{1}{8} & 0 & 0 \end{bmatrix} \end{aligned} \tag{6.25}$$

The equation of motion in the transformed coordinate system and the near-identity transform may now be written as

$$\ddot{u} + 2\zeta\omega_n \mathrm{D}^\beta u + \omega_n^2 u + 3\alpha\left(u_p^2 u_m + u_p u_m^2\right) = 0, \tag{6.26}$$

considering that this is a SDOF system which gives that $x = q = v$ and to ε^1 order of accuracy, it is possible to write

$$v = u + n^* u^* = u + \frac{\alpha}{8\omega_n^2}\left(u_p^3 + u_m^3\right) \tag{6.27}$$

Using the trial solution in Eq. 6.16, for $\omega_r = \Omega$ and $\mathbf{P_u r} = \mathbf{P_x r} = R\cos(\Omega)$ it is possible write

$$\begin{aligned} \left(\omega_n^2 - \Omega^2\right)\frac{U}{2}\left(\mathrm{e}^{\mathbf{i}(\Omega t-\phi)} + \mathrm{e}^{-\mathbf{i}(\Omega t-\phi)}\right) + 2\zeta\omega_n\left(\eta_1\mathrm{e}^{\mathbf{i}(\Omega t-\phi)} + \eta_2\mathrm{e}^{-\mathbf{i}(\Omega t-\phi)}\right) + \\ \frac{3\alpha U^3}{8}\left(\eta_1\mathrm{e}^{\mathbf{i}(\Omega t-\phi)} + \eta_2\mathrm{e}^{-\mathbf{i}(\Omega t-\phi)}\right) = \frac{R}{2}\left(\mathrm{e}^{\mathbf{i}\Omega t} + \mathrm{e}^{-\mathbf{i}\Omega t}\right) \end{aligned} \tag{6.28}$$

By balancing the exponential terms

$$\mathrm{e}^{\mathbf{i}(\Omega t-\phi)}: \quad \left(\omega_n^2 - \Omega^2\right)U + 4\zeta\omega_n\eta_1 + \frac{3}{4}\eta_1\alpha U^3 = R\mathrm{e}^{\,\mathbf{i}\phi} \tag{6.29a}$$

$$\mathrm{e}^{-\mathbf{i}(\Omega t-\phi)}: \quad \left(\omega_n^2 - \Omega^2\right)U + 4\zeta\omega_n\eta_2 + \frac{3}{4}\eta_2\alpha U^3 = R\mathrm{e}^{-\,\mathbf{i}\phi} \tag{6.29b}$$

it is important to consider that, compared to the case of viscous damping (i.e. $\beta = 1$), the fractional order system involves higher mathematical complexities when trying to find the real and imaginary parts of the

solution; the Gamma functions in Eq. 6.20 illustrate combinations of real and imaginary sets of solutions depending on the values of ω_n and t. However, it is convenient to proceed with the DNF analysis keeping in mind that η_1 and η_2 are complex numbers and they are not complex conjugates, thus by balancing the exponential terms, the real and imaginary parts in Eq. 6.29a become:

$$\text{Re: } \left(\omega_n^2 - \Omega^2\right) U + 4\zeta\omega_n \Re\{\eta_1\} + \frac{3}{4}\Re\{\eta_1\}\alpha U^3 = R\cos\phi \tag{6.30a}$$

$$\text{Im: } 4\zeta\omega_n \Im\{\eta_1\} = R\sin\phi \tag{6.30b}$$

where $\Re\{\eta_1\}$ and $\Im\{\eta_1\}$ are the real and imaginary parts of η_1, respectively. Now, by squaring and adding these two equations together it is possible obtain an expression for the backbone curve of this system,

$$\left[\left(\omega_n^2 - \Omega^2\right) U + 4\zeta\omega_n \Re\{\eta_1\} + \frac{3}{4}\Re\{\eta_1\}\alpha U^3\right]^2 + \left[4\zeta\omega_n \Im\{\eta_1\}\right]^2 = R^2 \tag{6.31}$$

Additionally, it is possible to obtain an expression for the phase relationship ϕ as

$$\phi = \tan^{-1}\left[\frac{4\zeta\omega_n \Im\{\eta_1\}}{\left(\omega_n^2 - \Omega^2\right) U + 4\zeta\omega_n \Re\{\eta_1\} + \frac{3}{4}\Re\{\eta_1\}\alpha U^3}\right] \tag{6.32}$$

Using Eq. 6.31 it is possible to find the frequency response of the system analytically, and hence it is possible to calculate the fractionally damped backbone curves of the system. In the following section, a method to obtain the numerical frequency response of the fractionally damped Duffing is discussed, which then can be used to verify the analytical results obtained by the DNF technique.

6.3 Comparison with numerical results

As described in [139], the relationship between the explicit numerical approximation and the power series method is described numerically by Grünwald-Letnikov's definition as

$$\mathrm{D}_{t_n}^{\beta}\left(y(t_n)\right) \approx \frac{1}{h^{\beta}} \sum_{j=0}^{n} C_j^{\beta} y(t_{n-j}) \tag{6.33}$$

where t_n, h and C_j^{β} are the sample points, sample step size and the fractional binomial coefficient, respectively.

Moreover, the sample points can be written as $t_n = nh$ and considering that $C_0^\beta = 1$, the fractional binomial coefficient is iteratively written as

$$C_j^\beta = \left(1 - \frac{1+\beta}{j}\right) C_{j-1}^\beta \tag{6.34}$$

thus, Eq. 6.33 is rewritten as

$$\mathrm{D}_{t_n}^\beta \left(y(t_n)\right) \approx \frac{1}{h^\beta} \sum_{j=0}^{n} \left(1 - \frac{1+\beta}{j}\right) C_{j-1}^\beta y(t_{n-j}), \quad C_0^\beta = 1 \tag{6.35}$$

Now, in order to investigate the accuracy of the amplitude-frequency relationship of the fractional Duffing oscillator in Eq. 6.31, the frequency response functions for Duffing oscillator with fractional damping are analytically computed from Eq. 6.31, and then the results are verified numerically using fractional order derivative of $\beta = 0.75$, forcing excitation amplitude of $R = 1$ and natural frequency of $\omega_n = 2$ rad/s. The Grünwald-Letnikov's definition in Eq. 6.35 is substituted in the EOM of Duffing oscillator, Eq. 6.14, and then the resulting equation is solved with sample step of $h = 0.005$ for a total computation time of 400 s. The temporary response in the first 200 s is skipped in order to get the steady-state response, and the peak values of the posterior response is considered to be the required numerically computed steady-state amplitudes, this process is repeated for various excitation frequencies. Fig. 6.1 shows a comparison between the analytical and numerical frequency response of the fractional Duffing oscillator.

The effect of varying the fractional order β to the oscillations amplitude is given by Fig. 6.2. Starting from $\beta = 1$, which represent the Duffing case oscillator with viscous damping term, when the order of the fractional derivative decreases, the amplitude of the oscillations rapidly increases and the peak nonlinear frequency is shifted to the right (i.e. to a higher magnitude), this can be related to the fact that the decreasing fractional order of the derivative leads to smaller damping effects, [161]. Moreover, it is possible to notice some slight imperfections to the curves when the stable and unstable solutions coincide, this could be related to the fact that the analytical solutions roots are changing at these turning points. Finally, contrary to continuation packages such as MatCont, it can be seen that the DNF technique, in its current form, is unable to detect the subharmonic resonances for this system. However, for potential future work, DNF can be modified to include subharmonic resonances.

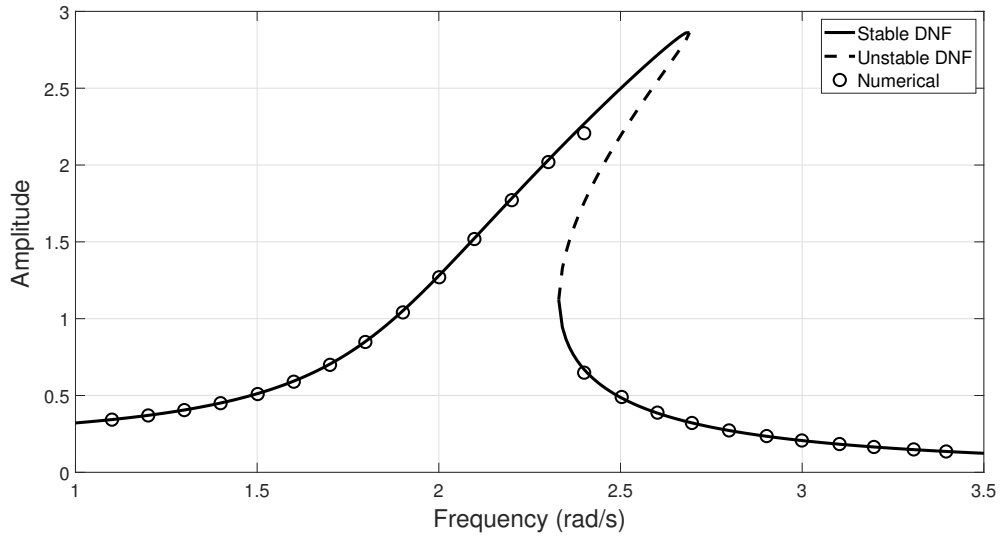

Figure 6.1: Frequency response relationship for Duffing oscillator with fractional damping term, the solid line represents the stable solution while the dashed line represents the unstable solution, both computed analytically using Eq. 6.31, while the circles represent the numerical solution computed using Eq. 6.35. Parameter values are: $\omega_n = 2$ rad/s, $\alpha = 0.2$, $R = 1$ and fractional order of $\beta = 0.75$.

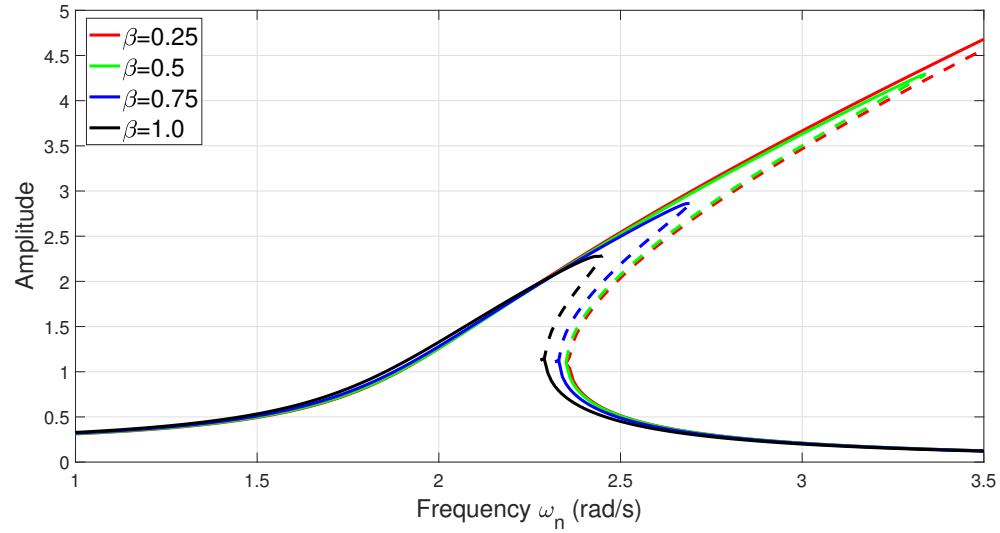

Figure 6.2: Frequency response relationship variations for Duffing oscillator with various fractional damping orders, the solid lines represent the stable solution while the dashed lines represent the unstable solution, all computed analytically using Eq. 6.31. Other parameter values are: $\omega_n = 2$ rad/s, $\alpha = 1.0$ and $R = 1$.

The effect of the excitation amplitude variations R to the oscillation amplitudes of the oscillator at fractional order derivative of $\beta = 0.75$ is shown in Fig. 6.3. In principle, when increasing the value of R, the same trend seen in Fig. 6.2 is repeated. Nevertheless, some differences are clearly noticed to the frequency responses away from the natural frequency of the system; increasing the values of R results in shifting the frequency

responses significantly; while this is not seen when decreasing the fractional order β. Overall, for a constant fractional order β, increasing the excitation amplitude will always yield to increased amplitude of the oscillator.

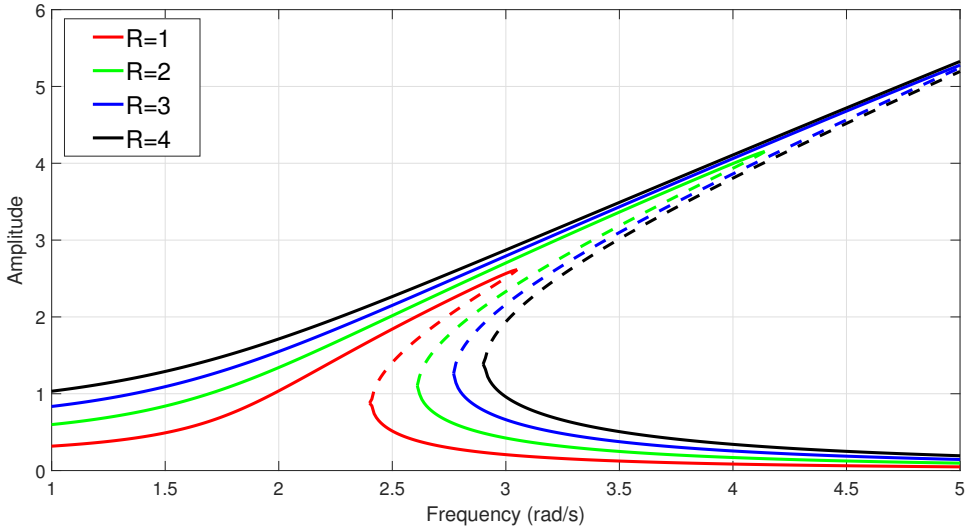

Figure 6.3: Frequency response relationship variations for Duffing oscillator with amplitudes of harmonic excitation, the solid lines represent the stable solution while the dashed lines represent the unstable solution, all computed analytically using Eq. 6.31. Other parameter values are: $\omega_n = 2$ rad/s, $\alpha = 1.0$ and $\beta = 0.75$

Finally, the effect of changing the nonlinear stiffness term coefficient α to the frequency responses of the oscillator is found in Fig. 6.4, the fractional order of the system is $\beta = 0.75$ and the excitation amplitude is $R = 1$. As expected, increasing α values will always lead to greater bending of the frequency-amplitude curves, this results in reducing the amplitudes while increasing the peak frequency of the system. This can also be noted for Duffing oscillators with viscous damping.

6.4 Comparisons to other methods

In this section, the results obtained using DNF method are to be compared to some results found in the literature using other methods. The Duffing oscillator with fractional damping has been studied in the literature using some traditional approximate techniques such as harmonic balance, averaging and multiple scales, some of these works can be found in [161] and references therein. The analysis presented in this section is based on the method of averaging shown in detail in [161] for a system with a viscous damping and a fractional damping terms. However, in this section, the analysis is reproduced for the system presented in Eq. 6.14, accordingly, it is possible to compare the results of both the DNF and averaging methods as will be briefly discussed. If the

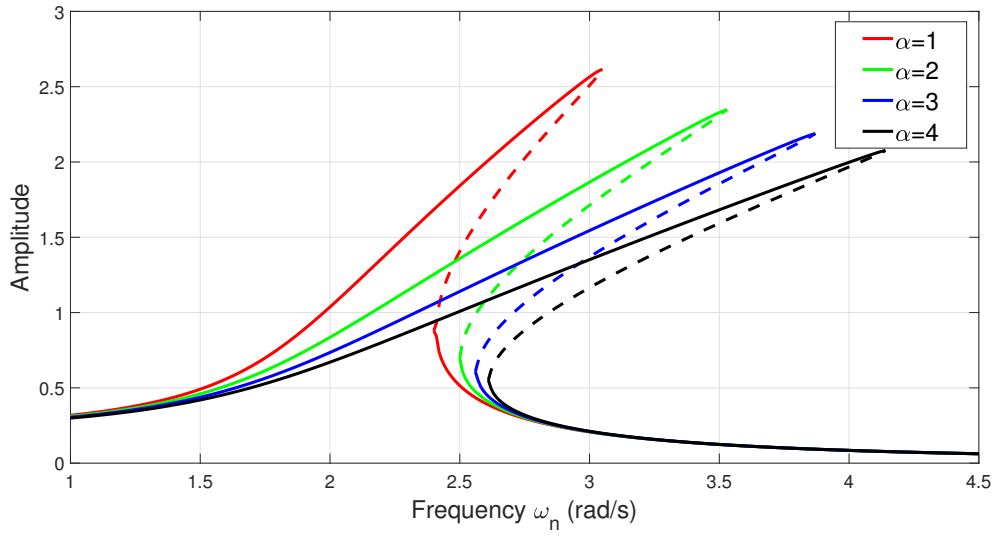

Figure 6.4: Frequency response relationship variations for Duffing oscillator with coefficient of the nonlinear cubic term, the solid lines represent the stable solution while the dashed lines represent the unstable solution, all solutions are computed analytically using Eq. 6.31. Other parameter values are: $\omega_n = 2$ rad/s, $R = 1.0$ and $\beta = 0.75$.

primary resonance is investigated for the Duffing oscillator in Eq. 6.14, the excitation frequency is considered to be close to the natural frequency, i.e. $\Omega \approx \omega_n$, and then, considering σ to be the detuning factor, the detuning frequency can be written as

$$\Omega^2 = \omega_n^2 + \varepsilon\sigma \tag{6.36}$$

Accordingly, Eq. 6.14 can be rearranged to be

$$\ddot{x}(t) + 2\varepsilon\zeta\omega_n \mathrm{D}^{\beta}x(t) + \left(\Omega^2 - \varepsilon\sigma\right)x(t) + \varepsilon\alpha x^3(t) = \varepsilon R\cos\left(\Omega t\right) \tag{6.37}$$

which can be written as

$$\ddot{x}(t) + \Omega^2 x(t) = \varepsilon\left(R\cos\left(\Omega t\right) - 2\zeta\omega_n \mathrm{D}^{\beta}x(t) + \sigma x(t) - \alpha x^3(t)\right) \tag{6.38}$$

Referring to Eq. 6.16, the assumed solution, in terms of $x(t)$ would be written as

$$x(t) = \left(\frac{X(t)}{2}\mathrm{e}^{-\mathrm{i}\phi(t)}\right)\mathrm{e}^{\mathrm{i}\omega_r t} + \left(\frac{X(t)}{2}\mathrm{e}^{\mathrm{i}\phi(t)}\right)\mathrm{e}^{-\mathrm{i}\omega_r t} = X(t)\cos\left(\Omega t - \phi\left(t\right)\right), \tag{6.39}$$

it is important to mention that both the displacement X and the phase ϕ are assumed to be functions of time to work in the generalised case, and this will enable the investigation of the steady-state solutions, as will be described in the following analysis. By differentiating Eq. 6.39 with respect to time, the following result is found

$$\dot{x}(t) = \dot{X}(t)\cos(\Omega t - \phi(t)) - X(t)\left(\Omega - \dot{\phi}(t)\right)\sin(\Omega t - \phi(t)), \tag{6.40}$$

nevertheless, if investigating the steady-state frequency-amplitude relationship near the resonance, both the amplitude X and the phase ϕ can considered to be slowly varying with time (or almost constant with time), this assumption is made in [160, 161] for which acceptable results are found. Thus, using Eq. 6.39, it is possible to write

$$\dot{x}(t) = -\Omega X(t)\sin(\Omega t - \phi(t)), \tag{6.41}$$

and when equating the results in Eq. 6.41 to that in Eq. 6.40, it is possible to write

$$\dot{X}(t)\cos(\Omega t - \phi(t)) - X(t)\dot{\phi}(t)\sin(\Omega t - \phi(t)) = 0, \tag{6.42}$$

now, by differentiating Eq. 6.41 with respect to time, the following is obtained

$$\ddot{x}(t) = -\Omega\dot{X}(t)\sin(\Omega t - \phi(t)) - X\Omega\left(\Omega + \dot{\phi}\right)\cos(\Omega t - \phi(t)), \tag{6.43}$$

Now, it is possible to substitute the value of $\ddot{x}(t)$ from Eq. 6.43 into Eq. 6.38 yielding to

$$-\Omega\dot{X}\sin(\Omega t - \phi) - X\Omega\left(\Omega + \dot{\phi}\right)\cos(\Omega t - \phi) + \Omega^2 x = \varepsilon\left(R\cos(\Omega t) - 2\zeta\omega_n \mathrm{D}^{\beta}x + \sigma x - \alpha x^3\right), \tag{6.44}$$

which can be rearranged as

$$\dot{X}\sin(\Omega t - \phi) + X\dot{\phi}\cos(\Omega t - \phi) = \frac{-\varepsilon}{\Omega}\left(\psi_1(U,\phi) + \psi_2(U,\phi)\right), \tag{6.45}$$

where,

$$\psi_1(U,\phi) = R\cos(\Omega t) + \sigma x + X\Omega^2\cos(\Omega t - \phi) - \Omega^2 x - \alpha x^3; \tag{6.46a}$$

$$\psi_2(U,\phi) = -2\zeta\omega_n \mathrm{D}^\beta x \tag{6.46b}$$

now, it is possible to solve Eq. 6.42 and Eq. 6.45 simultaneously for $\dot{U}$ and $\dot{\phi}$, which gives

$$\dot{U} = \frac{-\sin(\Omega t)}{\Omega}\left(\psi_1(U,\phi) + \psi_2(U,\phi)\right), \tag{6.47a}$$

$$\dot{\phi} = \frac{-\cos(\Omega t)}{U\Omega}\left(\psi_1(U,\phi) + \psi_2(U,\phi)\right) \tag{6.47b}$$

Considering the time interval $[0 \quad T]$, it is possible to apply the standard averaging method to Eq. 6.47, the averaging method is discussed in detail in [18, 21, 162] and it implies that if the formerly defined functions, Eq. 6.46 are periodic it is possible to select the period as $T = 2\pi$, and this is perfectly applicable to ψ_1. On the other hand, when the functions in Eq. 6.46 are aperiodic, the period should be defined as $T = \infty$, and this is applicable to ψ_2. Furthermore, in order to evaluate the integrals resulting by the averaging method, $\varphi(t) = \varphi = \Omega t + \phi$ is defined, which is sometimes called the generalised phase [160, 161]. Thus,

$$\dot{U} = \frac{-1}{T\Omega}\int_0^T [\psi_1 + \psi_2]\cos(\varphi)\,\mathrm{d}\varphi = \frac{-1}{2\pi\Omega}\int_0^{2\pi} \psi_1\sin(\varphi)\,\mathrm{d}\varphi + \lim_{T\to\infty}\frac{-1}{T\Omega}\int_0^T \psi_2\sin(\varphi)\,\mathrm{d}\varphi, \tag{6.48a}$$

$$\dot{\phi} = \frac{-1}{TU\Omega}\int_0^T [\psi_1 + \psi_2]\cos(\varphi)\,\mathrm{d}\varphi = \frac{-1}{2\pi U\Omega}\int_0^{2\pi} \psi_1\cos(\varphi)\,\mathrm{d}\varphi + \lim_{T\to\infty}\frac{-1}{TU\Omega}\int_0^T \psi_2\cos(\varphi)\,\mathrm{d}\varphi \tag{6.48b}$$

In both integrals in Eq. 6.48, the first term, ψ_1, is directly integrated over the period of 2π with the aid of Eq. 6.46 and basic trigonometric integration rules, however, the second term, ψ_2, needs further investigation to be integrated. Consequently, if defining $\dot{U} = \dot{U}_1 + \dot{U}_2$, and $\dot{\phi} = \dot{\phi}_1 + \dot{\phi}_2$ which represent the integration of ψ_1 and ψ_2, respectively, one can initially get

$$\dot{U}_1 = \frac{-1}{2\pi\Omega}\int_0^{2\pi} \psi_1\sin(\varphi)\,\mathrm{d}\varphi) = -\frac{\varepsilon R}{2\Omega} \tag{6.49a}$$

$$\dot{\phi}_1 = \frac{-1}{2\pi U\Omega}\int_0^{2\pi} \psi_1\cos(\varphi)\,\mathrm{d}\varphi = -\frac{\varepsilon}{2\Omega U}\left(R\cos(\phi) + \sigma U - \frac{3}{4}\alpha U^3\right) \tag{6.49b}$$

to find the second part of each integration in Eq. 6.48 it is possible to write

$$\dot{U}_2 = \lim_{T\to\infty} \frac{-1}{T\Omega} \int_0^T \psi_2 \sin(\varphi)\, \mathrm{d}\varphi = \lim_{T\to\infty} \frac{-1}{T\Omega} \int_0^T -2\zeta\omega_n \mathrm{D}^\beta [X\cos(\varphi)] \sin(\varphi)\, \mathrm{d}\varphi, \tag{6.50a}$$

$$\dot{\phi}_2 = \lim_{T\to\infty} \frac{-1}{TU\Omega} \int_0^T \psi_2 \cos(\varphi)\, \mathrm{d}\varphi = \lim_{T\to\infty} \frac{-1}{TU\Omega} \int_0^T -2\zeta\omega_n \mathrm{D}^\beta [X\cos(\varphi)] \cos(\varphi)\, \mathrm{d}\varphi \tag{6.50b}$$

now, in order to solve the two integrations in Eq. 6.50, one could refer to the two following formulas, which are normally used when dealing with dynamical systems with fractional order equations of motion,

$$\xi_1 = \lim_{T\to\infty} \int_0^T \frac{\sin(\Omega t)}{t^\beta}\, \mathrm{d}t, \tag{6.51a}$$

$$\xi_2 = \lim_{T\to\infty} \int_0^T \frac{\cos(\Omega t)}{t^\beta}\, \mathrm{d}t \tag{6.51b}$$

which can be transformed using $t = s^{1/(1-\beta)}$ into

$$\xi_1 = \frac{1}{1-\beta} \lim_{T\to\infty} \int_0^{T^{1-\beta}} \sin\left(\Omega s \frac{1}{1-\beta}\right) \mathrm{d}s, \tag{6.52a}$$

$$\xi_2 = \frac{1}{1-\beta} \lim_{T\to\infty} \int_0^{T^{1-\beta}} \cos\left(\Omega s \frac{1}{1-\beta}\right) \mathrm{d}s \tag{6.52b}$$

Now, it is possible to apply the residual theorem and contour integration, as discussed in [124], which gives

$$\xi_1 = \frac{\Omega^{\beta-1}\Gamma(2-\beta)}{1-\beta} \cos\left(\frac{\beta\pi}{2}\right) = \Omega^{\beta-1}\Gamma(1-\beta)\cos\left(\frac{\beta\pi}{2}\right) \tag{6.53a}$$

$$\xi_2 = \frac{\Omega^{\beta-1}\Gamma(2-\beta)}{1-\beta} \sin\left(\frac{\beta\pi}{2}\right) = \Omega^{\beta-1}\Gamma(1-\beta)\sin\left(\frac{\beta\pi}{2}\right) \tag{6.53b}$$

Using the results in Eq. 6.53, it is now possible to evaluate the two integrals appearing in Eq. 6.50, as mentioned earlier, this derivation is done in detail in [161] for a system with a viscous damping term and a fractional damping term. Nevertheless, the detailed derivation to obtain Eq. 6.54 below is listed in Appendix F.

$$\dot{U}_2 = -\varepsilon\zeta\omega_n U\Omega^{\beta-1} \sin\left(\frac{\beta\pi}{2}\right) \tag{6.54a}$$

$$\dot{\phi}_2 = \varepsilon\zeta\omega_n\Omega^{\beta-1} \cos\left(\frac{\beta\pi}{2}\right) \tag{6.54b}$$

Combining Eq. 6.49 and Eq. 6.54, it is possible to write the following

$$\dot{U} = -\frac{\varepsilon R}{2\Omega} - \varepsilon\zeta\omega_n U\Omega^{\beta-1}\sin\left(\frac{\beta\pi}{2}\right) \tag{6.55a}$$

$$\dot{\phi} = -\frac{\varepsilon}{2\Omega U}\left(R\cos(\phi) + \sigma U - \frac{3}{4}\alpha U^3\right) + \varepsilon\zeta\omega_n\Omega^{\beta-1}\cos\left(\frac{\beta\pi}{2}\right) \tag{6.55b}$$

Having found $\dot{U}$ and $\dot{\phi}$, the steady-state solutions are desired, which can be found by setting both $\dot{U}$ and $\dot{\phi}$ to be zeros, then by rearranging the equations it is possible to write

$$R = -2U\zeta\omega_n\Omega^{\beta}\sin\left(\frac{\beta\pi}{2}\right) \tag{6.56a}$$

$$R\cos(\phi) + \sigma U - \frac{3}{4}\alpha U^3 = 2U\zeta\omega_n\Omega^{\beta}\cos\left(\frac{\beta\pi}{2}\right) \tag{6.56b}$$

by squaring and adding the above two equations, the following is obtained

$$R^2 + \left(R\cos(\phi) + \sigma U - \frac{3}{4}\alpha U^3\right)^2 = \left(2U\zeta\omega_n\Omega^{\beta}\right)^2 \tag{6.57}$$

by substituting the value of R from Eq. 6.56 and recalling that $\sigma = \Omega^2 - \omega_n^2$, it is possible to find

$$\left(\left(\omega_n^2 - \Omega^2\right)U + 2U\zeta\omega_n\Omega^{\beta}\sin\left(\frac{\beta\pi}{2}\right)\cos(\phi) + \frac{3}{4}\alpha U^3\right)^2 + \left(2U\zeta\omega_n\Omega^{\beta}\right)^2 = R^2 \tag{6.58}$$

The frequency-amplitude relationship in Eq. 6.58 can be used to plot the steady-state frequency amplitude manifolds and those can be compared to the results of DNF appearing in Eq. 6.31. In the following figure, the results obtained from the two methods are compared using the numerical values of $\omega_n = 2$ rad/s, $\alpha = 0.2$, $R = 1$ and fractional order of $\beta = 0.75$. As clearly seen, perfect matching between the two responses which indicates that accurate results are obtained using DNF compared to other results in the literature.

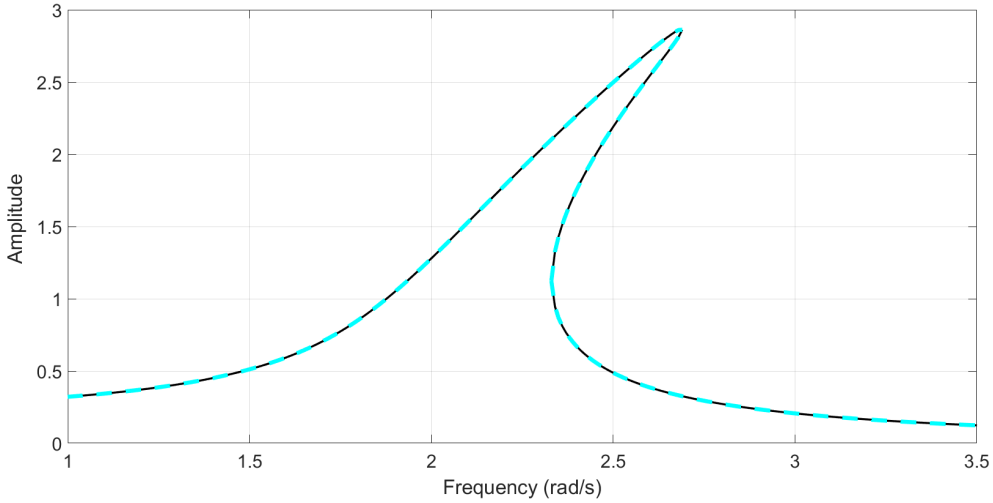

Figure 6.5: Comparing the DNF and averaging method steady-state frequency response for Duffing oscillator with fractional damping, the solid black line represents the DNF results, Eq. 6.31, while the dashed navy blue line shows results of the averaging method, Eq. 6.58. Parameter values are: $\omega_n = 2$ rad/s, $\alpha = 0.2$, $R = 1$ and fractional order of $\beta = 0.75$.

6.5 DNF analysis of fractional Van-der-Pol oscillator

The equation of motion of the fractionally damped Van-der-Pol oscillator is given by, [167]

$$\ddot{x}(t) + \mu\left(x^2(t) - 1\right) \mathrm{D}^{\beta} x(t) + \omega_n^2 x(t) = R\cos\left(\Omega t\right) \tag{6.59}$$

where, as discussed before, μ is a constant, $x(t)$ denotes the displacement of the oscillator, $\mathrm{D}^{\beta}x(t)$ denotes the fractional damping of the system with β being the order of the fractional order of the system $0 < \beta < 1$ and when $\beta = 1$ then the system is viscously damped. Additionally, R and Ω appears in the right-hand-side of the equation represent the forcing amplitude and frequency, respectively. Finally, ε is a bookkeeping parameter and α is a constant denoting the smallness of the weak nonlinearity. To apply DNF analysis for the fractionally damped Van-der-Pol oscillator, some elementary steps are similar to the viscously damped Van-der-Pol, Subsection 5.4.1, except for replacing the first derivative with the fractional derivative, however, at a certain stage the author needed to refer to the Davison-Essex fractional derivative used in the case of fractionally damped Duffing oscillator. For convenience, all solution steps are to be mentioned here, these steps can then be followed to repeat the analysis for any type of non-conservative oscillators. To start, it is convenient to

introduce the following,

$$\begin{aligned}\mathbf{P_x} &= \left\{\frac{R}{2}, \frac{R}{2}\right\} \\ \mathbf{r} &= \{r_p, r_m\}^\intercal = \{\mathrm{e}^{\,\mathrm{i}\Omega t}, \mathrm{e}^{-\,\mathrm{i}\Omega t}\}^\intercal \\ \widetilde{\mathbf{N}}\left(\mathbf{q}, \mathrm{D}^\beta\{\mathbf{q}\}, \mathbf{r}\right) &= \mu\left(q^2(t)-1\right)\mathrm{D}^\beta q(t)\end{aligned} \tag{6.60}$$

and thus the equation of motion becomes

$$\ddot{x}(t) + \omega_n^2 x(t) + \widetilde{\mathbf{N}}\left(\mathbf{q}, \mathrm{D}^\beta\{\mathbf{q}\}, \mathbf{r}\right) = \mathbf{P_x r} \tag{6.61}$$

The linear modal transformation is $\mathbf{q} = \mathbf{x} = x$ since SDOF is considered, thus

$$\ddot{q} + \Lambda q + N_q\left(\mathbf{q}, \mathrm{D}^\beta\{\mathbf{q}\}, \mathbf{r}\right) = \mathbf{P_q r} \tag{6.62}$$

where $\Lambda = \omega_n^2$, $N_q\left(\mathbf{q}, \mathrm{D}^\beta\{\mathbf{q}\}, \mathbf{r}\right) = \mu\left(q^2-1\right)\mathrm{D}^\beta q$ and $\mathbf{P_q} = \mathbf{P_x}$. Now, the forcing transformation is considered to be $\mathbf{q} = \mathbf{v} + \mathbf{er}$, this transformation is used to eliminate the non-resonant forcing terms. Due to the fact that the analysis is close to resonant, $\Omega = \omega_r$ and $[\mathbf{e}] = 0$, this results in

$$\ddot{v} + \Lambda v + N_v\left(\mathbf{v}, \mathrm{D}^\beta\{\mathbf{v}\}, \mathbf{r}\right) = \mathbf{P_v r} \tag{6.63}$$

with $N_v\left(\mathbf{v}, \mathrm{D}^\beta\{\mathbf{v}\}, \mathbf{r}\right) = \mu\left(v^2-1\right)\mathrm{D}^\beta v$ and $\mathbf{P_v} = \mathbf{P_q}$. The near-identity transformation is computed to ε^1 accuracy, by rewriting the nonlinear terms using $\mathbf{u}$, one should obtain $n_1\left(\mathbf{u}, \mathrm{D}^\beta\{\mathbf{u}\}, \mathbf{r}\right) = \mu\left(u^2-1\right)\mathrm{D}^\beta u$ for which $\mathbf{u} = \mathbf{u_p} + \mathbf{u_m}$. At this stage some differences occur compared to the case of viscously damped Van-der-Pol oscillator; the fractional derivative appearing in the previous analysis needs to be treated in a similar way to the case of fractional Duffing; that is

$$\mathrm{D}^\beta u = \eta_1 u_p + \eta_2 u_m \tag{6.64}$$

accordingly, the matrix manipulations for the fractionally damped Van-der-Pol become

$$\begin{aligned}
\mathbf{u}^* = \begin{bmatrix} u_m^3 \\ u_p^3 \\ u_p u_m^2 \\ u_p^2 u_m \\ u_m \\ u_p \end{bmatrix} \rightsquigarrow \mathbf{n}^* = \mu \begin{bmatrix} \eta_2 \\ \eta_1 \\ \eta_1 + 2\eta_2 \\ 2\eta_1 + \eta_2 \\ -\eta_2 \\ -\eta_1 \end{bmatrix}^{\mathsf{T}} \rightsquigarrow \boldsymbol{\beta}^* = \omega_r^2 \begin{bmatrix} 8 \\ 8 \\ 0 \\ 0 \\ 0 \\ 0 \end{bmatrix}^{\mathsf{T}} \rightsquigarrow \\
\mathbf{h}^* = \frac{\mu}{8\omega_r^2} \begin{bmatrix} \eta_2 \\ \eta_1 \\ 0 \\ 0 \\ 0 \\ 0 \end{bmatrix}^{\mathsf{T}} \rightsquigarrow \mathbf{n}_{\mathbf{u}}^* = \mu \begin{bmatrix} 0 \\ 0 \\ \eta_1 + 2\eta_2 \\ 2\eta_1 + \eta_2 \\ -\eta_2 \\ -\eta_1 \end{bmatrix}^{\mathsf{T}}
\end{aligned} \tag{6.65}$$

For ε^1 accuracy, the equation of motion can then be written in the u-transformed coordinates as

$$\ddot{u} + \omega_n^2 u + \mu\left(\eta_1 + 2\eta_2\right) u_p u_m^2 + \mu\left(2\eta_1 + \eta_2\right) u_p^2 u_m - \mu\left(\eta_1 u_p + \eta_2 u_m\right) = R\cos\left(\omega_r t\right) \tag{6.66}$$

and by substituting the assumed solution, it is possible to write

$$\begin{aligned}
&\frac{U}{8}\mu\left(\left(3U^2 - 4\right)\left(\eta_1 + \eta_2\right) + \omega_n^2 - \omega_r^2\right)\left(\frac{\mathrm{e}^{\,\mathbf{i}(\omega_r t - \phi)}}{2} + \frac{\mathrm{e}^{-\,\mathbf{i}(\omega_r t - \phi)}}{2}\right) \\
&-\frac{\mu}{16}\left(\eta_1 - \eta_2\right)\left(U^2 - 4\right)\left(\frac{\mathrm{e}^{\,\mathbf{i}(\omega_r t - \phi)}}{2} - \frac{\mathrm{e}^{-\,\mathbf{i}(\omega_r t - \phi)}}{2}\right) = R\cos\left(\omega_r t\right)
\end{aligned} \tag{6.67}$$

the term $R\cos(\omega_r t)$ can be converted into its equivalent exponential form using Euler's identity, and then one of the exponential terms of Eq. 6.67 can be balanced, performing that to $e^{\mathbf{i}(\omega_r t-\phi)}$ gives

$$\frac{U}{8}\mu\left(\left(3U^2-4\right)(\eta_1+\eta_2)+\omega_n^2-\omega_r^2\right)-\frac{\mu}{16}(\eta_1-\eta_2)\left(U^2-4\right)=Re^{\mathbf{i}\phi} \tag{6.68}$$

considering that the functions η_1 and η_2 have both real and imaginary components, it is necessary to balance the real and imaginary terms of Eq. 6.68, yielding to

$$\begin{aligned}\text{Re: } &\frac{U}{8}\mu\left(\left(3U^2-4\right)(\Re\{\eta_1\}+\Re\{\eta_2\})+\omega_n^2-\omega_r^2\right)-\\ &\frac{\mu}{16}(\Re\{\eta_1\}-\Re\{\eta_2\})\left(U^2-4\right)=R\cos(\phi) \qquad (6.69a)\\ \text{Im: } &\frac{U}{8}\mu\left(\left(3U^2-4\right)(\Im\{\eta_1\}+\Im\{\eta_2\})\right)-\\ &\frac{\mu}{16}(\Im\{\eta_1\}-\Im\{\eta_2\})\left(U^2-4\right)=R\sin(\phi) \qquad (6.69b)\end{aligned}$$

Finally, by squaring and adding the real and imaginary components, the amplitude-frequency relationship are found, and if upon dividing them the phase relationship for the fractionally damped Van-der-Pol oscillator is also obtained. Further mathematical investigation of the relationship of η_1 and η_2, their real and imaginary components, and how the results in Eq. 6.69 can be refined to simpler forms are all needed for future works. However, having reached this form of solution it can be sufficient to study the amplitude-frequency behaviour of this oscillator for various orders of the fractional derivatives.

6.6 Summary

In this Chapter, a novel implementation of the DNF method for fractionally damped oscillators is shown. This application is based on using fractional calculus approach, in which the Davison-Essex (D-E) definition of fractional derivatives is adopted. Two examples are discussed, the Duffing oscillator with fractional damping and the fractionally damped Van-der-Pol oscillator. For verification purposes, comparisons with numerical results and other methods are practised. Based on this Chapter analysis, the followings are observed;

- Compared to both numerical and other methods found in the literature, the proposed ε^1 DNF technique show acceptable levels of accuracy, nevertheless, further analysis regrading the effects of higher order

accuracies could be an interesting future research.

- For the example of fractionally damped Duffing oscillator, the presence of the fractional damping term led to significant changes to the frequency response curves, refer to Fig. 6.2-Fig. 6.4 and the corresponding discussions.

- For the both fractionally damped Duffing and fractionally damped Van-der-Pol oscillators, analytical expressions of the backbone curves are obtained using the method of DNF computed to ε^1 accuracy. Nevertheless, these expressions need more investigations to be refined to simpler forms, specifically the terms $\Re\{\eta_i\}$ and $\Im\{\eta_i\}$ appearing in the response relationships.

Chapter 7

Applications to MDOF systems

In this Chapter, the DNF analysis is extended to systems of MDOF. Firstly, in order to show the validity of the proposed symbolic DNF technique for MDOF systems, two verification problems are to be presented; the Vertical-horizontal-spring-mass oscillator (or as called Touzé 2-DOF system), and 3-DOF system with cubic nonlinear stiffness coupling terms, the dynamics of these two systems are investigated in the literature as will be demonstrated.

Having proved the effectiveness of the proposed DNF technique for MDOF systems, a detailed analysis of the non-resonant 2-DOF cubic-quintic oscillator is introduced. Initially, the investigation presented is shown to demonstrate how the *single-mode* backbone curves of the two degree-of-freedom system can be computed in an analogous manner to the approach used for the cubic-quintic SDOF oscillator, Section 5.1. Then, the analysis is extended to study the *double-mode* interactions in order to investigate the resulting backbone curves.

7.1 Verification problem 1: Vertical-horizontal-spring-mass oscillator

In this subsection, a verification problem of an oscillator system consisting of a mass supported by vertical and horizontal springs is considered, for which two springs are attached to solid supports — as shown schematically in Fig. 7.1 (a).

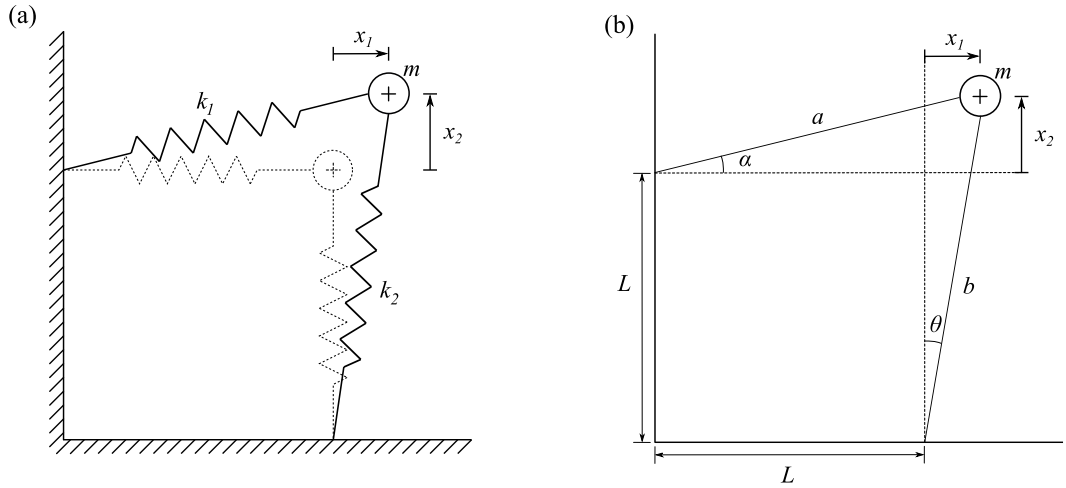

Figure 7.1: The vertical-horizontal-spring-mass oscillator considered in Section 7.1.

This system has been studied in-depth by several previous authors [45, 46, 70]. However, only a non-physical derivation of the EOMs of the system is presented in these studies. Primarily, an alternate model based on a strong-form, physics based set of equations of motion is derived, this step-by-step derivation of the EOMs is presented in Appendix C. Initially the case of conservative system is considered (i.e when there is no damping or external forcing). As a result the only forces in the system are the inertial force related to the mass, m and the restoring forces relating to the linear springs, k_1 and k_2. The geometry of the system at an arbitrary displacement is shown in Fig. 7.1 (b).

7.1.1 Direct normal forms solutions for the conservative system

In this section, the application of DNF method previously described is shown, in order to obtain the backbone curves of the undamped unforced system, i.e. Eq. C.11. Maple code was written that enables the author to perform all of these complicated calculations, since Maple is a powerful symbolic computation tool, it can be implemented for symbolic programming of DNF method introduced by [8]. It is important to mention that, according to many researches, the Touzé two-degree-of-freedom system has many interesting aspects that can make it unique; the modal coupling between the two modes can cause rotary motion under the influence of excitation in one direction. Another interesting finding is that ε^2 solution gives completely different behaviour compared to ε^1 results, although this behaviour needs more extended studies, it can yield to completely new understanding of the expansions and their contribution to total solution. Furthermore, mathematically speaking, the mixed nonlinearity of X_1 and X_2 can be studied, this type of nonlinearities can usually be seen in MDOF

systems, and as discussed earlier using Maple software, corresponding computation can be easily performed. Reconsidering the undamped, unforced two-degree-of-freedom Touzé system, and by expanding Eq. C.11, Appendix C, it is possible to get

$$\begin{aligned}
\ddot{X}_1 &+ \omega_1^2 X_1 + \frac{3\omega_1^2}{2} X_1^2 + \frac{\omega_1^2}{2} X_2^2 + \omega_2^2 X_1 X_2 + \frac{\omega_1^2+\omega_2^2}{2} X_1 X_2^2 + \frac{\omega_1^2+\omega_2^2}{2} X_1^3 = 0, \\
\ddot{X}_1 &+ \omega_2^2 X_2 + \frac{3\omega_2^2}{2} X_2^2 + \frac{\omega_2^2}{2} X_1^2 + \omega_1^2 X_2 X_1 + \frac{\omega_2^2+\omega_1^2}{2} X_2 X_1^2 + \frac{\omega_2^2+\omega_1^2}{2} X_2^3 = 0.
\end{aligned} \tag{7.1}$$

Since this is a two-degree-of-freedom-system, the application of DNF method differs from SDOF systems, and the complexity of this method is directly related to degree-of-freedom of the system, hence, our method using Maple software can greatly help in the analysis. The first step is writing the system of equations in standard matrix form, that is

$$\ddot{\mathbf{q}} + \mathbf{\Lambda}\,\mathbf{q} + \mathbf{N}_q(\mathbf{q}) = 0, \tag{7.2}$$

where $\Lambda = \begin{bmatrix} \omega_1^2 & 0 \\ 0 & \omega_2^2 \end{bmatrix}$ and

$$\mathbf{N}_q(\mathbf{q}) = \begin{Bmatrix} \frac{3\omega_1^2}{2} q_1^2 + \frac{\omega_1^2}{2} q_2^2 + \omega_2^2 q_1 q_2 + \left(\frac{\omega_1^2+\omega_2^2}{2}\right) q_1 q_2^2 + \left(\frac{\omega_1^2+\omega_2^2}{2}\right) q_1^3 \\ \frac{3\omega_2^2}{2} q_2^2 + \frac{\omega_2^2}{2} q_1^2 + \omega_1^2 q_1 q_2 + \left(\frac{\omega_2^2+\omega_1^2}{2}\right) q_2 q_1^2 + \left(\frac{\omega_2^2+\omega_1^2}{2}\right) q_2^3 \end{Bmatrix} \tag{7.3}$$

where ω_1 and ω_2 are the first and second natural frequencies of this system, respectively. Now, applying near identity transform from $\mathbf{q}$ to $\mathbf{u}$, and considering all nonlinear terms to be of ε^1 order, the power series of the solution is truncated to $\mathbf{N}_q = \varepsilon \mathbf{n}_1$. And then the usual substitution of $\mathbf{u}_j = \mathbf{u}_{\mathrm{pj}} + \mathbf{u}_{\mathrm{mj}}$ is performed and $\mathbf{n}_1$, in matrix notation can be expressed as $\mathbf{n}_1(\mathbf{u}) = \mathbf{n}^* \mathbf{u}^*(\mathbf{u}_p,\ \mathbf{u}_m)$. Accordingly, the polynomial terms vector $\mathbf{u}^*$ and the coefficient matrix $\mathbf{n}^*$ are now constructed which have 30 elements. Furthermore, using Eq. 3.15 and Eq. 3.16, $\boldsymbol{\beta}^*$ matrix is constructed and it is used to find coefficient matrices of resonant and nonlinear harmonic terms $\mathbf{h}_1$ and $\mathbf{n}_{u1}$. Denoting h as the relation between the two forcing frequencies, i.e. $h = \dfrac{\omega_{r2}}{\omega_{r1}}$. Then, the detailed matrices for the solution are briefly shown in Appendix D.

It is important to mention that all terms of the solution are included in ε^1; since it is the basic solution, and all the following solutions will depend on ε^1. However, if the analysis is extended to higher order accuracies,

such as ε^2, the number of terms included in the analysis will significantly increase, which traditionally implies some reduction techniques for which certain terms are included in the analysis, and so the order of the matrices are reduced to make it possible to construct the solution, refer to [47]. However, when using Maple software for the analysis, where it can be possible to deal with massive algebraic terms, the researcher has enhanced flexibility to investigate the effect of all terms included.

To continue with the analysis, it is possible to write $\mathbf{n}_{u(1)}$ in terms of $\mathbf{u}$ as follows

$$\mathbf{n}_{u(1)} = \begin{Bmatrix} \frac{3\omega_1^2}{2}U_1^2 + \frac{\omega_1^2}{2}U_2^2 + \omega_2^2 U_1 U_2 + \left(\frac{\omega_1^2+\omega_2^2}{2}\right)U_1 U_2^2 + \left(\frac{\omega_1^2+\omega_2^2}{2}\right)U_1^3 \\ \frac{3\omega_2^2}{2}U_2^2 + \frac{\omega_2^2}{2}U_1^2 + \omega_1^2 U_1 U_2 + \left(\frac{\omega_2^2+\omega_1^2}{2}\right)U_2 U_1^2 + \left(\frac{\omega_2^2+\omega_1^2}{2}\right)U_2^3 \end{Bmatrix} \tag{7.4}$$

Now, to find the resonant nonlinear terms for ε^2 order, one needs to find $\frac{\partial}{\partial u}\mathbf{n}_{q(\mathbf{u})}$, and it is convenient to write $\mathbf{n}_{q(\mathbf{u})} = \widetilde{\mathbf{n}}_{q(\mathbf{u})} + \mathscr{O}(u^3)$, for which $\widetilde{\mathbf{n}}$ includes the quadratic terms only, so it is possible to write

$$\widetilde{\mathbf{n}}_{q(\mathbf{u})} = \begin{Bmatrix} \frac{3\omega_1^2}{2}U_1^2 + \frac{\omega_1^2}{2}U_2^2 + \omega_2^2 U_1 U_2 \\ \frac{3\omega_2^2}{2}U_2^2 + \frac{\omega_2^2}{2}U_1^2 + \omega_1^2 U_1 U_2 \end{Bmatrix} \tag{7.5}$$

This system is studied in detail by Liu and Wagg, [47], and they obtained the same results for ε^1, furthermore, they used the assumption of selecting quadratic terms only to construct ε^2 solution. In this work, the analysis is performed using the same assumption of adopting quadratic terms only, and this will generate 30 terms in $\mathbf{n}_{(2)}$, while if using both quadratic and cubic terms, $\mathbf{n}_{(2)}$ will be very massive (it will contain 168 elements). When using ε^2, the physical behaviour of the system changes from hardening to softening, this very interesting finding was also obtained by Liu and Wagg, [47]; and this unexpected behaviour of the second truncated term in the solution of ε^2 can be related to the magnitude of nonlinear terms; where usually these nonlinear terms are very small compared to linear terms but in Touzé system these nonlinear terms are not assumed to be small. Due to the massive size of $\mathbf{n}_{(2)}$, only $\mathbf{n}_{u(2)}$ is written in this thesis, and it can be found in Appendix D.

Now, the resulting equations for the non-resonant case can be written as

$$\begin{aligned}
&\ddot{u}_1 + \omega_1^2 U_1 + \eta_1(\omega_{r1},\omega_{r2})\left(u_{p1}^2 u_{m1} + u_{p1}u_{m1}^2\right) + \eta_2(\omega_{r1},\omega_{r2})\left(u_{p1}u_{p2}u_{m2} + u_{m1}u_{m2}u_{p2}\right) = 0,\\
&\ddot{u}_2 + \omega_2^2 U_2 + \eta_3(\omega_{r1},\omega_{r2})\left(u_{p2}^2 u_{m2} + u_{p2}u_{m2}^2\right) + \eta_4(\omega_{r1},\omega_{r2})\left(u_{p1}u_{p2}u_{m1} + u_{m1}u_{m2}u_{p1}\right) = 0.
\end{aligned} \tag{7.6}$$

where

$$\begin{aligned}
\eta_1(\omega_{r1},\omega_{r2}) &= \frac{3}{2}\left(\omega_1^2+\omega_2^2\right) - \frac{90}{12\omega_{r1}^2}\omega_1^4 + \frac{3\omega_{r2}^2 - 8\omega_{r1}^2}{2\omega_{r2}^2\left(4\omega_{r1}^2-\omega_{r2}^2\right)}\omega_2^4,\\
\eta_2(\omega_{r1},\omega_{r2}) &= \left(\omega_1^2+\omega_2^2\right) + \frac{2}{\omega_{r2}^3 - 4\omega_{r1}^2}\omega_2^4 - \frac{3}{\omega_{r1}^2}\omega_1^4 + \frac{2}{\omega_{r1}^2 - 4\omega_{r2}^2}\omega_1^4 - \frac{3}{\omega_{r2}^2}\omega_2^4,\\
\eta_3(\omega_{r1},\omega_{r2}) &= \frac{3}{2}\left(\omega_1^2+\omega_2^2\right) - \frac{90}{12\omega_{r2}^2}\omega_2^4 + \frac{3\omega_{r1}^2 - 8\omega_{r2}^2}{2\omega_{r1}^2\left(4\omega_{r2}^2-\omega_{r1}^2\right)}\omega_1^4,\\
\eta_4(\omega_{r1},\omega_{r2}) &= \left(\omega_1^2+\omega_2^2\right) + \frac{2}{\omega_{r1}^3 - 4\omega_{r2}^2}\omega_1^4 - \frac{3}{\omega_{r2}^2}\omega_2^4 + \frac{2}{\omega_{r2}^2 - 4\omega_{r1}^2}\omega_2^4 - \frac{3}{\omega_{r1}^2}\omega_1^4.
\end{aligned} \tag{7.7}$$

It worth mentioning that, for this particular system, it is difficult to write the previous expressions explicitly for ω_{r1} and ω_{r2}, however, to proceed with the analysis, those functions are adopted to construct the backbone curves. Finally, the system of time-independent frequency equations are written as

$$\begin{aligned}
U_1\left[\left(\omega_1^2-\omega_{r1}^2\right) + \frac{1}{4}\eta_1(\omega_{r1},\omega_{r2})U_1^2 + \frac{1}{4}\eta_2(\omega_{r1},\omega_{r2})U_2^2\right] = 0\\
U_2\left[\left(\omega_2^2-\omega_{r2}^2\right) + \frac{1}{4}\eta_3(\omega_{r1},\omega_{r2})U_2^2 + \frac{1}{4}\eta_4(\omega_{r1},\omega_{r2})U_1^2\right] = 0
\end{aligned} \tag{7.8}$$

Solving the system of equations it is possible to find the *single-mode* backbone curves for this system

$$\begin{aligned}
S1: \quad \omega_{r1}^2 &= \omega_1^2 + \frac{1}{4}\eta_1(\omega_{r1},\omega_{r2})U_1^2\\
S2: \quad \omega_{r2}^2 &= \omega_2^2 + \frac{1}{4}\eta_3(\omega_{r1},\omega_{r2})U_2^2
\end{aligned} \tag{7.9}$$

In order to verify these results, numerical results for the undamped unforced case are used, where the two natural frequencies are $\omega_1 = 2$ rad/s and $\omega_2 = 4.5$ rad/s, Fig. 7.2 shows the two backbone curves of this system versus the first amplitude of vibration U_1. It is worth mentioning that further more discussions regarding this system can be held, including modal interactions, bifurcations and stability of this system, further details regarding the dynamics of such system can be found in [45–47].

From Fig. 7.2 several findings can be noticed;

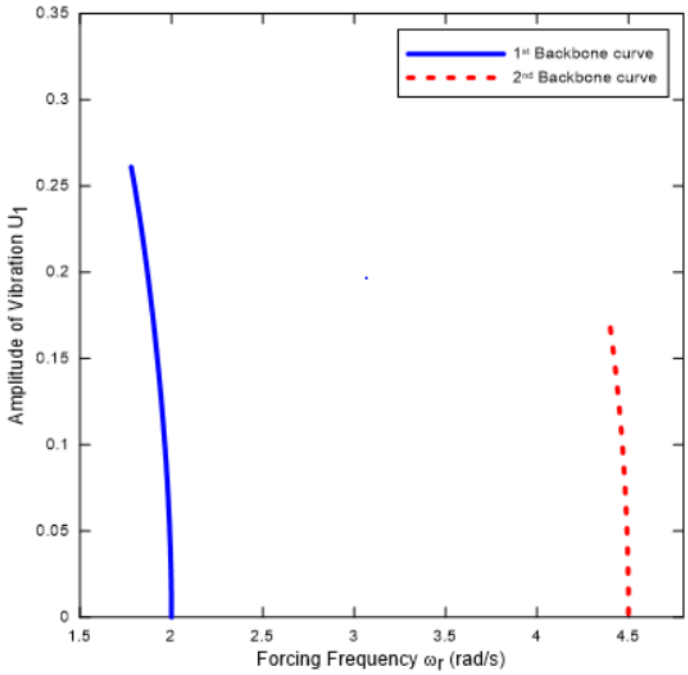

Figure 7.2: Backbone curves for the first and second natural frequencies versus the first amplitude of vibration U_1. Parameter values are: $\omega_1 = 2$ rad/s and $\omega_2 = 4.5$ rad/s.

- This figure shows the effect of the two nonlinear frequencies, ω_{r1} and ω_{r2}, to the first amplitude of vibration U_1, similarly, another figure of the effect of these two frequencies to the second amplitude of vibration U_2 can be plotted.

- In this figure, the dominant forcing frequency is ω_{r1}, while ω_{r2} will be dominant if U_2 is plotted. However, in both cases, the effect of the other forcing frequency is minor, but normally effective, hence, the visualisation of both forcing frequencies in a single plot can help understanding their effect.

- For systems of higher degrees-of-freedom (i.e. 3 or more), the effect of the additional forcing frequencies can be also plotted.

- This representation, with the aid of COCO forced frequency manifolds, can yield to a skeleton diagram that shows the effect of all forcing frequencies on any chosen system response (i.e. $U_1, U_2, \ldots$).

- Finally, much more in-depth analysis can be practised for this system as performed in [45–47], where many interesting aspects regarding the dynamics of such system are revealed. In this thesis, the system has been studied using the symbolic DNF approach which enabled the researcher to overcome complex mathematical manipulations involved.

Even though it mostly appears to be a theoretical (or mathematical) system, practical applications of Touzé two-degree-of-freedom can be found in the literature; one of these applications is illustrated in the stability analysis and vibration isolation in manufacturing equipment, [71], in which the mechanism investigated perfectly shows the nonlinear mode coupling of two perpendicular degrees-of-freedom problem. Under linear assumptions and simplifications, the model proposed by [71] has been investigated and results are accordingly generated, but in some cases where the force amplitudes are considerable then linear assumptions may not be valid and nonlinear analysis is necessary.

7.2 Verification problem 2: DNF analysis of 3-DOF system

In this section, the dynamics of 3-DOF system presented in Fig. 7.3 are explored, the system has a bilaterally symmetric structure which consists of three lumped masses, all have the mass m, attached to three identical linear springs of k stiffness, and three identical viscous dampers c. Moreover, the middle mass is connected to two nonlinear springs with linear and nonlinear cubic stiffnesses of $\bar{k}$, and κ, respectively, and two viscous dampers $\bar{c}$. Thus, the nonlinear springs have elastic forces of $F = \bar{k}(\Delta x) + \kappa(\Delta x)^3$. Additionally, the masses are excited with sinusoidally driving forces of the form $P_i \cos(\Omega t)$, in which Ω denotes the driving frequency and P_i is the amplitude of each force, and x_i is the displacement response of each mass given that $i = 1, 2, 3$. This system has been extensively studied by Liu in his PhD thesis, [72], using traditional DNF method applied with hand calculations, however, in this Section, the analysis done by Liu is reproduced using DNF method applied symbolically and truncated to ε^1 accuracy.

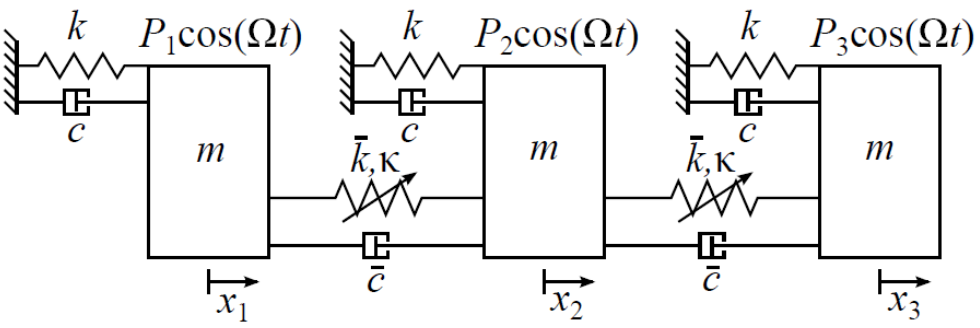

Figure 7.3: Schematic diagram of the bilaterally symmetric 3-DOF system with cubic nonlinear springs.

In reference to Eq. 3.3, the EOM of this system, in terms of the coordinates of physical displacement response $\mathbf{x} = [x_1 \quad x_2 \quad x_3]^\intercal$ can be written as

$$\begin{bmatrix} m & 0 & 0 \\ 0 & m & 0 \\ 0 & 0 & m \end{bmatrix} \ddot{\mathbf{x}}(t) + \begin{bmatrix} c+\bar{c} & -\bar{c} & 0 \\ -\bar{c} & c+2\bar{c} & -\bar{c} \\ 0 & -\bar{c} & c+\bar{c} \end{bmatrix} \dot{\mathbf{x}}(t) + \begin{bmatrix} k+\bar{k} & -\bar{k} & 0 \\ -\bar{k} & k+2\bar{k} & -\bar{k} \\ 0 & -\bar{k} & k+\bar{k} \end{bmatrix} \mathbf{x}(t) + \kappa \begin{Bmatrix} (x_1-x_2)^3 \\ (x_2-x_1)^3+(x_2-x_3)^3 \\ (x_3-x_2)^3 \end{Bmatrix} = \frac{1}{2} \begin{bmatrix} P_1 & P_1 \\ P_2 & P_2 \\ P_3 & P_3 \end{bmatrix} \tag{7.10}$$

Thus, the nonlinear stiffness matrix, which will be used to start the DNF solution is as follows

$$\mathbf{N}_x = \begin{bmatrix} c+\bar{c} & -\bar{c} & 0 \\ -\bar{c} & c+2\bar{c} & -\bar{c} \\ 0 & -\bar{c} & c+\bar{c} \end{bmatrix} \dot{\mathbf{x}}(t) + \kappa \begin{Bmatrix} (x_1-x_2)^3 \\ (x_2-x_1)^3+(x_2-x_3)^3 \\ (x_3-x_2)^3 \end{Bmatrix} \tag{7.11}$$

Now, it is required to apply linear modal transform, which is applied to decouple the linear stiffness terms, which yields to the EOM in the modal displacement responses $\mathbf{q}$, as mentioned in Eq. 3.8. Then, the matrices of modal natural frequencies, and linear mode shapes, $\mathbf{\Lambda}$ and $\mathbf{\Phi}$, are obtained upon solving the eigenvalue problem in Eq. 3.5, which gives, [72]

$$\mathbf{\Lambda} = \begin{bmatrix} \omega_{n1}^2 & 0 & 0 \\ 0 & \omega_{n2}^2 & 0 \\ 0 & 0 & \omega_{n3}^2 \end{bmatrix} = \frac{1}{m} \begin{bmatrix} k & 0 & 0 \\ 0 & k+\bar{k} & 0 \\ 0 & 0 & k+3\bar{k} \end{bmatrix}, \tag{7.12a}$$

$$\mathbf{\Phi} = \begin{bmatrix} 1 & 1 & 1 \\ 1 & 0 & -2 \\ 1 & -1 & 1 \end{bmatrix} \tag{7.12b}$$

The vector of nonlinear stiffness and damping terms is obtained using Eq. 3.16, that is

$$\mathbf{N}_q = \begin{Bmatrix} c\dot{q}_1 \\ \dfrac{2cm\dot{q}_2 + \kappa q_2\left(q_2^2 + 27q_3^2\right)}{m} \\ \dfrac{(c+3\bar{c})\,m\dot{q}_3 + 9\kappa q_3\left(q_2^2 + 3q_3^2\right)}{m} \end{Bmatrix} \tag{7.13}$$

Moreover, the force amplitudes transformed vector is written as, [72]

$$\mathbf{P}_q = \frac{1}{2}\begin{bmatrix} P_{m1} & P_{m1} \\ P_{m2} & P_{m2} \\ P_{m3} & P_{m3} \end{bmatrix} = \frac{1}{12m}\begin{bmatrix} 2P_1 + 2P_2 + 2P_3 & 2P_1 + 2P_2 + 2P_3 \\ 3P_1 - 3P_3 & 3P_1 - 3P_3 \\ P_1 - 2P_2 + P_3 & P_1 - 2P_2 + P_3 \end{bmatrix} \tag{7.14}$$

The forcing transform is then applied, the forcing frequency Ω is assumed to be close to the natural frequencies of the system, i.e. $\Omega \approx \omega_{ni}$ where $i = 1,2,3$. This assumption is reasonable if the coupling springs linear stiffnesses are sufficiently small compared to the grounding springs stiffnesses, i.e. $\bar{k} \ll k$, [72]. Then, it is possible to apply the transform $\mathbf{v} = \mathbf{q}$ considering that $\mathbf{e} = [\mathbf{0}]_{\{3\times 2\}}$, and referring to Eq. 3.11 and Eq. 3.21, in view of Eq. 3.14, it is possible write

$$\mathbf{N}_v(\mathbf{v}, \dot{\mathbf{v}}) = \mathbf{N}_q(\mathbf{v}, \dot{\mathbf{v}}), \tag{7.15a}$$

$$\mathbf{P}_v = \mathbf{P}_q \tag{7.15b}$$

Finally, the nonlinear near-identity transform leads to the resonant EOM in terms of $\mathbf{u}$ coordinates, as seen in Eq. 3.26. For this system, ε^1 accuracy is adopted, the results of this accuracy level compared to numerical results is investigated in detail in [72] in which good agreement can be observed. By substituting the assumed solution, Eq. 3.27 into Eq. 7.15a, one can find the the polynomial terms vector, $u^*_{(1)}$, and the corresponding coefficient matrix, $[n_v(1)]$, then the matrix $\boldsymbol{\beta}$ is computed using Eq. 3.26. Thus, in Appendix E the matrix manipulations for this system are presented assuming that $\Omega = \omega_{r2} = \omega_{r3}$ corresponding to the condition that $\Omega \approx \omega_{n2} \approx \omega_{n3}$ as in [72].

Now, it is possible to apply the conditions in Eq. 3.16 to find the vector of nonlinear and damping terms, thus

$$\mathbf{N}_u = \left\{ \begin{array}{c} \mathbf{i}c\omega_{r1}\left[u_{p1}-u_{m1}\right] \\ \mathbf{i}\left(c+\bar{c}\right)\omega_{r2}\left[u_{p2}-u_{m2}\right]+u_2\left[3u_{p2}u_{m2}+54u_{p3}u_{m3}\right]+27\left[u_{m2}u_{p2}^2+u_{p2}u_{m3}^2\right] \\ \mathbf{i}\left(c+3\bar{c}\right)\omega_{r3}\left[u_{p3}-u_{m3}\right]+u_3\left[18u_{p2}u_{m2}+81u_{p3}u_{m3}\right]+9\left[u_{m3}u_{p2}^2+u_{p3}u_{m2}^2\right] \end{array} \right\} \tag{7.16}$$

Accordingly, for $\omega_{r2}=\omega_{r3}$ and $\phi_2-\phi_3$ being the phase difference between the second and third modes, respectively, the time-invariant complex coefficients, in terms of $\mathrm{e}^{\mathbf{i}\omega_{ri}t}$, for each row in Eq. 6.25 can be found as

$$N_{u1}^{+}=\mathbf{i}c\omega_{r1}\mathrm{e}^{-\mathbf{i}\phi_1}, \tag{7.17a}$$

$$N_{u2}^{+}=\mathbf{i}\left(c+\bar{c}\right)\omega_{r2}\mathrm{e}^{-\mathbf{i}\phi_2}+\frac{3\kappa}{8m}\mathrm{e}^{-\mathbf{i}\phi_2}U_2\left[U_2^2+18U_3^2+9\mathrm{e}^{2\mathbf{i}(\phi_2-\phi_3)}U_3^2\right], \tag{7.17b}$$

$$N_{u3}^{+}=\mathbf{i}\left(c+3\bar{c}\right)\omega_{r3}\mathrm{e}^{-\mathbf{i}\phi_3}+\frac{9\kappa}{8m}\mathrm{e}^{-\mathbf{i}\phi_3}U_3\left[2U_2^2+9U_3^2+\mathrm{e}^{-2\mathbf{i}(\phi_2-\phi_3)}U_2^2\right] \tag{7.17c}$$

Moreover, it is possible to eliminate the terms ϕ_i in Eq. 7.17 to get the analytical expressions for the time-invariant equations for this system, which are

$$\left\{\left[\omega_{n1}^2-\omega_{r1}^2\right]^2+\left(c\omega_{r1}\right)^2\right\}U_1^2=P_{m1}^2, \tag{7.18a}$$

$$\left\{\left[\omega_{n2}^2-\omega_{r2}^2+\frac{3\kappa}{4m}\left[U_2^2+\left(18+9\mathrm{e}^{2\mathbf{i}(\phi_2-\phi_3)}U_3^2\right)\right]\right]^2+\left(\left(c+\bar{c}\right)\omega_{r2}\right)^2\right\}U_2^2=P_{m2}^2, \tag{7.18b}$$

$$\left\{\left[\omega_{n3}^2-\omega_{r3}^2+\frac{3\kappa}{4m}\left[27U_3^2+\left(6+3\mathrm{e}^{-2\mathbf{i}(\phi_2-\phi_3)}U_2^2\right)\right]\right]^2+\left(\left(c+3\bar{c}\right)\omega_{r3}\right)^2\right\}U_3^2=P_{m3}^2 \tag{7.18c}$$

Finally, the previous expressions, with some different notations, were obtained by Liu in [72] using the traditional hand-calculated DNF technique, in this work, using our proposed symbolic DNF technique applied with Maple software, the author has been able to obtain the same results with much less efforts. In the next subsection, the analysis is extended to compute the corresponding backbone curves of this system.

7.2.1 Computations of conservative backbone curves

In order to find the conservative backbone curves of the 3-DOF system in Eq. 7.11, it is possible to set all damping and forcing terms in Eq. 7.18 to be zeros, which gives;

$$\left[\omega_{n1}^2 - \omega_{r1}^2\right] U_1 = 0, \tag{7.19a}$$

$$\left[\omega_{n2}^2 - \omega_{r2}^2 + \frac{3\kappa}{4m}\left[U_2^2 + \left(18 + 9\mathrm{e}^{2\mathbf{i}(\phi_2-\phi_3)}U_3^2\right)\right]\right] U_2 = 0, \tag{7.19b}$$

$$\left[\omega_{n3}^2 - \omega_{r3}^2 + \frac{3\kappa}{4m}\left[27U_3^2 + \left(6 + 3\mathrm{e}^{-2\mathbf{i}(\phi_2-\phi_3)}U_2^2\right)\right]\right] U_3 = 0 \tag{7.19c}$$

In Eq. 7.19 when $U_1 = U_2 = U_3 = 0$ no motion is occurring and thus the trivial solution of the system is considered. Moreover, if each mode is independently behaving, three more sets of solutions can also be observed for which the phenomena of *single-mode* backbone curves is obtained. Setting $U_2 = U_3 = 0$, $U_1 = U_3 = 0$ and $U_1 = U_2 = 0$ in Eq. 7.19a, Eq. 7.19b, Eq. 7.19c, respectively, leads to the analytical expressions of ε^1 conservative *single-mode* backbone curves, labelled as $S1$, $S2$ and $S3$, such that;

$$S1: \quad U_1 \neq 0, U_2 = 0, U_3 = 0, \qquad \omega_{r1}^2 = \omega_{n1}^2, \tag{7.20a}$$

$$S2: \quad U_1 = 0, U_2 \neq 0, U_3 = 0, \qquad \omega_{r2}^2 = \omega_{n2}^2 + \frac{3\kappa}{4m}U_2^2, \tag{7.20b}$$

$$S3: \quad U_1 = 0, U_2 = 0, U_3 \neq 0, \qquad \omega_{r3}^2 = \omega_{n3}^2 + \frac{81\kappa}{4m}U_3^2, \tag{7.20c}$$

The previous expressions of the *single-mode* backbone curves are also obtained by Lui, [72], and then he extended the analysis to include *double-mode* backbone curves for both hardening and softening cases, furthermore, he used the stability of the steady-state solution, given in Section 3.3, to investigate the stability of the backbone curves introduced. Nevertheless, having reached the *single-mode* backbone curves in Eq. 7.20, it is possible conclude that our proposed implementation of symbolically practised DNF works well compared to traditional DNF technique. Thus, in this thesis, the discussions for this 3-DOF system are limited to this point, and the interested reader can refer to [72] for more in-depth investigations of this system in addition to more complicated 3-DOF systems.

7.3 Analysis of 2-DOF oscillator with cubic and quintic nonlinearities

In this section, the two degree-of-freedom oscillator shown in Fig. 7.4 is considered, for which the spring forces are governed by both linear and nonlinear terms, and the nonlinear term contains cubic and quintic orders of polynomial nonlinearities. The main purpose of this Section is to show how the type of analysis carried out for SDOF systems can be applied to oscillators of more than one degree-of-freedom. As a result, the system is assumed to be conservative (undamped and unforced), and the corresponding *single-mode* backbone curves are computed (e.g., neglecting the resonant cases).

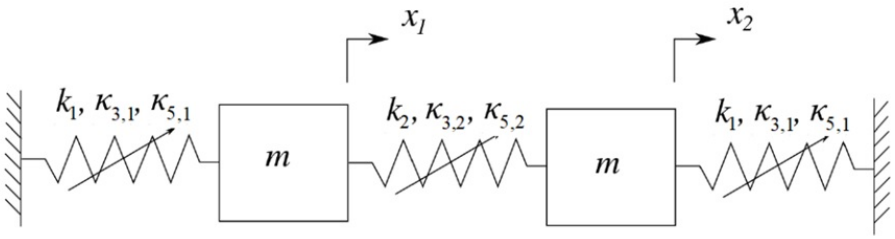

Figure 7.4: Schematic diagram of the 2-DOF cubic-quintic oscillator in Section 7.3.

In matrix form, the system equations of motion can be written as

$$\begin{bmatrix} m & 0 \\ 0 & m \end{bmatrix} \ddot{x} + \begin{bmatrix} k_1+k_2 & -k_2 \\ -k_2 & k_1+k_2 \end{bmatrix} x + \begin{bmatrix} \kappa_{3,1}x_1^3 - \kappa_{3,2}(x_2-x_1)^3 + \kappa_{5,1}x_1^5 - \kappa_{5,2}(x_2-x_1)^5 \\ \kappa_{3,1}x_2^3 + \kappa_{3,2}(x_2-x_1)^3 + \kappa_{5,1}x_2^5 + \kappa_{5,2}(x_2-x_1)^5 \end{bmatrix} = \begin{bmatrix} 0 \\ 0 \end{bmatrix} \tag{7.21}$$

where $\boldsymbol{x} = \{x_1, x_2\}^\intercal$ and the two masses are of identical mass m, and the linear stiffness coefficients are k_1 and k_2. The nonlinear stiffnesses are denoted by κ with subscripts that reflect both the order of the nonlinearity and the spring number, thus, the cubic stiffness coefficients are $\kappa_{3,1}$ and $\kappa_{3,2}$ and the quintic stiffness coefficients are $\kappa_{5,1}$ and $\kappa_{5,2}$, respectively. This form of the subscript is chosen to help generalisation of this problem to include higher orders of odd nonlinearities. The analysis of such a system starts by obtaining the linear version of Eq. 7.21, by setting all the nonlinear stiffnesses to be zeros. Following that, the linear modal analysis leads to a modal transformation of

$$\boldsymbol{x} = \boldsymbol{\Phi}\boldsymbol{q} \quad \text{where} \quad \boldsymbol{\Phi} = \begin{bmatrix} 1 & 1 \\ 1 & -1 \end{bmatrix} \tag{7.22}$$

herein, $\omega_{n1}^2 = \dfrac{k}{m}$, $\omega_{n2}^2 = \dfrac{k_1+2k_2}{m}$ are the natural frequencies.

Now, following the steps of the DNF procedure for MDOF systems as previously described (see [8, 30] for more details), one can compute approximate analytical expressions for backbone curves. For this system of coupled cubic-quintic oscillators, considering the non-resonant case, where $\omega_{r2} \neq \omega_{r1}$, the following expressions of the backbone curves are found

$$U_1 \left\{ \omega_{n1}^2 - \omega_{r1}^2 + \frac{3\kappa_{3,1}}{4m}\left[U_1^2 + 2U_2^2(2+p)\right] + \frac{5\kappa_{5,1}}{8m}\left[U_1^4 + 2U_2^4(2+p)\right] \right\} = 0, \tag{7.23a}$$

$$U_2 \left\{ \omega_{n2}^2 - \omega_{r2}^2 + \frac{3\kappa_{3,1}}{4m}\left[\gamma_1 U_2^2 + 2U_1^2(2+p)\right] + \frac{5\kappa_{5,1}}{8m}\left[\gamma_2 U_2^4 + 2U_1^4(2+p)\right] \right\} = 0 \tag{7.23b}$$

where $\gamma_1 = 1 + \dfrac{8\kappa_{3,2}}{\kappa_{3,1}}$ and $\gamma_2 = 1 + \dfrac{32\kappa_{5,2}}{\kappa_{5,1}}$, and p denotes two main cases corresponding to the *in-unison* and *out-of-unison* cases as follows:

- $p = +1$ stands for the *in-unison* case, where the phase difference $|\phi_1 - \phi_2| = 0$ for the *in-phase* case and $|\phi_1 - \phi_2| = \pm n\pi$ for $n = 1, 2, 3...$ which represents the *out-of-phase* case.
- $p = -1$ stands for the *out-of-unison* case where the phase difference $|\phi_1 - \phi_2| = \pm\dfrac{n\pi}{2}$ for $n = 1, 2, 3...$ which represents the *out-of-unison* case.

Accordingly, it is possible to consider two cases of the backbone curves; namely, *single-mode* and *double-mode* backbone curves, [8, 119].

7.3.1 Single-mode backbone curves

The *single-mode* backbone curve, usually denoted by S, can be generated for this system by setting $U_2 = 0$ in Eq. 7.23a, or $U_1 = 0$ in Eq. 7.23b. Therefore, the *single-mode* backbone curves for this system are obtained in [101] and can be written as,

$$\begin{aligned} S_1 \quad &\rightsquigarrow \quad U_2 = 0 \quad \rightsquigarrow \quad \omega_{r1}^2 = \omega_{n1}^2 + \frac{3\kappa_{3,1}}{4m}U_1^2 + \frac{5\kappa_{5,1}}{8m}U_1^4 \\ S_2 \quad &\rightsquigarrow \quad U_1 = 0 \quad \rightsquigarrow \quad \omega_{r2}^2 = \omega_{n2}^2 + \frac{3\kappa_{3,1}}{4m}\gamma_1 U_2^2 + \frac{5\kappa_{5,1}}{8m}\gamma_2 U_2^4 \end{aligned} \tag{7.24}$$

In these *single-mode* backbone curves, no phase coupling occurs between the two modal coordinates, u_1 and u_2. In order to explore the case of phase coupling between the two modal coordinates, it is possible to consider the *in-unison* case when $p = +1$. In the literature, some research has been conducted to study the *double-mode* (or

two mode) modal interactions, see [8] as an example. In Fig. 7.5 sample results of the *single-mode* backbone curves for this oscillator are shown. However, the case of *double-mode* modal interactions are shown in the following subsection.

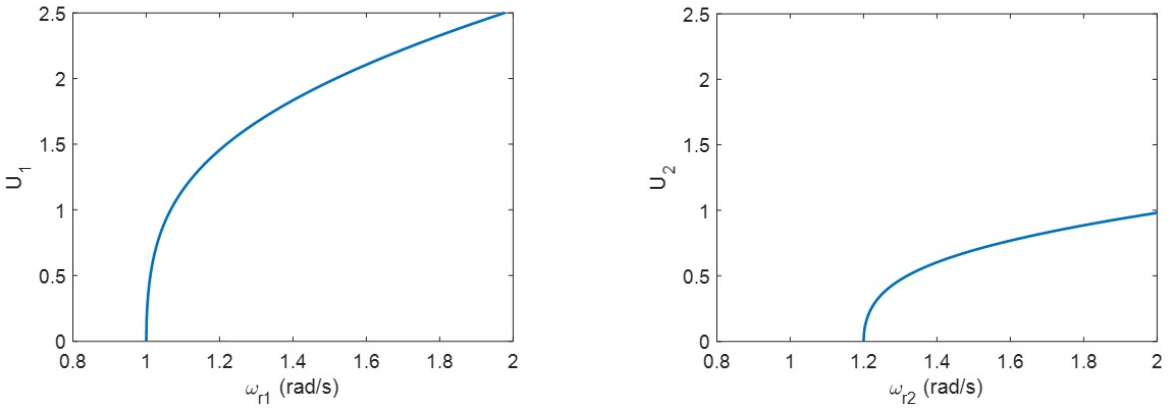

(a) (b)

Figure 7.5: *Single-mode* backbone curves of the 2-DOF oscillator studied in Section 7.3: (a) S_1 backbone curve which represents the projection of U_1 against ω_{r1}, (b) S_2 backbone curve which represents the projection of U_2 against ω_{r2}. Parameter values are: $\omega_{n1} = 1$ rad/s, $\omega_{n2} = 1.2$ rad/s and $\kappa_{3,1} = \kappa_{3,2} = \kappa_{5,1} = \kappa_{5,2} = 0.1$.

The key point is to notice the similarity between the *single-mode* backbone curves for the 2-DOF system, Eq. 7.4, and the corresponding results of the SDOF cubic-quintic oscillator, Eq. 5.10. Hence, the *single-mode* backbone curves, truncated to ε^1 accuracy, for a 2-DOF nonlinearly couple oscillators with odd polynomial nonlinear stiffness terms, can be written as

$$\begin{aligned} S_1 \quad &\rightsquigarrow \quad \omega_{r1}^2 = \omega_{n1}^2 + \sum_{j=1}^{R} \frac{1}{2^{2j}} \binom{2j+1}{j+1} \kappa_{2j+1,1} U^{2j+1} \\ S_2 \quad &\rightsquigarrow \quad \omega_{r2}^2 = \omega_{n2}^2 + \sum_{j=1}^{R} \frac{1}{2^{2j}} \binom{2j+1}{j+1} \kappa_{2j+1,1} \gamma_j U^{2j+1} \end{aligned} \tag{7.25}$$

where $\gamma_j = 1 + (2)^{(2j+1)} \left(\dfrac{\kappa_{2j+1,2}}{\kappa_{2j+1,1}} \right)$. Using Eq. 7.24, the *single-mode* backbone curves of the 2-DOF oscillator with odd polynomial nonlinearities is computed. This example shows how (at least for the relatively simple case of *single-mode* backbone curves) the analysis for cubic-quintic SDOF oscillators relates to the 2-DOF case.

7.3.2 Double-mode backbone curves

In order to consider the resonant case, it is convenient to introduce Ω as a general frequency response parameter and then rewrite Eq. 7.23 considering responses of both equations at a certain Ω value, thus it is convenient to write

$$\begin{aligned}\Omega^2 &= \omega_{n1}^2 + \frac{3\kappa_{3,1}}{4m}\left[U_1^2 + U_2^2(2+p)\right] + \frac{5\kappa_{5,1}}{8m}\left[U_1^4 + 2U_2^4(2+p)\right] \\ &= \omega_{n2}^2 + \frac{3\kappa_{3,1}}{4m}\left[\gamma_1 U_2^2 + U_1^2(2+p)\right] + \frac{5\kappa_{5,1}}{8m}\left[\gamma_2 U_2^4 + 2U_1^4(2+p)\right]\end{aligned} \tag{7.26}$$

where $p = \mathrm{e}^{2\ \mathrm{i}(\phi_1-\phi_2)}$. In order to maintain real solutions, $p = \pm 1$ is required, such that

- when $p = +1$ the *in-unison* case is considered denoting that either in-phase (0) or out-of-phase ($\pm n\pi$) occurs, corresponding to $|\phi_1 - \phi_2| = 0, \pm n\pi$, for $n = 1, 2, 3...$,

- when $p = -1$ the *out-of-unison* case is considered denoting that phase differences in the response behaviour are ($\pm n\pi/2$), corresponding to $|\phi_1 - \phi_2| = \pm n\pi/2$, for $n = 1, 2, 3....$

Herein, only the case of $p = +1$ is shown, nevertheless, further details of the *out-of-unison* case can be found in [31], for instance. Setting $p = +1$ and $n = 1$ yields to two backbone curves, labelled $D12_i^+$ and $D12_i^-$, with the phase differences

$$D12_i^+ : \quad |\phi_1 - \phi_2| = 0\,, \qquad\qquad D12_i^- : \quad |\phi_1 - \phi_2| = \pi\,. \tag{7.27}$$

It is noteworthy that, for double (or two) mode interaction, the notation D is followed by the two interacting modes while the subscript i means in-unison, furthermore, the plus and minus signs refer to the *in-phase* and *out-of-phase* cases, respectively. Substituting $p = +1$ in Eq. 6.35 leads to the following expressions for $D12_i^{\pm}$;

$$U_1^2 = \frac{\sqrt{150U_2^4(\gamma_2+5)\kappa_{5,1}^2 + 40\left(\left(\omega_{n1}^2 - \omega_{n2}^2\right)m + \frac{9}{4}U_2^2\kappa_{3,1}\right)(\gamma_2+5)\kappa_{5,1} + 9\kappa_{3,1}^2(\gamma_1+2)^2} + (-3\gamma_1-6)\kappa_{3,1}}{5\kappa_{5,1}(\gamma_2+5)} \tag{7.28}$$

and,

$$\Omega^2 = \frac{-3\kappa_{3,1}\left(\gamma_1-\gamma_2-3\right)\sqrt{150U_2^4\left(\gamma_2+5\right)\kappa_{5,1}^2+40\left(\omega_{n1}^2 m-\omega_{n2}^2 m+\frac{9}{4}U_2^2\kappa_{3,1}\right)\left(\gamma_2+5\right)\kappa_{5,1}+9\kappa_{3,1}^2\left(\gamma_1+2\right)^2}}{20\kappa_{5,1}\left(\gamma_2+5\right)^2 m}$$
$$+\frac{75U_2^4\left(\gamma_2+6\right)\left(\gamma_2+5\right)\kappa_{5,1}^2+20\left(\frac{9U_2^2(\gamma_2+6)\kappa_{3,1}}{4}+m\left(\gamma_2\omega_{n1}^2+6\omega_{n1}^2-\omega_{n2}^2\right)\right)\left(\gamma_2+5\right)\kappa_{5,1}+9\kappa_{3,1}^2\left(\gamma_1+2\right)\left(\gamma_1-\gamma_2-3\right)}{20\kappa_{5,1}\left(\gamma_2+5\right)^2 m} \tag{7.29}$$

From the expression in Eq. 7.28 the following conditions need to be imposed so that real solutions are ensured;

$$U_2^2 > \frac{-9\kappa_{3,1}+\sqrt{240m\kappa_{5,1}\left(\omega_{n2}^2-\omega_{n1}^2\right)+81\kappa_{3,1}^2}}{30\kappa_{5,1}}, \quad \text{and} \quad 240m\kappa_{5,1}\left(\omega_{n2}^2-\omega_{n1}^2\right)+81\kappa_{3,1}^2>0. \tag{7.30}$$

Numerically computed results are shown in Fig. 7.6 (a) and (b). If the middle spring linking the two masses is much less stiff than the springs connecting the masses to the hard walls at either end, e.g. $k_2 \ll k_1$, $\kappa_{3,2} \ll \kappa_{3,1}$ and $\kappa_{5,2} \ll \kappa_{5,1}$, then the numerical findings in Fig. 7.6 will hold. In the literature, this type of system is normally called *weakly coupled*, in which, for very small amplitudes, both masses on $S1$ and $S2$ curves will oscillate at a frequency very close to one. Thus, as U_i amplitudes increase, it can be seen that the $S2$ backbone curve has a bifurcation at which point the stable $D12_i^{\pm}$ curves coincide with $S2$. More discussions regarding the bifurcation points for a system of 2-DOF with cubic nonlinear coupling term can be found in [104, 119].

7.4 Summary

In this Chapter, analysis of MDOF systems using the proposed symbolic DNF is shown, two verification problems are considered; the vertical-horizontal-spring-mass oscillator (or Touzé 2-DOF system), and 3-DOF system with cubic nonlinear stiffness coupling terms. Then, a system of 2-DOF cubic-quintic oscillator is discussed. Based on the discussions in this Chapter, the followings are observed;

- For the Touzé 2-DOF system, a new derivation of the EOM is introduced, contrary to the derivations found in the literature, this proposed derivation is based on a physically strong-form set of equations of motion as seen in Appendix C.

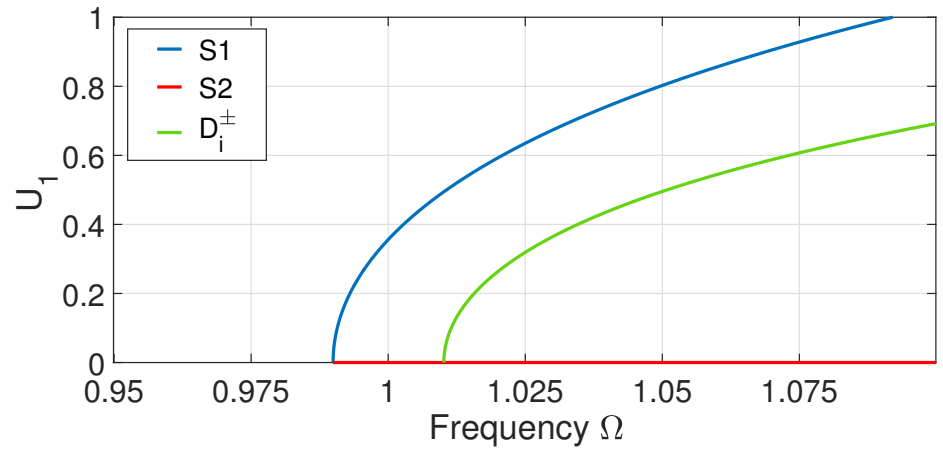

(a)

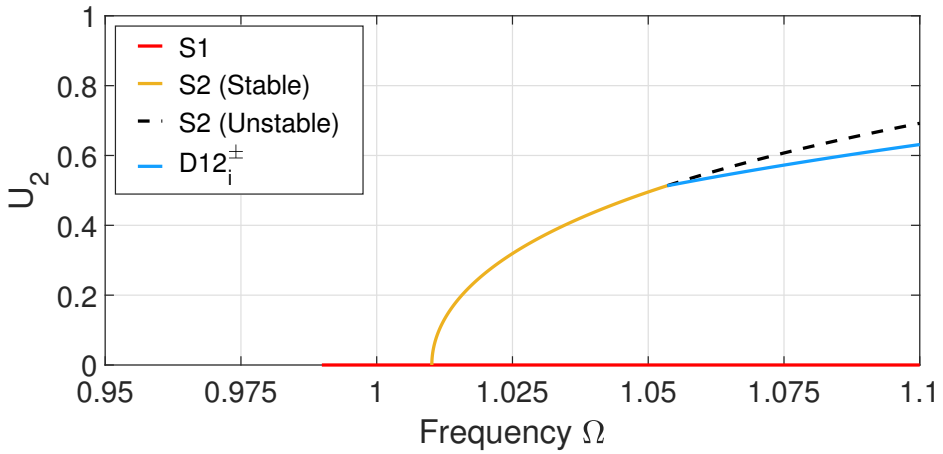

(b)

Figure 7.6: The two-degree-of-freedom cubic-quintic oscillator, (a) *Single-mode* backbone curves; the backbone curves in the projection of U_1 against Ω. (b) Projection of U_2 against Ω, where the dashed black line represents the unstable part of the backbone curve. Parameter values are $m = 1$ kg, $k_1 = 0.98$ N/m, $k_2 = 0.0202$ N/m, $\kappa_{3,1} = 0.2$ N/m^3, $\kappa_{3,2} = 0.02$ N/m^3, $\kappa_{5,1} = 0.1$ N/m^5 and $\kappa_{5,2} = 0.01$ N/m^5.

- The two verification problems illustrate the possibility of using the method of DNF applied symbolically for the investigation of MDOF systems, however, more in-depth future works are needed to expand the implementation of symbolic DNF technique for systems with higher degrees of freedom.

- For the 2-DOF cubic-quintic system studied in Section 7.3, the *single-mode* and *double-mode* backbone curves are generated, however, those are computed to ε^1 accuracy. Thus, future works can involve expanding the analysis to ε^2 accuracy to compare both results.

- In addition to being applied for the DNF analysis, and due to the complexity of the calculations involved in the analysis of the 2-DOF cubic-quintic system, Maple software was used for the mathematical manipulations for this system.

- Starting by the analysis performed in this Chapter, further future works can be conducted regarding MDOF system, this can include, as priorly mentioned, higher degrees of freedom systems. Moreover, based on the analysis in Section 4.4, computing damped backbone curves for MDOF systems can also be an interesting topic for future studies.

Chapter 8

Conclusions and future work

In this final Chapter of the thesis, upon reviewing the overall investigations held, discussions regarding the overall novelties and contributions of this research are performed, this is followed by more specific discussions of the key conclusions. Finally, discussions of potential future works are also presented.

8.1 Discussions of the overall novelties and contributions of this research

In this research, the method of DNF has been explored symbolically with Maple software, which lead to significant improvements to the method and its applications in the field of nonlinear mechanical vibrations. Firstly, the method of DNF, when used effectively, is a powerful tool for researchers to adopt. DNF method enables the investigations of the dynamics of nonlinear EOMs for both SDOF and MDOF systems, under numerous resonant and non-resonant cases, besides, compared to other methods such as harmonic balance, it can effectively deal with imperfections appearing in the system such as discontinuities in the nonlinear terms, which, for instance, makes it a good choice for analysts to study non-smooth nonlinearities.

In terms of the DNF method accuracy, thanks to the symbolic computations approach, a novel contribution of this research is introducing a generalised analytical closed form solution that can be used, in principle, to truncate the results of the method to any ε accuracy, Section 4.2, and this has been discussed with some exam-

ples in Section 4.3 in this thesis. On the other hand, the topic of damped backbone curves has been discussed in detail, and novel procedure of the analytical computations of obtaining these curves is shown in Section 4.4.

Moreover, the symbolic implementation of the DNF method, as this thesis reveals, resulted in enhanced tools for researchers to explore nonlinear SDOF systems with high orders of polynomial geometric nonlinearities, Section 5.3, SDOF systems with combinations of polynomial nonlinear stiffness and viscous damping terms, Section 5.4, SDOF systems with fractional order damping, Section 6.2 and Section 6.5, and finally MDOF systems with high orders of polynomial nonlinear stiffness terms, Section 7.3. All of these novel contributions indicate that the symbolic implementation approach of the method leads to desirable outcomes that add to the value of the proposed work. In the following subsections, more specific details of the main findings and conclusions that can be drawn from the proposed work are discussed.

8.1.1 Higher order accuracies and Damped backbone curves

In Section 4.1 of this thesis, a novel improvement to the accuracy of DNF technique has been shown, which was demonstrated by raising the accuracy of the DNF method to any desired ε order. By proposing a general closed-form pattern of ε^n accuracy, the author has been able to study some nonlinear SDOF examples to conclude that raising the accuracy of the DNF method can lead to some improved findings of the resulting backbone curves.

Furthermore, in Section 4.4, the problem of viscously damped nonlinear oscillators with geometric polynomial stiffness nonlinearities is discussed in detail. The proposed technique is based on a combination of Burton's work and the normal form method. Damped backbone curves (DBBC) are analytically truncated and compared to the numerically computed forced-damped manifolds, and the overall results show good matching between the analytical and numerical results. Furthermore, when the damping is relatively small, the proposed technique is directly used to analyse higher orders of polynomial nonlinearities, and straightforward approximations to the DBBC's are obtained in the form of explicit expressions truncated to ε^1 order.

While the proposed technique can be directly implemented for many engineering applications, some restrictions need to realised; the technique can be used for small damping cases, and for ε^1 accuracy. Moreover, the technique needs to be improved to study MDOF systems, and, in principle, nonlinear normal modes (NNMs) can typically be practical engineering applications to clarify the advantages of this technique.

8.1.2 Oscillators with geometric nonlinear stiffness terms

In Chapter 5 of this thesis, the DNF method has been used to study nonlinear oscillators with higher order polynomial stiffness nonlinear terms. For the SDOF case, the analysis has been performed for two orders of series expansion, ε^1 and ε^2, and the related backbone curves were derived for both of cases. The results were compared with a selection of other methods already available in the published literature. One point of interest was that in the case of only odd nonlinear terms (like the cubic-quintic) the ε^2 order solutions were not always more accurate than the ε^1 order solutions (when compared to the benchmark case). When even nonlinear terms were added, as with the generic cubic-quintic SDOF oscillator this changed, and here the ε^2 order solutions were always more accurate than the ε^1 order solutions – as would be expected.

In addition, it was shown that, for the SDOF oscillators considered with only odd nonlinear terms, the expression for the backbone curve of the system to ε^1 order could be generalized. This was not the case when even nonlinearities were present and in this case, ε^2 accuracy was needed.

In terms of methodology, the use of symbolic computations helped deal with algebraic complexity, for the higher orders nonlinearities and/or degrees-of-freedom. As a more complex example, a two degree-of-freedom cubic-quintic oscillator was considered. Here it was shown that, for *single-mode* backbone curves (ignoring potential resonances and out-of-unison responses) there was a similar structure in the approximate expressions for the backbone curves when compared to the equivalent SDOF cubic-quintic cases. This demonstrates that a possible general relationship exists for SDOF and MDOF oscillators of this type, at least in the simplest cases. This may be a worthwhile topic for future research.

Moreover, the method of DNF is used to study the dynamical behaviour of Van-der-Pol and Rayleigh oscillators driven by a single harmonic force near resonance, the purpose of the applying DNF is to analytically investigate the steady-state frequency responses of these oscillators. Several oscillator cases are studied, the Van-der-Pol oscillator, Duffing Van-der-Pol, cubic-quintic Van-der-Pol, Rayleigh oscillator, Rayleigh-Duffing and finally cubic-quintic Rayleigh oscillator. In order to make all required calculations Symbolic computations using Maple were implemented, and this enabled the author to manipulate massive algebraic mathematical expressions.

8.1.3 Applications to SDOF and MDOF systems

In Chapter 4 and Chapter 5 of this thesis, numerous DNF applications are discussed in detail, most of the analysis performed in that area are performed symbolically using Maple software. Based on the overall investigations held, it can be concluded that, for geometrically nonlinear stiffness terms, some frequency-amplitude (or backbone) curves patterns are observed in the order of the nonlinearity and, specifically, the order of the ε^1 terms.

Moreover, it can be concluded that higher order nonlinearities can be tackled succinctly using the proposed symbolic DNF technique. This leads to the fact that this symbolic approach can be applied to a variety of classical oscillator problems with acceptable levels of accuracy compared to numerical techniques. Therefore, a key contribution to knowledge of this thesis is the demonstration that symbolic computation approaches have indeed shed new light on the intricate nonlinear dynamics of oscillatory mechanical systems.

8.1.4 Fractionally damped oscillators

In Chapter 6 of this work, DNF approximate analytical technique is modified to investigate the dynamics of fractionally damped Duffing oscillator, for which the fractional damping order of the oscillator is β, where $0 < \beta < 1$ and if $\beta = 1$ then the viscously damped Duffing oscillator is resulted. According to the author best knowledge, the DNF technique has never been used to study such a type of fractionally damped systems; thus, this work shows a novel implementation of the DNF to investigate Duffing oscillators with any order of fractional derivative β where $0 < \beta < 1$. Practically, Davison-Essex's definition of the fractional derivative is

used to write the fractional derivatives in a form that enhances applicability of DNF technique; accordingly, the author has been able to perform the analysis to the oscillator with different orders of the fractional derivative, and approximate analytical expressions for the frequency-amplitude and frequency-phase relationships are generated.

In order to explore the accuracy of the proposed results, numerical solutions of the oscillator are obtained using Grünwald-Letnikov's numerical technique, and those are compared to the corresponding DNF results, the comparison shows acceptable levels of accuracy of the DNF in reference to the numerically computed frequency-amplitude figure. Additionally, in order to compare the proposed DNF results to other results found in the literature, the averaging method is used to investigate the frequency-amplitude relationship of the fractionally damped Duffing oscillator. As a result, when compared to the averaging technique, the DNF outcomes perfectly fit the corresponding results of the averaging technique which denotes the accuracy of the proposed work.

8.1.5 Value of this research in the wider engineering context

The overall discussions held in this thesis are inherently connected to the wider context of engineering applications; the main concern of this research is to improve the capabilities of the DNF method so that it can be efficiently adopted for more complex physical engineering applications, specifically those mathematically modelled by nonlinear EOMs. The traditional applications of the DNF techniques are restricted to nonlinear systems those modelled by low orders of polynomial nonlinear stiffness terms, nevertheless, many modern engineering applications require more complicated models, including; higher orders of polynomial geometric stiffness terms, combinations of geometric nonlinear stiffness and viscous damping terms, in addition to systems with fractional orders of damping that can be found, for instance, in designs adopting polymeric materials. All of these applications are discussed in this research where the dynamics of such models are discussed in detail using the symbolic approach of the DNF technique.

Moreover, some real-life engineering applications are discussed in this research; for example, as shown in Section 7.1, engineering practical applications of Touzé system should not be overlooked, for instance; the stability analysis and vibration isolation in manufacturing equipment is one important application of this system, the need of finding a sustainable design of these equipments could impose improving the design of the equipments by adopting nonlinear modelling methods such as the proposed DNF symbolic technique. In addition, the increased use of polymeric materials in engineering applications requires finding a suitable approach for the design and analysis, for which the fractional damping technique proposed in Chapter 6 can be adopted.

8.2 Future work

In this Section, based on the overall findings and conclusions, discussions regarding some relevant future works of the proposed research are held.

In Section 4.2, the proposed novel generalisation of the DNF method to any desired ε accuracy has been discussed with some selected examples, nevertheless, more in-depth future work need to be performed to explore the effects of higher order accuracies, specifically for systems with even polynomial nonlinear terms and systems with combinations of polynomial stiffness nonlinear and damping terms.

Additionally, according to the discussions in Section 4.4, as a potential future work, the proposed direct technique of obtaining the damped backbone curves needs to be further improved to include more complicated SDOF and MDOF systems. For SDOF systems, the technique still needs more specific research to be applied for systems with combinations of polynomial stiffness and damping nonlinearities, and it could be beneficial to investigate the technique for higher orders accuracies. For MDOF systems, more in-depth research can be performed, considering the fact, when generating the frequency-amplitude relationship for weakly nonlinear MDOF systems with light damping, the undamped natural frequencies can be directly replaced with the damped natural frequencies and then the backbone curves can be compared to the forced frequency response curves.

For the analysis performed in Section 5.4, some findings can be adopted for future research; for instance, the effects of sub-harmonics to the frequency responses of the systems under study can be clearly noticed in

the numerical continuation results, see for example Fig. 5.8, Fig. 5.10, Fig. 5.11, Fig. 5.13, etc, these effects are not captured by the DNF method, which imply the need of improving the method to achieve results that have better matching to those captured numerically. One possible improvement to the DNF method is to modify the assumed solutions by adding more terms that reflect the effects of these sub and super harmonics. Furthermore, in Rayleigh oscillators, and due to the considerable differences between the analytical and numerical frequency responses, Fig. 5.16-Fig. 5.18, more specific research can be held to investigate the effects of including higher orders of the damping terms, i.e. $\dot{x}^3$, for these oscillators, the application of DNF technique needs to be improved.

For the DNF applications of MDOF systems, Chapter 7, many future works can be performed; the application of DNF for systems with 3-DOF or even more need to explored, specifically when high orders of polynomial stiffness nonlinear coupling terms are located in the EOMs, this can be studied for variuos conditions including resonant or non-resonant terms, where the DNF method has the potential to be applied for all of these conditions, and with the aid of symbolic computations approach, the computations could be performed with less time and efforts. Additionally, as discussed in damped backbone topic, this technique can be applied to MDOF systems to refine the DNF results so that less differences compared to the numerical results are achieved.

Finally, in regards of the discussions in Chapter 6, the application of DNF technique for investigating fractionally damped systems needs to be significantly improved, this improvement can include studying more complicated systems such as SDOF systems with higher orders of geometric stiffness terms, systems with combinations of stiffness and fractional damping terms (such as the fractional Van-der-Pol Duffing oscillator), and MDOF systems with fractional damping terms.

Bibliography

[1] C. Zhang, J. Yang and Z. Chang, *Machinery Dynamics*. Academic Press, 2022.

[2] Matthew Cartmell, *Introduction to linear, parametric and nonlinear vibrations*. Chapman and Hall London, 1990.

[3] Jack K. Hale, *Oscillations in nonlinear systems*. McGraw-Hill, 1963.

[4] Gérard Iooss and Daniel D Joseph, *Elementary stability and bifurcation theory*. New York, 1990.

[5] Jerrold Marsden and Marjorie McCracken, *The Hopf bifurcation and its applications*. Volume 19. Springer-Verlag, 1976.

[6] Minoru Urabe, *Nonlinear autonomous oscillations: Analytical theory*. Volume 34, Academic Press, 1967.

[7] J.H.G. Macdonald, M.S. Dietz, S.A. Neild, A. Gonzalez-Buelga, A.J. Crewe and D.J. Wagg. Generalised modal stability of inclined cables subjected to support excitations. *Journal of Sound and Vibration*, vol. 329, p.p. 4515–4533, 2010.

[8] Wagg, D. J. and S. A. Neild, *Nonlinear vibration with control*. 2nd edition, Springer, 2015.

[9] Wanda Szemplińska-Stupnicka. The generalized harmonic balance method for determining the combination resonance in the parametric dynamic systems. *Journal of Sound and Vibration*, Volume 58 (3), pp.347-361, 1978.

[10] K. Worden, G.R. Tomlinson. *Nonlinearity in Structural Dynamics: Detection, Identification, and Modeling*. Institute of Physics Publishing, Bristol and Philadelphia, 2001.

[11] P. Mellodge. *Characteristics of Nonlinear Systems*, in *A Practical Approach to Dynamical Systems for Engineers*, Woodhead Publishing, 2016.

[12] U. Parlitz, A. Hornstein, D. Engster, Al-Bender Farid, Lampaert Vincent, Tjahjowidodo Tegoeh, Fassois Spilios, Rizos Demosthenis, C. Wong, K. Worden & Manson, Graeme. Identification of pre-sliding friction dynamics. *Chaos: An Interdisciplinary Journal of Nonlinear Science*, 14(2), 420–430, 2004. https://doi.org/10.1063/1.1737818.

[13] M. Heller, T. Baier and F. Schuck. Lateral fly-by-wire control system dedicated to future small aircraft. In: Chu, Q., Mulder, B., Choukroun, D., van Kampen, EJ., de Visser, C., Looye, G. (eds) *Advances in Aerospace Guidance, Navigation and Control*. Springer, Berlin, Heidelberg, 2013. https://doi.org/10.1007/978-3-642-38253-6_22.

[14] Manson, Graeme & Worden, Keith. Frequency Response Functions for Uncertain Nonlinear Systems. *Materials Science Forum*. 440-441. 37-44. 10.4028, 2003. www.scientific.net/MSF.440-441.37.

[15] K. Worden, & G. Manson. Random vibrations of a duffing oscillator using the Volterra series. *Journal of sound and vibration*. 1998, Vol 217, Num 4, pp 781-789

[16] K. Worden, & G. Manson. A Volterra series approximation to the coherence of the Duffing oscillator. *Journal of Sound and Vibration*. 286. 529-547. 10.1016/j.jsv.2004.10.028, 2005.

[17] Eugene L. Allgower and Kurt Georg, *Introduction to Numerical Continuation Methods*, SIAM Classics in Applied Mathematics 45, 2003.

[18] A. H. Nayfeh, D. T. Mook, *Nonlinear oscillations*. John Wiley: New York, 1995.

[19] Everett Minnich Baily. “Steady-state harmonic analysis of nonlinear networks”. PhD thesis, Department of Electrical Engineering, Stanford University, 1968.

[20] John C Lindenlaub, An approach for finding the sinusoidal steady-state response of nonlinear systems. In Proc. 7th, *Ann. Allerton Conf. Circuit and System Theory*. University of Illinois, 1969.

[21] Jan A Sanders, Ferdinand Verhulst, and James A Murdock. *Averaging methods in nonlinear dynamical systems*. Volume 59. Springer, 2007.

[22] Ferdinand Verhulst. *Nonlinear differential equations and dynamical systems*. 2nd Edition, Springer Science & Business Media, 2006.

[23] Vladimir I. Arnold. *Geometrical methods in the theory of ordinary differential equations*. Vol. 250, Springer Science & Business Media, 2012.

[24] Kenneth Meyer, Glen Hall, and Dan Offin, *Introduction to Hamiltonian dynamical systems and the n-body problem: A Mechanised Logic of Computation*. Volume 90. Springer Science & Business Media, 2008.

[25] Richard H. Enns & George C. McGuire. *Nonlinear physics with Mathematica for scientists and engineers*. Birkhauser Boston, 2001.

[26] Wang S. and Huseyin K. (1992)., *'Maple' Analysis of nonlinear oscillations*. Mathematical and Computer Modelling 16(11), 49-57, 1992.

[27] Z.F. Xin, S. A. Neild, D. J. Wagg, and Z. X. Zuo. Resonant response functions for nonlinear oscillators with polynomial type nonlinearities. *Journal of Sound and Vibration* 332 (7), 1777–1788, 2013.

[28] A.D. Shaw, S.A. Neild, and D.J. Wagg. Dynamic analysis of high static low dynamic stiffness vibration isolation mounts, *Journal of Sound and Vibration*. 332, 1437–1455, 2012.

[29] A. Cammarano, S. A. Neild, S. G. Burrow, D. J. Wagg, and DJ Inman. Optimum resistive loads for vibration-based electromagnetic energy harvesters with a stiffening nonlinearity. *Journal of Intelligent Material Systems and Structures*, 2014.

[30] A. Cammarano, T.L. Hill, S.A. Neild, and D.J. Wagg. Bifurcations of backbone curves for systems of coupled nonlinear two mass oscillator, *Nonlinear Dynamics*, 77(1-2), 311–320, 2014.

[31] T. L. Hill, A. Cammarano, S. A. Neild, and D. J. Wagg. Out-of-unison resonance in weakly nonlinear coupled oscillators. In Proceedings of the *Royal Society of London A: Mathematical, Physical and Engineering Sciences*, volume 471, page 20140659. The Royal Society, 2015.

[32] T.L. Hill, A. Cammarano, A. Neild, and D.J. Wagg. An analytical method for the optimisation of weakly nonlinear systems. Proceedings of *EURODYN 2014*, pages 1981–1988, 2014.

[33] A. H. Nayfeh, D. T. Mook, *Perturbation Methods*. Wiley, New York, 1973.

[34] F. Schilder, H. Dankowicz. *Recipes for Continuation*. SIAM Computational Science and Engineering, 2013.

[35] F. Schilder, H. Dankowicz. *Continuation core and toolboxes (coco) [onine]*. Available at: https://sourceforge.net/projects/cocotools/, 2017.

[36] J. Thomsen. *Vibrations and Stability: Order and Chaos*. McGraw Hill, 1997.

[37] D. Richards. *Advanced mathematical methods with Maple*. Cambridge University Press, 2009.

[38] R. Enns, G. McGuire. *Nonlinear physics with Maple for scientists and engineers*. Springer, 2000.

[39] S. Bellizzi and R. Bouc. A new formulation for the existence and calculation for nonlinear normal modes. *Journal of Sound and Vibration* 287(3), 545-569, 2005.

[40] X. Lui. *Symbolic Tools for the Analysis of nonlinear dynamical systems*. PhD thesis, Department of Applied Mathematics, University of Western Ontario, London, 1999.

[41] Gaëtan Kerschen, Maxime Peeters, Jean-Claude Golinval, and Alexander F Vakakis. Nonlinear normal modes, part i: A useful framework for the structural dynamicist. *Mechanical Systems and Signal Processing*, 23(1):170–194, 2009.

[42] Gaëtan Kerschen, Maxime Peeters, Jean Claude Golinval, and Cyrille Stéphan. Nonlinear modal analysis of a full-scale aircraft. *Journal of Aircraft*, 2013.

[43] Hamed Haddad Khodaparast, Hadi Madinei, Michael I Friswell, Sondipon Adhikari, Simon Coggon, and Jonathan E Cooper. An extended harmonic balance method based on incremental nonlinear control parameters. *Mechanical Systems and Signal Processing*, 85:716–729, 2017.

[44] Ali H Nayfeh and Balakumar Balachandran. *Applied nonlinear dynamics: analytical, computational and experimental methods*. John Wiley & Sons, 2008.

[45] C. Touzé, O. Thomas, & A. Chaigne. Hardening/softening behaviour in non-linear oscillations of structural systems using non-linear normal modes. *Journal of Sound and Vibration* 273, 77–101, 2004.

[46] C. Touzé, & M. Amabili. Nonlinear normal modes for damped geometrically nonlinear systems: Application to reduced-order modelling of harmonically forced structures. *Journal of Sound and Vibration* 298, 958–981, 2006.

[47] X. Liu & D. J. Wagg. ε^2-order normal form analysis for a two-degree-of-freedom nonlinear coupled oscillator. *Nonlinear Dynamics of Structures, Systems and Devices*. Springer, 25–33, 2020.

[48] Roy Craig and Mervyn Bampton. Coupling of substructures for dynamic analyses. *AIAA journal*, 6(7):1313–1319, 1968.

[49] Scott W Doebling, Charles R Farrar, Michael B Prime, and Daniel W Shevitz. Damage identification and health monitoring of structural and mechanical systems from changes in their vibration characteristics: a literature review, 1996.

[50] Jimin He and Zhi-Fang Fu, "Modal analysis of a damped MDoF system", in *Modal Analysis*, Butterworth-Heinemann, Oxford, 2001. https://doi.org/10.1016/B978-075065079-3/50006-1.

[51] The Math Works, Inc. *MATLAB. Version 2020a*, the Math Works, Inc. Computer Software, 2020.

[52] Lawrence N. Virgin, Christopher George, Ashwath Kini, Experiments on a non-smoothly-forced oscillator, *Physica D: Nonlinear Phenomena*, Volume 313, Pages 1-10, 2015.

[53] Simon A Neild and David J Wagg. Applying the method of normal forms to second order nonlinear vibration problems. Proceedings of the *Royal Society A: Mathematical, Physical and Engineering Science*, 467(2128):1141–1163, 2011.

[54] Eusebius J Doedel. *Auto: A program for the automatic bifurcation analysis of autonomous systems*. Congr. Numer, 30:265–284, 1981.

[55] Eusebius J Doedel, Alan R Champneys, Thomas F Fairgrieve, Yuri A Kuznetsov, B E Oldeman, R C Paffenroth, B Sandstede, X J Wang, and C Zhang. *Auto-07p: Continuation and bifurcation software for ordinary differential equations*. Available at http://cmvl.cs.concordia.ca/auto, 2017.

[56] Annick Dhooge, Willy Govaerts, and Yu A Kuznetsov. *MatCont: a MATLAB package for numerical bifurcation analysis of odes*. ACM Transactions on Mathematical Software (TOMS), 29(2): 141–164, 2003.

[57] Annick Dhooge, Willy Govaerts, Yu A Kuznetsov, Hil Gaétan Ellart Meijer, and Bart Sautois. New features of the software MatCont for bifurcation analysis of dynamical systems. *Mathematical and Computer Modelling of Dynamical Systems*, 14(2): 147–175, 2008.

[58] Annick Dhooge,Willy Govaerts, Yu A Kuznetsov, Hil Gaétan Ellart Meijer, and Bart Sautois. *MatCont: numerical bifurcation analysis toolbox in MATLAB*. Available at https://sourceforge.net/projects/matcont/, 2017.

[59] Maxime Peeters, Régis Viguié, Guillaume Sérandour, Gaëtan Kerschen, and J-C Golinval. Nonlinear normal modes, part ii: Toward a practical computation using numerical continuation techniques. *Mechanical systems and signal processing*, 23(1):195–216, 2009.

[60] M Peeters, L Renson, and G Kerschen. *Nnmcont: A MATLAB package for the continuation of nonlinear normal modes*. Available at http://www.ltasvis.ulg.ac.be/cmsms/index.php?page=nnm, 2016.

[61] Ludovic Renson, Jean-Philippe Noël, and Gaëtan Kerschen. Complex dynamics of a nonlinear aerospace structure: numerical continuation and normal modes. *Nonlinear Dynamics*, 79(2):1293–1309, 2015.

[62] Z. Ahsan, H. Dankowicz, M. Li et al. Methods of continuation and their implementation in the COCO software platform with application to delay differential equations. *Nonlinear Dynamics* Volume 107, Pages 3181–3243, 2022.

[63] L Renson, A Gonzalez-Buelga, DAWBarton, and SA Neild. Robust identification of backbone curves using control-based continuation. *Journal of Sound and Vibration*, 367:145–158, 2016.

[64] Sanjiv Sharma, Etienne B Coetzee, Mark H Lowenberg, Simon A Neild, and Bernd Krauskopf. Numerical continuation and bifurcation analysis in aircraft design: an industrial perspective. *Phil. Trans. R. Soc. A*, 373(2051):20140406, 2015.

[65] LI Manevich and Iu V Mikhlin. On periodic solutions close to rectilinear normal vibration modes. *Journal of Applied Mathematics and Mechanics*, 36(6): 988–994, 1972.

[66] Richard H Rand. A higher order approximation for non-linear normal modes in two degree of freedom systems. *International Journal of Non-Linear Mechanics*, 6(4): 545–547, 1971.

[67] Alexander F Vakakis. *Analysis and identification of linear and nonlinear normal modes in vibrating systems*. PhD thesis, California Institute of Technology, 1991.

[68] Steven W Shaw and Christophe Pierre. Normal modes for non-linear vibratory systems. *Journal of sound and vibration*, 164(1):85–124, 1993.

[69] P. B. Kahn and Y. Zarmi. *Nonlinear dynamics: Exploration through normal forms*. Dover Publications, New York, USA, 2014.

[70] T. Breunung, & G.Haller. Explicit backbone curves from spectral submanifolds of forced-damped nonlinear mechanical systems. *Proc. R. Soc. A* 474, 20180083, 2018.

[71] J. Tlusty, Manufacturing processes and equipment. Upper Saddle River, NJ: Prentice Hall. ISBN 02-014-9865-0, 2000.

[72] Liu Xuanang. *Backbone Curve Analysis of Nonlinear Mechanical Systems*. PhD Thesis. University of Sheffield, 2018.

[73] F. Benedettini, G. Rega, and R. Alaggio. Non-linear oscillations of a nonlinear model of a suspended cable. *Journal of Sound and Vibration*, 182, 775–798, 1995.

[74] F. Casciati and F. Ubertini. Nonlinear vibration of shallow cables with semi-active tuned mass damper. *Nonlinear Dynamics*, 53(1-2), 89–106, 2008.

[75] M. El-Attar, A. Ghobarah, and , T.S. Aziz. Non-linear cable response to multiple support periodic excitation. *Engineering Structures*, 22, 1301–1312, 2000.

[76] V. Gatulli, M. Lepidi, J. Macdonald, and C.Taylor. One to two global local interaction in a cable-stayed beam observed through analytical, finite element and experimental models. *International Journal of Nonlinear Mechanics*, 40, 571– 588, 2005.

[77] A. Gonzalez-Buelga, S. Neild, D. Wagg, and J. Macdonald. Modal stability of inclined cables subjected to vertical support excitation. *Journal of Sound and Vibration*, 318, 565–579, 2008.

[78] H.M. Irvine and T.K. Caughey. The linear theory of free vibrations of a suspended cable. Proc. of *Roy. Soc. A*, 341(1626), 299–315, 1974.

[79] Y. Warnitchai, T. Fujino, and A. Susumpov. A nonlinear dynamic model for cables and its application to a cable structure-system. *Journal of Sound and Vibration*, 187(3), 695–712, 1995.

[80] S. S. Rao, *Mechanical Vibrations*, 6th Edition, Pearson, 2018.

[81] A. H. Nayfeh, P. F. Pai, *Linear and Nonlinear Structural Mechanics*, Wiley, New York, 2004.

[82] Thomas L Hill. *Modal interactions in nonlinear systems*. PhD thesis, University of Bristol, 2016.

[83] S.K. Lai, C.W. Lim, B.S. Wu, C. Wang, Q.C. Zeng, and X.F. He. Newton-harmonic balancing approach for accurate solutions to nonlinear cubic-quintic Duffing oscillator. *Applied Mathematical Modelling*, 33(2), 852-866, 2009.

[84] Reinhardt Mathias Rosenberg. Normal modes of nonlinear dual-mode systems. *Journal of Applied Mechanics*, 27(2):263–268, 1960.

[85] L. Jezequel and C.H. Lamarque. Analysis of nonlinear dynamic systems by the normal form theory, *Journal of Sound and Vibration*, 149(3), 429–459, 1991.

[86] A.H. Nayfeh. *The Method of normal forms*. Wiley, New York, 1993.

[87] I. Kovacic, M.J. Brennan. *The Duffing Equation: Nonlinear Oscillators and their behaviour*. John Wiley & Sons, 2011.

[88] A.M. Nasir, N.D. Sims and D.J. Wagg. Computing backbone curves for nonlinear oscillators with higher order polynomial stiffness terms. In: Papadrakakis, M., Fragiadakis, M. and Papadimitriou, C., (eds.) EURODYN 2020: Proceedings of the XI International Conference on Structural Dynamics. *EURODYN 2020: XI International Conference on Structural Dynamics*, 23-26 Nov 2020, Athens, Greece. European Association for Structural Dynamics (EASD), pp. 318-334. ISBN 9786188507203, 2020.

[89] M. Krack, *Nonlinear modal analysis of non-conservative systems: extension of the periodic motion concept*. Computers & Structures 154, 59-71, 2015.

[90] T. Burton. On the amplitude decay of strongly non-linear damped oscillators, *Journal of Sound and Vibration*, 87 (4), 535-541, 1983.

[91] F. J. Bourland, R. Haberman. The modulated phase shift for strongly nonlinear, slowly varying, and weakly damped oscillators. *SIAM Journal on Applied Mathematics*, 48 (4), 737-748, 1988.

[92] A. C. King, J. Billingham, S. R. Otto. *Differential equations*, Cambridge, 2003.

[93] G. Wentzel. Eine verallgemeinerung der quantenbedingungen für die zwecke der wellenmechanik, *Zeitschrift für Physik*, 38 (6-7), 518-529, 1926.

[94] L. Brillouin. La mécanique ondulatoire de schrödinger; une méthode générale de résolution par approximations successives, *Compt. Rend. Hebd. Seances Acad*. Sci. 183, 24-26, 1926.

[95] H. A. Kramers. Wellenmechanik und halbzahlige quantisierung, *Zeitschrift für Physik*, 39 (10-11) 828-840, 1926.

[96] G. Stephenson, P. M. Radmore. *Advanced mathematical methods for engineering and science students*. Cambridge, 1990.

[97] L. Brillouin. A practical method for solving Hill's equation, *Quarterly of Applied Mathematics*, 6 (2), 167-178, 1948.

[98] P. D. Kourdis, A. F. Vakakis. Some results on the dynamics of the linear parametric oscillator with general time-varying frequency, *Applied mathematics and computation*, 183 (2), 2006. 1235–1248.

[99] A. Elliott, A. Cammarano, S. Neild, T. Hill, D. Wagg. Using frequency detuning to compare analytical approximations for forced responses, *Nonlinear Dynamics*, 98 (4), 2795-2809, 2019.

[100] D. T. Kawano, R. G. Salsa Jr, F. Ma, M. Morzfeld, A canonical form of the equation of motion of linear dynamical systems, Proceedings of the *Royal Society A: Mathematical, Physical and Engineering Sciences*, 474 (2211), 20170809, 2018.

[101] A. Nasir, N. Sims, and D. Wagg. Direct normal form analysis of oscillators with different combinations of geometric nonlinear stiffness terms. *Journal of Applied and Computational Mechanics*, 7:1167–1182, 2021.

[102] M. Sulemen & Q. Wu. Comparative solution of nonlinear quintic cubic oscillator using modified homotopy method. *Advances in Mathematical Physics*, 2015.

[103] Razzak, M., An analytical approximate technique for solving cubic-quintic Duffing oscillator. *Alexandria Engineering Journal*. (55) 2959-2965, 2016.

[104] S. A. Neild and D. J. Wagg. Applying the method of normal forms to second-order nonlinear vibration problems. *Proceedings of the Royal Society of London A*, 467, (2128), 1141-1163, 2011.

[105] A. Nasir, N. Sims, D.J. Wagg. Exploring the Dynamics of Viscously Damped Nonlinear Oscillators via Damped Backbone Curves: A Normal Form Approach. In: Lacarbonara, W., Balachandran, B., Leamy, M.J., Ma, J., Tenreiro Machado, J.A., Stepan, G. (eds) *Advances in Nonlinear Dynamics*. NODYCON Conference Proceedings Series. Springer, Cham. https://doi.org/10.1007/978-3-030-81162-4_14, 2022.

[106] A. F. Ghaleb, M. S. Abou-Dina, G. M. Moatimid and M. H. Zekry. Analytic approximate solutions of the cubic–quintic Duffing–van der Pol equation with two-external periodic forcing terms: Stability analysis. *Mathematics and Computers in Simulation*, 180, 129–151, 2021.

[107] Z. Zhihong, Y. Shaopu. Application of van der Pol–Duffing oscillator in weak signal detection. *Computers and Electrical Engineering*, 41, 1–8, 2015.

[108] H. Chen and L. Zou. Global study of Rayleigh–Duffing oscillators. *J. Phys A*, 49, 165202, 2016.

[109] J. L. P. Felix, J. M. Balthazar and R.M. Brasil. Comments on nonlinear dynamics of a non-ideal Duffing–Rayleigh oscillator: numerical and analytical approaches. *J. Sound Vib.*, 319, 1136–1149, 2009.

[110] W. Herfort and H. Troger. Robust modelling of flow induced oscillations of bluff bodies. *Math. Model. Sci. Technol*, 8, 251–255, 1987.

[111] Y. Kanai, H. Yabuno. Creation-annihilation process of limit cycles in the Rayleigh–Duffing oscillator. *Nonlinear Dyn.*, 70, 1007–1016, 2012.

[112] M. Bikdash, B. Balachandran and A.H. Nayfeh. Melnikov analysis for a ship with a general Roll-damping model. *Nonlinear Dyn.*, 6, 101–124, 1994.

[113] A.H. Nayfeh and B. Balachandran. *Applied Nonlinear Dynamics*. Wiley, Weinheim, 2004.

[114] H. Chen, D. Huang and Y. Jian. The saddle case of Rayleigh-Duffing oscillators. *Nonlinear Dyn.*, 93, 2283–2300, 2018.

[115] C. H. He, D. Tian, G. Moatimid, H. Salman and M. Zekry. Hybrid rayleigh–van der pol–duffing oscillator: Stability analysis and controller. *Journal of Low Frequency Noise, Vibration and Active Control*, Vol. 41(1) 244–268, 2022.

[116] W. Govaerts, Yu. A. Kuznetsov, V. De Witte, A. Dhooge, H.G.E. Meijer, W. Mestrom, A.M. Riet and B. Sautois. *MATCONT and CL MATCONT: Continuation toolboxes in MATLAB*, Utrecht University, The Netherlands, 2011.

[117] A. Dhooge, W. Govaerts and Yu. A. Kuznetsov, MATCONT : A MATLAB package for numerical bifurcation analysis of ODEs. *ACM Transactions on Mathematical Software*, 29(2), pp. 141-164, 2003.

[118] Volvert, Martin, and Gaetan Kerschen. "Resonance phase lags of a Duffing oscillator." arXiv preprint arXiv:2202.07556, 2022.

[119] David. J. Wagg. Normal form transformations for structural dynamics: An introduction for linear and nonlinear systems. *Journal of Structural Dynamics*, Issue 1, (pp. 138-216), 2022. URL: https://popups.uliege.be/2684-6500/index.php?id=84

[120] D. Hong, T. L. Hill, and S. A. Neild. Conditions for the existence of isolated backbone curves. Proceedings of the *Royal Society A*, 475(2232):20190374, 2019.

[121] Veskos, Paschalis & Demiris, Yiannis. Experimental Comparison of the van der Pol and Rayleigh Nonlinear Oscillators for a Robotic Swinging Task. In: Proceedings of the *AISB 2006 Conference, Adaptation in Artificial and Biological Systems*, pp. 197-202, Bristol, 2006.

[122] S. Chakraverty, Diptiranjan Behera, *Dynamic responses of fractionally damped mechanical system using homotopy perturbation method*. Alexandria Engineering Journal, Volume 52, Issue 3, 2013, Pages 557-562, ISSN 1110-0168.

[123] K.S. Miller, B. Ross. *An Introduction to the Fractional Calculus and Fractional Differential Equations*. Wiley, New York, 1993.

[124] I. Podlubny. *Fractional Differential Equations*. Academic Press, San Diego, 1999.

[125] K. Adolfsson, M. Enelund and P. Olsson. On the fractional order model of viscoelasticity. Mech. Time Depend. *Mechanics of Time-Dependent Materials*, Volume 9, Pages 15-34, 2005.

[126] O. Zarraga, I. Sarría, J. García-Barruetabeña and F. Cortés. An Analysis of the Dynamical Behaviour of Systems with Fractional Damping for Mechanical Engineering Applications. *Symmetry*, Volume 11, Pages 1499-1514, 2019.

[127] P. J. Torvik and R. L. Bagley. On the Appearance of the Fractional Derivative in the Behaviour of Real Materials. *Journal of Applied Mechanics*, Volume 51, Pages 294–298, 1984.

[128] R.L. Bagley and P. J. Torvik. A theoretical basis for the application of fractional calculus to viscoelasticity. *Journal of Rheology*, Volume 27, Pages 201–210, 1983.

[129] M. Di Paola, A. Pirrotta and A. Valenza. Viscoelastic behaviour through fractional calculus: An easier method for best fitting experimental results. *Mechanics of Materials*, Volume 43, Pages 799–806, 2011.

[130] P. G. Nutting. A new general law of deformation. *Journal of the Franklin Institute* Volume 191, Pages 679–685, 1921.

[131] A. Gemant. A method of analyzing experimental results obtained from elasto-viscous bodies. *Physics*, Volume 7, Pages 311–317, 1936.

[132] F. P. Pinnola, G. Zavarise, A. D. Prete, R. Franchi. On the appearance of fractional operators in non-linear stress–strain relation of metals. *International Journal of Non-Linear Mechanics*, Volume 105, Pages 1–8, 2018,

[133] N. Makris. Three-dimensional constitutive viscoelastic laws with fractional order time derivatives. *Journal of Rheology*, Volume 41, Pages 1007–1020, 1997.

[134] G. Alotta, O. Barrera, A. C. Cocks and M. Di Paola. On the behaviour of a three-dimensional fractional viscoelasticn constitutive model. *Meccanica*, Volume 52, Pages 2127–2142, 2017.

[135] G. Alotta, O. Barrera, A. C. Cocks and M. Di Paola. The finite element implementation of 3D fractional viscoelastic constitutive models. *Finite Elements in Analysis and Design*, Volume 146, Pages 28–41, 2018.

[136] N. Heymans and I. Podlubny. Physical interpretation of initial conditions for fractional differential equations with Riemann-Liouville fractional derivatives. *Rheologica Acta*, Volume 45, Pages 765–771, 2006.

[137] M. Di Paola, F. P. Pinnola and M. Zingales. A discrete mechanical model of fractional hereditary materials. *Meccanica*, Volume 48, Pages 1573–1586, 2013.

[138] H. Schiessel, R. Metzler, A. Blumen and T.F. Nonnenmacher. Generalized viscoelastic models: their fractional equations with solutions. *Journal of Physics A: Mathematical and General*, Volume 28, Page 6567-6584, 1995.

[139] I. Petras. *Fractional-Order Nonlinear Systems*. Higher Education Press, Beijing, 2011.

[140] Concepcion A. Monje, C. YangQuan, M.V. Blas, X. Dingyu, and F. Vicente. *Fractional-order Systems and Controls Fundamentals and Applications*. Advances in Industrial Control, Springer, 2010.

[141] Changpin Li, Weihua Deng. Remarks on fractional derivatives, *Applied Mathematics and Computation*, Volume 187, Issue 2, Pages 777-784, 2007.

[142] HongGuang Sun, Yong Zhang, Dumitru Baleanu, Wen Chen, YangQuan Chen. A new collection of real world applications of fractional calculus in science and engineering, *Communications in Nonlinear Science and Numerical Simulation*, Volume 64, Pages 213-231, 2018.

[143] Edmundo Oliveira, and Jose Antonio Machado. Review Article: A Review of Definitions for Fractional Derivatives and Integral. *Hindawi Publishing Corporation, Mathematical Problems in Engineering*, Volume, 2014.

[144] M. Davison and C. Essex. Fractional differential equations and initial value problems, *The Mathematical Scientist*, vol. 23, no. 2, pp. 108–116, 1998.

[145] G.S. Teodoro, J.T. Machado and E.C. De Oliveira. A review of definitions of fractional derivatives and other operators. *Journal of Computational Physics*, Vol. 388, Pages 195–208, 2019.

[146] Roberto Garrappa. On linear stability of predictor–corrector algorithms for fractional differential equations. *International Journal of Computer Mathematics*, 87:10,2281-2290, 2010.

[147] Roberto Garrappa. Trapezoidal methods for fractional differential equations: Theoretical and computational aspects. *Mathematics and Computers in Simulation*, Volume 110, Pages 96-112, 2015.

[148] R. Garrappa, E. Kaslik and M. Popolizio. Evaluation of Fractional Integrals and Derivatives of Elementary Functions: Overview and Tutorial. *Mathematics*, 7, 407, 2019. https://doi.org/10.3390/math7050407.

[149] O. Brandibur, R. Garrappa and E. Kaslik. Stability of Systems of Fractional-Order Differential Equations with Caputo Derivatives. *Mathematics*, 9, 914, 2021. https://doi.org/10.3390/math9080914.

[150] R. Garrappa. *Predictor-corrector PECE method for fractional differential equations*. MATLAB Central File Exchange, 2011.

[151] Roberto Garrappa. "Short tutorial: Solving fractional differential equations by MATLAB codes". 2014.

[152] K. Diethelm, N.J. Ford and A.D. Freed. A predictor–corrector approach for the numerical solution of fractional differential equations. *Nonlinear Dyn.*, 29, 3–22, 2002.

[153] K. Diethelm, N.J. Ford, A.D. Freed and Y. Luchko. Algorithms for the fractional calculus: a selection of numerical methods. *Comput. Methods Appl. Mech. Eng.*, 194, 743–773, 2005.

[154] K.B. Oldham, J. Spanier. *The Fractional Calculus*. New York: Academic Press, 1974.

[155] P. Ostalczyk. The non-integer difference of the discrete-time function and its application to the control system synthesis. International Journal of Systems Science, 31(12):1551–1561, 2000.

[156] A. Dzieliński, D. Sierociuk. Stability of discrete fractional order state-space systems. *Journal of Vibration and Control*, 14(9-10):1543–1556, 2008.

[157] D. Sierociuk. *Fractional Order Discrete State-Space System Simulink Toolkit User Guide. [online]*. www.https://www.ee.pw.edu.pl/~dsieroci/fsst/fsst.htm.

[158] A. Dzieliński, D. Sierociuk. Simulation and experimental tools for fractional order control education. Proceedings of *17th World Congress The International Federation of Automatic Control*, Seoul, Korea, July 6-11. IFAC WC, 11654–11659, 2008.

[159] Yong Xu, Yongge Li, Di Liu, Wantao Jia and Hui Huang. Responses of Duffing oscillator with fractional damping and random phase. *Nonlinear Dyn.*, 2013. 74:745-753DOI 10.1007/s11071-013-1002-9.

[160] Sujuan Li, Jiangchuan Niu, and Xianghong Li: Primary resonance of fractional-order Duffing–van der Pol oscillator by harmonic balance method, *Chin. Phys. B*, Vol. 27, No. 12, 120502, 2018.

[161] Shen, Yongjun, Shaopu Yang, Haijun Xing, and Guosheng Gao. Primary resonance of Duffing oscillator with fractional-order derivative. *Communications in Nonlinear Science and Numerical Simulation*, 17, no.7, 3092-3100, 2012.

[162] Burd Vladimir. *Method of averaging for differential equations on an infinite interval: theory and applications*. Taylor & Francis Group, 2007.

[163] F. Afzali, E. Kharazmi, B.F. Feeny. Resonances of a Forced van der Pol Equation with Parametric Damping. In: Lacarbonara, W., Balachandran, B., Leamy, M.J., Ma, J., Tenreiro Machado, J.A., Stepan, G. (eds) *Advances in Nonlinear Dynamics*. NODYCON Conference Proceedings Series. Springer, Cham, 2022.

[164] Z. Zhihong, Y. Shaopu: Application of van der Pol–Duffing oscillator in weak signal detection. *Computers and Electrical Engineering*, 41, 1–8, 2015.

[165] R. S. Barbosa, J. A. T. Machado, I. M. Ferreira and J. K. Tar. Dynamics of the fractional-order Van-der-Pol oscillator. *Second IEEE International Conference on Computational Cybernetics*, 2004. ICCC 2004., pp. 373-378, doi: 10.1109/ICCCYB.2004.1437752.

[166] Barbosa RS, Machado JAT, Vinagre BM, Calderón AJ. Analysis of the Van-der-Pol Oscillator Containing Derivatives of Fractional Order. *Journal of Vibration and Control*, 13(9-10):1291-1301, 2007. doi:10.1177/1077546307077463.

[167] V. Mishra, S. Das, H. Jafari, S.H. Ong, Study of fractional order Van-der-Pol equation, *Journal of King Saud University - Science*, Volume 28, Issue 1, Pages 55-60, 2016. ISSN 1018-3647. https://doi.org/10.1016/j.jksus.2015.04.005.

[168] Y.J. Shen, P. Wei & S.P. Yang. Primary resonance of fractional-order van der Pol oscillator. *Nonlinear Dyn*, 77, 1629–1642, 2014. https://doi.org/10.1007/s11071-014-1405-2.

[169] A.Y.T. Leung, H.X. Yang, Z.J. Guo. The residue harmonic balance for fractional order van der Pol like oscillators. *Journal of Sound and Vibration*, Volume 331, Issue 5, Pages 1115-1126, 2012. ISSN 0022-460X, https://doi.org/10.1016/j.jsv.2011.10.023.

[170] C.H He and Y.O El-Dib. A heuristic review on the homotopy perturbation method for non-conservative oscillators. *Journal of Low Frequency Noise, Vibration and Active Control*. 41(2):572-603, 2022. doi:10.1177/14613484211059264.

-

Appendices

A Matrix manipulation for the cubic-quintic nonlinear oscillator

Table A.1: ε^2 DNF matrix results for the cubic-quintic oscillators

$\mathbf{u}_l^*$	β_l^*	$\mathbf{n}_{\mathbf{u},l}^*$	$\mathbf{h}_l^*$	$\mathbf{u}_l^*$	β_l^*	$\mathbf{n}_{\mathbf{u},l}^*$	$\mathbf{h}_l^*$
u_m^3	$8\omega_r^2$	0	$\frac{\alpha_1\left(\omega_n^2-\omega_r^2\right)}{64\omega_r^4}$	$u_p^2u_m^7$	$24\omega_r^2$	0	$\frac{55\alpha_2^2}{96\omega_r^4}$
u_m^5	$24\omega_r^2$	0	$\frac{9\alpha_1^2+\alpha_2\left(\omega_n^2-\omega_r^2\right)}{576\omega_r^4}$	$u_p^3u_m^2$	0	$\frac{3\alpha_1^2}{8\omega_r^2}$	0
u_m^7	$48\omega_r^2$	0	$\frac{\alpha_1\alpha_2}{64\omega_r^4}$	$u_p^3u_m^4$	0	$\frac{5\alpha_1\alpha_2}{\omega_r^2}$	0
u_m^9	$80\omega_r^2$	0	$\frac{\alpha_2^2}{384\omega_r^4}$	$u_p^3u_m^6$	$8\omega_r^2$	0	$\frac{235\alpha_2^2}{96\omega_r^4}$
u_p^3	$8\omega_r^2$	0	$\frac{\alpha_1\left(\omega_n^2-\omega_r^2\right)}{64\omega_r^4}$	$u_p^4u_m$	$8\omega_r^2$	0	$\frac{6\alpha_1^2+5\alpha_2\left(\omega_n^2-\omega_r^2\right)}{64\omega_r^4}$
u_p^5	$24\omega_r^2$	0	$\frac{9\alpha_1^2+\alpha_2\left(\omega_n^2-\omega_r^2\right)}{576\omega_r^4}$	$u_p^4u_m^3$	0	$\frac{5\alpha_1\alpha_2}{\omega_r^2}$	0
u_p^7	$48\omega_r^2$	0	$\frac{\alpha_1\alpha_2}{64\omega_r^4}$	$u_p^4u_m^5$	0	$\frac{95\alpha_2^2}{6\omega_r^2}$	0
u_p^9	$80\omega_r^2$	0	$\frac{\alpha_2^2}{384\omega_r^4}$	$u_p^5u_m^2$	$8\omega_r^2$	0	$\frac{61\alpha_1\alpha_2}{64\omega_r^4}$
$u_pu_m^4$	$8\omega_r^2$	0	$\frac{6\alpha_1^2+5\alpha_2\left(\omega_n^2-\omega_r^2\right)}{64\omega_r^4}$	$u_p^5u_m^4$	0	$\frac{95\alpha_2^2}{6\omega_r^2}$	0
$u_pu_m^6$	$24\omega_r^2$	0	$\frac{37\alpha_1\alpha_2}{192\omega_r^4}$	$u_p^6u_m$	$24\omega_r^2$	0	$\frac{37\alpha_1\alpha_2}{192\omega_r^4}$
$u_pu_m^8$	$48\omega_r^2$	0	$\frac{95\alpha_2^2}{1152\omega_r^4}$	$u_p^6u_m^3$	$8\omega_r^2$	0	$\frac{235\alpha_2^2}{96\omega_r^4}$
$u_p^2u_m^3$	0	$\frac{3\alpha_1^2}{8\omega_r^2}$	0	$u_p^7u_m^2$	$24\omega_r^2$	0	$\frac{55\alpha_2^2}{96\omega_r^4}$
$u_p^2u_m^5$	$8\omega_r^2$	0	$\frac{61\alpha_1\alpha_2}{64\omega_r^4}$	$u_p^8u_m^1$	$48\omega_r^2$	0	$\frac{95\alpha_2^2}{1152\omega_r^4}$

B Some results obtained for different types of oscillators

Table B.1: Backbone curves of SDOF oscillators with polynomial nonlinear term truncated to ε^1 and ε^2 accuracies

Nonlinear vector	ε^1 Backbone curve	ε^2 Backbone curve
$\alpha x^2(t)$	ω_n^2	$\omega_n^2 - \frac{5}{6\omega_r^2}\alpha^2 U^2$
$\alpha x^3(t)$	$\omega_n^2 + \frac{3}{4}\alpha U^2$	$\omega_n^2 + \frac{3}{4}\alpha U^2 + \frac{3}{128\omega_r^2}\alpha^2 U^4$
$\alpha x^4(t)$	ω_n^2	$\omega_n^2 - \frac{63}{80\omega_r^2}\alpha^2 U^6$
$\alpha x^5(t)$	$\omega_n^2 + \frac{5}{8}\alpha U^4$	$\omega_n^2 + \frac{5}{8}\alpha U^4 + \frac{95}{1536\omega_r^2}\alpha^2 U^8$
$\alpha x^6(t)$	ω_n^2	$\omega_n^2 - \frac{1287}{1792\omega_r^2}\alpha^2 U^{10}$
$\alpha x^7(t)$	$\omega_n^2 + \frac{35}{64}\alpha U^6$	$\omega_n^2 + \frac{35}{64}\alpha U^6 + \frac{6405}{65536\omega_r^2}\alpha^2 U^{12}$
$\alpha x^8(t)$	ω_n^2	$\omega_n^2 - \frac{12155}{18432\omega_r^2}\alpha^2 U^{14}$
$\alpha x^9(t)$	$\omega_n^2 + \frac{36}{128}\alpha U^8$	$\omega_n^2 + \frac{63}{128}\alpha U^8 + \frac{84393}{655360\omega_r^2}\alpha^2 U^{16}$
$\alpha x^{10}(t)$	ω_n^2	$\omega_n^2 - \frac{440895}{720896\omega_r^2}\alpha^2 U^{18}$
$\alpha x^{11}(t)$	$\omega_n^2 + \frac{231}{512}\alpha U^{10}$	$\omega_n^2 + \frac{231}{512}\alpha U^{10} + \frac{1955107}{12582912\omega_r^2}\alpha^2 U^{20}$
$\alpha x^{12}(t)$	ω_n^2	$\omega_n^2 - \frac{3900225}{6815744\omega_r^2}\alpha^2 U^{22}$
$\alpha x^{13}(t)$	$\omega_n^2 + \frac{429}{1024}\alpha U^{12}$	$\omega_n^2 + \frac{429}{1024}\alpha U^{12} + \frac{20941713}{117440512\omega_r^2}\alpha^2 U^{24}$
$\alpha x^{14}(t)$	ω_n^2	$\omega_n^2 - \frac{4524261}{8388608\omega_r^2}\alpha^2 U^{26}$
$\alpha x^{15}(t)$	$\omega_n^2 + \frac{6435}{16384}\alpha U^{14}$	$\omega_n^2 + \frac{6435}{16384}\alpha U^{14} + \frac{1703280825}{8589934592\omega_r^2}\alpha^2 U^{28}$

Table B.2: Backbone curves of ε^2 accuracy for SDOF oscillators with combined polynomial nonlinear term truncated

Nonlinear vector	ε^2 Backbone curve
$\alpha_1 x^2(t)+\alpha_2 x^3(t)$	$\omega_n^2+\frac{3}{128\omega_r^2}\alpha_2^2U^4+\frac{3}{4}\alpha_2U^2-\frac{5}{6\omega_r^2}\alpha^2U^2$
$\alpha_1 x^2(t)+\alpha_2 x^4(t)$	$\omega_n^2-\frac{63}{80\omega_r^2}\alpha_2^2U^6-\frac{7}{4\omega_r^2}\alpha_1\alpha_2U^4-\frac{5}{6\omega_r^2}\alpha_1^2U^2$
$\alpha_1 x^2(t)+\alpha_2 x^5(t)$	$\omega_n^2+\frac{95}{1536\omega_r^2}\alpha_2^2U^8+\frac{5}{8}\alpha_2U^4-\frac{5}{6\omega_r^2}\alpha^2U^2$
$\alpha_1 x^2(t)+\alpha_2 x^6(t)$	$\omega_n^2-\frac{1287}{1792\omega_r^2}\alpha_2^2U^{10}-\frac{15}{8\omega_r^2}\alpha_1\alpha_2U^6-\frac{5}{6\omega_r^2}\alpha_1^2U^2$
$\alpha_1 x^2(t)+\alpha_2 x^7(t)$	$\omega_n^2+\frac{6405}{65536\omega_r^2}\alpha_2^2U^{12}+\frac{35}{64}\alpha_2U^6-\frac{5}{6\omega_r^2}\alpha^2U^2$
$\alpha_1 x^2(t)+\alpha_2 x^8(t)$	$\omega_n^2-\frac{12155}{18432\omega_r^2}\alpha_2^2U^{14}-\frac{385}{192\omega_r^2}\alpha_1\alpha_2U^8-\frac{5}{6\omega_r^2}\alpha_1^2U^2$
$\alpha_1 x^2(t)+\alpha_2 x^9(t)$	$\omega_n^2+\frac{84393}{655360\omega_r^2}\alpha_2^2U^{16}+\frac{63}{128}\alpha_2U^8-\frac{5}{6\omega_r^2}\alpha^2U^2$
$\alpha_1 x^3(t)+\alpha_2 x^4(t)$	$\omega_n^2-\frac{63}{80\omega_r^2}\alpha_2^2U^6+\frac{3}{128\omega_r^2}\alpha_1^2U^4+\frac{3}{4}\alpha_1U^2$
$\alpha_1 x^3(t)+\alpha_2 x^5(t)$	$\omega_n^2+\frac{3}{4}\alpha_1U^2+\frac{5}{8}\alpha_2U^4+\frac{3}{128\omega_r^2}\alpha_1^2U^4+\frac{5}{64\omega_r^2}\alpha_1\alpha_2U^6+\frac{95}{1536\omega_r^2}\alpha_2^2U^8$
$\alpha_1 x^2(t)+\alpha_2 x^3(t)+\alpha_3 x^5(t)$	$\omega_n^2+\frac{3}{4}\alpha_1U^2+\frac{5}{8}\alpha_2U^4+\frac{3}{128\omega_r^2}\alpha_1^2U^4+\frac{5}{64\omega_r^2}\alpha_1\alpha_2U^6+\frac{95}{1536\omega_r^2}\alpha_2^2U^8-\frac{5}{6\omega_r^2}\alpha_1^2U^2$
$\alpha_1 x^2(t)+\alpha_2 x^3(t)+$ $\alpha_3 x^4(t)+\alpha_4 x^5(t)+\alpha_5 x^6(t)$	$\omega_n^2+\frac{3}{4}\alpha_1U^2+\frac{5}{8}\alpha_2U^4+\frac{3}{128\omega_r^2}\alpha_1^2U^4+\frac{5}{64\omega_r^2}\alpha_1\alpha_2U^6+\frac{95}{1536\omega_r^2}\alpha_2^2U^8-\frac{5}{6\omega_r^2}\alpha_1^2U^2-\frac{1287}{1792\omega_r^2}\alpha_5^2U^{10}-\frac{99}{64\omega_r^2}\alpha_5\alpha_3U^8-\frac{15}{8\omega_r^2}\alpha_5\alpha_1U^6-\frac{63}{80\omega_r^2}\alpha_3^2U^6-\frac{7}{4\omega_r^2}\alpha_3\alpha_1U^4$

C Derivation of the vertical-horizontal-spring-mass oscillator EOMs

Using the geometric definitions shown in Fig. 7.1, the following equations of motion are resulted

$$\begin{aligned} m\ddot{x}_1 + k_1(a-L)\cos(\alpha) + k_2(b-L)\sin(\theta) = 0, \\ m\ddot{x}_2 + k_1(a-L)\sin(\alpha) + k_2(b-L)\cos(\theta) = 0. \end{aligned} \tag{C.1}$$

Now, elimination of a, b, α and θ is to be considered, so that the restoring forces are expressed in terms of x_1 and x_2. From Fig. 7.1(b) it is possible to find that

$$\begin{aligned} a = \frac{x_2}{\sin(\alpha)} = \frac{x_1+L}{\cos(\alpha)}, \quad b = \frac{x_1}{\sin(\theta)} = \frac{x_2+L}{\cos(\theta)}, \\ a = \sqrt{x_2^2 + (L+x_1)^2} \quad \text{and} \quad b = \sqrt{x_1^2 + (L+x_2)^2}. \end{aligned} \tag{C.2}$$

which can be used to eliminate the trigonometric functions from Eq. C.1 giving

$$\begin{aligned} m\ddot{x}_1 + k_1\frac{(a-L)}{a}(L+x_1) + k_2\frac{(b-L)}{b}x_1 = 0, \\ m\ddot{x}_2 + k_1\frac{(a-L)}{a}x_2 + k_2\frac{(b-L)}{b}(L+x_2) = 0. \end{aligned} \tag{C.3}$$

Now, it is possible to write

$$\frac{(a-L)}{a} \equiv 1 - \frac{L}{a} \quad \text{and} \quad a = L\sqrt{1 + \frac{(x_2^2 + 2Lx_1 + x_1^2)}{L^2}}. \tag{C.4}$$

Then using the binomial expansion

$$(1+z)^n = 1 + (n)(z) + \frac{n(n-1)}{2!}(z)^2 + ..., \tag{C.5}$$

it can be shown that

$$\frac{1}{a} \approx \frac{1}{L}\left(1 - \frac{(x_2^2 + 2Lx_1 + x_1^2)}{2L^2}\right) + ..., \tag{C.6}$$

such that

$$\frac{(a-L)}{a} \equiv 1 - \frac{L}{a} = 1 - \frac{L}{L}\left(1 - \frac{(x_2^2 + 2Lx_1 + x_1^2)}{2L^2}\right) = \frac{(x_2^2 + 2Lx_1 + x_1^2)}{2L^2}. \tag{C.7}$$

Similarly

$$\frac{(b-L)}{b} \equiv 1 - \frac{L}{b} = 1 - \frac{L}{L}\left(1 - \frac{(x_1^2 + 2Lx_2 + x_2^2)}{2L^2}\right) = \frac{(x_1^2 + 2Lx_2 + x_2^2)}{2L^2}. \tag{C.8}$$

Then it is possible to write

$$\begin{aligned}
k_1\frac{(a-L)}{a}(L+x_1) &= k_1\left(x_1 + \frac{3x_1^2}{2L} + \frac{x_2^2}{2L} + \frac{x_1x_2^2}{2L^2} + \frac{3x_1^3}{2L^2}\right),\\
k_1\frac{(a-L)}{a}x_1 &= k_1\left(\frac{x_1^2}{L} + \frac{x_2^2x_1}{2L^2} + \frac{x_1^3}{2L^2}\right),\\
k_2\frac{(b-L)}{b}(L+x_2) &= k_2\left(x_2 + \frac{3x_2^2}{2L} + \frac{x_1^2}{2L} + \frac{x_2x_1^2}{2L^2} + \frac{3x_2^3}{2L^2}\right),\\
k_2\frac{(b-L)}{b}x_2 &= k_2\left(\frac{x_2^2}{L} + \frac{x_1^2x_2}{2L^2} + \frac{x_2^3}{2L^2}\right).
\end{aligned} \tag{C.9}$$

Now, by eliminating a and b in Eq. C.3 it is possible to write

$$\begin{aligned}
m\ddot{x}_1 &+ k_1x_1 + \frac{3k_1}{2L}x_1^2 + \frac{k_1}{2L}x_2^2 + \frac{k_2}{L}x_1x_2 + \frac{k_1+k_2}{2L^2}x_1x_2^2 + \frac{k_1+k_2}{2L^2}x_1^3 = 0,\\
m\ddot{x}_2 &+ k_2x_2 + \frac{3k_2}{2L}x_2^2 + \frac{k_2}{2L}x_1^2 + \frac{k_1}{L}x_1x_1^2 + \frac{k_2+k_1}{2L^2}x_1x_2 + \frac{k_2+k_1}{2L^2}x_2^3 = 0.
\end{aligned} \tag{C.10}$$

These equations can be divided by m to give

$$\begin{aligned}
\ddot{x}_1 &+ \omega_1^2x_1 + \frac{3\omega_1^2}{2L}x_1^2 + \frac{\omega_1^2}{2L}x_2^2 + \frac{\omega_2^2}{L}x_1x_2 + \frac{\omega_1^2+\omega_2^2}{2L^2}x_1x_2^2 + \frac{\omega_1^2+\omega_2^2}{2L^2}x_1^3 = 0,\\
\ddot{x}_2 &+ \omega_2^2x_2 + \frac{3\omega_2^2}{2L}x_2^2 + \frac{\omega_2^2}{2L}x_1^2 + \frac{\omega_1^2}{L}x_1x_1^2 + \frac{\omega_2^2+\omega_1^2}{2L^2}x_1x_2 + \frac{\omega_2^2+\omega_1^2}{2L^2}x_2^3 = 0.
\end{aligned} \tag{C.11}$$

hence, Eq. C.11 are now in exactly the same form to those derived by [45] with $L = 1$. As can be noted, dividing by L again and defining $X_1 = \frac{x_1}{L}$ and $X_2 = \frac{x_2}{L}$ gives

$$\begin{aligned}
\ddot{X}_1 &+ \omega_1^2X_1 + \frac{\omega_1^2}{2}\left(3X_1^2 + X_2^2\right) + \omega_2^2X_1X_2 + \frac{\omega_1^2+\omega_2^2}{2}X_1\left(X_2^2 + X_1^2\right) = 0,\\
\ddot{X}_1 &+ \omega_2^2X_2 + \frac{\omega_2^2}{2}\left(3X_2^2 + X_1^2\right) + \omega_1^2X_2X_1 + \frac{\omega_2^2+\omega_1^2}{2}X_2\left(X_1^2 + X_2^2\right) = 0.
\end{aligned} \tag{C.12}$$

Which are the same as the equations considered in [45, 46, 70]. In this case the system is *partially* non-dimensionalised.

D Matrix manipulations for Touzé two-degree-of-freedom system, Subsection 7.1.1

$$
\mathbf{u}^{*}=\left\{\begin{array}{c}
u_{p1}^{2}\\ u_{m1}^{2}\\ u_{p1}u_{m1}\\ u_{p1}u_{p2}\\ u_{m1}u_{m2}\\ u_{p1}u_{m2}\\ u_{m1}u_{p2}\\ u_{p2}^{2}\\ u_{m2}^{2}\\ u_{p2}u_{m2}\\ u_{p1}^{3}\\ u_{m1}^{3}\\ u_{p1}^{2}u_{m1}\\ u_{p1}u_{m1}^{2}\\ u_{p1}u_{p2}^{2}\\ u_{m1}u_{m2}^{2}\\ u_{p1}u_{m2}^{2}\\ u_{m1}u_{p2}^{2}\\ u_{p1}u_{p2}u_{m2}\\ u_{m1}u_{p2}u_{m2}\\ u_{p1}^{2}u_{p2}\\ u_{m1}^{2}u_{m2}\\ u_{p1}^{2}u_{m2}\\ u_{m1}^{2}u_{p2}\\ u_{p1}u_{m1}u_{p2}\\ u_{p1}u_{m1}u_{m2}\\ u_{p2}^{3}\\ u_{m2}^{3}\\ u_{p2}^{2}u_{m2}\\ u_{p2}u_{m2}^{2}
\end{array}\right\}\rightarrow\beta^{*\mathsf{T}}=\omega_{r1}^{2}\left[\begin{array}{cc}
3 & 4-h^{2}\\ 3 & 4-h^{2}\\ -1 & -h^{2}\\ h^{2}+2h & 1+2h\\ h^{2}+2h & 1+2h\\ h^{2}-2h & 1-2h\\ h^{2}-2h & 1-2h\\ 4h^{2}-1 & 3h^{2}\\ 4h^{2}-1 & 3h^{2}\\ -1 & -h^{2}\\ 8 & 9-h^{2}\\ 8 & 9-h^{2}\\ 0 & 1-h^{2}\\ 0 & 1-h^{2}\\ 4h^{2}+4h & 3h^{2}+4h+1\\ 4h^{2}+4h & 3h^{2}+4h+1\\ 4h^{2}-4h & 3h^{2}-4h+1\\ 4h^{2}-4h & 3h^{2}-4h+1\\ 0 & 1-h^{2}\\ 0 & 1-h^{2}\\ 4h^{2}+4h+3 & 4+4h\\ 4h^{2}+4h+3 & 4+4h\\ 4h^{2}-4h+3 & 4-4h\\ 4h^{2}-4h+3 & 4-4h\\ h^{2}-1 & 0\\ h^{2}-1 & 0\\ 9h^{2}-1 & 8h^{2}\\ 9h^{2}-1 & 8h^{2}\\ h^{2}-1 & 0\\ h^{2}-1 & 0
\end{array}\right]\rightarrow\mathbf{n}_{(1)}{}^{\mathsf{T}}=\left[\begin{array}{cc}
1.5\omega_{1}^{2} & 0.5\omega_{2}^{2}\\ 1.5\omega_{1}^{2} & 0.5\omega_{2}^{2}\\ 3\omega_{1}^{2} & \omega_{2}^{2}\\ \omega_{2}^{2} & \omega_{1}^{2}\\ \omega_{2}^{2} & \omega_{1}^{2}\\ \omega_{2}^{2} & \omega_{1}^{2}\\ \omega_{2}^{2} & \omega_{1}^{2}\\ 0.5\omega_{1}^{2} & 1.5\omega_{2}^{2}\\ 0.5\omega_{1}^{2} & 1.5\omega_{2}^{2}\\ \omega_{1}^{2} & 3\omega_{2}^{2}\\ 0.5\left(\omega_{1}^{2}+\omega_{2}^{2}\right) & 0\\ 0.5\left(\omega_{1}^{2}+\omega_{2}^{2}\right) & 0\\ 1.5\left(\omega_{1}^{2}+\omega_{2}^{2}\right) & 0\\ 1.5\left(\omega_{1}^{2}+\omega_{2}^{2}\right) & 0\\ 0.5\left(\omega_{1}^{2}+\omega_{2}^{2}\right) & 0\\ 0.5\left(\omega_{1}^{2}+\omega_{2}^{2}\right) & 0\\ 0.5\left(\omega_{1}^{2}+\omega_{2}^{2}\right) & 0\\ 0.5\left(\omega_{1}^{2}+\omega_{2}^{2}\right) & 0\\ 1.5\left(\omega_{1}^{2}+\omega_{2}^{2}\right) & 0\\ 1.5\left(\omega_{1}^{2}+\omega_{2}^{2}\right) & 0\\ 0 & 0.5\left(\omega_{1}^{2}+\omega_{2}^{2}\right)\\ 0 & 0.5\left(\omega_{1}^{2}+\omega_{2}^{2}\right)\\ 0 & 0.5\left(\omega_{1}^{2}+\omega_{2}^{2}\right)\\ 0 & 0.5\left(\omega_{1}^{2}+\omega_{2}^{2}\right)\\ 0 & \left(\omega_{1}^{2}+\omega_{2}^{2}\right)\\ 0 & \left(\omega_{1}^{2}+\omega_{2}^{2}\right)\\ 0 & 0.5\left(\omega_{1}^{2}+\omega_{2}^{2}\right)\\ 0 & 0.5\left(\omega_{1}^{2}+\omega_{2}^{2}\right)\\ 0 & 1.5\left(\omega_{1}^{2}+\omega_{2}^{2}\right)\\ 0 & 1.5\left(\omega_{1}^{2}+\omega_{2}^{2}\right)
\end{array}\right]
$$

$$\mathbf{n}_{u(1)}{}^{\mathsf{T}} = \begin{bmatrix} 0 & 0 \\ 0 & 0 \\ 0 & 0 \\ 0 & 0 \\ 0 & 0 \\ 0 & 0 \\ 0 & 0 \\ 0 & 0 \\ 0 & 0 \\ 0 & 0 \\ 0 & 0 \\ 0 & 0 \\ 0 & 0 \\ 1.5\left(\omega_1^2+\omega_2^2\right) & 0 \\ 1.5\left(\omega_1^2+\omega_2^2\right) & 0 \\ 0 & 0 \\ 0 & 0 \\ 0 & 0 \\ 0 & 0 \\ \left(\omega_1^2+\omega_2^2\right) & 0 \\ \left(\omega_1^2+\omega_2^2\right) & 0 \\ 0 & 0 \\ 0 & 0 \\ 0 & 0 \\ 0 & 0 \\ 0 & \left(\omega_1^2+\omega_2^2\right) \\ 0 & \left(\omega_1^2+\omega_2^2\right) \\ 0 & 0 \\ 0 & 0 \\ 0 & 1.5\left(\omega_1^2+\omega_2^2\right) \\ 0 & 1.5\left(\omega_1^2+\omega_2^2\right) \end{bmatrix} \rightarrow \mathbf{h}_{(1)}{}^{\mathsf{T}} = \frac{1}{\omega_{r1}^2} \begin{bmatrix} 0.5\omega_1^2 & \frac{\omega_2^2}{8-2h^2} \\ 0.5\omega_1^2 & \frac{\omega_2^2}{8-2h^2} \\ -3\omega_1^2 & \frac{-2\omega_2^2}{h^2} \\ \frac{\omega_2^2}{h_2+2h} & \frac{\omega_1^2}{1+2h} \\ \frac{\omega_2^2}{h_2+2h} & \frac{\omega_1^2}{1+2h} \\ \frac{\omega_2^2}{h_2-2h} & \frac{\omega_1^2}{1-2h} \\ \frac{\omega_2^2}{h_2-2h} & \frac{\omega_1^2}{1-2h} \\ \frac{0.5\omega_1^2}{4h^2-1} & \frac{\omega_2^2}{2h^2} \\ \frac{0.5\omega_1^2}{4h^2-1} & \frac{\omega_2^2}{2h^2} \\ -\omega_1^2 & \frac{-3\omega_2^2}{h^2} \\ \frac{\left(\omega_1^2+\omega_2^2\right)}{16} & 0 \\ \frac{\left(\omega_1^2+\omega_2^2\right)}{16} & 0 \\ 0 & 0 \\ 0 & 0 \\ \frac{\left(\omega_1^2+\omega_2^2\right)}{8h^2+8h} & 0 \\ \frac{\left(\omega_1^2+\omega_2^2\right)}{8h^2+8h} & 0 \\ \frac{\left(\omega_1^2+\omega_2^2\right)}{8h^2+8h} & 0 \\ \frac{\left(\omega_1^2+\omega_2^2\right)}{8h^2+8h} & 0 \\ 0 & 0 \\ 0 & 0 \\ 0 & \frac{\left(\omega_1^2+\omega_2^2\right)}{8+8h} \\ 0 & \frac{\left(\omega_1^2+\omega_2^2\right)}{8+8h} \\ 0 & \frac{\left(\omega_1^2+\omega_2^2\right)}{8+8h} \\ 0 & \frac{\left(\omega_1^2+\omega_2^2\right)}{8+8h} \\ 0 & 0 \\ 0 & 0 \\ 0 & \frac{\left(\omega_1^2+\omega_2^2\right)}{16h^2} \\ 0 & \frac{\left(\omega_1^2+\omega_2^2\right)}{16h^2} \\ 0 & 0 \\ 0 & 0 \end{bmatrix}$$

$$\mathbf{n}_{u(2)}{}^{\mathsf{T}} = \frac{1}{\omega_{r1}^2}\begin{bmatrix}
0 & 0\\
0 & 0\\
0 & 0\\
0 & 0\\
0 & 0\\
0 & 0\\
0 & 0\\
0 & 0\\
0 & 0\\
0 & 0\\
0 & 0\\
0 & 0\\
\frac{-90}{12}\omega_1^4+\frac{9h^2-24}{2h^2(4-h^2)}\omega_1^2\omega_2^2 & 0\\
\frac{-90}{12}\omega_1^4+\frac{9h^2-24}{2h^2(4-h^2)}\omega_1^2\omega_2^2 & 0\\
0 & 0\\
0 & 0\\
0 & 0\\
0 & 0\\
\frac{2}{(h^2-4)}\omega_2^4-3\omega_1^4+\frac{2}{(1-4h^2)}\omega_1^4-\frac{1}{3\,h^2}\omega_2^4 & 0\\
\frac{2}{(h^2-4)}\omega_2^4-3\omega_1^4+\frac{2}{(1-4h^2)}\omega_1^4-\frac{1}{3\,h^2}\omega_2^4 & 0\\
0 & 0\\
0 & 0\\
0 & 0\\
0 & 0\\
0 & 0\\
0 & -3\omega_1^4+\frac{2}{h^2-4}\omega_2^4-\frac{2}{h^2}\omega_1^2\omega_2^2+\frac{2}{1-4h^2}\omega_1^4\\
0 & -3\omega_1^4+\frac{2}{h^2-4}\omega_2^4-\frac{2}{h^2}\omega_1^2\omega_2^2+\frac{2}{1-4h^2}\omega_1^4\\
0 & 0\\
0 & 0\\
0 & \frac{3-8h^2}{8h^2-2}\omega_1^4-\frac{90}{12h^2}\omega_2^4\\
0 & \frac{3-8h^2}{8h^2-2}\omega_1^4-\frac{90}{12h^2}\omega_2^4
\end{bmatrix}$$

E Matrix manipulations for the 3-DOF system, Section 7.2

$$
\mathbf{u}^{*}_{(1)} = \left\{ \begin{array}{c}
u_{p2}^3 \\ u_{m2}^3 \\ u_{p2}^2 u_{m2} \\ u_{p2} u_{m2}^2 \\ u_{p2} u_{p3}^2 \\ u_{m2} u_{m3}^2 \\ u_{p2} u_{p3} u_{m3} \\ u_{m2} u_{p3} u_{m3} \\ u_{p2} u_{m3}^2 \\ u_{m2} u_{p3}^2 \\ u_{p2}^2 u_{p3} \\ u_{m2}^2 u_{m3} \\ u_{p2} u_{m2} u_{p3} \\ u_{p2} u_{m2} u_{m3} \\ u_{p2}^2 u_{p3} \\ u_{p2}^2 u_{m3} \\ u_{p3}^3 \\ u_{m3}^3 \\ u_{p3}^2 u_{m3} \\ u_{p3} u_{m3}^2 \\ u_{p1} \\ u_{m1} \\ u_{p2} \\ u_{m2} \\ u_{p3} \\ u_{m3}
\end{array} \right\} \rightarrow [n_{v(1)}]^{\mathsf{T}} = \frac{\kappa}{m} \left[\begin{array}{ccc}
0 & 1 & 0 \\ 0 & 1 & 0 \\ 0 & 3 & 0 \\ 0 & 3 & 0 \\ 0 & 27 & 0 \\ 0 & 27 & 0 \\ 0 & 54 & 0 \\ 0 & 54 & 0 \\ 0 & 27 & 0 \\ 0 & 27 & 0 \\ 0 & 0 & 9 \\ 0 & 0 & 9 \\ 0 & 0 & 18 \\ 0 & 0 & 18 \\ 0 & 0 & 9 \\ 0 & 0 & 9 \\ 0 & 0 & 27 \\ 0 & 0 & 27 \\ 0 & 0 & 81 \\ 0 & 0 & 81 \\ \frac{\omega_{r1} mc}{\kappa} & 0 & 0 \\ -\frac{\omega_{r1} mc}{\kappa} & 0 & 0 \\ 0 & \frac{\omega_{r2} m(c+\bar{c})}{\kappa} & 0 \\ 0 & -\frac{\omega_{r2} m(c+\bar{c})}{\kappa} & 0 \\ 0 & 0 & \frac{\omega_{r3} m(c+3\bar{c})}{\kappa} \\ 0 & 0 & -\frac{\omega_{r3} m(c+3\bar{c})}{\kappa}
\end{array} \right] \rightarrow \boldsymbol{\beta}^{\mathsf{T}}_{(1)} = \omega_{r2}^2 \left[\begin{array}{ccc}
\_ & 8 & \_ \\ \_ & 8 & \_ \\ \_ & 0 & \_ \\ \_ & 0 & \_ \\ \_ & 8 & \_ \\ \_ & 8 & \_ \\ \_ & 0 & \_ \\ \_ & 0 & \_ \\ \_ & 0 & \_ \\ \_ & 0 & \_ \\ \_ & \_ & 8 \\ \_ & \_ & 8 \\ \_ & \_ & 0 \\ \_ & \_ & 0 \\ \_ & \_ & 0 \\ \_ & \_ & 0 \\ \_ & \_ & 8 \\ \_ & \_ & 8 \\ \_ & \_ & 0 \\ \_ & \_ & 0 \\ 0 & \_ & \_ \\ 0 & \_ & \_ \\ \_ & 0 & \_ \\ \_ & 0 & \_ \\ \_ & \_ & 0 \\ \_ & \_ & 0
\end{array} \right]
$$

F Detailed derivation of Eq. 6.54

In this appendix the derivation of Eq. 6.54a is introduced, while the same procedure can be followed for Eq. 6.54b. Starting with the following

$$\begin{aligned}\dot{U}_2 &= \lim_{T\to\infty}\frac{2\varepsilon\zeta\omega_n}{T\Omega}\int_0^T\{\mathrm{D}^\beta[U\cos(\Omega t+\phi)]\sin(\Omega t+\phi)\}\,\mathrm{d}t\\ &= -\varepsilon\frac{2U\zeta\omega_n}{\Gamma(1-\beta)}\lim_{T\to\infty}\frac{1}{T}\int_0^T\left(\int_0^t\left[\frac{\sin(\Omega u+\phi)}{(t-u)^\beta}\,\mathrm{d}u\right]\sin(\Omega t+\phi)\right)\mathrm{d}t\end{aligned} \tag{F.1}$$

Using the transformation $s=t-u$ which gives $\mathrm{d}s=-\mathrm{d}u$, it is possible to write

$$\begin{aligned}\dot{U}_2 &= \frac{-2\varepsilon\zeta\omega_n U}{\Gamma(1-\beta)}\lim_{T\to\infty}\frac{1}{T}\int_0^T\left[\int_0^t\frac{\sin(\Omega t+\phi-\Omega s)}{s^\beta}\,\mathrm{d}s\right]\sin(\Omega t+\phi)\,\mathrm{d}t\\ &= \frac{-2\varepsilon\zeta\omega_n U}{\Gamma(1-\beta)}\lim_{T\to\infty}\frac{1}{T}\int_0^T\left[\int_0^t\frac{\cos(\Omega s)}{s^\beta}\,\mathrm{d}s\right]\sin^2(\Omega t+\phi)\,\mathrm{d}t\\ &+\frac{2\varepsilon\zeta\omega_n U}{\Gamma(1-\beta)}\lim_{T\to\infty}\frac{1}{T}\int_0^T\left[\int_0^t\frac{\sin(\Omega s)}{s^\beta}\,\mathrm{d}s\right]\sin(\Omega t+\phi)\cos(\Omega t+\phi)\,\mathrm{d}t\end{aligned} \tag{F.2}$$

It is now possible to integrate the two components of the previous equation separately, using integration by parts for each component; if assumed that $\dot{U}_2=\Upsilon_1+\Upsilon_2$, then the first component Υ_1 is expressed as

$$\begin{aligned}\Upsilon_1 &= \frac{-\varepsilon\zeta\omega_n U}{2\Omega\Gamma(1-\beta)}\lim_{T\to\infty}\left\{\frac{2\Omega t-\sin(2\Omega t+2\phi)}{T}\left[\int_0^t\frac{\cos(\Omega s)}{s^\beta}\,\mathrm{d}t\right]\right\}\Bigg|_0^{\mathrm{T}}\\ &+\frac{\varepsilon\zeta\omega_n U}{2\Omega\Gamma(1-\beta)}\lim_{T\to\infty}\left\{\frac{1}{T}\int_0^t\left[\frac{\cos(\Omega t)[2\Omega t-\sin(2\Omega t+2\phi)]}{t^\beta}\,\mathrm{d}t\right]\right\}\end{aligned} \tag{F.3}$$

by using Eq. 6.51 to Eq. 6.53, and simplifying the results, one can get

$$\Upsilon_1=-\varepsilon\zeta\omega_n U\Omega^{\beta-1}\sin\left(\frac{\beta\pi}{2}\right) \tag{F.4}$$

similarly, if the same procedure is repeated one may find that $\Upsilon_2=0$ when $T\to\infty$. Finally, it is possible to write

$$\dot{U}_2=-\varepsilon\zeta\omega_n U\Omega^{\beta-1}\sin\left(\frac{\beta\pi}{2}\right) \tag{F.5}$$

In order to find the second part of Eq. 6.54, $\dot{\phi}$, the same procedure is followed which finally yields to

$$\dot{\phi}_2=\varepsilon\zeta\omega_n\Omega^{\beta-1}\cos\left(\frac{\beta\pi}{2}\right) \tag{F.6}$$